Dynamics and Conformation of Hairy-Rod Polymers in Isotropic Solutions

George Petekidis

A Thesis Submitted to the
Physics Department
Univeristy of Crete

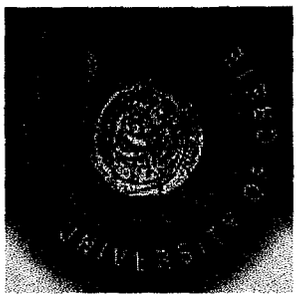

Heraklion, December 1997

TABLE OF CONTENTS

Chapter 2

Polymer Solutions

A polymer solution is a physical system with very interesting thermodynamic as well as dynamic behavior. The physical properties of a polymer solution depend on solvent, temperature and concentration but also from the conformation of the polymer chain; flexible, semistiff or rodlike macromolecules can exhibit different behavior in solutions. From the thermodynamic point of view, the significant and solvent-polymer interactions, which are of an extremely unsymmetrical nature, lead to strong deviations from ideality as is defined by Rault's and van't Hoff's laws [1]. In determining the thermodynamic properties of polymer solutions the free energy, F, and the osmotic pressure, π, have to be calculated. The later plays the same role in the description of a solution that pressure plays for convectional gases; moreover since it is the main force opposing concentration fluctuations in a polymer solution is closely related with the relaxation phenomena or in general with the dynamics of macromolecules in solution [2, 3].

Polymer solutions can be classified according to concentration and according to the interactions between solvent and solute molecules. In the latter case, the solvents for polymers are broadly classified into two categories, good and poor solvents. If the effective potential between the polymer chains in the medium of the solvent molecules is repulsive, the system is under *good solvent* conditions. This attractive interactions between polymers and solvent molecules is realized by an easy dissolution of the polymer. If, to the contrary, the interaction between the solvent and the polymer chains is repulsive then the effective potential between macromolecules is attractive, the system is under *poor solvent* conditions and phase separation may occur. Finally, a polymer solution is in a *theta state* if there is zero effective interaction between the polymer chains. The second virial coefficient A_2 is also used often to define the solvent quality. It is zero at theta temperature (Θ), positive for good solvents while for bad solvents it can become negative [4].

2.1 Chain Conformation

The conformation of a polymer chain is not only a fundamental subject in polymer science but also a prerequisite for almost all investigations in the field. Several, mainly scattering, experimental techniques are utilized, to investigate the characteristics of single polymer chains such as the size, conformation and flexibility.

From the theoretical point of view, the most simple model describing an ideal polymer chain is the *Freely Joined Chain* which is composed of a sequence of n rigid segments, each of length l_o with no rotational restrictions, no valence bond angles and no volume excluded by the chain. A measure of the size of the chain is the mean square end to end vector $< R^2 >$, (fig. 2.1a) which for the freely joined chain is [5, 4]:

$$< R^2 >= nl_o^2 \tag{2.1}$$

The average is taken over all possible conformations of the chain. An ideal polymer chain has a Gaussian probability distribution function $P_n(R)$ due to the fact that the orientational correlations diminish with distance exponentially. The Gaussian coil is a system with low density and intense concentration fluctuations with correlation size of the magnitude of the size of the coil [4]. A more realistic model for describing polymer chains is the *Rotational Isomeric State Model,* (RIS) [5, 6], proposed by Flory, in which the chain conformation and shape are described using molecular parameters such as conformational energies and torsional angle (fig. 2.1b).

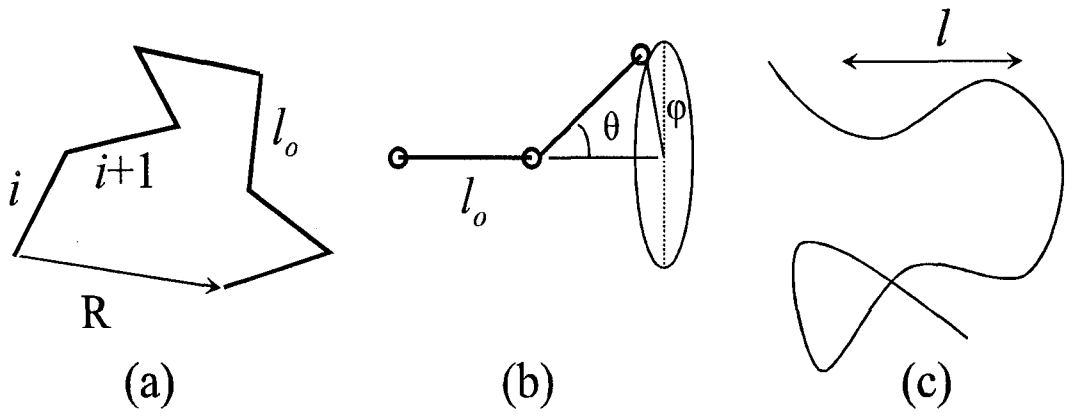

Figure 2.1: Conformation of a polymer chain: (a) Freely jointed chain, (b) RIS chain with valence angle θ and internal rotational angle φ, (c) wormlike chain with a persinstence length l

In general, any long macromolecule exhibits some flexibility, but different polymers have different mechanisms of flexibility, which can be described by

different models. Even if the straight-chain conformation corresponds to the absolute minimum of the energy of a macromolecule, the thermal excitation energy ($\sim k_B T$) produces small deformations, so that the atomic framework of the polymer can be regarded as a thin elastic, homogeneous filament obeying Hooke's law under deformation [4]. Such a model of a polymer chain is called *persistent* or *Wormlike Model*. In this way, even small fluctuation bendings can lead to a total coiling of a sufficiently long chains, because different sections bend to different sides. The flexibility of a polymer chain is determined by the *persistence length, l*, and can vary from ten to few thousands Angstroms, depending on the chemical structure of the macromolecule. Polymers with large flexibility (small l) are called flexible, while those with small flexibility are called stiff polymers, and depending on the total length of their chain (contour length) they can have a rodlike or a coiled conformation. Stiffness can be introduced in a polymer chain by linear rigid connection between monomers or by steric interaction of the neighboring monomers or by helical supramolecular structures. The first two cases are more common in synthetic macromolecules like poly(p-phenylenes) and poly(phthalocyaninatosiloxanes) respectively, while the latter is very often found in biopolymers such as DNA [7].

A real polymer can be treated effectively as a freely joined chain made of $n = L/l_\kappa$ segments. This is the *Kuhn Model* [8, 9] and l_κ (Kuhn segment length), which characterizes the flexibility of the chain, is defined by $< R^2 > = L\ l_\kappa$. Probably the best model for treating semiflexible chains is the wormlike model of Kratky & Porod [10, 11], which was qualitatively described above. In this model, the path that the polymer chain follows is described by a continuous differentiable space curve $\mathbf{r}(s)$, where s determines a point along the chain. Actually the Kratky-Porod wormlike model is defined as the continuous limit of the freely joined chain with supplementary valence bond angle θ, and is an interpolation from the random coil limit $L/l_\kappa \rightarrow \infty$, where $< R^2 >= Ll_\kappa$, to the rigid rod limit $L/l_\kappa \rightarrow 0$, where $< R^2 >= L^2$ [12].

The persistence length, l ,can roughly be considered as the maximum chain section that remains straight; at greater lengths bending fluctuations destroy the memory of chain direction. In all models, l can be defined by

$$< cos\theta(s) > \equiv < \mathbf{u}(s) \cdot \mathbf{u}(0) >= \exp(-s/l) \tag{2.2}$$

where $\mathbf{u}(s) = \partial \mathbf{r}(s)/\partial s$ is the unit tangent vector at the point s. For a wormlike chain the persistence length is related to the effective bending modulus per unit length of the chain, κ , according to $l = \kappa\ /\ k_B T$ [4].

For a wormlike chain the mean square end-to-end vector is [13, 4]:

$$< R^2 >= 2l^2\{\frac{L}{l} - 1 + exp(-L/l)\} \tag{2.3}$$

while the radius of gyration defined by [4, 14]:

$$< R_g^2 >= \frac{1}{n} < \sum_i (\mathbf{r}_i - \mathbf{R})^2 >= \frac{1}{2} N^{-2} < \sum_i \sum_j (\mathbf{r}_i - \mathbf{r}_j)^2 > \qquad (2.4)$$

(**R** denoting the center of mass of the chain) is [13, 15]:

$$< R_g^2 >= l^2 \{ \frac{L}{3l} - 1 + \frac{2l}{L} - \frac{2l^2}{L^2} [1 - exp(-L/l)] \} \qquad (2.5)$$

For a Gaussian chain the mean square radius of gyration, in the limit $n \gg 1$ is found to be $< R_g^2 >= \frac{1}{6} < R^2 >$.

The radius of gyration, the molecular weight, the contour length, and the persistence length can be determined experimentally by light scattering from dilute polymer solutions where interactions between different chains are not important. The determination of the flexibility of different series of stiff polymers by such scattering techniques is a part of the present work.

2.2 Concentration Regimes

Polymer solutions in good solvents can be divided in three regions according to concentration. In dilute polymer solutions the individual polymer chains are isolated while in more concentrated solutions the polymer chains overlap. In rodlike polymers it is the length L and the diameter b of the molecule which defines these regimes, whereas for flexible chains it is the radius of gyration R_g. The concentration regimes are (Fig. 2.2):

i) **Dilute region**: The solution is so dilute, that the polymers are separated from each other and polymer-polymer interactions are so small, that at most only pair interactions should be considered. At this region, all physical quantities are expressed as a power series with respect to concentration. For flexible polymers, this region corresponds to a number concentration $\rho < \rho^* = \frac{1}{(4/3)\pi R_g^3}$, while for rodlike polymers to $\rho < \rho^* = \frac{1}{L^3}$. For semiflexible chains the onset of the semidilute region is indicated by $\rho^* = \frac{1}{Ll^2}$. The characteristic length observed in experiments like light scattering is the size of the molecule R_g.

ii) **Semidilute region**: The polymer chains are now close enough that they can overlap. For rodlike molecules, the region is defined by $\rho^* = 1/L^3 < \rho < \rho^{**} = 1/(bL^2)$, while for semiflexible coils it is the region where $\rho^* = 1/Ll^2 < \rho < \rho^{**} = 1/(bLl)$. In this regime excluded volume interactions are still small. It must be noted that the polymer concentration is still quite small in a solute numbers; for example polystyrene, a flexible polymer, with molecular weight 10^6,the overlap concentration is $c^* \simeq 0.5\%$ by weight, while a rodlike poly (p-phenylene) with molecular weight 10^4 it is $c^* \simeq 0.1\%$, due to its extended shape. In this region, as well as in the dilute one, the fluctuations of the polymer segment density are large (fig. 2.2) and with a correlation length of the order of the interchain distance, ξ.

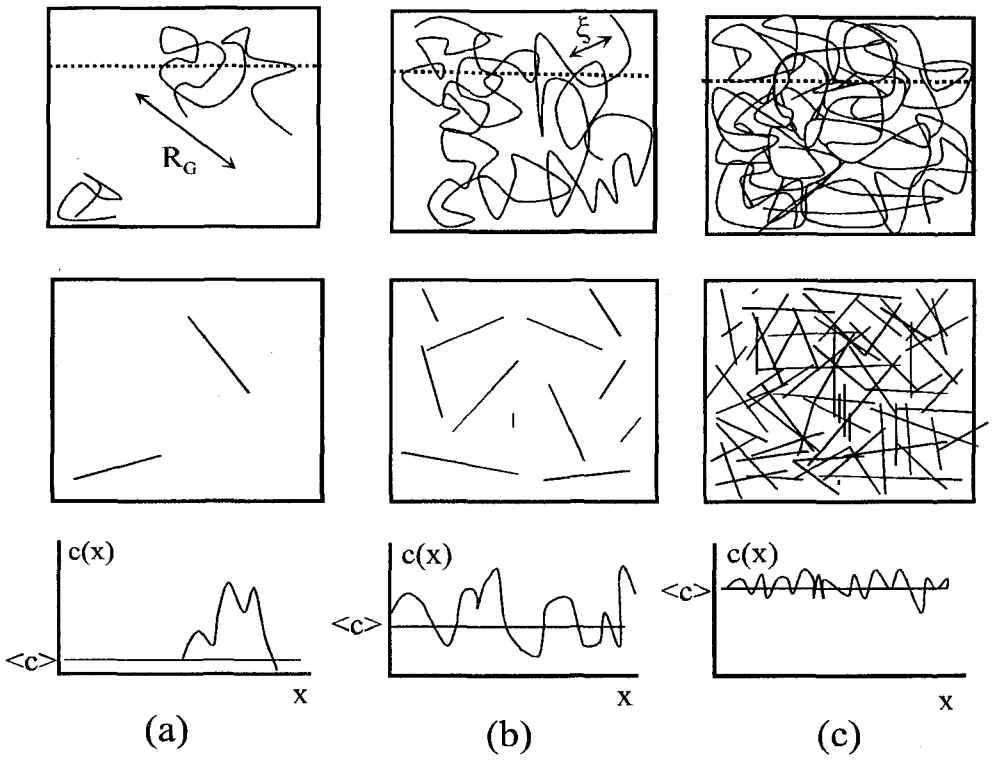

Figure 2.2: Concentration regimes of flexible (top) and rodlike (bottom) polymer solutions: (a) dilute, (b) semidilute, (c) concentrated. c(x) denotes the concentration profile along the dashed line. The characteristic lengths in these regimes are shown: R_G (dilute) and ξ (semidilute and concentrated).

iii) **Concentrated region**: At high concentrations there is a significant interpenetration of the polymer chains, which leads to a strong entanglement if the molecular weight is large enough. The fluctuations in the segment density become small and can be treated by mean field theory [3]. On the other hand for rodlike polymers there is strong enmeshment which, as in the case of their flexible counterparts, affects both the dynamic and static properties a great deal. Moreover, in solutions of rodlike macromolecules, when the concentration becomes larger than a critical value c_n, the molecules align in nearly parallel direction and the solution becomes an anisotropic liquid [4, 3] (fig. 2.4).

It should be mentioned that this classification of polymer solutions is rather conceptual since the crossover between various regimes is not sharp and experimentally it is often difficult to identify the crossover concentration. In a poor solvent the situation is more complicated since the attractive forces between the polymers can lead to aggregation and finally phase separation.

2.3 Phase Separation

The phenomenon of phase separation of flexible polymer chains has been treated theoretically by Flory and Huggins [16, ?, 2, 17]. The theory predicts a biphasic region for temperatures lower than a critical temperature, T_c, where the system separates into two isotropic phases with different concentrations; a small c_A and a large c_B (fig. 2.3).

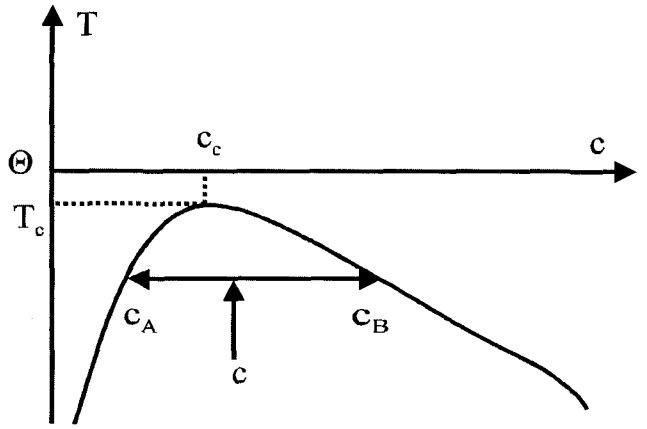

Figure 2.3: Phase diagram of solutions of a flexible polymer. In the biphasic region the system at concentration c will phase separate into two phases with concentrations c_A and c_B .

This phase diagram can be very much altered if the polymer chains are rodlike or if they possess stiff parts either, in their backbone or in side chains. As the concentration is increased in a solution of rodlike molecules, the repulsive interactions among the rods become stronger and can lead to an ordered phase, even in the absence of any specific energetic interactions. In such cases pure steric reasons make impossible the arrangement of such anisodiametric molecules isotropically when the system is sufficiently concentrated [18, 19, 20]. Then a transition takes place from an isotropic liquid to a liquid-crystalline (LC) solution, a state with properties intermediate between those of a liquid and a crystalline solid. Like liquids, liquid crystals lack of long range translational order, while they maintain long-range orientational order and thus they are anisotropic like crystalline solids. Liquid-crystalline polymer melts are often called thermotropic polymeric liquid crystals since in such systems the transition from the isotropic to the LC state can happen by changing the temperature, whereas polymer solutions which can form LC phases are called lyotropic systems and the transition can happen by changing the concentration. Polymeric LC's like their small molecule analogous can be found in three types: nematic, smectic and cholesteric (fig. 2.4).

The two main theoretical approaches, which describe the nematic ordering in solutions of long rigid rods are the Onsager theory [21] and the Flory lattice theory [22]. Onsager treated the case of an athermal solution of cylindrical rods of length L and diameter b, in which only repulsive forces act, due to the mutual impenetrability between two molecules. The fundamental approximation of the Onsager theory is that the interactions between rods are taken into account in the second virial approximation and thus this method is applicable only at low concentrations ($\rho \ll 1/Lb^2$). Nevertheless, it is found that for $L \gg b$ the isotropic to nematic transition indeed occurs at such small concentrations and is a first-order phase transition. The critical concentration at which the transition to a nematic liquid crystal phase occurs according to this theory is $\rho_n \simeq \frac{4}{A_{2,c}} = \frac{16}{\pi bL^2} = \frac{16}{\pi}\rho^{**}$ (or a volume fraction $\phi_n \simeq 4/x$, with $x = L/b$ the axial ratio of the rod), where $A_{2,c}$ is the osmotic second virial coefficient. Actually the Onsager approach predicts that when $\phi_i < \phi < \phi_a$ the solution separates into an isotropic and an anisotropic phase, while for $\phi > \phi_n$ it is completely in the liquid crystalline phase. These concentrations are: $\phi_i = 3.34/x$ and $\phi_a = 4.49/x$. The order parameter $s =< 3cos^2\theta - 1 > /2$ at ϕ_a is also calculated, $s(\phi_a) = 0.84$ [21, 20].

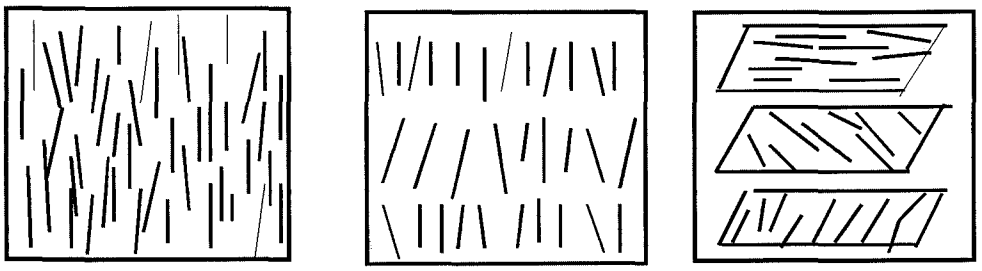

Figure 2.4: Anisotropic Liquid Crystalline phases: (a) nematic, (b) smectic, (c) cholesteric.

Flory [23, 22] developed a lattice theory for rods where he could take into account energetic interactions, which are usually present in real systems, via an interaction parameter χ. The phase diagram which he predicted (fig. 2.5) is much different than the one for flexible coils. The most important difference is that whereas for flexible coils an interaction parameter $\chi_{cr} > 0.5$ is needed for phase separation to occur, rodlike solutions phase separation occurs even at $\chi_{cr} \approx 0$. The reason is that configurational entropy, some of which must dissipate from random coil polymers before phase separation can occur, is completely absent in rodlike polymers. The Flory phase diagram has a narrow biphasic region at large T's (the "chimney") and a much wider one for the smaller T's. In the chimney region, a liquid crystalline phase coexists with an isotropic phase of a

similar concentration. The first appearance of the anisotropic phase occurs, in the limit of high axial ratio's, at a twice the value predicted by Onsager. Under poor solvent conditions, in the wide biphasic region at low T's, the difference in the concentrations of the two phases becomes larger and thus the induced coupling of concentration with orientation is enhanced. The later feature has also significant effects in the dynamics of such systems. The Flory phase diagram is quantitatively the same with the one experimentally determined by Miller et al [24] for solutions of the helical rodlike polymer PBLG. It is not clear yet which approach is more accurate since in real systems additional effects like flexibility, polydispersity have to be considered. There is evidence that the Onsager theory is very accurate only for truly stiff and monodisperse rods [25, 26].

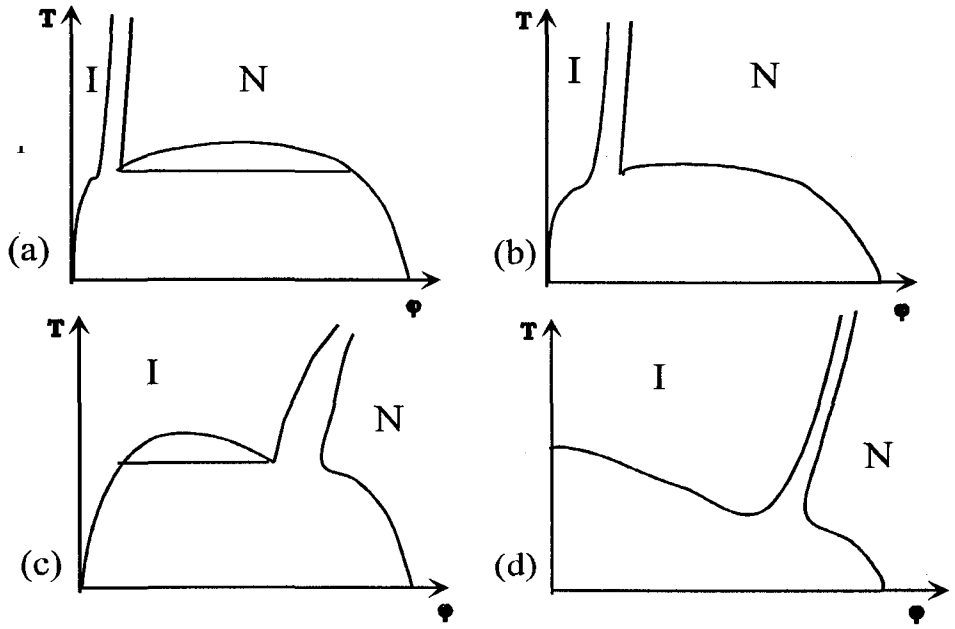

Figure 2.5: Phase diagrams of rod-like polymers with high (a) and low aspect ratio (c), for wormilike polymers with small (b) and large flexibility (d).

The effect of polydispersity on the nematic transition has been analyzed by using both approaches and the results qualitatively coincide. The nematic transition is expected to occur at $\phi_n \sim (b/L_w)$, where L_w is the weight average length of the rods, while the biphasic region is expected to increase (fig. 2.5). Moreover the fraction of the longer rods in the anisotropic phase is considerably greater than in the isotropic phase meaning that the phase separation is accompanied by a strong fractionation [20].

The case of athermal solutions of partially flexible polymers and it is found that orientational ordering depends strongly both on the persinstence length, l,

and on the character of the flexibility [20]. For the persistent flexibility mechanism, which describes better most of the semistiff polymers, it is predicted that even a small amount of flexibility ($L/l \sim 0.1$) suffices to make the properties of the LC transition closer to the case of semiflexible chains rather than to rigid rods, although the geometric shape of the molecule is closer to rodlike [27]. For an athermal solution of semiflexible chains it was shown that the orientational ordering occurs at much larger concentrations compared to rigid rods and with a much smaller order parameter [28]. Experimental investigations on semistiff chains with persistent flexibility such as poly(γ-benzyl-a,L-glutamate) (PBLG), a helical rodlike polymer, poly(p-phenylenterephthalamide) (PPTP) and poly(p-benzamide) (PBA) are at least in a qualitative agreement with theoretical predictions [20].

In the case of non-athermal systems the effects of polydispersity and flexibility affect the phase diagram in a similar way to that of athermal solutions [29, 30]. It is predicted that for different values of l/b, the phase diagram can be qualitatively different (fig. 2.5), revealing biphasic regions where the system phase separates not only in an isotropic and an anisotropic phase, but also for large values of l/b (> 125) in two anisotropic phases and for small values of l/b (< 50) in two isotropic phases with different concentrations. In the latter case, one of the isotropic phases is very dilute and the system resembles the phase separated flexible polymer systems.

2.4 Polymer Dynamics

In addition to their rich thermodynamics, macromolecules in solution exhibit various complex translational, rotational and bending motions, which dominate the dynamic behavior of the system. In a two-component system composed of rigid particles and liquid three types of force act on the particle [31]:

a) the "Brownian" force which arises from the collisions with the thermally agitated molecules of the liquid medium,

b) the forces due to direct interactions between particles i.e., shielded Coulomb interactions between charged particles, repulsive "excluded volume" or "hard-sphere" and attractive van der Waals forces between uncharged particles.

c) the hydrodynamic forces which originate from the coupling between the motion of particles transmitted indirectly by the flows induced in the liquid.

In addition to the above a polymer chain in solution is subjected to bending and stretching forces, due to its nonrigid character, which change their shape. Measurement of the relaxation time constants associated with such motions is

important for the understanding of the dynamics of these systems and the prediction of their macroscopic behavior in solution and bulk. In addition, these complex systems provide a challenging many body-problem and a testing ground for fundamental statistical and hydrodynamic theories of liquids which exhibit multiple relaxations over several time and length scales.

In dilute solutions most theories for the diffusion coefficients treat the macromolecule as a particle immersed in a hydrodynamic continuous medium, while the surface of the macromolecule is considered to be smooth, ignoring complex molecular characteristics. Using hydrodynamic methods and usually stick (non-slip) boundary conditions, the diffusion coefficients can be calculated, in the limit of infinitely dilution, in terms of the geometric characteristics such as L, and b for rigid rods and also l, in the case of semiflexible molecules (see chapter 4 and appendix therein). Of course, the effect of the solvent also enters through its viscosity η_0. In general, the translational diffusion coefficient D is given by Einstein's relation, $D = k_BT/f$, while the rotational diffusion coefficient by $D_R = k_BT/f_R$, where f and f_R are the translational and the rotational friction coefficients respectively and is a function η_0, L, b and l.

The Brownian motion can be studied by a microscopic approach, starting from the dynamical equation of motion of the Brownian particle and the fluid molecules, as well as by a more phenomenological approach which regards the Brownian motion as a stochastic process and constructs an equation describing the phenomenon based on macroscopic laws. The second approach which originated by Einstein, is limited by several conditions such as that the time-scale and the length scale of the Brownian particle is much longer than those of the solvent molecules and that there is a linear relation between the forces and the fluxes [3]. For polymer solutions and suspensions, these conditions are normally satisfied. The phenomenological approach is also more useful in calculating dynamic quantities and it is based on an equation for Brownian motion which appears in two different forms: the *Smoluchowski equation* and the *Langevin equation.* The Smoluchowski equation is derived from a generalization of the diffusion equation and is related to the thermodynamics of irreversible processes; in one dimension and under the influence of an external potential U, it is written as [3]:

$$\frac{\partial c}{\partial t} = \frac{\partial}{\partial x}\frac{1}{f}(k_BT\frac{\partial c}{\partial x} + c\frac{\partial U}{\partial x}) \tag{2.6}$$

The diffusion coefficient D characterizes the thermal motion of the particles whereas the friction coefficient f specifies the response to an external force. This relation is a special case of the more general *fluctuation-dissipation theorem*, which states that the characteristics of the response of the spontaneous thermal fluctuations are related to the characteristics of the response of the system to an external field [3]. The Smoluchowski equation holds also for the evolution of the probability distribution function $G\ (x,t)$ and can then be applied to describe the fluctuations of physical quantities such as concentration. The potential $U(x)$

determines the force acting on the Brownian particle and can also be regarded as the free energy which determines the equilibrium distribution of the quantities under investigation.

A classical example for the usage of such a method in polymer physics is the investigation of the dynamic behavior of a flexible macromolecules in dilute solution [3, 17]. In the framework of the Rouse model [32] the dynamic behavior of a flexible chain is calculated with the use of above phenomenological equation and disregarding the excluded volume interaction and the hydrodynamic interaction. The center of mass position is found to diffuse with a diffusion coefficient $D_s = \frac{k_B T}{N f} \propto M^{-1}$, while the rotational relaxation time is $\tau_R \propto M^2$; predictions which disagree with experimental findings in dilute solutions of flexible polymers. However, when the hydrodynamic interactions are taken into account (as was done by Zimm model [33] in the preaveraging approximation), we are led to $D_s \propto M^{-1/2}$ and $\tau_R \propto M^{3/2}$, in agreement with experimental findings. The results of the Zimm model can also be predicted using scaling law ideas [2].

If the concentration of a polymer solution exceeds c^*, the polymer molecules start to overlap and excluded volume, hydrodynamic and entanglement interactions strongly affect the molecular motion. From the theoretical side, the calculations become complicated and rigorous treatment of the entanglements from first principle is very difficult. The current theories for the dynamics of concentrated polymer solutions are based on two general models which capture some features of the motion very well, but cannot describe all aspects of the dynamics [17]. The first theory describes *concentration fluctuations* ignoring entanglements and considering the combined cooperative motions of parts of the polymer chain. The second one is the *reptation theory* which describes both diffusion and viscoelasticity in concentrated polymer solutions and melts, where the effect of the entanglements is dominant, and which considers the motion of individual chains while cooperative motions are neglected. One of the central questions of polymer solution dynamics is the validity of the reptation idea which is actually a plausible hypothesis rather than the result of a rigorous molecular theory. It can also be realized [3] as a kind of a mean-field approximation which describes the detailed constraints by an average constraint, i.e., the tube.

In nondilute polymer solutions one expects a slowing down of the motion of the polymer chains and thus a decrease of diffusivity due to mutual hinderance and interpenetration of neighboring polymer chains. This is the steric effect in the diffusion, which is manifested as an increase of the friction. But as the concentration increases the solution begins to act more and more as a thermodynamic and hydrodynamic continuum. The solution is characterized by concentration fluctuations in space and time, which are opposed partly by hydrodynamic friction, and partly by the osmotic pressure. A measure of the driving force that can relax concentration fluctuations is the osmotic modulus $(\partial\pi/\partial c)_{T,P}$. The osmotic pressure increases with polymer concentration due to the increase of the excluded

volume and acts so that it makes the concentration uniform as fast as possible. Thus, there are two opposing terms; the increasing friction which tends to slow down the polymer motion and the increasing osmotic pressure which tends to speed up the diffusion so that the concentration fluctuations are relaxed faster.

A quantity which directly reflects the above forces is the *cooperative diffusion* coefficient, D_c, through which the concentration fluctuations relax. The cooperative diffusion (or mutual) represents the average response of a collection of molecules in a weak concentration gradient imposed by thermal fluctuations and is a one of the main quantities studied by *dynamic light scattering.* D_c is related with the osmotic modulus according to [1, 34]:

$$D_c = (\frac{M}{N_A})(1-\phi)^2(\partial\pi/\partial c)_{T,P} \ / \ f_m \tag{2.7}$$

where f_m is the mutual friction coefficient and is not necessarily the same with the self-diffusion friction coefficient f_s.

In the virial regime, where the intermolecular interactions are weak enough to be treated only at a level of pair interactions, friction and thermodynamic parameters such as the osmotic pressure π, as well as dynamical constants such as mutual diffusion coefficient can be expressed as power series expansion in the polymer concentration. Thus in this regime the mutual friction coefficient $f_m(c)$, and the mutual diffusion coefficient $D_c(c)$ can be written as [35]:

$$f_m = f_0(1 + k_f c + ...) \tag{2.8}$$

and

$$\begin{aligned} D_c &= D_o(1-v_s c)(1+2A_2Mc+...)/(1+k_f c+...) && (2.9)\\ &\simeq D_o(1+k_D c+...) && (2.10) \end{aligned}$$

with k_f representing the change in the friction and $k_D = (2A_2M - v_s - k_f)$. Since k_f and v_s (the polymer specific volume) are always positive, the mutual diffusion coefficient can either increase with concentration (which is the most usual under good solvent conditions), or decrease if $2A_2M$ is small or negative (theta or bad solvent conditions). In the limit of zero concentration the mutual diffusion and the self diffusion of the chain are equal ($D_0 = D_{s(c=0)}$) and k_D and D_0 can be measured from the concentration dependence of the diffusion coefficient.

Another quantity which is largely affected by the strong interparticle interactions and the enmeshment (or entanglement) of the chains, is the rotational diffusion coefficient D_R. Especially in the case of rodlike and stiff polymer solutions the concentration dependence of D_R, as well as the relaxation mechanisms for relaxing the orientation fluctuations are of great interest.

References

[1] H. Yamakawa. *Modern Theory of Polymer Solutions.* Harper and Row, London, 1971.

[2] P.G. de Gennes. *Scaling Concepts in Polymer Physics.* Cornell University Press, Ithaca, 1979.

[3] M. Doi and S.F. Edwards. *The Theory of Polymer Dynamics.* Oxford University Press, New York, 1986.

[4] A.Y. Grosberg and A.R. Khokhlov. *Statistical Physics of Macromolecules.* AIP Press, New York, 1994.

[5] P. Flory. *Statistical Mechanics of Chain Molecules, 2nd ed.* Hanser Publishers, Munchen, 1989.

[6] P.J. Flory. *Macromolecules*, 7:381, 1974.

[7] M. Ballauff. *Angew. Chem.*, 28:253, 1989.

[8] W. Kuhn. *Kolloid-Z.*, 68:2, 1934.

[9] W. Kuhn. *Kolloid-Z.*, 87:3, 1937.

[10] O. Kratky and G. Porod. *Recl.Trav.Chim.Pays-Bas*, 68:1106, 1949.

[11] G. Porod. *Monatsh.Chem.*, 80:251, 1949.

[12] H. Yamakawa. *Ann. Rev. Phys. Chem.*, 35:23, 1984.

[13] H. Benoit and P.J. Doty. *J. Phys. Chem.*, 57:958, 1953.

[14] J.B. Berne and R. Pecora. *Dynamic Light Scattering.* Willey Interscience Publications, New York, 1976.

[15] H. Benoit and J.S. Higgins. *Polymers and Neutron Scattering.* Oxford Science Publications, Oxford, 1994.

[16] P. Flory. *Principles of Polymer Chemistry.* Cornell Univ. Press, Ithaca,New York, 1953.

[17] M. Doi and H. See. *Indroduction to Polymer Physics.* Clarendon Press, Oxford, 1996.

[18] P.G. de Gennes. *The Physics of Liquid Crystals.* Clarendon Press, Oxford, 1974.

[19] S. Chandrasenkhar. *Liquid Crystals.* Cambridge University Press, Cambridge, 1977.

[20] A.N. Semenov and A.R. Kokhlov. *Sov. Phys. Usp.*, 31:988, 1988.

[21] L. Onsager. *Ann. N.Y. Acad. Sci.*, 51:627, 1949.

[22] P.J. Flory and G. Ronca. *Mol.Cryst.Liq.Cryst.*, 54:289, 1979.

[23] P.J. Flory. *Proc.Roy.Soc.London, Ser. A*, 234:73, 1956.

[24] W.G. Miller, C.C. Wu, E.L. Wee, G.L. Santee, J.L. Rai, and K.G. Goebel. *Pure Appl. Chem.*, 38:37, 1956.

[25] K. Kubo and K. Ogino. *Mol. Cryst. Liq. Cryst.*, 53:207, 1979.

[26] T. Odijk. *Macromolecules*, 19:2313, 1986.

[27] A.R. Kokhlov and A.N. Semenov. *Physica A*, 112:605, 1982.

[28] A.R. Kokhlov and A.N. Semenov. *Physica A*, 108:546, 1981.

[29] A.R. Kokhlov and A.N. Semenov. *J. Stat. Phys.*, 38:161, 1985.

[30] A. Matsuyama, Y. Sumikawa, and T. Kato. *J. Chem. Phys.*, 107:4711, 1997.

[31] P.N. Pusey and R.J.A. Tough. *Dynamic Light Scattering; Applications of Photon Correlation Spectroscopy*, page 85. Plenum Press, 198593.

[32] P.E. Rouse. *J. Chem. Phys.*, 21:1272, 1953.

[33] B.H. Zimm. *J. Chem. Phys.*, 24:269, 1956.

[34] J.M. Schurr. *Chem. Phys.*, 111:55, 1987.

[35] M.A. Tracy and R. Pecora. *Annu. Rev. Phys. Chem.*, 43:525, 1992.

Chapter 3

Light Scattering

The interaction of Electomagnetic radiation with matter is one of the most important tools of physics for the investigation of both structure and dynamics. When photons impinge on a molecule they can either gain or impart energy from its translational, rotational, vibrational and the electronic degrees of freedom. These interactions can cause both scattering and absorption of light; the former also involves frequency shifts. The scattering from the translational and rotational degrees of freedom which cause only a small Doppler shift to the incident light frequency is regarded as elastic scattering and is called *Rayleigh Scattering.* The vibrational degrees of freedom cause the *Raman scattering,* which consists of resonant peaks in the spectrum at the frequencies of the corresponding transitions. The interaction with thermal waves in the medium give rise to additional scattering, a doublet in the frequency spectrum which is called *Brillouin doublet.* The phenomena of light interaction with matter can be accurately described by a quantum field theory (the theory of quantum electrodynamics); nevertheless, several of these phenomena, such as light scattering can be understood very well in the framework of classical Electromagnetic theory. According to the later when light impinges on matter, its electric field polarizes the molecules which acting as oscillating dipoles radiate (scatter) light. The frequency shifts, the angular distribution, the polarization and the intensity of the scattered light are determined by the size, shape, and molecular interactions in the scattering material [1, 2].

The basic theory of Rayleigh scattering was developed by Rayleigh, Mie, Einstein, Smoluchowski and Debye more than half a century ago. Einstein and Smoluchowski [3, 4] developed the theory of scattering from liquids, which they considered as continuous medium where thermal fluctuations give rise to density or concentration fluctuations. According to their *fluctuation (or thermodynamic) theory of light scattering,* the scattered intensity can be calculated from the mean-square fluctuations of thermodynamic quantities such as density, concentration or temperature which cause in turn fluctuations of the dielectric constant of the medium. It can also be shown that a similar approach can be followed to describe light scattering caused by fluctuations of non-thermodynamic variables

such as orientation [5, ?]. Thus, in this semimacroscopic view the light scattering is a result of the local fluctuations of the dielectric constant. If there are no fluctuations of the dielectric constant there will be no light scattered, except in the forward direction, due to the cancelation of the wavelets scattered from different regions and having all the same amplitude but, in pairs, opposite phases. Besides the above phenomenological approach there is also a *molecular approach of light scattering* which of course involves some degree of approximation [1].

Like most scattering techniques, light scattering provides information in the reciprocal rather than the real space; *Dynamic Light Scattering* (DLS) observes the relaxation of fluctuations in a spatial Fourier component of wavelength $2\pi/q$, where q is the scattering vector (see eq. 3.4). For non-interacting particles, a characteristic time $(q^2 D_0)^{-1}$ is associated with this wavelength; it is the time that a particle needs to diffuse for a distance $1/q$. In general, the low-q measurements probe large-scale slow motions, whereas large-q measurements probe small-scale fast motions. In the so-called thermodynamic or hydrodynamic limit $q\xi \ll 1$ (ξ being the interparticle distance), dynamic light scattering probes fluctuations of macroscopic scale. It should be noted that while the thermodynamic limit is always reachable (going towards zero scattering angle), the high q-limit ($q\xi \gg 1$) is limited by the maximum scattering angle of 180^o (backscattering experiment) and the wavelength of the incident light. Thus very often, in order to observe static local phenomena like ordering in polymeric systems, one has to use incident radiation of smaller wavelength such as like x-rays or neutrons. In the case, though, of dynamic investigation the use of light scattering is almost unique; only the technique of neutron-spin echo can provide an alternative dynamic information in smaller length scales, lacking of course the ability of *Photon Correlation Spectroscopy* (PCS) to investigate multiple relaxation systems. An extension of conventional light scattering (based on single scattering events) is the *Diffusive Wave Spectroscopy* (DWS) in multiply scattering systems which provides a way to detect very local and fast motions [6, 7].

3.1 Classical Electromagnetic theory

The incident electric field, in a medium with average dielectric constant ε_0 can be written in the form of a plane wave:

$$E_i(r,t) = \mathbf{n}_i E_0 \exp i(\mathbf{k}_i \cdot \mathbf{r} - \omega_i t) \tag{3.1}$$

where $\mathbf{n}_i$ is the unit vector in the direction of the incident electric field, E_0 is the amplitude of the field, $\mathbf{k}_i$ ($|\mathbf{k}_i| = 2\pi n_0/\lambda_i$) the incident wave vector, ω_i the frequency of the incident radiation, λ_i the wavelength and n_0 ($= \sqrt{\varepsilon_0}$) the average refractive index of the medium.

The scattering medium is considered as nonconducting, nonmagnetic and non-absorbing with a local dielectric tensor:

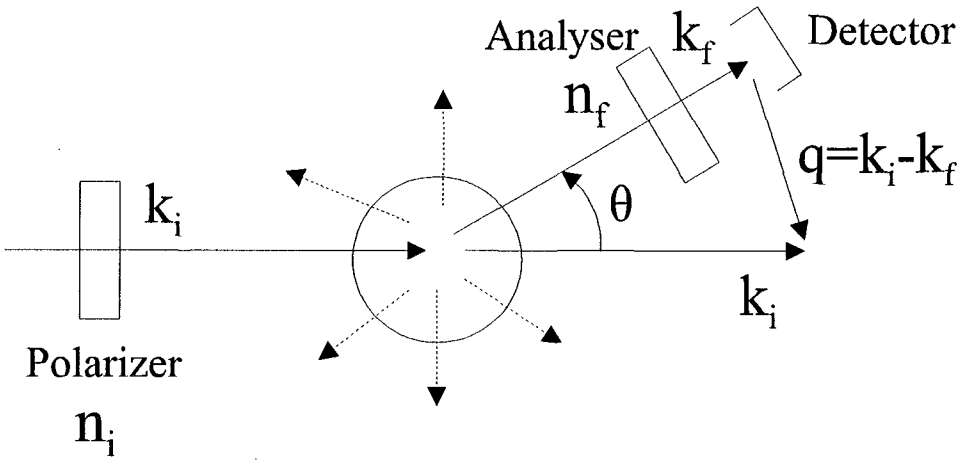

Figure 3.1: The incident light with polarization $\mathbf{n}_i$ and wavevector $\mathbf{k}_i$ is scattered by the sample in all directions. A scattered beam with $\mathbf{n}_f$ and $\mathbf{k}_f$ is measured by the detector at an angle θ. The scattering wavevector $\mathbf{q} = \mathbf{k}_i - \mathbf{k}_f$ is defined by the geometry.

$$\varepsilon = \varepsilon_0 \mathbf{I} + \delta\varepsilon(\mathbf{r},t) \tag{3.2}$$

where $\mathbf{I}$ is the unit tensor and $\delta\varepsilon(\mathbf{r},t)$ is the fluctuation of the dielectric constant at position $\mathbf{r}$ and time t. The Maxwell equations can be used to obtain the basic equation for the scattered field [1, 8]. Neglecting double scattering contributions (or second order term $\delta\varepsilon \cdot \mathbf{E}_s$), the scattered electric field at large distances R from the scattering volume is obtained:

$$\mathbf{E}_s = \frac{-k_f^2 E_0}{4\pi R\varepsilon_0} \exp i(k_f R - \omega_i t)\delta\varepsilon_{if}(\mathbf{q},t) \tag{3.3}$$

where $\delta\varepsilon_{if}(\mathbf{q},t) \equiv \mathbf{n}_f \cdot \delta\varepsilon(\mathbf{q},t) \cdot \mathbf{n}_i$ is the component of the spatial Fourier transform of the dielectric fluctuation tensor, $\delta\varepsilon(\mathbf{q},t) = \int_V d^3r \ \delta\varepsilon(\mathbf{r},t) \exp i\mathbf{q} \cdot \mathbf{r}$, along the initial, $\mathbf{n}_i$, and final, $\mathbf{n}_f$., polarization directions. The vector $\mathbf{q} \equiv \mathbf{k}_i - \mathbf{k}_f$ is defined by the directions of propagation of the incident and the scattered wave and is called *scattering wavevector*. Since we are discussing the case of elastic light scattering : $|\mathbf{k}_i| \cong |\mathbf{k}_f| = \frac{2\pi n_0}{\lambda_i}$ and thus

$$q = \frac{4\pi n_0}{\lambda_i} \sin\frac{\theta}{2} \tag{3.4}$$

with θ the scattering angle.

The spectrum of the scattered light is determined by the time-correlation function of the scattered electric field according to:

$$I_{if}(\mathbf{q},\omega) = \frac{1}{2\pi}\int_{-\infty}^{\infty} dt < E_s^*(0)E_s(t) > \exp(-i\omega_f t) \tag{3.5}$$

$$= A\frac{1}{2\pi}\int_{-\infty}^{\infty} dt < \delta\varepsilon_{if}^*(\mathbf{q},0)\delta\varepsilon_{if}(\mathbf{q},t) > \exp(-i\omega\ t)$$

where

$$A = \frac{k_f^4 I_0}{16\pi^2 R^2 \varepsilon_0^2} \tag{3.6}$$

is a proportionality constant revealing the characteristic λ^{-4} dependence of Rayleigh scattering and the R^{-2} attenuation of any spherical wave. The difference $\omega \equiv \omega_i - \omega_f$ is the frequency change in the scattering process due to the motion of the scatterers. This frequency change occurs only if $\delta\varepsilon(\mathbf{q},t)$ varies with time; scattering could occur from temporally frozen fluctuations but with a frequency identical with that of the incident beam. The spectrum of light can be measured with any detector together with an optical spectrometer like a Fabry-Perot interferometer. The total scattered intensity, measured directly by any square-law detector (like a photomultiplier) is then

$$I_{if}(\mathbf{q}) = \int_{-\infty}^{\infty} I_{if}(\mathbf{q},\omega)d\omega =< |\delta\varepsilon_{if}(\mathbf{q})|^2 > \tag{3.7}$$

In this approach, the scattering which results in a frequency shift ω and a wavevector change $\mathbf{q}$ is due entirely to the fluctuations of the dielectric constant. To calculate the light scattering spectrum we must then have a model describing these fluctuations.

An alternative approach is the *molecular theory of scattering* which attributes the scattering to the fluctuations of the polarizability tensor of the scatterers. According to this approach, when a monochromatic light impinges on a molecule with a polarizability tensor $\boldsymbol{\alpha}$, the induced dipole moment $\boldsymbol{\mu}(t) = \boldsymbol{\alpha} \cdot \mathbf{E}(t)$ varies with time and thus it radiates light. The scattered field with polarization $\mathbf{n}_f$, is then proportional to $\mathbf{n}_f \cdot \boldsymbol{\alpha}(t) \cdot \mathbf{n}_i\ e^{i\mathbf{q}\cdot\mathbf{r}(t)} \equiv \boldsymbol{\alpha}_{if}(t)e^{i\mathbf{q}\cdot\mathbf{r}(t)}$; $\boldsymbol{\alpha}_{if}(t)$varies with time due to the rotation and vibration of the molecules while $e^{i\mathbf{q}\cdot\mathbf{r}(t)}$ due to translation. In a liquid, if the molecules are electronically weakly coupled, the scattered field will be proportional to a superposition of the amplitudes scattered from each molecule in the illuminated volume $\delta\boldsymbol{\alpha}_{if}(\mathbf{q},t) = \sum_j \boldsymbol{\alpha}_{if}^j(t)e^{i\mathbf{q}\cdot\mathbf{r}(t)}$, leading to interference which is modulated by the motion of the molecules. The power spectrum (or spectral density) of the scattered light is

$$I_{if}(\mathbf{q},\omega) = \frac{1}{2\pi}\int_{-\infty}^{\infty} dt < \delta\boldsymbol{\alpha}^*_{if}(\mathbf{q},0)\delta\boldsymbol{\alpha}_{if}(\mathbf{q},t) > \exp(-i\omega\ t) \tag{3.8}$$

where

$$I_{if}(\mathbf{q},t) =< \delta\boldsymbol{\alpha}^*_{if}(\mathbf{q},0)\delta\boldsymbol{\alpha}_{if}(\mathbf{q},t) > \tag{3.9}$$

is the correlation function of the polarizability tensor flucutation.

In this approximate approach, the effect of the collision between the molecules, which is the origin of excess scattering (collision-induced scattering is discussed in chapter 6), has be neglected. The polarizability tensor also varies due to the vibration of the molecules giving rise to the *vibration-rotation Raman spectrum.* Thus, if the polarizability tensor is written as a sum of the equilibrium nuclear configuration value and a term linear in the vibrational displacements of the molecule, then eq. 3.8 will yield both the Rayleigh and the Raman spectra. The latter is related to the various normal modes, $Q(t) \sim \cos(\Omega\ t)$, of the vibrational displacements which are active in Raman Scattering if they can produce some change in the polarizability tensor i.e., if $(\partial\boldsymbol{\alpha}_{if}/\partial Q(t))_0 \neq 0$.

3.2 Measured quantities in light scattering

In a Rayleigh light scattering experiment, the measured quantity is the total scattered intensity $I(q,t)$ or its spectrum $I(q,\omega)$. In the former case $I(q,t)$ can be either used directly to provide information about the system under investigation (*Static Light Scattering*) or it can be manipulated to form its autocorrelation function:

$$G^{(2)}(q,t) \equiv< I_s(q,0)I_s(q,t) > \tag{3.10}$$

(*Dynamic Light Scattering*). The scattered intensity is commonly measured in two geometries, the *polarized geometry* (VV) where both the incident on the sample and the measured by the detector radiation are polarized perpendicular to the scattering plane, and the *depolarized geometry* (VH) where the incident beam is polarized vertical and the scattered beam horizontally (with respect to the scattering plane) (fig. 3.1).

Dynamic Light Scattering-Optical Mixing Techniques

The polarized and depolarized correlation functions $G^{(2)}_{VV}(q,t)$and $G^{(2)}_{VH}(q,t)$, as will be discussed below, give information for the concentration or density fluctuations and the orientation fluctuations of the system, respectively. The intensity correlation function is normally measured under *homodyne* conditions, when only the scattered light impinges on the photomultiplier [1]. $G^{(2)}(q,t)$, measured with the homodyne method can be related with the field correlation function,

$$\boxed{G^{(1)}(q,t) \equiv < E_s^*(q,0)E_s(q,t) >= AI(q,t)} \tag{3.11}$$

which is directly connected with dynamic behavior of the investigated system. The scattering volume V can be subdivided into subregions small compared to the wavelength of light and the scattered field is then a superposition of all the scattered fields from these subregions ($E_s = \sum_n E_s^{(n)}$). Moreover, if the subregions are large enough to permit independent motions of the molecules inside each one of them, the scattered fields $E_s^{(n)}$ can be regarded as independent random variables. In this case, the total scattered field E_s is a random variable following a Gaussian distribution and [1] $G^{(2)}(q,t)$ is related to $G^{(1)}(q,t)$ by the *Siegert relation*

$$G^{(2)}(t) = |G^{(1)}(0)|^2(1 + \frac{|G^{(1)}(t)|^2}{|G^{(1)}(0)|^2}) \tag{3.12}$$

In practice, what is measured in a PCS experiment is the normalized intensity correlation function:

$$\boxed{g^{(2)}(q,t) \equiv \frac{G^{(2)}(q,t)}{|G^{(1)}(q,0)|^2} = 1 + f^*(aC(q,t))^2} \tag{3.13}$$

where

$$C(q,t) = \frac{G^{(1)}(q,t)}{G^{(1)}(q,0)} \tag{3.14}$$

is the normalized field correlation function and: f^* is an instrumental factor (see chapter 5) and a the fraction of the intensity with dynamics inside the correlator's time window.

As mentioned above, E_s is proportional to $\delta\varepsilon_{if}(\mathbf{q},t)$(or $\delta\boldsymbol{\alpha}_{if}(\mathbf{q},t)$) and thus $G^{(2)}(t) \propto < |\delta\varepsilon_{if}(\mathbf{q},0)|^2|\delta\varepsilon_{if}(\mathbf{q},t)|^2 >$ and $G^{(1)}(t) \propto < \delta\varepsilon_{if}^*(\mathbf{q},0)\delta\varepsilon_{if}(\mathbf{q},t) >$; a theory is then needed to calculate the correlation functions of the dielectric (or polarizability) fluctuations of the system and relate them to quantities such as concentration, orientation, size and shape of molecules, as well as the interactions among them. This will be discussed in the next section. All the dynamic light scattering measurements in this work were carried out under homodyne conditions. The Gaussian approximation was fulfilled in almost all cases; a case of possible exception discussed in chapter 7.

Spectral Experiments-Filter Techniques

For an incident laser beam with frequency ω_0, the spectrum of the scattered light, $I(\omega)$, is measured by an interferometer or a diffraction grating and contains information not only about the elastic part of scattering (the Rayleigh peak is the central band around the frequency of the laser ω_0) but also about the inelastic

contributions (bands with shifted frequency). The latter consists of the Brillouin doublets and the Raman spectrum [1, 2]. The Brillouin doublets are due to the inelastic collision between photons and the fluid, in which a photon gains or looses energy to the phonons (or sound waves) and thus suffers a frequency shift $\pm\omega(q)$. The frequency shift is related to the sound velocity, c_s, in the medium ($\omega(q) = c_s q$) and the width of these bands gives the lifetime ($q^2\Gamma$) of a classical phonon of wavevector q. The Raman lines provide information about the vibrational states of local groups within the molecule, giving the Stokes (at shifted frequency $-\Omega$) and the anti-Stokes (at shifted frequency Ω) band. Finally, the elastic part (the Rayleigh peak) in a binary mixture (like a polymer solution) mainly consists of two Lorentzian contributions; the thermal diffusivity and the particle diffusion. Thus, not only the correlation functions but also the spectral density profile can give information on the dynamics of the system, mainly through the width of the Rayleigh peak. Nevertheless, as will be apparent in the next chapters, the technique of PCS provides much more clear, dynamic informations for complex systems with multiple relaxation processes.

The scattering from macromolecular solutions can be discussed for the case of dilute systems, where particle independence simplifies the calculations, and more concentrated systems were the analysis becomes more complicated.

3.3 Scattering from dilute systems

In dilute solutions of large molecules like polymers, the basic characteristics related with the scattering of light are:

a) The polarizability of the macromolecule is enormous compared with that of the solvent molecule and thus the macromolecules scatter much more light than the solvent molecules,

b) The macromolecules move much more slowly than the solvent molecules and thus the two dynamics are timewise separable.

In general, when scattering from large, compared to the wavelength of light, particles is considered, Maxwell equations must be solved inside the particle and outside in the medium with the proper boundary conditions and properly add the contributions from all scatterers in order to calculate the scattering radiation. Complete solutions of the problem are available for spherical particles of arbitrary size and refractive index (Mie scattering) and some solutions for cylindrical particles [9]. In Mie scattering, the relative magnitude and phase of the electric field are altered by the presence of the scattering particle in contrast to the Rayleigh -Debye scattering where they are not affected. In the case of macromolecules though, it is still possible to use the Rayleigh-Debye approximation despite the fact that very often the overall size of the polymer molecules is of the

order of the wavelength of the incident light or even larger. This is mainly due to the rather loose structure of a polymer molecule which either in a coil conformation or in a rigid rod conformation looks more like a linear chain immensed in a medium rather than a three dimensional particle of the same dimensions. Consequently, a convenient artifice is to consider the basic scattering element of a polymer molecule to be a polymer segment rather than the whole molecule. In this way, the scattering form factor can be calculated. Each segment is chosen so that its size l_0 is small compared to $1/q$ ($ql_0 \ll 1$) to ensure that it behaves like a point scatterer. In general the Rayleigh-Debye approximation breaks down when the particles become large and very different optically from the medium.. For particles with a well defined inside and outside (not like a polymer), a rough criterion for the validity of the approximation is: $\frac{4\pi}{\lambda}R|m-1| \ll 1$ where m is the ratio of the refractive index inside and outside the particle of radius R [1].

3.3.1 Scattering from small molecules

Before discussing the case the scattering by a macromolecular system we consider the basic characteristics of scattering by a system of small molecules. For a symmetric top molecule the polarizability tensor can be expressed as:

$$\alpha_{\alpha\beta} = \alpha\delta_{\alpha\beta} + \beta(u_\alpha u_\beta - \frac{1}{3}\delta_{\alpha\beta}) \tag{3.15}$$

where $\alpha \equiv \frac{1}{3}(\alpha_\parallel + 2\alpha_\perp)$ is the isotropic part of the polarizability, $\beta \equiv (\alpha_\parallel - \alpha_\perp)$ the anisotropic part and u_α is the αth component of the unit vector u along the symmetry axes of the top. β is also called the optical anisotropy since it characterizes the ability of a molecule to depolarize the incident light.

To deduce both the total scattering intensities $I_{if}(\mathbf{q})$ and the correlation functions $G^{(1)}(q,t)$ and $G^{(2)}(q,t)$ we have to calculate $I_{if}(\mathbf{q},t)$ (eq. 3.9). For identical particles (with the same polarizability), $I_{VV}(\mathbf{q},t)$ and thus the polarized field correlation function, $G^{(1)}_{VV}(q,t)$ is related with the correlation function of the concentration (or density) fluctuations:

$$I_{if}(\mathbf{q},t) \sim < \delta c^*(q,t)\delta c(q,0) > \tag{3.16}$$

since $\sum_i \exp i\mathbf{q}\cdot\mathbf{r}_i(\mathbf{t})$ is the Fourier transform of the concentration of them $c(q,t)$.

In general, $I_{if}(\mathbf{q},t)$ (eq. 3.9) can be splited into two terms, in the *molecular self-part* ($i = j$) and the molecular pair (or distinct)-part ($i \neq j$):

$$\begin{aligned} I_{if}(\mathbf{q},t) &= < \sum_i \boldsymbol{\alpha}^i_{if}(0)\boldsymbol{\alpha}^i_{if}(t)\exp i\mathbf{q}\cdot(\mathbf{r}_i(\mathbf{t}) - \mathbf{r}_i(0)) > \\ &+ < \sum_{i\neq j} \boldsymbol{\alpha}^i_{if}(0)\boldsymbol{\alpha}^j_{if}(t)\exp i\mathbf{q}\cdot(\mathbf{r}_j(\mathbf{t}) - \mathbf{r}_i(0)) > \end{aligned} \tag{3.17}$$

For dilute systems were the particles rarely collide with each other, we can assume that two different **scatterers are statistically independent** and thus the distinct term vanishes. If in addition the **position and the orientation of a scatterer are also independent** and **all scatterers are identical**, we get:

$$I_{if}(\mathbf{q},t) =< N >< \boldsymbol{\alpha}_{if}(0)\boldsymbol{\alpha}_{if}(t) > F_s(q,t) \tag{3.18}$$

since $\boldsymbol{\alpha}^i_{if}(t)$ depends only on the rotation of the particle and $\exp i\mathbf{q}\cdot(\mathbf{r}_j(\mathbf{t}) - \mathbf{r}_j(0))$ only on its translation. The translational factor

$$\boxed{F_s(q,t) \equiv < \exp i\mathbf{q}\cdot(\mathbf{r}_j(\mathbf{t}) - \mathbf{r}_j(0)) >} \tag{3.19}$$

is called *Self-Intermediate Scattering Function.*

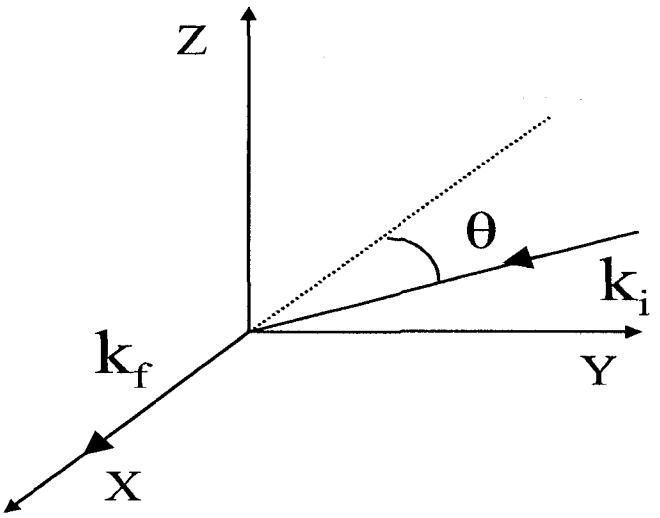

Figure 3.2: Light scattering geometry: The XY is the scattering plane, θ is the scattering angle, k_i and k_f the incident and scattered wavevectors respectively.

If the scattering geometry of figure 3.2, is used then $I_{VV}(\mathbf{q},t) \propto < \boldsymbol{\alpha}_{zz}(0)\boldsymbol{\alpha}_{zz}(t) >$ and $I_{VH}(\mathbf{q},t) \propto < \boldsymbol{\alpha}_{yz}(0)\boldsymbol{\alpha}_{yz}(t) >$. Further, it can be shown [1] that for symmetric top molecules (with $\mathbf{u}$ the unit vector along their main axis) eq. 3.18 leads to:

$$I_{VV}(\mathbf{q},t) =< N > [\alpha^2 + \frac{4}{45}\beta^2 < P_2(\mathbf{u}(0)\cdot\mathbf{u}(t)) >]F_s(q,t) \tag{3.20}$$

and

$$I_{VH}(\mathbf{q},t) =< N > \frac{1}{15}\beta^2 < P_2(\mathbf{u}(0)\cdot\mathbf{u}(t)) > F_s(q,t) \tag{3.21}$$

where $P_2(\mathbf{u}(0)\cdot\mathbf{u}(t)) \equiv (3[\mathbf{u}(0)\cdot\mathbf{u}(t)]^2 - 1)/2$ is the second Legendre polynomial. To end-up with this result, a **random orientation of the scatterers** ($< P_2(\mathbf{u}(t)\cdot\mathbf{u}(t)) >= 0$) **is assumed.** Thus, we see that depolarized scattering ($I_{VH}(\mathbf{q},t)$) depends on both translational motion (through F_s) and rotational motion (through P_2) while the isotropic part of the polarized scattering:

$$\boxed{I_{iso}(\mathbf{q},t) = I_{VV}(\mathbf{q},t) - \tfrac{4}{3}I_{VH}(\mathbf{q},t)} \tag{3.22}$$

depends only on the translational motion.

The functions $F_s(q,t)$ and $< P_2(\mathbf{u}(0)\cdot\mathbf{u}(t)) >$ are expressing the dynamic behavior of the system. For a particle which does an **independent translational and an rotational diffusion**, the probability distribution, $c(\mathbf{u},\mathbf{R},t)$, obeys the diffusion equation:

$$\frac{\partial c}{\partial t} = D\nabla^2 c - D_R\mathbf{I}^2 c \tag{3.23}$$

where $-\mathbf{I}^2$ is the angular part of the Laplacian operator, F_s and P_2 are exponentially relaxing functions related, respectively, with the translational and rotational diffusion coefficients of the scatterer [1]. The field correlation function $G^{(1)}(q,t)$ in the VV and VH geometry is:

$$\boxed{G^{(1)}_{VV}(q,t) \sim I_{VV}(\mathbf{q},t) =< N > [\alpha^2 + \tfrac{4}{45}\beta^2\exp(-6D_Rt)]\exp(q^2Dt)} \tag{3.24}$$

and

$$\boxed{G^{(1)}_{VH}(q,t) \sim I_{VH}(\mathbf{q},t) =< N > \tfrac{1}{15}\beta^2\exp(-6D_Rt)\exp(q^2Dt)} \tag{3.25}$$

These are the basic equations for the investigation of the dynamics by PCS, the technique which, in the homodyne geometry, measures the intensity correlation function $G^{(2)}(q,t)$, usually related to $G^{(1)}(q,t)$ through the Siegert relation (eq. 3.12). In the frequency space the Rayleigh peak is described by Lorentzians. This is observed if a spectrum analyzer is used instead of an autocorrelator.. Hence, the Fourier transform of eqs. 3.24 and 3.25 gives:

$$I_{iso}(\mathbf{q},\omega) = \frac{N\alpha^2}{\pi}\frac{q^2D}{(q^2D)^2+\omega^2} \tag{3.26}$$

and

$$I_{VH}(\mathbf{q},\omega) = \frac{N\beta^2}{15\pi}\frac{q^2D+6D_R}{(q^2D+6D_R)^2+\omega^2} \tag{3.27}$$

Before discussing how the polymeric nature of macromolecules affects the picture described above, two additional points should be mentioned. In the case

of very dilute systems, the intensity correlation function $G^{(2)}(q,t)$ contains an additional to the Gaussian (eq. 3.12) term, $< \delta N(0)\delta N(t) >$ where $\delta N(t)$ is the number fluctuation. This fluctuation occur at a time scale τ which is required for a particle to traverse the scattering volume. Finally, lets consider the general case of particles moving in the scattering volume with a Gaussian probability of displacements $\mathbf{R}$, and a mean square displacement $< \Delta\mathbf{R}^2(\mathbf{t}) >$. This situation can describe Brownian motion of particles, but also the more rare case of freely moving particles in random directions with a Gaussian distribution of velocities. Then, the self-intermediate scattering function can be written as:

$$F_s(q,t) = \exp(-q^2 < \Delta\mathbf{R}^2(t) > /6) \tag{3.28}$$

For diffusing particles, $< \Delta\mathbf{R}^2(\mathbf{t}) >= 6Dt$, while for freely moving particles with velocity v, $< \Delta\mathbf{R}^2(t) >= < v^2 > t^2$.

3.3.2 Scattering from macromolecules

When molecules are large, intramolecular interference must be taken into account in calculating the light scattering properties. As mentioned above, the Rayleigh-Debye approximation is still used, assuming scattering from segments of the polymer chain. It is exactly this method that introduces the *molecular (or particle) form factor*, through the interference of radiation scattered by different parts of the macromolecule. The total dynamic correlation function contains the summation over pairs of segments of the same and different molecules:

$$\boxed{I_{if}(\mathbf{q},t) =< \sum_{P,Q}^{N} \sum_{l,m}^{n} \boldsymbol{\alpha}_P^l(0)\boldsymbol{\alpha}_Q^m(t) \exp i\mathbf{q} \cdot (\mathbf{r}_Q^m(t) - \mathbf{r}_P^l(0)) >} \tag{3.29}$$

where the indices P, Q refer to the N different chains in the scattering volume and the indices l, m to the n segments associated with each polymer chain.

For **non-interacting polymer chains**, where only the self part ($P = Q$), of the correlation function, $I_{if}(\mathbf{q},t)$ ($P = Q$) survives, 3.29 simplifies to:

$$I_{if}(\mathbf{q},t) =< N >< \sum_{l,m}^{n} \boldsymbol{\alpha}_{if}^l(0)\boldsymbol{\alpha}_{if}^m(t) \exp i\mathbf{q} \cdot (\mathbf{r}_l(t) - \mathbf{r}_m(0)) > \tag{3.30}$$

where the indices l and m run over segments of the some chain. The isotropic component, $I_{iso}(\mathbf{q},t)$, of the polarized dynamic correlation function, $I_{VV}(\mathbf{q},t)$, is related with the *single molecule dynamic form factor*:

$$P(q,t) \equiv \frac{1}{n^2} < \sum_{l,m}^{n} \exp i\mathbf{q} \cdot (\mathbf{r}_l(t) - \mathbf{r}_m(0)) > \tag{3.31}$$

through $I_{iso}(\mathbf{q},t) = a_M^2 NP(q,t)$ where $a_M = na$ is the molecular polarizability of the polymer chain. The zero-time correlation function

$$\boxed{P(q) \equiv \frac{1}{n^2} < \sum_{l,m}^{n} \exp i\mathbf{q} \cdot (\mathbf{r}_l - \mathbf{r}_m) >} \tag{3.32}$$

is the *molecular form factor* which contains all the intermolecular interference of the scattered light and gives information on the shape and size of the scatterer. Due to the destructive interference of the scattering from different parts of the particle, for all kind of scatterers, $P(q)$ decreases with q. Note that at the thermodynamic limit, $q = 0$, $P(0) = 1$ and thus there is no destructive interference.

For large macromolecules, consisting of n identical, cylindrically symmetric segments, the general relations for VV and VH static intensities, in the scattering geometry of fig. 3.2 are [1]:

$$\begin{aligned} I_{VV}(\mathbf{q}) &= N\alpha^2 < \sum_{l,m}^{n} \exp i\mathbf{q} \cdot (\mathbf{r}_l - \mathbf{r}_m) > \\ +\frac{N}{9}\beta^2 &< \sum_{l,m}^{n} (3\cos^2\theta_l - 1)(3\cos^2\theta_m - 1) \exp i\mathbf{q} \cdot (\mathbf{r}_l - \mathbf{r}_m) > \\ +\frac{2N}{3}\alpha\beta &< \sum_{l,m}^{n} (3\cos^2\theta_l - 1) \exp i\mathbf{q} \cdot (\mathbf{r}_l - \mathbf{r}_m) > \end{aligned} \tag{3.33}$$

and

$$I_{VH}(\mathbf{q}) = N\beta^2 < \sum_{l,m}^{n} (\sin\theta_l \cos\theta_l \sin\phi_l)(\sin\theta_m \cos\theta_m \sin\phi_m) \exp i\mathbf{q} \cdot (\mathbf{r}_l - \mathbf{r}_m) > \tag{3.34}$$

where the angles (θ_l, ϕ_l) represent the orientation angles of segment l in a laboratory-fixed spherical coordinate system. Note that the third term in the equation for $I_{VV}(\mathbf{q})$, is a cross term in $\alpha\beta$; this is an extra term, compared to eq. 3.20, which survived because we did not assume isotropic distribution for θ_l. However, for $q \to 0$ or for cases where orientations of different segments are uncorrelated, the cross term vanishes and eq. 3.22 is recovered.

Molecular Size determination

For macromolecules of arbitrary shape, $P(q)$ is related to the radius of gyration, R_G. The most convenient form of this relation is

$$\boxed{P^{-1}(q) \cong 1 + \frac{q^2}{3} R_g^2 + ...} \tag{3.35}$$

This is a classical way of measuring the size of a particle, in dilute solutions, from the angular dependence of the light scattering intensity.

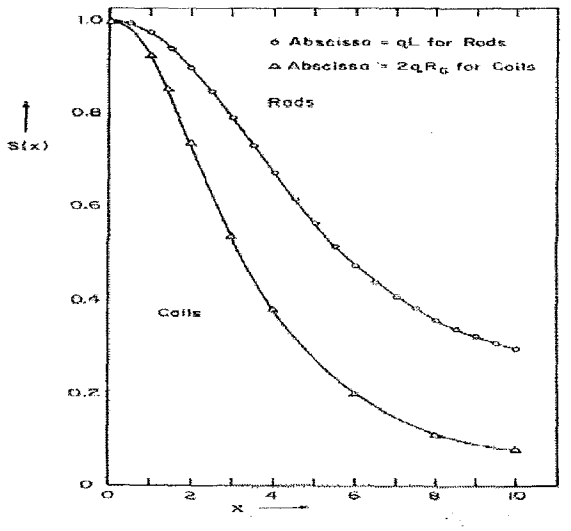

Figure 3.3: Form factor of rodlike chains and Gaussian coils.

The form factors of various particles have been calculated (fig. 3.3); for example, the form factor of thin rods is:

$$P(q) = \frac{2}{x}\int_0^x dz \frac{\sin z}{z} - (\frac{2}{x}\sin(\frac{x}{2}))^2 \tag{3.36}$$

with $x = qL$, while its radius of gyration is $R_g = L/\sqrt{12}$. For a Gaussian coil we have:

$$P(q) = \frac{2}{y^4}[e^{-y^2} - 1 + y^2] \tag{3.37}$$

with $y = qR_G$.

Molecular Weight determination

In addition to the size, the molecular weight of the scatterers can be measured by Static Light Scattering in dilute solutions. This is achieved at $q \to 0$ to avoid intramolecular interactions and at $\rho \equiv N/V \to 0$ to avoid intermolecular interactions. For this calculation, only the isotropic intensity I_{iso} should be used; thus, for particles with important optical anisotropy the depolarized contribution, I_{VH} must be substracted from the measured I_{VV} (eq. 3.22). The isotropic intensity

per unit volume is $I_{iso} = Ba_m^2 \rho P(q)$ with $B = \frac{k_I^4 E_o^2}{\varepsilon^2 R^2}$ according to eq. 3.3. The molecular polarizability is usually related to the excess dielectric constant increment $\Delta\varepsilon = n_s^2 - n_o^2$ ($\approx (\frac{\partial\varepsilon}{\partial\rho})\rho = 2n_o(\frac{\partial n_s}{\partial\rho})\rho$), where n_s ($= \sqrt{\varepsilon_s}$)is the refractive index of the solution and n_o ($= \sqrt{\varepsilon_s}$) of the solvent, by $\Delta\varepsilon = 4\pi\rho a_m$ [1, 2]. Thus, using 3.35 for a monodisperce system at infinite dilution we get:

$$\frac{Bca_M^2}{N_A I_{iso}(\mathbf{q})} = \frac{1}{M}(1 + \frac{q^2}{3}R_g^2 + ...) \tag{3.38}$$

where $a_M = \frac{a_m N_A}{M}$ is the polarizability per unit mass. This result is valid for infinitely diluted system where there are no interactions. For a polydisperse system the scattered light is:

$$I_{iso}(\mathbf{q}) = \frac{Bca_M^2}{N_A}\sum_i M_i c_i S_i(\mathbf{q}) \tag{3.39}$$

and thus the measured molecular weight by eq. 3.38 is the weight average molecular weight $M_w = \sum_i M_i c_i \;/\; \sum_i c_i$.

For convenience, Eq. 3.38 is usually rewritten as:

$$\frac{Kc}{R_{iso}} = \frac{1}{M_w}\left(1 + \frac{q^2}{3}R_G^2 + ...\right) = \frac{1}{M_w P(q)} \tag{3.40}$$

with $K = 4\pi^2 n_o^2 (\frac{\partial n_s}{\partial\rho})^2 / \lambda_o^4 N_A$ and the *Rayleigh ratio*, $R_{iso} = I_{iso}R^2/V_s E_o^2$. The latter normalizes the scattered intensity with the intensity of the incident beam, the scattering volume V_s, and the distance at which the scattered intensity is measured.

Dynamics

In the small qR_G region, the intramolecular interference is small and $P(q,t)$ is related to the translational diffusion of the center of mass ($\mathbf{R}(t)$) of the polymer chain:

$$P(q,t) \approx F_s(\mathbf{q},t) =< \exp i\mathbf{q}\cdot(\mathbf{R}(t) - \mathbf{R}(0) >\sim \exp(-q^2 Dt) \tag{3.41}$$

similarly with the case of small molecules. At infinite dilution, the translational diffusion, D, is actually the self-diffusion coefficient, D_s, of the polymer. For $qR_G \geq 1$ the intramolecular interference must be taken into account in $P(q,t)$.

The dynamic structure factor for Gaussian coils of n segments was calculated in the framework of the Rouse-Zimm model discussed in chapter 2. It may be expanded in a sum of exponentials [1]:

$$P(q,t) = S_o(y^2)\exp(-q^2 Dt) + S_2(y^2)\exp(-(q^2 D + \frac{2}{\tau_r})t) + ... \tag{3.42}$$

with the terms S_2 and higher representing the contributions of the internal modes of motion in the relaxation of the dynamic structure factor. The characteristic times of the normal modes are $\tau_p = \tau_r/p^2$ for the Rouse model and $\tau_p = \tau_r/p^{-3/2}$ for the Zimm model, with τ_r being rotational relaxation time or the longest relaxation time of the end-to-end vector correlation time. These terms are important only for high qR_G ($q^2R_G^2 \geq 3$). Another way of investigating the dynamic structure factor is to calculate it in the high and low qR_G regimes and to describe the dynamics of the system through the its initial decay rate $\Gamma_q^{(0)} \equiv -\frac{d}{dt}ln[P(q,t)]$. In this way it is shown that while for $qR_g \ll 1$ the structure factor decays through the center of mass translation ($\Gamma_q^{(0)} = Dq^2$), for $qR_g \gg 1$, where the internal dynamics (higher order in eq. 3.42) dominate $\Gamma_q^{(0)} = Dq^4R_G^2$ for the Rouse model and $\Gamma_q^{(0)} = Dq^3R_G$ in the Zimm model [10].

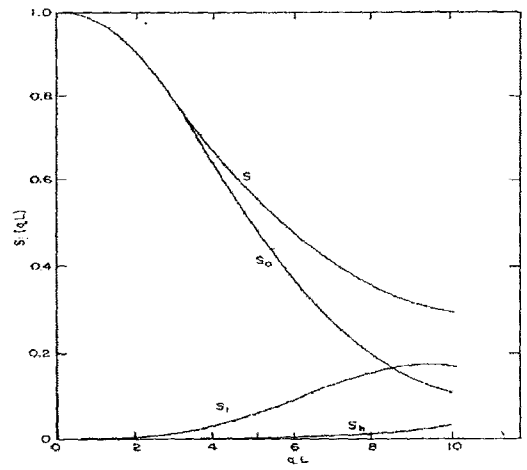

Figure 3.4: $S_i(qL)$contributions in the dynamic form factor $P(q,t)$ of rodlike particles.

For rigid rods, assuming independent rotational and translational motion, the dynamic structure factor is a sum of exponentials:

$$P(q,t) = S_o(qL)\exp(-q^2Dt) + S_1(qL)\exp(-(q^2D + 6D_R)t) + ... \qquad (3.43)$$

Thus, for rodlike particles, even the isotopic part in the polarized correlation function contains a contribution from the rotational motion of the particle ($S_1(qL)$ term). Nevertheless, this contribution of the rotational diffusion in the dilute regime is only seen by dynamic light scattering for quite large rodlike polymers ($S_1(qL)$ is larger than 10% of the total $P(q)$ only for $qL \geq 5$) (fig. 3.4). As will be discussed below, the coupling of the translational to rotational diffusion for rodlike systems is expected to be more evident in the dynamic structure factor at higher concentrations, although this is of a different nature.

3.4 Scattering from interacting systems

At finite concentrations there is always some interference between the scattered light from different particles. When the intermolecular interactions do not vanish the pair term in eq. 3.29 must be kept; for the static isotropic scattering these yield the *Intermolecular Structure Factor*:

$$\boxed{S'(\mathbf{q}) = \frac{1}{n^2N(N-1)} < \sum_{P\neq Q}^{N}\sum_{l,m}^{n} \exp i\mathbf{q}\cdot(\mathbf{r}_Q^m - \mathbf{r}_P^l) >} \tag{3.44a}$$

and the total intensity scattered by the macromolecule can be represented by:

$$\frac{Kc}{R_{iso}} = \frac{1}{MP(q) + VN_AS'(q)c} \tag{3.45}$$

Since it is not possible to calculate rigorously the interactions between all the segments of different chains in the above expression, Zimm [11, 2] considered the special case where only one segment of each chain is in physical contact with another chain (one contact approximation). By associating the distance between the interacting segments with the center of mass position, **R**, of the macromolecules, it can be shown that $S'(q)$ can be written as product of the intermolecular structure factor of a system of interacting point particles, $S'_R(\mathbf{q})$, and the square of the molecular form factor $P(q)$:

$$S'(\mathbf{q}) = S'_R(\mathbf{q})P^2(q) \tag{3.46}$$

with

$$S'_R(\mathbf{q}) = \frac{1}{N^2} < \sum_{P\neq Q}^{N}\sum_{Q=1}^{N} \exp i\mathbf{q}\cdot(\mathbf{R}_P - \mathbf{R}_Q) > \tag{3.47}$$

The latter relates to the pair distribution function $g_{1,2}(\mathbf{r})$through:

$$S'_R(\mathbf{q}) = \frac{1}{V}\int_0^\infty d\mathbf{r}(g_{1,2}(\mathbf{r}) - 1)\exp(i\mathbf{q}\cdot\mathbf{r}) \tag{3.48}$$

We can see that for $\mathbf{q}\cdot\mathbf{r} \ll 1$, the above is essentially the second virial coefficient, $B_2 = -1/2\int_0^\infty (g_{1,2}(\mathbf{r}) - 1)d\mathbf{r}$. Hence,

$$\frac{Kc}{R_{iso}} = \frac{1}{MP(q)}\frac{1}{1 - 2A_2MP(q)c} \tag{3.49}$$

with $A_2 = N_AB_2/M^2$. Relative to non-interacting particles, repulsive interactions ($g_{1,2}(\mathbf{r}) < 1$) lead to a decrease in scattered light intensity, whereas attractive interactions ($g_{1,2}(\mathbf{r}) > 1$) lead to an increase of the scattered intensity.

Consequently, for relatively low concentrations, were only pair interactions are important, the scattering intensity is related not only with molecular characteristics, such as M_w and R_G, but also with the interactions between molecules described by the second virial coefficient A_2, according to:

$$\boxed{\frac{Kc}{R_{iso}} = \frac{1}{M_w}\left(1 + \frac{q^2}{3}R_g^2 + ...\right) + 2A_2c + ...} \tag{3.50}$$

From the above it is obvious that the determination of M_w requires a double extrapolation to $q = 0$ and $c = 0$; the slope of Kc/R_{iso} with q^2 yields $R_G^2/3$, while the slope with respect to c gives A_2. This kind of static light scattering analysis is called a *Zimm plot.*

In practice the "self" and the "pair" contributions to the total isotropic scattering intensity can not be separated and thus, a *Solution Structure Factor,* $F(q)$, is defined through:

$$\boxed{I_{iso} = Ba_m^2\rho P(q)(1 + S'(q)/P(q)) \equiv Ba_m^2\rho P(q)F(q)} \tag{3.51}$$

In general, the static structure factor, defined (eq. 3.16) as $S(q,c) = \frac{1}{cV} < |c(q)|^2 >$ is the multiplication of the intramolecular factor $P(q,c)$(the molecular form factor) with the intermolecular factor $F(q,c)$(solution structure factor). Experimentally the behavior of $S(q,c)$ at small q's define the correlation length, $\xi(c)$which represents the range of regularity of the polymer segment density, according to:

$$\boxed{S(q,c) = \frac{S(0,c)}{1+q^2\xi^2(c)+...}} \tag{3.52}$$

The calculation of $S(q,c)$in requires the knowledge of the segment-segment pair distribution function, $g_{1,2}(\mathbf{r})$, and thus is calculated approximately; for example Random Phase Approximation (RPA) has been used to calculate $S(q,c)$ for flexible polymers [12, 10] and wormlike chains [13].

A more complicated task is to calculate the polarized, $S(\mathbf{q},t) = C_{iso}(\mathbf{q},t)$, and the depolarized, $C_{VH}(\mathbf{q},t)$, dynamic structure factor (eq. 3.29), of nondilute polymer systems. For concentrated solutions of rigid rods these functions were calculated in the framework of RPA and with the help of fluctuation dissipation theorem [14, 15]. The correlation functions are complicated and were either approximated as a single exponential for $q \to 0$, or computed numerically at arbitrary q; the characteristic times were can be estimated in the form of the initial decay rate. These results will be discussed in the next chapter. The general form of the correlation functions are:

$$C_{iso}(\mathbf{q},t) = \frac{1}{\rho LV} < c(\mathbf{q},t)c(-\mathbf{q},0) > \tag{3.53}$$

$$= \frac{L}{c}\int_t^\infty dt' \int d\mathbf{u} s(\mathbf{q},\mathbf{u}) \exp(-t'\Omega(\mathbf{q})\Theta(\mathbf{q}))s(\mathbf{q},\mathbf{u})$$

$$C_{VH}(\mathbf{q},t) = \frac{1}{\rho LV} < E_{VH}(\mathbf{q},t)E^*_{VH}(\mathbf{q},0) > \quad (3.54)$$

$$= \frac{L}{4\pi}\int_t^\infty dt' \int d\mathbf{u} E_{VH}(\mathbf{q},t) \exp[-\Omega(\mathbf{q})t']\Theta(\mathbf{q}))E^*_{VH}(\mathbf{q},0)$$

where $s(\mathbf{q},\mathbf{u}) = \frac{1}{L}\int_{-L/2}^{L/2} \exp(i\mathbf{q}\cdot\mathbf{u}s)ds$ expresses the intramolecular interference, $E_{VH}(\mathbf{q},t) = \alpha_{VH}(\mathbf{u})s(\mathbf{q},\mathbf{u})$and $\Omega(\mathbf{q}) = \Theta(\mathbf{q})\Phi(\mathbf{q})$, with $\Theta(\mathbf{q})$and $\Phi(\mathbf{q})$operators for the translation-rotation diffusion of the rod and the rod-rod interaction in the mean field approximation, respectively.

3.4.1 Scattering from Hydrodynamic modes

In dense systems such as pure liquids, binary mixtures or nondilute polymer solutions, the positions of neighboring molecules are highly correlated both with respect to their spatial distribution and their motions. Under such conditions, the collective nature of light scattering is more evident and the use of the thermodynamic approach is more appropriate than the approximate molecular approach.. Then, as mentioned before, the scattered intensity is related with the correlation function of dielectric constant $< \delta\varepsilon^*_{if}(\mathbf{q},0)\delta\varepsilon_{if}(\mathbf{q},t) >$ similarly with eq. 3.8. The relative dielectric fluctuations, of wavelength of the order of that of light, involve the collective motions of large number of molecules and consequently can be described by the laws of macroscopic physics, such as thermodynamics and hydrodynamics.

3.4.2 Isotropic fluctuations

Statics

The dielectric constant ε is in general a function of density ρ, temperature T , and concentration c, an thus the isotropic part of the local dielectric fluctuation can be related with the fluctuations of these quantities:

$$\delta\varepsilon(\mathbf{r},t) = \left(\frac{\partial\varepsilon}{\partial\rho}\right)_{T,c}\delta\rho(\mathbf{r},t) + \left(\frac{\partial\varepsilon}{\partial T}\right)_{\rho,c}\delta T(\mathbf{r},t) + \left(\frac{\partial\varepsilon}{\partial c}\right)_{\rho,T}\delta c(\mathbf{r},t) \quad (3.55)$$

Consequently, the light scattering intensity (eq. 3.7) will involve autocorrelation terms of $\delta\rho, \delta T$ and δc such as $\left(\frac{\partial\varepsilon}{\partial\rho}\right)^2 < \delta\rho^*(\mathbf{r},t)\delta\rho(\mathbf{r},t) >$ and $\left(\frac{\partial\varepsilon}{\partial T}\right)^2 <$

$\delta T^*(\mathbf{r},t)\delta T(\mathbf{r},t) >$ as well as cross correlation terms of the above quantities. Note that the microscopic theory completely ignores temperature fluctuations. Fortunately $\left(\frac{\partial\varepsilon}{\partial T}\right)$ is found to be very small and hence ε can be considered mainly as a function of ρ and c (in solutions). Of course, in the case of polymer solutions the dominant contribution is that of polymer concentration fluctuations $\delta c(\mathbf{r},t)$.

For one component systems, where $S(0) =< |\delta\rho(\mathbf{0})|^2 >=< \delta N^2 >$, statistical fluctuation theory suggests that at $q \to 0$ the intensity of scattered light is related with the isothermal compressibility of the liquid $\chi_T = (1/\rho)(\partial\rho/\partial p)_T$ [4, 1]:

$$I_{iso} = \left(\frac{\partial\varepsilon}{\partial\rho}\right)^2_{P,T} Vk_BT\rho^2\chi_T \tag{3.56}$$

For a polymer solution the scattering intensity mainly originates from the concentration fluctuations, $S(q) =< |\delta c(\mathbf{q})|^2 >$ and the isotropic intensity at $q \to 0$ is related with $(\partial c/\partial\mu)_{T,P}$ or the osmotic compressibility $(\partial c/\partial\pi)_{T,P}$ [2, 1]:

$$\boxed{I_{iso} \sim \left(\frac{\partial n_s}{\partial c}\right)^2_{P,T} k_BT\left(\frac{\partial c}{\partial\mu}\right)_{T,P} = A\frac{c}{N_A}4n_o^2\left(\frac{\partial n_s}{\partial c}\right)^2_{P,T} k_BT\left(\frac{\partial\pi}{\partial c}\right)^{-1}_{T,P}} \tag{3.57}$$

where μ is an effective chemical potential per unit mass and A a constant (eq. 3.6). In the limit of infinite dilution, $(\partial\pi/\partial c)_{T,P} \to k_BT/M$ (eq. 2.1). In a pure liquid, the isothermal compressibility diverges at the gas-liquid critical point and thus $< \delta\rho^2 >$ and the scattering intensity diverge too (*critical opalescence*). Likewise at the critical consolute point of a binary mixture $(\partial c/\partial\mu)_{T,P}$ diverges and thus the scattering intensity diverge. In such cases the density or concentration fluctuations become large and are correlated at long distances.

Dynamics

To calculate the dynamic structure factor of the system we should find the relaxation equations that the involved quantity (ρ, c, T) obeys. In light scattering from solutions the relaxation equation of concentration equation is used. In relation to the thermodynamics of irreversible processes Onsager suggested the "*Regression Hypothesis*", according to which a spontaneous fluctuation in a property $A(\mathbf{r},t)$ relaxes back to equilibrium according to the same relaxation equation that describes the macroscopic relaxation process after an external macroscopic disturbance. Hence, the thermally induced concentration fluctuations in an equilibrium solution should satisfy the macroscopic diffusion equation:

$$\frac{\partial}{\partial t}\delta c(\mathbf{q},t) = -q^2 D_c \delta c(\mathbf{q},t) \tag{3.58}$$

and thus the correlation function of concentration fluctuations has a similar relaxation to that in the dilute regime,

$$\boxed{I_{iso}(q,t) \sim < \delta c^*(q,t)\delta c(q,0) > = < |\delta c(q)|^2 > \exp(-q^2 D_c t)} \quad (3.59)$$

governed by the cooperative diffusion coefficient D_c. As it is already mentioned in chapter 2, this diffusion is related with the osmotic compressibility $(\partial c/\partial \pi)_{T,P}$ and the mutual friction coefficient f_m (eq. 2.10).

The general way to calculate the light scattering spectrum involves the deduction of relaxation equations and subsequently the calculation of the correlation functions which followed eq. 3.55. The relaxation equation can be obtained by connecting a conservation equation and a constitutive equation. In this way, the Rayleigh-Brillouin spectrum of a pure monatomic fluid can be obtained using the conservation laws of density, momentum and energy. The fluctuations of conserved quantities become infinitely long-lived as $q \to 0$ and are called *hydrodynamic modes.* If they there is no propagation frequency $\omega(q)$ (no shift from the frequency of the incident beam) the mode is called a purely *diffusive mode*; otherwise it is called *propagating mode.* In a pure liquid there are three longitudinal and two transverse hydrodynamic modes. Only the longitudinal contribute to the light scattering spectrum and consist of one diffusive mode (originating from heat diffusion or entropy fluctuations) and a two propagating modes (due to sound waves or fluctuations of pressure). The latter give rise to the Brillouin doublets.

3.4.3 Orientation fluctuations

It has been shown that the self-part of the depolarized correlation function $G_{VH}(\mathbf{q},t)$ (eq. 3.25) for a system of symmetric top scatterers decays exponentially with a characteristic decay rate $\Gamma_{VH} = q^2 D + 6D_R$. However, for dense systems such as concentrated solutions or pure liquids, the rotations are no more unrestricted and the neighboring scatterers do not move independently. Then, as in the case of the polarized light scattering, the collective motions of the fluid should be considered. In the molecular approach discussed above, the distinct term of the VH dynamic structure factor (eq. 3.29) which includes dynamical correlations both of the orientation and the translation must be calculated. In the thermodynamic approach the problem lies in deriving a set of "hydrodynamic equations" which include rotations. Unfortunately, this is not as straight forward as in the case of isotropic density fluctuations. The problem is that orientation is not a thermodynamic variable and thus it can not be connected directly with the thermodynamic variables of the system; in this respect the situation resembles the internal field problem in depolarized light scattering (see Appendix 4). The derivation of the kinetic equations for the orientational relaxation in a dense liquid is based on the *Zwanzig-Mori formalism* [5, 1]. Following this approach, Keyes and Kivelson [16] proposed a theory in the approximation of **independent translation and rotation** which relates the single molecule rotational

relaxation with the collective relaxation measured by light scattering in a dense liquid. Their theory as applied to symmetric top optically anisotropic molecules in a solution of optically isotropic solvent, predicts a VH dynamic structure factor:

$$\boxed{I_{VH}(\mathbf{q},t) = \frac{N}{15}\beta^2(1+\rho F)\exp[-6D_R\frac{(1+\rho G)}{(1+\rho F)}t]\exp(q^2Dt)} \tag{3.60}$$

where F measures the static and G the dynamic orientation correlations between the molecules. The static correlation factor F can be written as [1]:

$$F = \frac{1}{N(N-1)} < \sum_{i \neq j} P_2(\mathbf{u}_i \cdot \mathbf{u}_j) > \tag{3.61}$$

For small molecules and isotropic polymers the dynamic correlation factor G has been found to be much smaller than the static. Hence, the collective rotational relaxation time $\tau_c \simeq (1+\rho F)\tau_s$ is larger than the single molecule relaxation time τ_s for $F > 0$ (parallel orientation) and smaller than τ_s for $F < 0$ (perpendicular orientation). The static correlations also induce an additional increase of the VH scattered intensity as seen in eq. 3.60.

The direct application of eq. 3.60 in systems of macromolecules (flexible or stiff) is questionable since the interactions among different segments of different chains (intermolecular interactions of polymeric nature) are not taken into account. The depolarized, as well as the polarized dynamic structure factors of concentrated polymer systems are usually very complicated and can be estimated only approximately (see chapter 4).

References

[1] J.B. Berne and R. Pecora. *Dynamic Light Scattering.* Willey Interscience Publications, New York, 1976.

[2] K.S. Schmitz. *Dynamic Light Scattering by Macromolecules.* Academic Press, London, 1990.

[3] M. Smoluchowski. *Ann. Phys*, 25:205, 1908.

[4] A. Einstein. *Ann.Phys*, 33:1275, 1910.

[5] R. Zwanzig. *Ann. Rev. Phys. Chem.*, 16:67, 1965.

[6] D.A. Weitz and D.J. Pine. *Dynamic Light Scattering: The Technique and Some Applications*, page 653. Oxford Press, 1993.

[7] G. Maret. *Mesoscopic Quantum Physics.* Elsevier Science B. V, 1995.

[8] L.D. Landau and E.M. Lifshitz. *Electrodynamics of Continiuous Media.* Addison Wesley, Reading, Mass., 1960.

[9] M. Kerker. *The Scattering of Light and Other Electromagnetic Radiation.* Academic Press, New York, 1969.

[10] M. Doi and S.F. Edwards. *The Theory of Polymer Dynamics.* Oxford University Press, New York, 1986.

[11] B.H. Zimm. *J. Chem. Phys.*, 16:1093, 1948.

[12] P.G. de Gennes. *Scaling Concepts in Polymer Physics.* Cornell University Press, Ithaca, 1979.

[13] T. Shimada, M. Doi, and K. Okano. *J. Chem. Phys.*, 88:2815, 1988.

[14] M. Doi, T. Shimada, and K. Okano. *J. Chem. Phys.*, 88:4070, 1988.

[15] T. Maeda. *Macromolecules*, 23:1464, 1990.

[16] T. Keyes and D. Kivelson. *J. Chem. Phys.*, 56:1057, 1974.

Chapter 4

Dynamics of Rodlike and Semistiff Polymers

In this chapter the dynamics of rodlike and semistiff macromolecules in isotropic solutions are presented. Some aspects of flexible polymer dynamics are also presented to reveal the differences with their stiff counterparts. An emphasis is given in the quantities which are related with dynamic light scattering, such as concentration and orientation correlation functions, diffusion coefficients and their concentration dependencies. First the dynamics in the dilute regime are addressed, and then in the nondilute concentration regime i.e. the semidilute and the concentrated regions.

4.1 Dilute regime

In the dilute region, polymer molecules can be regarded as independently diffusing particles which in general can have three kinds of motion, translation of their center of mass, rotation, and internal motion for polymers which posses internal degrees of freedom, i.e., not rigid macromolecules. Since the molecular motion is essentially unrestricted dilute solutions, are the appropriate system for the determination of the transport coefficients and their dependencies on the size and the shape of polymer chain. The theoretical treatment of rodlike polymers is much easier than that of their flexible counterparts since rigid rods lack internal motions. From the physical point of view, in systems of rodlike polymers the importance of the orientational degrees of freedom and the unusual nature of the topological constraints are clearly manifested in the dynamics. More specifically some of the problems involved in systems of suspended rodlike particles are the coupling between diffusion and rotation, hydrodynamic interaction, flexibility and molecular architecture. Despite significant recent work there is no completely satisfactory theory which incorporates all these factors [1, 2, 3].

4.1.1 Dilute Rigid Rods

The diffusion coefficients are calculated by using hydrodynamic methods in terms of the rod length and diameter, while for semiflexible chains the persistence length is also involved. Translation of large slender rods along their molecular axis is faster than perpendicular to it, and thus the rate of translational displacement in a given laboratory-fixed frame direction depends on the orientation of the molecule, resulting to the so-called translational-rotational coupling. For thin long rods, the parallel to the axes translational diffusion is twice the perpendicular one [4]: $D_{\parallel} = 2D_{\perp}$ and the rotational diffusion $D_R = 9D/L^2$, where D is the isotropically averaged diffusion constant $D = \frac{D_{\parallel}+2D_{\perp}}{3}$. Some polarized dynamic light scattering measurements on very large rods ($qL \gg 1$) [5, 6] have found evidence for this coupling due to the anisotropic diffusion.

For rigid rods the diffusion is described by the Smoluchowski equation for both translation and rotation [4]:

$$\frac{\partial c(\mathbf{r},\mathbf{u},t)}{\partial t} = \frac{\partial}{\partial \mathbf{R}} \cdot [D_{\parallel}\mathbf{uu} + D_{\perp}(\mathbf{I}-\mathbf{uu})] \cdot [\frac{\partial c}{\partial \mathbf{R}} + \frac{c}{k_B T}\frac{\partial U}{\partial \mathbf{R}}] + \widehat{R} D_R [\widehat{R}c + \frac{c}{k_B T}\widehat{R}U] \tag{4.1}$$

where $\widehat{R} \equiv \mathbf{u}\times\partial/\partial\mathbf{u}$ is the rotational operator. U is an external potential which for a free rod (dilute region) is zero, whereas, in the semidilute and concentrated regime or under flow represents the excluded volume, the nematic, or the flow field. The effect of anisotropic diffusion $D_{\parallel} - D_{\perp} = \Delta D \neq 0$ can be included in eq. 4.1 by a term $\Delta D(\mathbf{u}\cdot\frac{\partial}{\partial \mathbf{R}})^2 - \frac{1}{3}\frac{\partial^2}{\partial \mathbf{R}^2})c$. The coupling of the rotation with the translation can act so that a concentration gradient of a rodlike polymer may induce an anisotropy in the orientation distribution. Thus, in an homogeneous system the rotational diffusion can be discussed only using the rotational part of Smoluchowski equation.

The expressions for the diffusion coefficients in general are obtained from the relation of the force with the flux which is calculated using the hydrodynamics of the problem. For rigid rods the diffusion coefficients are of the form [7, 8]:

$$\boxed{D_0 = (k_B T/3\pi\eta_s L)\ln[(2L/b) - \gamma]} \tag{4.2}$$

$$\boxed{D_{R,0} = (3k_B T/\pi\eta s L^3)\ln[(2L/b) - \zeta]} \tag{4.3}$$

with η_s being the solvent viscosity and γ and ζ are functions of the aspect ratio (L/b), which describe the corrections due to end effects. There are several different models which calculate these coefficients with main differences in the correction terms [1]. In our work, the Broesma relations for smooth cylinders are used for calculations in the rod limit. An overview of these expressions, together with the respective for semistiff rods are given in Appendix B.

Equations 4.2 and 4.3 have been used successfully by Tirado et al [9] to obtain the hydrodynamic dimensions of several rodlike molecules from the measured diffusion coefficients and also by Eimer et al [10] to determine the aspect ratio of several rodlike DNA in solution. A more sophisticated model, were the actual atomic surface of the molecule that is accessible to the solvent and the amount of solvation is calculated (iteratively using experimental data), has been proposed by Pastor [11]. Correlation techniques have been used for the determination of the diffusion coefficients of numerous stiff molecules from rodlike viruses [12, 13, 14], to synthetic macromolecules such as poly-γ-benzyl-L-glutamate (PBLG) [15], poly-n-hexyl isocyanante [16] and poly-phenylene-benzbistiazole (PBT) [14].

In the dilute region, where PCS probes single molecule dynamics, the correlation function for short ($qL < 1$), molecules is a single exponential decay function [17]:

$$\boxed{I_{VV}(q,t) = 4Nn^2(\partial n/\partial c)^2 exp[-(q^2Dt] + \tfrac{4N}{45}\beta^2 exp[-(q^2D + 6D_R)t} \quad (4.4)$$

$$\boxed{I_{VH}(q,t) = \tfrac{N}{15}\beta^2 exp[-(q^2D + 6D_R)t]} \quad (4.5)$$

for the VV and the VH geometries, respectively. The first term of eq. 4.4 corresponds to the isotropic fluctuations of the polarizability tensor (which are proportional to α^2) and the second the contribution of the depolarized scattering ($\frac{4}{3}I_{VH}$) (eq. 3.22). According to 4.5, at $q = 0$ the depolarized correlation function depends only on the rotation of the molecule since the translational component of $\Gamma_{VH} = q^2D + 6D_R$ is eliminated. For larger rods ($qL > 1$) the dynamic form factor $P(q,t)(\sim I_{iso}(q,t))$(eq. 3.31), even in the dilute region, has a contribution from the rotational movement of the particles through smaller in amplitude terms as Pecora has shown (see eq. 3.43) assuming that rotation and translation are decoupled [18]. The terms except the first $S_0(q,t)$, become important only for large rods. The total $S(q) = \sum_p S_p(q)$ is the rodlike structure factor (eq. 3.36).

The dimensions of rodlike polymers in dilute solutions may be obtained by combining measurements of the rotational and the translational diffusion coefficients [2, 3]. In the case of semistiff polymers, in addition to the above, the persistence length must be known. A common way for the determination of the translational diffusion coefficient is dynamic light scattering in the polarized geometry (applying eq. 4.4). For the rotational diffusion coefficient, the same technique in the depolarized geometry (eq. 4.5), may be applied in the dilute region only for relatively large polymers (larger than about 200 nm) which have a rotational relaxation time larger than $3 \times 10^{-7}s$; the lower end of the correlator's window is at present $10^{-7}s$. For smaller rods (smaller than $10nm$), or semiflexible polymers the width of the Rayleigh peak, measured with a Fabry-Perot interferometer, can by used to determine the rotational time (eq. 3.27) [19, 10].

For intermediate lengths, transient electric birefringence decay (TEB) or electric dichroism decay can be applied. It must be noted though, that only PCS has the ability of investigating systems with multiple relaxations, with decay times separated less than one decade.

A practical problem concerning the PCS measurements in the dilute regime is the low scattering intensity; especially for longer rods, measurements in the actual dilute region ($\rho < \rho^* = 1/L^3$) are difficult due to the very small values of ρ^* (typically 0.05% by weight for a rod of $L = 50nm$). Consequently long data collection is needed in the dilute region, which range up to several hours. The depolarized PCS is even more difficult and requires molecules with large inherent optical anisotropy. This is related with the off-diagonal components of the polarizability tensor of the molecule or of its repeating unit. If $\beta = a_{||} - a_{\perp}$ is large, as in the case of many synthetic polymers with highly conjugated backbone, the molecule has a high capability to depolarize an incident polarized light. On the other hand, helical rodlike molecules usually have small optical anisotropy although they are rodlike in shape. Nevertheless PCS is a very powerful technique even for dilute solution measurements because it does not require any modification of the macromolecular structure (like the addition of fluorophore for fluorescence studies) and also observes the equilibrium state directly (in contrast to electric birefringence).

The calculation of the dynamic structure factor, $P(q,t)$, discussed above, does not take into account the anisotropy of the translational diffusion ($D_{\parallel} = D_{\perp}$). Moreover, the rotational diffusion coefficient of rods slows down as the length increases, much more dramatically than the translational diffusion, since $D_R \sim L^{-3}$ while $D \sim L^{-1}$ and thus, for large rods the rotation of the molecule might not be fast enough to sample an isotropic orientation distribution in the time needed to translate over a distance of $2\pi/q$. Then the translational motion is not decoupled from the rotation, and the trace of the translational diffusion tensor is not measured. A measure of the importance of this coupling is the parameter $\gamma = q^2(D_{\parallel} - D_{\perp})/D_R$; if it is small, then the rod will rotate many times during an interval q^2D , the diffusion tensor will be appropriately averaged and no coupling effects will be seen. On the other hand, if the translational diffusion was isotropic ($D_{\parallel} = D_{\perp}$) this averaging would be unimportant.

Corrections to eq. 3.43 due to the anisotropic translational diffusion have been calculated by other authors [20, 21, 18] who used the coupling parameter γ. All these studies lead to lower amplitudes for the faster mode ($S_1(q,t)$) and faster apparent relaxation rotational times; in the limit of no coupling ($\gamma \to 0$) eq. 3.43 is recovered. In general, in such studies two different formulations of the dynamics may been used; the first cummulant or initial decay rate approach and the presentation of the correlation function as a sum of exponentials. The first approach is easier, since the initial decay of the correlation function obtained is $\Gamma^{(0)} = \lim_{t\to 0}[\frac{dg^{(1)}(q,t)}{dt}]/g^{(1)}(q,t)$ and can be always calculated. The second one is

not always possible as the theoretical correlation function may be complicated or can be calculated only numerically. Nevertheless, the latter approach is more elegant and physically meaningful since it may relate the different terms with physical relaxation mechanisms of the fluctuations which are investigated.

Maeda and Fujime [22] calculated the initial decay rate, $\Gamma^{(0)}$, for the isotropic correlation function of large rods, taking into account the anisotropy in D :

$$\Gamma^{(0)}_{iso}/q^2 = D_\perp + (L^2/12)D_R f_1(qL) - (D_\parallel - D_\perp)f_2(qL) \tag{4.6}$$

The weight factors f have the limiting behavior: $f_1(qL) \to 0$ and $f_2(qL) \to \frac{1}{3}$ for $qL \to 0$, $f_1(qL) \to 1$ and $f_2(qL) \to 0$ for $qL \to \infty$. In the high q-limit it is found that $\Gamma^{(0)}_{iso}/q^2 = D_\perp + (L^2/12)D_R$, meaning that the motion of the rod along its axis does not contribute in scattering. This is because this motion can do little to relax the correlation function; a movement of a segment over a distance of $2\pi/q$ will always be followed by the movement of another segment over the same distance. Thus neither the phase nor the amplitude of the scattered field will be changed. To the contrary lateral translations and rotations will relax the correlation function much more effectively. Note that due to the coupling of the rotation with the translation the term containing D_R exhibits a q^2 (diffusive) behavior. This dependence of the rotational decay rate arises, in the initial decay rate approach, from the amplitudes of the composite functions, whereas the q^2 dependence of the translational decay rate arises from the diffusion process. It has been pointed out [23, 24, 1] that due to the insignificance of the axial diffusion the very small values of D_R, and the directed scattering of very long rods, the diffusion process can reduce to a planar diffusion, leading to an non exponential correlation function. For polydisperse samples the apparent diffusion, $\Gamma^{(0)}_{VV}/q^2$, exhibits a larger slope when plotted against q^2, since at high q's the scattered intensity from larger molecules falls off and the smaller ones are emphasized. Analogous expressions have been derived by other authors [6, 25, 20].

Aragon and Pecora [18] taking into account not only the anisotropic diffusion but also the optical anisotropy of the rods, wrote the dynamic structure factor $P(q,t)$ as a sum of exponential decays similarly with eq. 3.43. In comparison with the later there is a term $w_{mj}(\gamma)$ which causes a splitting of the relaxation modes. This splitting however is usually too small to be detected experimentally. As a general guideline, one can say that when the $S_1(qL)$ term in the original Pecora theory (eq. 3.43) becomes important one has to take into account the coupling in the correlation function in all approaches. Only when γ is larger than 25 the split modes differ by a factor of two and can be detected experimentally. Such values of the coupling parameter can be achieved only in semidilute concentrations where the rotational diffusion is slowed down more than the translational one due to strong intermolecular hinderance.. At this regime however, the interpretation of dynamic light scattering relaxation modes is more complicated since they are of cooperative rather than molecular nature.

4.1.2 Dilute Semistiff Polymers

Perfectly rigid rods are almost an idealization which can be very rarely be used for true macromolecules; even the stiffer of them have enough flexibility to look more like coils when their contour length is large. Most of the theoretical studies on the dynamic and static behavior of polymers have been done for the two limiting cases; the flexible and the rodlike polymers. The theory for the dynamics of semiflexible chains is much less developed despite the scientific and practical importance of such molecules.

It has been shown that the application of the Rouse-Zimm model for flexible chains, in macromolecules with high stiffness, such as DNA does not yield the correct static and dynamic properties even if they are long enough to resemble more a coil rather than a rod [6, 26]. Similar discrepancies are found in other stiff synthetic and natural macromolecules and seem to increase with increasing stiffness [27]; this discrepancy may be due to the finite stiffness that such molecules possess that makes them different from the RZ chain which is very flexible even in small length scales.

Wormlike model

The Kratky-Porod wormlike chain can be extended to calculate not only equilibrium static, but also dynamic properties, assuming that the *static persistence length* is the same with the *dynamic* one; the latter is used to characterize the dynamic bending of the chain . The experimental evidence so far show, that these two quantities are similar [2, 1], although Song and Schurr [28] raise the possibility that the dynamic persinstence length determining the bending force constant is higher than the static one for molecules that have permanent bends like DNA. Several authors have presented expressions for both the translation and the rotation diffusion coefficients [29, 30, 31] in terms l, L and b and the coefficients are given by different expressions for large or small L/l ratio. Several of these expressions are given in Appendix C.

The theories for the translational diffusion coefficient of wormlike chains give good agreement with experimental findings although some discrepancies have been found [32, 2]. On the other hand the measured rotational diffusion coefficients of DNA are generally not in agreement with the theoretical predictions, unless an L dependent persistence length l, is used [33, 34, 35]. This disagreement may be due to the sensitivity of the experimental techniques, such as dynamic light scattering, birefringence and dichroism decay, also in the internal motions of wormlike chains [2]. This explanation has been supported by Brownian dynamics simulation of semistiff chains [36].

Semistiff polymers exhibit, in addition to translation and rotation, significant internal motions which result from long range shape fluctuations. The internal dynamics and the coupling with the translational and rotational motion is not

easily quantified. Based on the Harris-Hearst approach [37] the Langevin equation for this model is:

$$\rho(\partial^2\mathbf{r}/\partial t^2) + f_L(\partial\mathbf{r}/\partial t) + \kappa(\partial^4\mathbf{r}/\partial s^4) - e(\partial^2\mathbf{r}/\partial s^2) = \mathbf{F}(s,t) \qquad (4.7)$$

where ρ is the linear mass density of the filament, f_L is the friction coefficient per unit length, κ is the transverse bending constant, and e is related to the length fluctuations of the chain. $\mathbf{F}(s,t)$ is a random force, per unit length acting on the chain due to the thermal bombardment from the molecules of the medium. The Harris-Hearst [37] and other similar models [1] do not include hydrodynamic interactions and interactions between the translational and rotational motions and the internal degrees of freedom. Moreover, they suffer from incorrect results in the rigid rod limit due to some chain length fluctuations. Several other models have been proposed to tackle this problem [38, 39, 2]. Aragon and Pecora [40] added a constrain to ensure constant contour length ($\mathbf{u}^2 = 1$) and solved eq. 4.7 for the pure bending model ($e = 0$) in the free draining approximation. The calculated normal modes have a characteristic decay rate: $\Gamma_l = lD(l)(2l+1)^4\pi^4/16L^3$, where $D(l) = k_BT/Lf_L$ is the translational diffusion coefficient which dependents on the persistence length (Appendix C). It is seen that stiff and short chains have faster characteristic decay for all relaxation modes. For $l = 0$ there are two degenerate eigenfunctions, which correspond to the translation and the rotation of the molecule in the rod limit whereas in the Rouse model there is only the translation. The most interesting, though, is that for stiff chains the relaxation modes of internal motions are separated much more ($\Gamma_{worm} \propto l^4$) than in the case of Rouse chains ($\Gamma_{Rouse} \propto l^2$) [1]. The polarized correlation function for the pure bending mode in the dilute region in the free draining limit is similar to eq. 3.43, except that the amplitudes B_j are now functions not only of qL but also of the persistence length l and time t.

Recently Harnau et al [27] presented an approach describing the static and dynamic properties of chains with arbitrary degree of stiffness. It is based on the maximum entropy principal to solve the equation of motion and includes also hydrodynamic interactions. This model suggests that at large scattering wavevectors ($ql > 1.5$), the chain stiffness becomes important for all macromolecules, even for very flexible. The model exhibits a cross over from stretching to bending modes for intramolecular modes. In the limit of high L/l, the relaxation times are proportional to L^2 and vary as n^{-2} in agreement with the Rouse model, while for smaller L/l, the relaxation times are proportional to L^4 and exhibit a $(2l-1)^{-4}$dependence. If only bending modes are considered, the decay rate, Γ, is approximately proportional to $q^{8/3}$ deviating from the Zimm model dependence (q^3). For flexible molecules there is an intermediate scattering vector regime where the decay rate is proportional to q^3. Such a regime does not exist in semiflexible molecules ($L/l < 20$) where for large wavevectors ($qR_G > 3$) the decay rate is proportional to $q^{8/3}$. Rodlike molecules exhibit a q^2 dependence of Γ

(plateau region) for large wavevectors. Finally, it is suggested that the dynamic structure factor for $qR_G > 1$ cannot represented by a single exponential decay but can be stretched exponentials in some limiting cases (only bending or only stretching modes).

4.1.3 Concentration dependence-Virial regime

In the dilute (virial) regime the concentration dependence of the diffusion coefficients is given by eq. ?? (chapter 2). The theories for the equilibrium properties of dilute solutions of hard rods have been treated by Zimm [41], Onsager [42] and Ishihara and Hayashida [43]. The later concluded that the second virial coefficient for rigid rods is

$$A_2 = (\pi N_A b^2 L/M^2)(1/4)x(1 + (3+\pi)/(2x) + (\pi/4)/x^2) \tag{4.8}$$

For large aspect ratio x becomes the same with the hard rods prediction given by Onsager and Zimm:

$$A_2 = \pi N_A L^2 b/4M^2 \tag{4.9}$$

The second virial coefficient was also calculated in the presence of attractive interactions [44, 45]. The sedimentation coefficient k_f in the case of uncharged rodlike molecules was calculated by Peterson [46]

$$k_f = \frac{k_B T}{3\eta_s}\frac{L^2}{D_o M}\left(\frac{3b}{8L}\right)^{2/3} \tag{4.10}$$

The passage from the dilute to the semidilute regime should be marked by a change in both the dynamic and static quantities of the solution; thus in a light scattering experiment in the diffusion coefficients and in the scattering intensity. The dynamic behavior of the macromolecules is becoming more complicated in the semidilute and the concentrated regime, but fortunately the dilute region dynamics are not affected crucially in the lower part of the semidilute region especially for rodlike polymers. This allows us to use the light scattering technique of photon correlation spectroscopy for the characterization of polymer dimensions. Nevertheless, it must be mentioned that usually is difficult to detect rod dynamics in the dilute regime ($c < 1/L^3$) due to weak scattering. However, as long as $c/c^* < 20$ excluded volume effects on the dynamic properties can be ignored as inferred from translational diffusion data [2]. A change in the behavior of D_c with concentration was observed by Tracy and Pecora [47, 2] at about $17c^*$ of a PBLG solution in DMF, marking according to the authors the passage to the semidilute region. The initial decrease of D_c was followed by an increase above $c/c^* > 17$. The diffusion data for the $c/c^* < 17$ regime gave a good aggreement with the value of k_f from eq. 4.10. It must be noted however that such a behavior of the cooperative diffusion was not found in any other case. This behavior means

that initially the friction term dominates over the thermodynamic term in eq. 2.9 for the low concentrations. Contrary to the above, in higher concentrations the thermodynamic speed up is the dominant factor in the diffusion, although it must be noted that the eq. 2.9 must be substituted by eq. 2.7. Deviations from the expected by eq. 4.10 were found in other studies of PBLG [48] and were attributed to flexibility, while poor aggreement was found in aqueous solutions of DNA [49] probably due to electrostatic interactions.

The rotational diffusion coefficient in the virial regime is less well studied. It is expected that the rotational diffusion is less affected by the thermodynamics than the translational diffusion. There is no analogous to eq. 2.7 and 2.9 expression for the rotational diffusion and few measurements exist. Measurements in small oligonucleotides [10] exhibit a virtually no concentration dependence in the dilute region.

4.2 Semidilute Region

The dynamics in the semidilute and the concentrated region are largely affected by direct and hydrodynamic intermolecular interactions, in contrast to the dilute region where they are negligible. The kinetic equation 4.1 has to include all these effects; in solving this equation all the effects are taken into account by the use of effective, concentration dependent, diffusion coefficients. The concentration dependence of these coefficients for solutions of rodlike and semistiff macromolecules is still under investigation although there are a lot of studies especially about the translational diffusivities. From the point of view of fundamental thermodynamics, it is of great interest to understand how dynamic properties such as the diffusion coefficients, and static properties such as the correlation length and the osmotic pressure behave, and also to resolve the relaxation mechanisms through which concentration and orientation fluctuations relax. Moreover, from the light scattering point of view, it is of great interest to understand how these relaxation processes are revealed in the polarized and depolarized correlation functions.

4.2.1 Doi-Edwards and related theories

The first theory for the dynamics of concentrated solutions of rigid rods was presented by Doi and Edwards [50, 4]. In its simplest form DE theory is a scaling theory based on the reptation concept, which was used earlier for flexible chains [51, 4]. It was formulated for infinitely thin, uncharged, rigid rods, whose only interaction is that they can not pass through each other. Thus, substantial restrictions on the possible motions of the molecules are imposed in nondilute solutions and are increasing as the concentration of rods is increased. DE proposed that these restrictions can be modeled by using the concept of an effective tube of radius α which is formed by the neighboring rods. Inside this tube, the

rodlike molecules can move freely along the axes of the tube while the translation in the perpedicular direction is restricted to about a distance α due to the presence of the neighboring rods. Hence, in the semidilute region normal diffusivity is almost frozen ($D_\perp \approx 0$) compared to the parallel diffusivity ($D_{||}$) which is considered unhindered and equal to its dilute solution value. The translational diffusion of a rod then decreases to almost half of its dilute value $D \simeq \frac{1}{2}D_o$ since $D = \frac{1}{3}(D_{||} + 2D_\perp)$ and $D_{0||} \cong 2D_{0\perp}$ and then is concentration independent in the semidilute region. In this theory, the effect of a finite diameter, of the molecular flexibility, of hydrodynamic interactions were not considered.

The DE theory predicts that the effect of the mutual hinderance on the rod's rotation is much more drastic than on the translational diffusion. As long as the molecule stays inside a certain tube, its direction is fixed by the direction of the tube and in order that the molecular orientation to change the rod has to move along the tube at least a distance $L/2$, disengage from the old tube and to pass into another. This passage from one tube into another involves a rotation of about $\varepsilon = \alpha/L$ and in order for the orientation of the test rod to lose its correlation with its initial orientation, it has to repeat the above process several times. Thus, the rotational and the translational movement are strongly coupled in the concentrated regime even for relatively small rods, in addition to the coupling that takes place in the dilute regime for long rigid rods. The average time, τ_d , necessary for the polymer to diffuse along the initial tube and escape is $\tau_d \simeq L^2/D_{\|,0}$, so that the rotational diffusion of the rod, $D_R \simeq \frac{\varepsilon^2}{\tau_d}$, becomes smaller than in the dilute regime: $D_R \simeq (\alpha/L)^2 D_{R,0}$ [4]. The radius α is then calculated in terms of the concentration c and L, to end up with the concentration dependence of the rotational diffusion coefficient [4]:

$$\boxed{D_R = \beta D_{R,0}(c^*/c)^2 \sim \rho^{-2}L^{-9}} \tag{4.11}$$

where β is a constant and ρ the number concentration of rods (c is the weight concentration). In the original DE theory was expected to assume values between 1 and 10. It is observed, however, that β is rather of the order of 10^3 [52, 15, 53, 54, 55] showing that enmeshment of rod-like particles is less likely than first suspected or in other words that the caging effect starts at a much higher concentration. It must be noted that in the above model it is implicitly assumed that the cage is undistorted, at least during τ_d . Actually, the tube can change during this time since it is formed by other rods which can also move a distance of the order of L, and thus release one of the constrains which was initially imposed on the test rod. Of course at the same time new constrains can be imposed by the same mechanism making the tube a rather dynamical formation. Doi argues [4] that since the characteristic time for the appearance and disappearance of these constraints is again τ_d and the step of the angular change they imply is again ε, resulting only in a change of the numerical coefficient and not in the functional form of D_R.

The zero-shear viscosity for dilute through concentrated solutions, neglecting hydrodynamic screening effects, is given by the general relation between η_0 and D_R [4]

$$\boxed{\eta_0 = \eta_s + (\rho k_B T/30 D_{R,0}) + (\rho k_B T/10 D_R)} \tag{4.12}$$

In the above expression the second term comes from the viscous stress, which arises from the energy dissipation by the friction between the rodlike molecule and the solvent and the third term corresponds to the elastic stress, which is produced by the orientational entropy loss of rods [56]. The asymptotic behavior in the semidilute region is given by:

$$\eta_0 = (k_B T L^6/10\beta D_{R,0})\rho^3 \tag{4.13}$$

The strong molecular weight dependence of the viscosity is in accordance with experimental findings although the precise exponent is difficult to extract, while the numerical factor β obtained from the viscosity data has again turned out to be similar to the experimentally found from D_R [4]. Moreover, in some cases the concentration dependence of η_0 was found to be stronger than ρ^3 possibly due to the rod jamming; an effect of the finite thickness of real rods [57]. On the other hand, at the low end of the semidilute regime a weaker concentration dependence should hold as eq. 4.12 indicates.

Experimental results but also theoretical considerations led to the need for modifications of the original DE theory. This refinements of the DE theory for rods can be classified on the basis of what is modified:

a) A recalculation of the tube size and geometry [53, 58, 59],

b) Different cage escape mechanisms [60],

c) Introducing the effect of finite thickness of the rods [61]

Next we give the results and a brief discussion of these modifications.

A) Recalculation of cage size

A recalculation of the cage size and geometry was done by Keep and Pecora [?, 62] assuming, like in the DE model, thin rigid rods and an isotropic equilibrium rod orientation. They actually calculate the concentration dependence of the average solid angle through which the rod can rotate in a cage and found a less strong c dependence of the rotational diffusion coefficient:

$$\boxed{D_R = 21.22 D_{R,0}/[f^2[(\rho L^3)^2 - 17.74(\rho L^3)]]} \tag{4.14}$$

with f being the fraction of L that a rod must translate to escape a cage (in the original version of the DE model $f \approx 1$); this expression converges to the classical DE prediction for $c/c^* > 500$. Comparison with experiments has shown that $f \approx 1/6$ [2]. Furthermore, it was argued that the rods can not be considered caged until $c/c^* \geq 50$ and also that isotropic orientation of the rods can not

be realized above $c/c^{**} < 2.3$ [62]. Thus, for thin rods it is expected that the DE cage theory will hold at high concentrations ($c/c^* > 500$) and the modified approach at a lower concentration regime ($50 < c/c^* < 500$).

Regardless the details of the cage concept, this picture clearly should be modified in low and high concentrations were other factors play important role. At the lower end of the semidilute regime, rods are insufficiently caged, while at the high end the finite thickness of the molecules can alter their dynamic behavior, since their lengthwise translation may no longer be free, due end-to-end collisions.

B) Alternative escape mechanisms

Another modification of the cage approach was done by Teraoka, Oukubo and Hayakawa [60, 63] who defined the tube by the projection of the hindering rods onto a sphere which incudes the test rod as its diameter. They also visualized two ways for the escape of the test rod; through the translation of one hindering by apart of its length L and by the translation of the test rod itself until it passes by the nearest hindering rod. Additionally they assumed that when the tube is enlarged by the above mechanisms the test rod may or may not pass to a new tube. This model predicted a similar to the DE rotational diffusion but with a much larger coefficient $\beta = 1350$ [60], which is closer to the available experimental findings.

Odell, Atkins and Keller [53] used computer simulation to show that for an isotropic solution of rods the rotational freedom of a test rod has a anisotropic distribution and that unexpectedly large rotational jumps can occur along certain directions up to an appreciable concentrations. This means that the cage is not closed in all directions and that the rotational diffusion has a less strong than c^{-2} dependence. Moreover, the L dependence would go towards L^{-3} rather than L^{-9} predicted by DE theory. Relating the above with the suggestions of Keep and Pecora it reasonable to expect that the mechanism proposed by Odell et al would apply for $1 \lesssim c/c^* \lesssim 50$, the region where the caging is incomplete.

C) Finite diameter effects

Edward and Evans [61] used a mean field theory to describe the diffusion of a rodlike molecule with finite thickness through a tube where the occasional hindrance in the sideways diffusion of the test rod by neighboring rods can be resembled by a linear diffusion through a series of doors which open and close. Utilizing a Green function perturbation expansion and a self-consistency argument for the tube model, they predict a slowing down of the parallel diffusion:

$$D_{\parallel} = \frac{3}{2} D_o (1 - C(\rho b L^2)^{3/2}) = \frac{3}{2} D_o (1 - \delta(\rho/\rho_n)^{3/2}) \qquad (4.15)$$

where C is constant of order of unity and $\delta = C(16/\pi)^{3/2}$. The above predicts freezing of the system at a concentration before the nematic transition (close to

$0.2\rho_n$); which is a quite strong suggestion which is not seen in real systems.

Teraoka and Hayakawa [64, 65] used this a Green function formulation that deals with the entanglement effect as perturbation, to calculate the decrease of the perpendicular diffusion. They predict

$$\boxed{D_\perp = D_{\perp,0}(1+\varepsilon\rho L^3)^{-2} = \tfrac{3}{4}D_{\perp,0}(1+\psi\rho/\rho_n)^{-2}} \tag{4.16}$$

where ε is a constant and $\psi = \varepsilon\rho_n L^3$, and the rotational diffusion:

$$D_R = D_{R,0}(1+\beta^{-1/2}\rho L^3)^{-2} \tag{4.17}$$

This expression reproduces the DE result for $\rho L^3 \gg 1$. An extension of the Edwards-Evans model to a wider concentration range was performed by Sato and Teramoto [56] yielding:

$$\boxed{D_\parallel = D_{\parallel,0}(1-aL^2b\rho)^2) = \tfrac{3}{2}D_0(1-\kappa\rho/\rho_n)^2} \tag{4.18}$$

with a a constant and $\kappa = a\rho_n L^2 b$. Moreover, these authors calculated the rotational diffusion and the zero-shear viscosity in the whole isotropic regime from dilute to concentrated solutions of rigid rods using a mean-field Green function method which does not use the tube model. They predict that:

$$\boxed{D_R = D_{R,0}[1+\beta^{-1/2}\rho L^3/(1-\alpha^{-1}L^2b\rho)]^{-2}} \tag{4.19}$$

while the zero-shear viscosity is calculated applying the above expression for D_R to the general relation between η_0 and D_R (eq. 4.12):

$$\frac{\eta_{sp}}{c} = [\eta]\{\frac{1}{4}+\frac{3}{4}(1+\frac{\beta^{-1/2}\rho L^3}{(1-\alpha^{-1}L^2b\rho)})\} \tag{4.20}$$

where η_{sp}, is the specific viscosity ($\equiv (\eta-\eta_s)/\eta$) and $[\eta]$ the intrinsic viscosity of the polymer.

From the above translational diffusivities. (eq. 4.16 and 4.18) the average diffusion coefficient can be written as:

$$\boxed{D = \tfrac{1}{2}D_0[(1-\kappa\rho/\rho_n)^2+(1+\psi\rho/\rho_n)^{-2}]} \tag{4.21}$$

4.2.2 Binary interaction theories

In an effort to use more rigorous formalism than the tube model, some authors have suggested theories based on more microscopic ideas, such as independent binary collisions or cooperative rod reorientations, to account for the influence of surrounding molecules [66, 67, 68, 69].

Fixman [66, 67] provided such an alternative, to the cage mechanism, model for the relaxation of orientation fluctuations of semidilute rigid-rod solutions.

The physical idea behind this model is that the elastic free energy of the system can relax through the DE mechanism of longitudinal diffusion, but also through a much faster mechanism for the short time decay of torque. This is the spreading of the elastic energy, which initially is concentrated in the few neighbors that make up the cage, among a larger number of neighboring molecules by small rotational movements. Hence, orientation fluctuations relaxes first at small times by cooperative reorientations of the neighboring rods and at later times by the DE longitudinal diffusions. Brownian dynamics simulations of rigid rods with finite thickness, in concentrations between 50 to $220\rho^*$, predicted a rotational movement which slows down with concentration as $(\rho L^3)^{-1}$ rather than the $(\rho L^3)^{-2}$ prediction of the DE theory. The rotational diffusion is written as:

$$\boxed{D_R = D_{R,0}[1 + (1/6\pi)cL^3Qfln[(1-f)/f]]^{-1}} \tag{4.22}$$

where $Q = 1 + (\pi/2)\rho L^3(b/L)(1-2f)^2$; f physically determines the matching of the rates of the two relaxation mechanisms. The importance of the axial ratio increases as the concentration increases meaning that at higher concentrations the concentration dependence may not be the same of small and larger rods. Fixman's approach indicates that DE model might not be valid at the whole semidilute and concentrated regime, because it is not the equilibrium size of the cage that is important, but rather the size of a dynamically distorted cage which is larger and also has a different c-dependence.

Bitsanis, Davis and Tirrel [70, 71] revealed a similar with Fixman dynamic behavior for semidilute solutions ($\rho = 5 - 150\rho^*$) of rodlike particles with aspect ratio $L/d = 50$, by Brownian dynamics simulations. These simulations show that the translational diffusion of the rods normal to their axes freezes at much higher concentration than predicted by DE theory. Actually $D_\perp$ drops to 10% of its dilute region value above $60\rho^*$ and frozen completely above $90\rho^*$ marking the passage to completely closed cages. At the same time, $D_\parallel$, decreases only about 20% at $150\rho^*$ due to the finite diameter of the rod. Moreover they supported the concentration dependence of D_R ($\sim \rho^{-1}$) up to about $70\rho^*$ and the two mechanisms for orientational relaxation suggested by Fixman's model. This work has also shown that the existence of solvent molecules is important because it makes the rotation a diffusive process by decorrelating the successive rod-rod collisions through solvent-polymer impacts. A consequence of this is that the rodlike polymer can sample more pathways as it rotates and thus is able to take advantage of small cage openings to escape from the cage in contrast to the case of a nondilute gas of rods [72]. In the range $70 - 150\rho^*$ the simulations give a rotational diffusion coefficient between the DE and the Fixman prediction; in this regime the Fixman model may not be applicable because it implies larger rotations of the rods inside the cages than what is really possible, since the cage is now more compact rather than dynamic, and thus closer to the original DE idealization. Recently, Sato and Teramoto [63] recalculated the diffusion data of

Bitsanis taking into account the anisotropy of the diffusion ($D_{\parallel,0} \neq D_{\perp,0}$) (in the original work it was assumed that $D_{\parallel,0} = D_{\perp,0}$), and showed that the recalculated data agree fairly well with the eq. 4.21.

Szamel and Schweizer [68, 69] presented an approximate microscopic theory based on the binary interactions approach to calculate the transverse translational diffusion coefficient and compare it with that derived from the reptation-tube theory. Their approximation takes into account the influence of the surrounding rods on the two-particle dynamics. They found that the transverse diffusion is the same for the two approaches in the semidilute region $\rho L^3 \geq 20$ and slow down similarly to the rotational diffusion coefficient

$$D_\perp \approx 18\pi \frac{D_{\parallel,0}}{(\rho L^3)^2} \tag{4.23}$$

For smaller semidilute concentrations, though, it follows a weaker concentration dependence while in the dilute regime is constant (similar to D_R). To make a deeper connection with the tube model they also calculate a relaxation time and an analog to the tube radius i.e., a localization length. For high concentrations they both follow the scaling laws of the reptation theory.

4.2.3 Flexibility Effects in the non-dilute region

The flexibility can have important effects on the dynamic behavior and very often deviations between experiments and theory of rods are attributed to it. For instance, a flexible end of a stiff macromolecule has some freedom to choose its own path when translating along its length, despite the fact that a large part of the chain may be caged and thus restricted to a certain orientation. The wormlike model has been in many cases the basis of the theoretical approaches for the dynamics of stiff chains in high concentrations. Another model for investigating the dynamics of semiflexible molecules is the fuzzy cylinder model [63].

Reptation models

Odijk [73, 74] has modeled the dynamics of wormlike chains in intermediate concentrations. He first treats the chain as trapped in a porous medium and then extends his theory to the case of a coil in a medium composed of the enmeshed neighboring chains. It is predicted that the effect of flexibility is large when the mean square deflection of the chain from linearity ($< \xi^2(s) >= 2s^3/3l$) is larger than the average cage size α, i.e., at high concentrations. Odijk uses the original DE formulas for calculating the cage size around a segment one persinstence length long, since such segments can be considered to rotate independently, and calculates a concentration independent rotational diffusion coefficient:

(i) $D_R \simeq kT/\eta_s L^2 l$, (for $\alpha^{2/3} l^{1/3} < L < l$)

(ii) $D_R \simeq kT/\eta_s L^3$, (for $L > l$) and

(iii) $D_R \simeq \alpha^2 kT/\eta_s L^5$, (if $\alpha < L < \alpha^{2/3} l^{1/3}$)

In the later case, the rotational diffusion coefficient is determined by the reptation-rotation of the rod and is concentration dependent through the change of the cage size α with concentration.

Doi [58] came to the same conclusions for the description of the Brownian dynamics of semiflexible polymers in concentrated solutions or in a network, assuming only reptational motion of the chain. The lateral diffusion of the chain is neglected and thus in the rod limit the result for D_R is not recovered. These theories do not agree with the observed dynamic behavior of concentrated solutions of stiff chains since they predict a c-independent rotational diffusion for $Ll \simeq 1$ and also suggest that $D_R \propto 1/L^{2-3}$ when it is found that $D_R \propto 1/L^{7-8}$. Moreover the predicted by Doi's theory magnitude of the numerical factor β in the expression of D_R is much smaller than the observed one. Doi suggests [58] that it is more realistic to think that during the reptation the semiflexible chain bends also and pushes its surrounding molecules so that the averaged out motion corresponds to the motion of a rod with an effective length $L_e =< \mathbf{u}(L/2) \cdot (\mathbf{R}(L) - \mathbf{R}(0)) >= 2l(1 - e^{-L/2l})$. Thus, the difference in the value β between experiments and the DE prediction can be attributed to flexibility effects and can be rationalized by a contour to an effective length ratio $L/L_e \simeq 2 - 3$.

In a scaling approach, Semenov investigated [75] the dynamics of concentrated solutions of stiff polymers in isotropic solutions. For concentrations smaller than $1/Ll^2$ the mean number of Kuhn segments in an l^3 volume is small and can be considered to move freely on scales comparable to their length. The solution is considered concentrated when $(4Ll^2)^{-1} \ll c \ll (2Llb)^{-1}$. In aggreement with the above Semenov predicts an isotropic rotational diffusion coefficient $D_R = 2D_{\|}/Ll$. Semenov also calculated the relaxation of the dynamic structure factor $S(q,t)$ which can be measured by scattering experiments with labelled chains and that of dynamic form factor $G(q,t)$ measured in coherent scattering experiments. The self-diffusion coefficient D_s, through which the dynamic structure factor decays (for $q^2 Ll \ll 1$) as $S(q,t) = \exp(-q^2 D_s t)$, is predicted to be c-independent:

$$D_s = D_{\|}(l/L + 2l)) \tag{4.24}$$

In the rod limit this gives the DE result, while in the flexible limit gives the reptation result $D_s \sim L^{-2}$.

For smaller wavelengths ($q^2 Ll \gg 1$), when a part of the chain is probed, four different relaxation regimes are predicted [75]. For $L \approx l$, the structure factor decays exponentially only for times larger than $\tau_3 = L^2/\pi^2 D_{\|}$, as $S(q,t) = \frac{8}{\pi qL} \exp(-t/\tau_3)$, whereas for times smaller than τ_3 (the time that a chain needs to diffuse a distance equal to its length), $S(q,t)$ decays linearly with t (for $t \ll q^2 D_{\|}$).

For $L \ll l$ the structure factor decays as in the limit of small wavevectors, if $1 \ll q(Ll/2)^{1/2} \ll l/L$, and as the above for the large wavevectors for $q(Ll/2)^{1/2} \gg l/L$. For $L \gg l$ the above dynamic behavior is correct if $ql \gg 1$, while for $ql \ll 1$ the dynamics are those of flexible chains. These findings demonstrate how in a scattering experiment the dynamic behavior probed dependents not only on the dimension and flexibility of the polymer chain, but also on the scattering wavelength i.e., on the characteristic length in which the system is observed.

Another theoretical approach based on scaling ideas by Tinland, Maret, and Rinaudo [76] which seems to hold not for very stiff chains, predicts that in the semidilute regime

$$D_s = \frac{9kT}{8\pi\eta_s} l^{-5} L^{-2} \rho^{-3} \tag{4.25}$$

while in the concentrated regime it is concentration independent

$$D_s = D_0 l/L \tag{4.26}$$

Fuzzy cylinder model

Sato, Takada and Teramoto [77] have used the "fuzzy cylinder" model to model stiff chains and extent their work on rodlike molecules [56, 78] in the case of isotropic solutions of semiflexible molecules. The the global motion of the chain can be identified with that of a segment-distribution model with cylindrical symmetry, the "fuzzy cylinder". The cylinder has a length equal to the root-mean-square end-to-end distance of the wormlike chain, $L_e =< R^2 >^{1/2}$, and an effective diameter, $b_e = [< H(L/2)^2 > + b^2\}^{1/2}$; with $< H(L/2)^2 >$ the mean square distance of the chain midpoint from the end-to-end displacement axis and b the diameter of the chain. In contrast to the work of Doi and Odijk, in this model internal motion of the stiff chain is allowed, which is probably acceptable for stiffer polymer chains in less concentrated solutions. In a way this is another realization of the Doi's suggestion that the motion of stiff chains can be described by a rod of an effective length L_e. The longitudinal diffusion is calculated by a mean-field Green function method and a hole theory; the basic assumption of the later is that the longitudinal diffusion of the test chain occurs only when a "hole" that is longer than a critical size exists in the front of the test chain. Both methods give a similar $D_\parallel$ with that predicted for rodlike molecules (eq. 4.18) by the same method, only with renormalized chain dimensions:

$$D_\parallel = D_{\parallel,0}(1 - B_{||} L_e^2 b_e \rho)^2) \tag{4.27}$$

The rotational diffusion coefficient is calculated by a mean-field Green function method and is found again similar with that for rodlike systems with renormalized dimensions (eq. 4.19):

$$D_R = D_{R,0}/[1 + \frac{\beta \mathrm{f}_R(b_e/L_e)\rho L_e^4/L}{(1 - B_{||}\ L_e^2 b_e \rho)}]^2 \tag{4.28}$$

where the function $\mathrm{f}_R(b_e/L_e)$ is a correction factor [63]. Thus D_R has a weaker than c^{-2} dependence in the intermediate concentrations, while at high concentrations D_R can decrease faster than c^{-2} due to the decrease of $D_{||}$. This model also predict a similar zero-shear viscosity with eq. 4.12.

The two models described above for the dynamics of semistiff molecules in nondilute solutions (fuzzy cylinder and reptation) are of a different nature. It is reasonable though, to expect that while the fuzzy cylinder model describes better the dynamics in the semidilute regime as the concentration is increased the polymer chain motion changes towards the reptation model mechanism. The onset of the crossover should depend on the degree in which the lateral motion is suppressed by entanglement with surrounding chains.

4.2.4 Experimental studies in the non-dilute region

Self-Diffusion

Rodlike and stiff polymer systems are much less studied compared to flexible one. The translational self-diffusion coefficient D_s of a polymer in concentrated solutions can be measured by techniques were the single particle motion is probed like forced Rayleigh scattering (FRS), fringe pattern recovery after photobleaching (FRAP), pulse-field gradient nuclear magnetic resonance (PFG-NMR) and computer simulations. The self-diffusion data on stiff polymers are yet very few. Measurements have been done on solutions of DNA [79, 80], xanthan (a stiff double-helical polysaccharide) [76], and PBLG [81], mainly by FRS and FRAP and indicate a decrease of the D_s with c.

Tinland et al.[76] have used several molecular weights of wormlike xanthan (with $L \simeq 10-200l$) and found a sigmoidal decrease of D_s with c (constant in the dilute, decreasing in the semidilute and leveling off at the concentrated region), except for the higher molecular weight were the decrease is monotonous. The decrease is more rapid for higher molecular weight and can be described only semiquantitatively for the three middle fractions by the "fuzzy cylinder model " predictions (eq. 4.21 and 4.27) [63]. An indication for a level off at higher concentrations was explained by Tinland et al. by the reptation mechanism which predicts a concentration independence of D_s as well as D_R.

More recently Bu et al. [81] have measured the self-diffusion of PBLG (with $L = 14nm - 160nm$, $l \sim 100nm$) by FRAP and again found two or three regimes depending on the molecular weight. On the contrary to Tinland et al. they found an indication of level off only for the two highest molecular weights. The D_s start to decrease well above $c^*(= 1/L^3)$; the data are not well fitted by any analytical theory but they are obeying a power low $c^{-1.13}L^{-1.8}$ dependence.

In the above studies the cessation of motion suggested by Edward and Evans [61] (eq. 4.15) for the high concentration was not observed. Concerning the level off of D_s at high concentrations for some of the measurements, Sato and Teramoto have pointed out [63] that it is in disagreement with the zero-shear viscosity dependence ($c^3 - c^7$) at high concentrations [78] since η_o is approximately proportional to c/D_R (eq. 4.12).

Rotational diffusion

The experimental studies on the rotational diffusion of stiff chains are like for the self-diffusion very few. Moreover, when the molecule posses some flexibility the determination of D_R becomes difficult especially by polarized light scattering and birefringence techniques, due to the internal motions of the chain. On the other hand the use of depolarized light scattering demands large molecular optical anisotropy. Concerning the slowing down of the rotational diffusion most authors [82, 63] find that these does not start until $c \approx 5 - 50c^*$ and persists well beyond c^{**}. In most investigations the rate of decrease was found to agree with the DE prediction c^{-2} above a certain concentration. The most common molecule in these studies is probably PBLG; it was used in light scattering experiments by Zero and Pecora [15] and Chu and coworkers [83, 84] and in electric birefringence experiments by Mori et al. [54]. It must be mentioned, though, that the depolarized scattering data in the above studies are quite poor due to the small optical anisotropy of PBLG. Moreover the measurements were done in one angle and the rotational diffusion coefficient was calculated from eq. using the translational diffusion value measured in the polarized geometry. This introduces an additional uncertainty since the in polarized scattering the cooperative diffusion coefficient is measured and it is questionable whether this should be used in eq. instead of the self diffusion coefficient.. To avoid such error the depolarized correlation function should be measured in several angles and then D_R must be obtained from an extrapolation of Γ_{VH} to $q = 0$.

Sato and Teramoto [63] compared these data with the predictions of the fuzzy cylinder model (eq. 4.28); the data of Mori et al seem to agree with the fuzzy cylinder prediction whereas the D_R data of the other groups exhibit a more delayed decrease with concentration compared to eq. 4.28; the deviation being larger for the larger molecular weights.. In all these experiments the c^{-2} dependence is approached at about $100c^*$. Similar concentration dependence was observed by computer simulations by Bitsanis et al [70, 71] and Doi et al. [72]; the later agree better with the prediction of eq. 4.19 while the D_R data by Bitsanis et al exhibit a delayed decrease with c possibly due to an overenhanced transverse diffusivity. There are also some other studies on the rotational diffusion of rod-like viruses (M-13, Tobacco mosaic, fd-virus) [85, 86, ?, 87]and other biological macromolecules [88, 89]. Nakamura and Okano [87] observed by transient magnetic birefringence measurements in isotropic solutions of fd-virus ($L = 890nm$,

$l = 2200nm$) a steeper than c^{-2} decrease of the rotational diffusion. It was attributed to the pretransitional behavior ($\tau_R \sim c/(c^* - c)$) in the vicinity of the isotropic to nematic transition. These phenomenon was considered to be due to short-range order effects (of the order of L) and was explained quantitatively by a Landau-de Gennes type of approach.

The magnitude of D_R which is related with the parameter β in all equations for the rotational diffusion is found in all experiments to be larger than was expected by the DE theory (β ranges from 4×10^2 to 10^4) [82]. Teraoka et al. [60] estimated β from calculations of stochastic geometry and probability of entanglement for infinitely thin rods with the cage model and obtained $\beta = 1350$. The length dependence of D_R in the nondilute region is predicted by DE to be L^{-9} (eq. 4.11) while the measured dependences are $1/L^{7-8}$ [15, 86, ?, 54]. Note, however that these kind of dependence is difficult to be confirmed due to flexibility effects and the fact that most samples are polydisperse.

Viscosity measurements

The zero-shear viscosity measurements are much easier and also less sensitive in polydispersity or aggregation effects than the measurements of the transport properties; especially the depolarized light scattering measurements of D_R. The measurements of aqueous xanthan solutions [78, 63] revealed a very strong concentration dependence of η_o ($\sim c^{3-6}$) and a molecular weight dependence which may exceed the flexible power law dependence ($M^{3.4}$) for high molecular weights. Similar behavior of the viscosity has been observed in other stiff-chain polymer solutions [63]. Recently, the zero-shear viscosity was measured for several molecular weights of the semiflexible PHIC (with $L/l = 1.6 - 200$) at a wide concentration range [90]. For high molecular weights ($L/l > 20$) a power law dependence was followed $c \propto c^{3.6}M^4$, similar to flexible polymer (although with different exponents). The predictions of the "fuzzy cylinder" model could fit the viscosity data only for $L/l < 16$ indicating the limitations of this model.

4.2.5 Light Scattering in non-dilute solutions

As discussed in chapter 3 the calculation of the dynamic structure factor (eq. 3.29) of interacting polymer systems is difficult. Here we discuss the case of rigid rods (mentioned also in chapter 3) since there is no theory which calculates the dynamic structure factor for semiflexible wormlike chains in the dilute and concentrated region.

We should also mention the calculation of the polarized and depolarized dynamic structure factors for optically anisotropic, randomly oriented rigid rods in nondilute solutions by Zero and Pecora [15], where the translational rotational coupling, which is important at these concentrations, is taken into account in the diffusion equation by a coupling term proportional to $\Delta D = D_{\parallel} - D_{\perp}$. Neverthe-

less, in this theory both the intramolecular and intermolecular interference were neglected, allowing eq. 3.29 to simplify to

$$I_{if}(q,t) =< N >< \alpha_{if}(0)G_s(q,t)\alpha_{if}(t) > \tag{4.29}$$

with $G_s(q,t)$the Fourier transform of the probability function. These simplification enable the authors to express the polarized and depolarized correlation functions as a sum of exponentials. These relations hold only for small coupling parameter $\gamma = q^2\Delta D/D_R(< 10)$and then the characteristic times are so similar that is difficult to distinguish experimentally. Thus, both the neglect of interference terms and the magnitude of the separation of times makes this approach not useful for comparisons with experiments.

Mean field-RPA theories

The most complete, so far, theoretical approach for the static and dynamic structure factors of rodlike molecules in the semidilute and concentrated regime has been presented by Doi, Shimada and Okano (DSO) [91, 92, 93] and subsequently reformulated by Maeda [94, 95]. DSO first presented a general theory to calculate the static structure factor of concentrated solutions of stiff (wormlike) polymers [91] and then applied it to calculate the dynamic structure factor [92]. This theory is a mean-field, random phase approximation theory which is proven to be analytically exact for rodlike polymers and it thus it may work better than for flexible chains where it is less successful than scaling predictions. On the other hand, in contrast to flexible polymers, where in a good solvent the mean field predictions become better with increasing concentration, for rods the nematic transition limits the usage of the mean field treatment. In the last paper of this series [93] they apply the theory to investigate the spinodal decomposition of rigid rod solutions and the thermal fluctuations in the isotropic regime as the system approaches the transition to a liquid crystalline phase. These investigations take into account the rotation - translation coupling of the rod diffusion and various types of interactions, which can not be neglected in nondilute systems, such as excluded volume interactions, entanglement effects and hydrodynamic interaction to calculate the dynamic structure factor for the isotropic scattering $S(q,t)$. Maeda reformulated the DSO theory to calculate $S(q,t)$ at the entire q and t regime [94] and also to calculate the depolarized dynamic structure factor $S_{VH}(q,t)$ [95].

Some of the predictions of the model regarding the static light scattering could have been deduced from the classical Onsager theory and Zimm's description of light scattering [96]. The osmotic pressure modulus, $(\partial\pi/\partial c)_{T,P}$, for isotropic solutions of rodlike particles is:

$$\boxed{(\tfrac{M}{RT})(\partial\pi/\partial c)_{T,P} = 1 + 8\rho/\rho_n} \tag{4.30}$$

while the static structure factor was calculated up to q^4 order [91]:

$$\boxed{S(0)/S(q) = 1 + \xi^2 q^2 + \psi q^4} \tag{4.31}$$

It is shown that the nematic interaction does not affect the apparent correlation length ξ, in the q^2 term, but only the q^4 term. A very interesting finding is that ψ changes sign as concentration increases above ρ_{inv} so that at high qL a negative deviation from the linearity is expected for the plot of $S(0)/S(q)$ vs. q^2. For rodlike polymers it was found that $\rho_{inv} = (7/27)\rho_n$ while for wormlike polymers this concentration can be very large, $\rho_{inv} = 45/(4l\upsilon_1)$; υ_1 is a constant of the order of the chain diameter, representing the strength of the nematic potential [91].

If such deviations from linearity are neglected, then the concentration dependence of the correlation length ξ can be found (in the $q\xi < 1$ regime). In the rigid rod limit:

$$\boxed{\xi = (L/6)(1 + 8\rho/\rho_n)^{-1/2}} \tag{4.32}$$

For large concentrations $\rho/\rho_n \gg 1/8$ this leads to $\xi \approx \rho^{-1/2}$. In the limit of flexible chains DSO predicts $\xi^2 = Ll/[9(1+\rho L\upsilon_0)]$, which is the known RPA result for flexible polymer [4, 51] ($\xi \sim \rho^{-1/2}$) with υ_0 the excluded volume parameter. In the semidilute region, however, the later does not agree with experimental data, and a better prediction is given by scaling theory ($\xi \sim \rho^{-3/4}$).

An important conclusion is that there is no anomaly in the static structure factor as the nematic transition is approached [91]; ξ does not diverge in contrast to what is expected in the case phase separation in flexible polymer solution. These is an indication that the scalar order parameter (concentration) is irrelevant in the phase separation of liquid crystalline polymers; the coupling between orientation and concentration affects only the q^4 term.

DSO also calculates the dynamic structure factor in the semidilute and concentrated regime for the case of rodlike polymers [92, 93]. The coupling of the rotation with translation was taken into account by writing a proper kinetic equation for the number density, ρ, of the rods. DSO wrote a kinetic equation for the distribution function which accounts both for the translation and the rotation the rods. Although this describes the time evolution of a single particle distribution function, it can be used to calculate pair correlation functions by applying the fluctuation dissipation function. The intermolecular correlation is accounted for by the mean field potential. In the limit of small q's, $S(q,t)$ is described by a single exponential ($\sim exp(-q^2 D_c t)$ [92] with a cooperative diffusion coefficient (which could also be deduced using the Onsager theory if eqs. 4.30 and 2.7 are combined):

$$\boxed{D_c = (\tfrac{k_B T}{f_c})(1 + 8\rho/\rho_n)(1 - \phi)^2} \tag{4.33}$$

If the $(1-\phi)$ term is neglected, and more importantly the mobility $\frac{k_BT}{f_c}$ is assumed to follow the same behavior as the one that the DE theory predicts ($D_s = D_{\parallel}/3$, $D_{\perp} = 0$), then it is found that $D_c = \frac{1}{3}D_{\parallel}(1 + 8\rho/\rho_n)$. If this equation is valid in the whole concentration regime then at $\rho/\rho_n < 1/8$ the cooperative diffusion coefficient should decrease from its dilute region value of $2D_{\parallel}/3$ towards $D_{\parallel}/3$, but before reaching this it should start to increase linearly with concentration and reach a value by factor of 9/2 larger than its dilute solution value. The 9 is a result of the thermodynamic driving force whereas the 2 from the increase of the friction. Small decreases in D_c, which are not associated with bad solvent conditions and aggregation, have been observed experimentally is few experiments in low concentrations [96, 47] but are in general are almost within experimental error and thus are difficult to be established.

For the high q's only the initial decay rate of the structure factor can be calculated [92]; it is given as a power series of the scattering vector q:

$$\Gamma_{iso}^{init}/q^2 = (\frac{k_BT}{f_c})(1 + 8\rho/\rho_n)[1 + B(\rho)(qL)^2] \tag{4.34}$$

where

$$B(\rho) = \frac{D_RL^2}{1080D_s} - \frac{(D_{\parallel} - D_{\perp})}{135D_s} - \frac{2\rho/\rho_n}{9(1 + 8\rho/\rho_n)} \tag{4.35}$$

For small concentrations, $B(\rho)$ is positive as it should be to account for the effects of the rotational motion which have already been described for the case of rods in dilute solutions. The usage of the dilute regime diffusion coefficients of rods results in:

$$B(\rho) = \frac{1}{36}[\frac{1}{10} - \frac{8\rho/\rho_n}{1 + 8\rho/\rho_n}] \tag{4.36}$$

which agrees with the prefactor of the q^2 term in the dilute region mentioned above (eqs.??). At higher concentrations, where $D_RL^2 \ll D_s$, the factor $B(\rho)$ takes negative values:

$$B(c) = -\frac{1}{9}[\frac{1}{5} + \frac{2\rho/\rho_n}{1 + 8\rho/\rho_n}] \tag{4.37}$$

This means that at high qL the apparent diffusion coefficient is predicted to be smaller than at low qL. This reflects the increased importance of local motions of individual rods in relaxing the correlation function; these motions are not subject to long-range driving forces such as the osmotic modulus which is measure in the macroscopic limit, at low qL. The change of sign of $B(\rho)$ happens for two reasons:

a) The decrease of the ratio D_R/D_s with concentration, due to entanglement interactions.

b) The last term of eqs. 4.35 which increases with concentration and represents the excluded volume interactions.

In addition to the initial decay rate DSO predicts the shape of the correlation function [1] for systems near the isotropic to nematic phase transition. In the small-angle, macroscopic limit, a double exponential for the isotropic correlation function is predicted [93]:

$$S(q,t) = A_1 e^{-\Gamma_1 \tau} + A_2 e^{-\Gamma_2 \tau} \tag{4.38}$$

with decay times $\Gamma_1 = (D_\parallel q^2/3)(1+8\rho/\rho_n)(1+\frac{4}{15}\beta)$, $\Gamma_2 = (D_\parallel q^2/3)(1+8\rho/\rho_n)(1+\frac{4}{15}\alpha)$and concentration dependent amplitudes A_1, A_2. The fast mode becomes faster with concentration, while its amplitude increases and the slow mode becomes weaker and slower. The two relaxation modes are diffusive and both describe the relaxation of the concentration fluctuations and are attributed to the coupling with orientation fluctuations which becomes more important as the system approaches the isotropic to nematic transition.

The fast mode is attributed to relaxing the concentration fluctuations without changing the orientation and gains amplitude while it becomes faster as the concentration increases. This is because with increasing concentration thermodynamic (or even purely steric) reasons make regions with increased orientation more stable, and consequently concentration fluctuations relax predominantly through axial diffusion (which is uncoupled to orientational relaxation).

The slow mode on the other hand corresponds to a relaxation which also changes the orientation of the rods, thus a mode where the coupling is dominant. This becomes slower and weaker as the concentration is increased [1].

It must be noted that the DSO theory considers optically isotropic rods and thus the change of orientation of the particles can be observed only indirectly through its coupling with the concentration fluctuations. Since in this approach both modes describe the behavior of the dynamic structure factor in the macroscopic limit (low qL), no q-dependence of their amplitudes is given. The decay rate of the fast mode follows very closely the concentration dependence of the initial decay rate.

Maeda reformulated the DSO theory to calculate the dynamic structure factor at the entire q and t regime [94] as well as to calculate the VH dynamic structure factor [95]. He introduced a q-dependent second virial coefficient, $A(qL,c)$ to account for the inability of the excluded volume interactions to couple efficiently to the short-range motions of the rods which can be observed at high qL by light scattering. Maeda's theory is a natural extension of two previous theories; the theory of light scattering of dilute solutions of rigid rods, which is valid for arbitrary q and t but only at $c = 0$, and the theory of the concentration dependence of the mutual diffusion which is valid only for $q = 0$ and $t = 0$. The quantity $A(qL,c)$ is a generalization of the repulsive thermodynamic term $(1+2A_2Mc+...)$,and explains the angular dependence of k_D, as will be explained

later. The dynamic structure factors were written in a matrix representation, which allowed the evaluation in the entire q and t regime. The initial decay rates calculated by the above theory are [94, 95]:

$$\Gamma_{VV}^{init} = [D_0 + (L^2/12)D_R f_1(qL) - (D_{\parallel} - D_{\perp})(1 - f_2(qL)]\ q^2\ A(qL, c) \quad (4.39)$$

$$\Gamma_{VH}^{init} = [D_{\perp} q^2 + D_R f_1^*(qL, \vartheta) + (D_{\parallel} - D_{\perp}) q^2 f_2^*(qL, \vartheta)]\ A^*(qL, c, \vartheta) \quad (4.40)$$

where f_1, f_2, f_1^*, f_2^* are weight factors and $A(qL, c)$ and $A^*(qL, c, \vartheta)$ the excluded volume terms. $D_{||}$ and $D_{\perp}$ denote the coefficients for diffusion parallel and normal to the rod axis respectively and as mentioned above, in the framework of DSO are treated as adjustables.

The quantities A and A^* express the ratio of the value of the VV and VH initial decay rates to their values at zero concentration, if we neglect the concentration dependence of the diffusion coefficients. The f weight factors for the isotropic decay rate have the limiting behavior: $f_1(qL) \rightarrow 0$ and $f_2(qL) \rightarrow \frac{1}{3}$ for $qL \rightarrow 0$, $f_1(qL) \rightarrow 1$ and $f_2(qL) \rightarrow 0$ for $qL \rightarrow \infty$ while $A(qL, c)$ is increasing with c and equals to one at $c \rightarrow 0$. So at the high qL limit, $\Gamma_{VV}^{init}/q^2 = D_{\perp} + (L^2/12)D_R$, which means that concentration fluctuations relax only through translation perpedicular to rod axis as well as through rotation. Of course this is reasonable since at high qL when one segment of the rod is moving a distance $2\pi/q$ along the rod axis another indentical segment will replace the first, so that there is neither a dephasing nor a change of the amplitude of the scattered light. The concentration dependence of the excluded volume parameter, for a constant value of qL, is almost linear. Maeda also concluded that due its form, the mean field interaction potential affects only the spatially long and temporarily slow modes of fluctuations in the solution.

The concentration dependence of the mutual diffusion coefficient at high concentration solutions depends on the concentration dependence and the relative magnitude of $2A_2(qL)M$ (the thermodynamic term) and of the frictional term. For $qL < 1$ the increase of the excluded volume factor $A(qL, c)$ with concentration exceeds the decrease of the self diffusion coefficients, so that the mutual diffusion coefficient $D_m(c)$ increases. However, for larger qL it is predicted that the increase of $A(qL, c)$ is weaker and thus the measured apparent mutual diffusion coefficient $\Gamma_{iso}^{init}/q^2 = D_m(c)$may decrease with concentration.

The calculation of the depolarized dynamic structure factor $S_{VH}(q, t)$and its initial decay rate (eqs. 4.40) reveals that the excluded volume interaction causes a decrease of the decay rate Γ_{VH}^{init}, in contrast to the isotropic scattering. This is due to a decrease of the excluded volume factor $A^*(qL, c, \vartheta)$; the effect is larger at low scattering angles. The apparent rotational diffusion coefficient $\Gamma_{VH}^{init}/\ f_1(qL, \vartheta)$ has the following limiting behavior:

$\Gamma_{VH}^{init}/\ f_1(qL,\vartheta) = D_r A^*(qL,c,\vartheta)$, for $qL \to 0$ and
$\Gamma_{VH}^{init}/\ f_1(qL,\vartheta) = [(L^2/12)D_\perp + D_R]A^*(qL,c,\vartheta)$, for $qL \to \infty$ and $\theta \to \pi$.

The latter is similar to the VV case at high qL limit. Only those rods that are perpendicular to the scattering wavevector q correspond to the scattering intensity, while their parallel translation does not contribute to the intensity fluctuation of the scattered light. Nevertheless, for intermediate values of qL and if the DE conjecture for the self-diffusivities. of rods holds ($D_\parallel \simeq D_{\parallel,0}$, $D_\perp \simeq 0$ and $D_R \simeq BD_{R,0}(\rho^*/\rho)^2$), the lengthwise term may dominate when the parallel diffusion coefficient is much larger than the other two.

It can been shown that the depolarized correlation function predicted by Maeda becomes identical to Zero-Pecora expression [15] in the limit $qL \to 0$ and $c \to 0$.

4.2.6 Light scattering experiments on stiff polymer solutions

Polarized scattering-Cooperative diffusion

There is a quite large number of experimental studies of the dynamics of rodlike and stiff polymer solutions by polarized dynamic light scattering. Both biological molecules, like DNA, Tobacco mosaic virus, fd-virus, xanthan and synthetic polymers like PBLG and PHIC have been used. The information from the dynamic studies concern both the number and origin of the relaxation processes and the concentration dependence of the diffusion coefficients.

In most of these polarized PCS experiments there are more than one modes from which one is attributed to the cooperative diffusion. The concentration dependence of the cooperative diffusion in solutions of stiff polymers in the semidilute region has been measured in several systems and in most cases is found to increase with concentration under good solvent conditions [96, 47, 80, 97, 49, 98]. In some cases D_c is found to be constant with c [99, 15, 100]. According to DSO, a c^1 dependence of $D_c/D_0 - 1$ and a slope of $8/\rho_n$ of D_c with c (eq. 4.33), should be found.

Delong and Russo [96] in their study of rodlike and stiff PBLG samples found four relaxation motions in the polarized correlation functions; the two of which were attributed to the cooperative modes predicted by DSO. Their initial decay rate exhibits a q-dependence similar with the predicted by DSO (eq. 4.34) and a linear increase with concentration in accordance with eq. 4.33. The origin of an ultra slow and of a fast mode were unclear. A linear c-dependence of the cooperative diffusion was also found by Bu et al. [101] in PBLG solutions and Seils and Pecora for DNA solutions [97]. The later actually find that only $D_c/D_0 - 1$ scales almost linearly with c in the total concentration region. Nevertheless, weaker increases with concentration (about 0.5-0.6) [98, 80] have also been found in experimental studies of other stiff molecules. Even in the cases were a c^1

was observed, the slope found was smaller than the $8/\rho_n$ prediction [96, 49, 47]. It must be reminded however, that in the derivation of eq. 4.34 the strong assumptions of DE theory for the translational diffusion coefficients were used. As we already discussed previously, in real systems it is not expected that $D_\perp = 0$ and $D_\parallel = D_{\parallel,0}$.

Depolarized scattering

Few depolarized studies of the orientation fluctuations existed so far in stiff polymer systems mainly due to the lack of model molecules with large inherent optical anisotropy [2, 1]. Thus there is very limited knowledge on the shape of the orientational structure factor and its concentration dependence in systems of rigid and semirigid rods. Actually, the investigations of the orientational dynamics, which are of primary interest in such anisotropic molecules were conducted more by electric birefringence and less by PCS experiments [86, 54, 15, 100], due to the small optical anisotropy of these systems, resulting in difficult, and sometimes ambiguous measurements. Advances in macromolecular chemistry have led to the synthesis of well-defined poly(p-phenylenes), PPP, with aliphatic side chains, with varying molecular weights and much higher optical anisotropy compared to other molecules [102, 103, 104].

Recently, there has been some activity in this direction, mostly with stiff biological macromolecules, such as DNA [97], tobacco mosaic virus [105], and F-actin [106, 100], using static and dynamic light scattering but most of the biological molecules, although very rigid, introduce further difficulties due to the presence of charges. In their study Drögemeier and Eimer presented good VH correlation functions from solutions of F-actin which could be fitted well by the dynamic structure factor of predicted by Maeda [95] for small molecular weights. On the other hand the larger molecular weights revealed significantly faster decays than the predicted; this was attributed to internal bending motions. In the semidilute regime these workers observe a slower mode increasing with concentration. No concentration dependecnce of the rotational diffusion was given.

Slow modes

In most of the investigations of concentrated solutions of both flexible (especially polyelectrolytes in low ionic strength) and rodlike polymers, the light scattering intensity correlation function shows slow modes. Researchers have explained these modes as polydispersity induced self-diffusion [39, 107] or attributed them to the presence of clusters or loose aggregates [80, 49, 107, 97,] or to the presence of gel-like phase [108]. The question of the slow modes is still open; it is possible though, that the there are multiple causes for the slow modes in the different types of systems studied. As mentioned above, DSO has predicted a slow mode in the vicinity of the isotropic to nematic transition the behavior of which is identified

with one of the slow modes found by DeLong and Russo [96] in solutions of PBLG. Tracy and Pecora [2] point out that the "transient aggregate' discussed by several authors [80, 109], appears similar to the entity that gives rise to the slow mode of DSO theory near the transition. However the theory does not give quantitative agreement with experiment.

References

[1] S.P Russo. *Dynamic Light Scattering: The Technique and Some Applications*, page 512. Oxford Science Publications, 1993.

[2] M.A. Tracy and R. Pecora. *Annu. Rev. Phys. Chem.*, 43:525, 1992.

[3] K. Zero and R. Pecora. *Dynamic Light Scattering, Applications of Photon Correlation Spectroscopy*, page 59. Plenum Press, New York and London, 1985.

[4] M. Doi and S.F. Edwards. *The Theory of Polymer Dynamics.* Oxford University Press, New York, 1986.

[5] K. Kubota, H. Urabe, Y. Tominaga, and Fujime S. *Macromolecules*, 17:2096, 1984.

[6] J. Wilcoxon and J.M. Schurr. *Biopolymers*, 22:849, 1983.

[7] S. Broesma. *J. Chem. Phys.*, 32:1626, 1960.

[8] S. Broesma. *J. Chem. Phys.*, 74:6989, 1981.

[9] J.G. de la Torre, M.M. Tirado, and C.L. Martinez. *J. Chem. Phys.*, 23:611, 1984.

[10] W. Eimer and R. Pecora. *J. Chem. Phys.*, 94:2324, 1991.

[11] R.M. Venable and R.W. Pastor. *Biopolymers*, 27:1001, 1988.

[12] T.A. King, A. Knox, and J.D.G. McAdam. *Biopolymers*, 12:1917, 1973.

[13] D.W. Schaefer, G.B. Benedek, P. Schofield, and E. Bradford. *J. Chem. Phys.*, 55:3884, 1970.

[14] C.R. Crosby, N.C. Ford, F.E. Karasz, and K.H. Langley. *J. Chem. Phys.*, 75:4298, 1981.

[15] K. Zero and R. Pecora. *Macromolecules*, 15:87, 1982.

[16] C.C.-C. Han and H. Yu. *J. Chem. Phys.*, 61:2650, 1974.

[17] J.B. Berne and R. Pecora. *Dynamic Light Scattering.* Willey Interscience Publications, New York, 1976.

[18] S.R. Aragon and R. Pecora. *J. Chem. Phys.*, 82:5346, 1985.

[19] W. Eimer, J.R. Williamson, S.G. Boxer, and R. Pecora. *Biochemistry*, 29:799, 1990.

[20] J.M. Rallison and L.G. Leal. *J. Chem. Phys.*, 74:4819, 1981.

[21] T. Maeda and S. Fujime. *Macromolecules*, 17:1157, 1984.

[22] T. Maeda and S. Fujime. *Macromolecules*, 17:2381, 1984.

[23] F.R. Hallet, B. Nickel, and T. Craig. *Biopolymers*, 24:947, 1985.

[24] K.S. Schmitz. *Dynamic Light Scattering by Macromolecules.* Academic Press, London, 1990.

[25] M. Schmidt and W.H. Stockmayer. *Macromolecules*, 17:509, 1984.

[26] J.M. Schurr. *Biopolymers*, 22:2207, 1983.

[27] L. Harnau, R.G. Winkler, and P. Reineker. *J. Chem. Phys.*, 104:6355, 1996.

[28] L. Song and J.M. Schurr. *Biopolymers*, 30:229, 1990.

[29] J.E. Hearst and W.H. Stockmayer. *J. Chem. Phys.*, 7:1425, 1962.

[30] H. Yamakawa and M. Fujii. *Macromolecules*, 6:407, 1973.

[31] P. J. Hagerman and B. H. Zimm. *Biopolymers*, 20:1481, 1981.

[32] S.S. Sorlie and R. Pecora. *Macromolecules*, 23:487, 1990.

[33] P.J. Hagerman. *Biopolymers*, 20:1503, 1981.

[34] P.J. Hagerman. *Biopolymers*, 22:811, 1983.

[35] R.J. Lewis, R. Pecora, and D. Eden. *Macromolecules*, 19:134, 1986.

[36] S.A. Allison. *Macromolecules*, 24:530, 1991.

[37] R.A. Harris and J.E. Hearst. *J. Chem. Phys.*, 44:2592, 1966.

[38] T. Maeda and S. Fujime. *Macromolecules*, 18:2430, 1985.

[39] S. Fujime, M. Takasaki-Ohsita, and T. Maeda. *Macromolecules*, 20:1292, 1987.

[40] S.R. Aragon and R. Pecora. *Macromolecules*, 18:1868, 1985.

[41] B.H. Rouse. *J. Chem. Phys.*, 14:164, 1946.

[42] L.S. Onsager. *Ann. N.Y. Acad. Sci.*, 51:627, 1949.

[43] A. Ishihara and T. Hayashida. *J. Phys. Soc. Japan.*, 6:40, 1951.

[44] P. van der Schoot and T. Odijk. *J. Chem. Phys.*, 97:515, 1992.

[45] T. Sato, Y. Jinbo, and A. Teramoto. *Macromolecules*, 27:6080, 1994.

[46] J.M. Peterson. *J. Chem. Phys.*, 40:2680, 1964.

[47] M.A. Tracy and R. Pecora. *Macromolecules*, 25:337, 1992.

[48] K. Kubota, Y. Tominaga, and Fujime S. *Macromolecules*, 19:1604, 1986.

[49] H.Tj. Goinga and R. Pecora. *Macromolecules*, 24:6128, 1991.

[50] M. Doi and S.F. Edwards. *J. Chem. Soc. Faraday Trans. II*, 74:560, 1978.

[51] P.G. de Gennes. *Scaling Concepts in Polymer Physics.* Cornell University Press, Ithaca, 1979.

[52] J.P. Maguire, M.C. Tague, and Rondelez. *Phys. Rev. Letters*, 45:1981, 1980.

[53] J.A. Odell, E.D.T. Atkins, and A. Keller. *Journal of Polymer Science:Polymer Letters Edition*, 21:289, 1983.

[54] Y. Mori, N. Ookubo, R. Hayakawa, and Y. Wada. *Journal of Polymer Science:Polymer Physics Edition*, 20:2111, 1982.

[55] K. Kubota and B. Chu. *Macromolecules*, 16:105, 1983.

[56] T. Sato and A. Teramoto. *Macromolecules*, 24:193, 1991.

[57] S.F. Edwards and K.E. Evans. *J. Chem. Soc. Faraday Trans. II*, 78:113, 1982.

[58] M. Doi. *Journal of Polymer Science:Polymer Symposium*, 73:93, 1985.

[59] G.T. Keep and R. Pecora. *Macromolecules*, 18:1167, 1985.

[60] I. Teraoka, N. Ookubo, and R.J. Hayakawa. *Phys. Rev. Letters*, 55:2712, 1985.

[61] S.F. Edwards and K.E. Evans. *Trans.Faraday Soc.*, 78:113, 1982.

[62] G.T. Keep and R. Pecora. *Macromolecules*, 21:817, 1988.

[63] T. Sato and A. Teramoto. *Adv. Pol. Sci.*, 126:85, 1996.

[64] I. Teraoka and R.J. Hayakawa. *J. Chem. Phys.*, 89:6989, 1988.

[65] I. Teraoka and R.J. Hayakawa. *J. Chem. Phys.*, 91:2643, 1989.

[66] M. Fixman. *Phys. Rev. Letters*, 54:337, 1985.

[67] M. Fixman. *Phys. Rev. Letters*, 55:2429, 1985.

[68] G. Szamel. *Phys. Rev. Letters*, 70:3744, 1993.

[69] G. Szamel and S. Schweizer. *J. Chem. Phys.*, 100:3127, 1994.

[70] I. Bitsanis, H.T. Davis, and M. Tirrell. *Macromolecules*, 21:2824, 1988.

[71] I. Bitsanis, H.T. Davis, and M. Tirrell. *Macromolecules*, 23:1157, 1990.

[72] M. Doi, I. Yamamoto, and F. Kano. *J. Phys. Soc. Japan.*, 53:3000, 1984.

[73] T. Odijk. *Macromolecules*, 16:1340, 1983.

[74] T Odijk. *Macromolecules*, 17:502, 1984.

[75] A.N. Semenov. *J. Chem. Phys.*, 82:317, 1986.

[76] B. Tinland, G. Maret, and M. Rinaudo. *Macromolecules*, 23:596, 1990.

[77] T. Sato, Y. Takada, and A. Teramoto. *Macromolecules*, 24:6262, 1991.

[78] Y. Takada, T. Sato, and A. Teramoto. *Macromolecules*, 24:6215, 1991.

[79] B.A. Scalettar, J.E. Hearst, and M.P. Klein. *Macromolecules*, 22:4550, 1989.

[80] L. Wang, M. M. Garner, and H. Yu. *Macromolecules*, 24:2368, 1991.

[81] M.B. Mustafa, D.L. Tipton, P.S. Russo, M.D. Barkley, and F.B. Blum. *Macromolecules*, 26:370, 1993.

[82] R. Pecora. *Journal of Polymer Science: Polymer Symposium*, 73:83, 1985.

[83] K. Kubota and B. Chu. *Biopolymers*, 22:1461, 1983.

[84] D. Statman and B. Chu. *Macromolecules*, 17:1537, 1984.

[85] J.M. Schurr and K.S. Schmitz. *Biopolymers*, 12:1021, 1973.

[86] J.F. Maguire, J.P. McTague, and F. Rondelez. *Phys. Rev. Letters*, 45:1891, 1980.

[87] H. Nakamura and K. Okano. *Phys. Rev. Letters*, 50:187, 1983.

[88] S. Highsmith, C-C. Wang, R. Pecora, and Jardetzky O. *Biochemistry*, 21:1192, 1982.

[89] A. Patkowski, W. Eimer, and Dorfm'

[90] A. Ohshima, H. Kudo, T. Sato, and A. Teramoto. 28:6095, 1995.

[91] T. Shimada, M. Doi, and K. Okano. *J. Chem. Phys.*, 88:2815, 1988.

[92] M. Doi, T. Shimada, and K. Okano. *J. Chem. Phys.*, 88:4070, 1988.

[93] T. Shimada, M. Doi, and K. Okano. *J. Chem. Phys.*, 88:7181, 1988.

[94] T. Maeda. *Macromolecules*, 22:1881, 1989.

[95] T. Maeda. *Macromolecules*, 23:1464, 1990.

[96] L. M. DeLong and P. S. Russo. *Macromolecules*, 24:6139, 1991.

[97] J. Seils and R. Pecora. *Macromolecules*, 28:661, 1995.

[98] T. Coviello, W. Burchard, M. Dentini, and V. Crescenzi. *Macromolecules*, 20:1102, 1987.

[99] Z. Bu and P.S. Russo. *Macromolecules*, 27:1187, 1994.

[100] J. Drogemeier and W. Eimer. *Macromolecules*, 27:96, 1994.

[101] Z. Bu, P.S. Russo, D.L. Tipton, and I.I. Negulescu. *Macromolecules*, 27:6871, 1994.

[102] J.K. Kallitsis, G. Wegner, and T. Pakula. *Makromol. Chem.*, 193:1031, 1992.

[103] U. Tiesler, T. Pulina, M. Rehahn, and M. Ballauff. 243:299, 1994.

[104] S. Vanhee, R. Rulkens, U. Lehmann, C. Rosenauer, M. Schulze, W. Koehler, and G. Wegner. *Macromolecules*, 29:5136, 1996.

[105] S. Fraden, G. Maret, and D.L.D. Caspar. *Phys. Rev. E*, 48:2816, 1993.

[106] J. Drogemeier, H. Hinssen, and W. Eimer. *Macromolecules*, 27:87, 1994.

[107] J. Buitenhuis, J.K.G. Dhont, and H.N.W. Lekkerkerker. *Macromolecules*, 27:7267, 1994.

[108] M.G. Fried and V.A. Bloomfield. *Biopolymers*, 23:2141, 1984.

[109] K.S. Schmitz and M. Lu. *Biopolymers*, 23:797, 1984.

Chapter 5

Experimental Techniques

The main experimental techniques used is Photon Correlation Spectroscopy (PCS) and Fabry-Perot Interferometry (FPI); the former for study the dynamics of polymer solutions and the latter for the determination of the chain conformation. For the study of the molecular orientation of stretched films we used the technique of Raman Scattering, together with Infrared Absorption and X-Ray Scattering. Moreover, in the study of the dynamics of rodlike polymer solutions, complementary to PCS, we used Pulse-Field Gradient NMR (PFG-NMR) and viscosity measurements. Below we describe the main techniques used i.e., PCS, FPI and Raman scattering and NMR while a brief description of the others is given in the relative chapters.

5.1 Photon Correlation Spectroscopy (PCS)

The autocorrelation function of the scattered light intensity is measured by Photon Correlation Spectroscopy in the homodyne geometry [1] (see also chapter 3). The PCS technique is also called dynamic light scattering because it relates the scattering of light with the dynamics (or relaxation phenomena) of the scattering medium. This is accomplished by correlating the scattering intensity, measured by a photomultiplier (PMT) which is a square law detector.

5.1.1 Correlator

The main component of the PCS, besides the optical scattering set up is the correlator which is an instrument (a electronic board) capable of obtaining the correlation function of an electrical signal [2]. The fundamental operations of a digital correlator are:

(1) counting the photoelectron pulses, $n(t)$, over *sampling time intervals* of width, t_s, during the real time, t , of the experiment,

(2) delaying these samples for some integer multiple of t_s, the *lag time* $\tau = kt_s$,

(3) multiplying direct and delayed data samples,

(4) summing these products

In this way it calculates the average of $n(q,t+\tau)n(q,t)$ during the total accumulation time of the experiment, for several values of τ (determined by the correlator channels). In practice, the theoretical autocorrelation function of measured photons,

$$G(\tau) =< n(t+\tau)n(t) >= \lim_{T\to\infty} \frac{1}{2T} \int_{-T}^{T} n(t+\tau)n(t)dt \tag{5.1}$$

is approximated by the temporally discrete function

$$G(kt_s) = \sum_{i=0}^{N-1} n_i n_{i+k} \tag{5.2}$$

where n_i is the number of photons measured in the ith t_s interval of the experiment. Actually what is given as an output by the correlator is the normalized correlation function:

$$g(q,t) =< n(q,t)n(q,0) > / < |n(q,0)| >^2 \tag{5.3}$$

It must be noted that the time autocorrelation function of photon counting data, $G(q,t)$, which is directly measured by the correlator, is equal to the autocorrelation function of the scattered intensity (*equality of photon correlation and intensity correlation*) [3].

In order to be able to measure several decays of characteristic relaxation times, modern correlators use a logarithmic lag time spacing. This requires the width of the sampling interval t_s to be increased in proportion to the lag time. In our experiments we used an ALV-5000/E multiple Tau digital correlator. In its normal version it uses 288 channels to measure correlation functions over the time range from 10^{-6} to about $10^3 s$. An additional fast card enables measurements of faster relaxation processes; using totally 320 channels, correlation functions over the time range from 10^{-7} to $10^3 s$ can be measured.

5.1.2 Optical set-up

The dynamic light scattering measurements were done using two different experimental set-up. In fig. 5.1 we show a schematic of the goniometer set up where we can measure at scattering angles from 11^o to 150^o. A fixed angle, home made, PCS set-up was also used, mainly for temperatures higher than 50^oC or when angular dependent study is not needed; a schematic is shown in fig. 5.2.

The polarization of the incident and the scattered beam, is determined by two Glan-Thomson (Halle, Berlin) polarizers ($P1$ and $P2$) of extinction ratio 10^{-6} and 10^{-7} respectively. In our experiments the incident polarization is always vertical to the scattering plane (V), while the analyzer ($P2$) in the scattered beam can be rotated, so that, we either measure the vertically (V) or the horizontally (H), polarized part of the scattered radiation. In this way the polarized, $I_{VV}(q)$, and the depolarized, $I_{VH}(q)$, scattered intensities are detected.

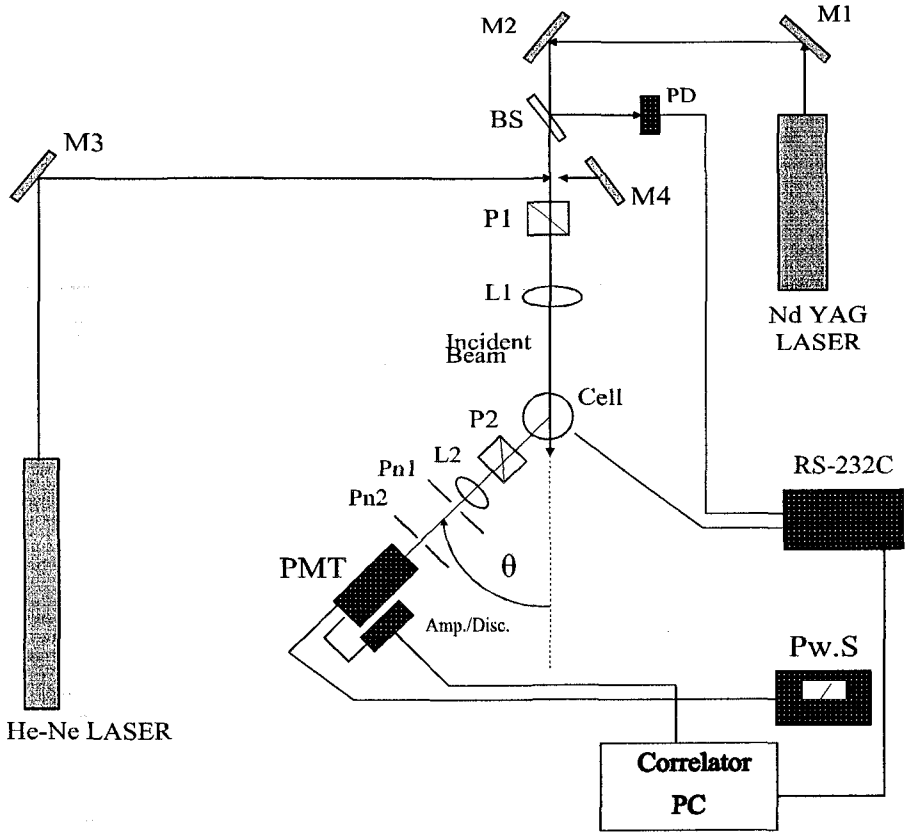

Figure 5.1: Goniometer Light Scattering Apparatus.

The goniometer set-up (fig. 5.1) consists of an automated ALV goniometer which uses as light source an Nd:YAG diode pumped air-cooled laser (Adlas DPY 315 II) with a single mode beam with wavelength of $\lambda = 532\ nm$ (frequency doubled) and maximum intensity $> 100\ mW$. The beam diameter is $0.32mm$ (Gaussian beam diameter of TEM_{00} mode) while the power used in our experiments was set to approximately 80 mW for stability reasons. The incident beam is focused in the sample with the use of an achromat lens ($L1$) with F=200 mm focal length. Both the intensity and the position of the incident beam are

monitored by a set of four photodiodes (PD). The sample cell, an optical quality glass tube of o.d. 10 mm, is placed in a liquid bath (Cell) which contains an index matching fluid (in our case toluene) to avoid reflections at the sample cell glass; in this way measurements at high (150^o) and especially at low angles ($11^o - 30^o$) are not affected by stray light. The scattered intensity is collected by the detector optics which utilizes a 2F/2F system i.e., a lens ($L2$) positioned in a distance 2F from the scattering volume and also form the last pinhole before the PMT ($Pn2$). A set of two pinholes (either 0.2 or 0.4 mm have been used) ($Pn1$ and $Pn2$) are used in front of the PMT (THORN EMI) to determine the scattering volume. The temperature of the bath, and consequently of the sample was regulated by circulation of a thermostated liquid (a mixture of water and glycol was used) with the use of a thermostat. The temperature was measured in the liquid bath by a thermocouple (ALV/Pt-100). The range of temperatures used in the goniometer set up was from 10 to 50^oC. All the functions of the goniometer were controlled by a PC with the help of the Bus Controller $RS - 232C$. In the goniometer set up we use the ALV-5000/E correlator with the additional fast correlator card. In the goniometer set-up a He-Ne Laser with a 633 nm wavelength and an intensity of 20 mW , was also used alternatively, to check the effect of the wavelength in some phenomena which are related to absorption.

The fixed angle set up (fig. 5.2) uses an Ar^+ laser light source (Spectra Physics Model 2020), usually a single line with wavelength of $\lambda = 488nm$ with an intensity of 300 mW. With this set up we can measure the intensity autocorrelation function simultaneously at two of the fixed scattering angles of the apparatus (45^o, 90^o and 135^o). For these angles the scattered beam is collected either by the convectional pinhole set up, or using a monomode fiber optics probe. In the first case two pinholes (from 0.2 to 0.4 mm diameter) ($Pn1$ and $Pn2$) are used in a distance of about 20 cm from each other to determine the scattering volume in the sample cell. The sample cell is placed in a electrically heated oven ($Hcell$) with working temperature ranging from 25^oC (room temperature) to 200^oC. Of course for the polymer solutions the upper temperature used is only around 80^oC. Again Glan-Thomson polarizers (were used in the incident and scattered beam ($P1$ and $P2$) and an achromat lenses (30 mm focusing length) ($L1$) was used to focus the incident beam in the cell. In the case of that a fiber optic detection unit was used, the scattered beam was collected into the fiber with a microlence (ML).

5.1.3 Coherence Area

The measured in a homodyne PCS experiment normalized autocorrelation function $g(q,t)$ of the scattering intensity is given by the Siegert relation [1, 3]:

$$\boxed{g(q,t) = 1 + f^* \left|\alpha\, C(q,t)\right|^2} \tag{5.4}$$

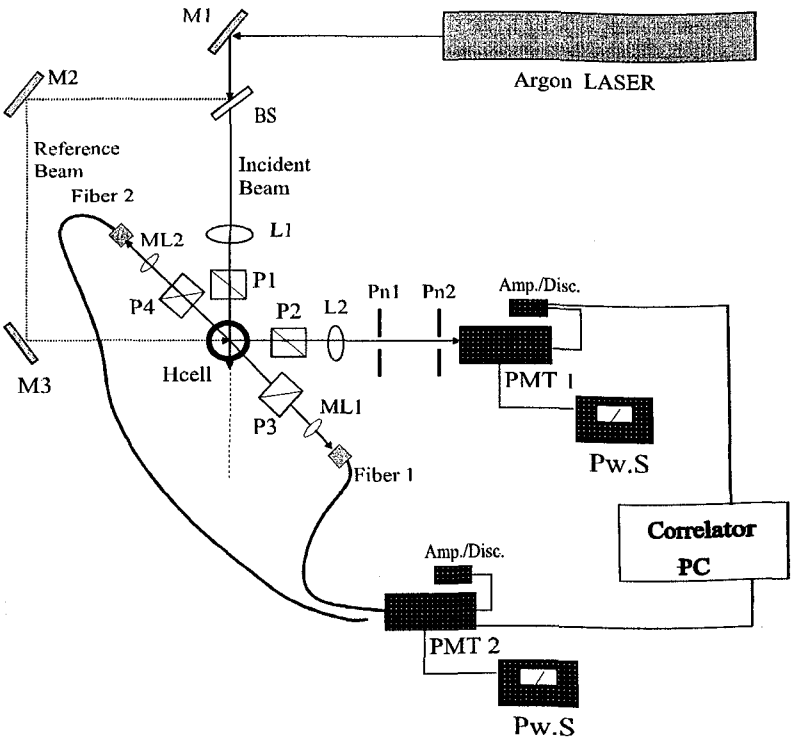

Figure 5.2: Fixed angle PCS set-up.

where f^* is an experimental instrument factor calculated by means of a standard. The constant f^* is related with the size of the scattering volume which is determined by the size of the pinholes collecting the scattered light, and with the coherence area. The coherence area is defined as the area from which all scattered photons measured on the detector's surface have the some phase. If the scattering volume (of radius α) or the distance, R, of the detector (of radius b) are large the photons coming from different parts of the scattering area will follow a different path length and thus will arrive in the detector out of phase. The fluctuations of the intensity in such a set-up will be the same as they would be at a point if the detector area is one coherence area, A_{coh}, or less where [2]:

$$A_{coh} = \pi b^2 = \frac{\lambda^2 R^2}{\pi a^2} \tag{5.5}$$

with λ being the wavelength of light. If the scattering volume has a radius a so that the scattering area πa^2 is larger than one coherence area then the PMT detects smaller fluctuations in the scattered intensity, since a larger area is observed. As the intensity fluctuations decrease (while the total intensity increases) less dynamic information from the scattering medium is detected since

the photons measured at the detector are no longer dephased only due to the fluctuations of the medium (for example motions of polymer chains) but also simply due to different distance that they cover. The result on the correlation function is a decrease of $g(q,0)-1$, from the maximum value of 1 to a value equal to f^*, in the case that $\alpha = 1$ i.e., all the scattering intensity has dynamics in the correlator's window. Based on the above we can calculate f^*, using a polymer solution with one dynamic process originating from the polymer molecules, which is inside the correlator's window. For this reason a dilute polystyrene solution in toluene is used and the factor f^* is calculated according to:

$$f^* = \frac{A}{(1-(1-\phi)I_{tol}/I_{pstol})^2} \tag{5.6}$$

where A $(= g(q,0)$) is the amplitude (contrast) of $g(q,t)$ from the standard solution (PS in toluene), I_{tol}, the scattering intensity of pure toluene, I_{pstol} the scattering intensity of the standard solution and ϕ the volume fraction of the polymer (PS) in the standard solution. The above holds simply because in the standard solution that we use all the intensity due to the polymer is inside the correlator's window and thus $\alpha = I_{ps}/I_{pstol} = (1-(1-\phi)I_{tol}/I_{pstol})$.

5.1.4 Analysis of the correlation function

Whenever possible, the analysis of the field correlation function, $C(q,t)$, was carried out by performing the inverse "Laplace transform" (ILT), using the program CONTIN [4, 5]. This method assumes that $C(q,t)$ is represented by a superposition of exponentials

$$\boxed{\alpha C(q,t) = \int_{-\infty}^{+\infty} L(\ln\tau)\exp(-t/\tau)d(\ln\tau)} \tag{5.7}$$

which describes a continuous spectrum of relaxation times $L(\ln\tau)$ which is actually the *distribution of relaxation times*. $L(\ln\tau)$ is used to determine the average characteristic relaxation times, τ, from the peak positions of the distribution, as well as the intensity of each relaxation process from the area under the corresponding peak. The inversion of an experimental $C(t_i)$ according to eq. 5.7 to get a general distribution function $w(\tau)$ (in our case $L(\ln\tau)$ because the data are taken in a logarithmic time scale) is not easy and can give several different $w(\tau)$ as a solution. CONTIN uses the regularization method in which the quantity minimized with respect to $w(\tau)$ is

$$\chi^2(a) = \sum_i (1/\sigma_i^2)[C(t_i) - \int w(\tau)\exp(-t/\tau)\,d\tau]^2 + a\left\|\frac{d^2w(\tau)}{d\tau^2}\right\| \tag{5.8}$$

where a is a regularizing parameter. In practice the larger a is, the more detailed is the distribution of relaxation times $L(\ln\tau)$. The choice of the proper $L(\ln\tau)$ is

made from the less detailed (with less peaks) solutions (in most of our data the solutions kept have a $a = 10^{-3} - 10^{-4}$) which give a good fit to the experimental $C(t_i)$.

The general procedure in analyzing dynamic light scattering data is the following:

A The distribution of relaxation times $L(\ln \tau)$, is found using the CONTIN algorithm.

B From $L(\ln \tau)$, the characteristic times, τ_i of the relaxation processes are determined from the peak positions of distribution in the case that the modes are well separated temporarily.. If the modes are not well separated an estimation of the characteristic times can be done by fitting $L(\ln \tau)$ with a number of Gaussians.. The later procedure is used only when there is strong evidence for the existence of two modes under a broad peak, usually by the appearance of a shoulder in the distribution.

C The dynamic character of the processes is determined by the dependence of the decay rate $\Gamma_i \equiv 1/\tau_i$ with q^2. For $\Gamma_i = A + Bq^2$ with $A = 0$ the mode is purely diffusive (like the translational diffusion process), while when $A \neq 0$ the mode has a non diffusive part (like the rotational diffusion process). If Γ_i is q -independent the mode corresponds to a not diffusive relaxation mechanism (like a structural relaxation or a viscoelastic mode).

D The diffusion coefficients are determined by an extrapolation of Γ_i/q^2 to $q = 0$.

E The intensity of each mode is calculated from the area under the corresponding peak of $L(\ln \tau)$ and from the total scattered intensity; most of the times the intensities are presented relative to the respective VV intensity of toluene.

F The q-dependence of the total intensity and the intensity of each mode is also used to identify the origin of the relaxation processes. The intensity at $q = 0$ (thermodynamic limit) is usually used in plots of concentration dependence.

In some cases involving relaxation processes which decay faster than single exponential, the ILT analysis is not adequate, and the correlation functions are represented by the Kohlrausch-Williams-Watts (KWW) function:

$$\boxed{C(q,t) = \exp[(-t/\tau)^{\beta}]} \tag{5.9}$$

where β is the shape parameter. Normally, $0 \leq \beta \leq 1$, with $\beta = 1$ corresponding to a single exponential relaxation mode; the rare case $\beta > 1$ is associated with

steeper than single exponential decays which physically involves some kind of ballistic motion or turbulence (eq. 3.31). Moreover, the use of KWW function to fit the correlation function is useful for the estimation of the broadness of the correlation ($\beta \leq 1$) which is an indication of either polydispersity or the existence of more than one relaxation modes.

5.2 Static Light Scattering

The ALV automated goniometer set-up (Fig. 5.1), described above, was employed for the static measurements as well. The range of angles scanned was 15^o to 150^o and the reference solvent was toluene. By static light scattering we often measure absolute values of molecular weights and thus the absolute value of the scattering intensity is needed. In such case the analysis (Zimm plot) is done using the Rayleigh ratio of a standard (here toluene) $R_{tol} = I_{tol}R^2/V_sE_o^2$ and utilizing eq. 3.43. The Rayleigh ratio of toluene used for polarized scattering and at a temperature $T = 25^oC$, is $R_{VV,tol} = 2.817 \times 10^{-5}cm^{-1}$ (for $\lambda = 532\ nm$); it is calculated from the value given by Bender et al. [6] for the 488 nm wavelength, $R_{VV,tol} = 3.96 \times 10^{-5}cm^{-1}$.

5.3 Fabry-Perot Interferometry

The Fabry-Perot interferometry set-up mainly consists of an Ar^+ laser light source (Spectra Physics Model 2020), operating in a single line of $\lambda = 488nm$ mode with an intensity of 300 mW, and a planar Fabry-Perot Interferometer (Spectra Physics Model 410) with a free spectral range of 983 GHz (40 cm^{-1}). The schematic of the optical set-up shown in fig. 5.3. It includes two Glan-Thomson polarizers (Halle, Berlin) ($P1$ and $P2$) of extinction ratio 10^{-6} and 10^{-7} respectively. In this experiment the incident polarization is vertical to the scattering plane (V), while the scattered beam analyzer ($P2$) is set in the horizontal (H) position since we measure the spectrum of the depolarized, I_{VH} intensity at 90^o scattering angle. The incident beam is focused by an achromat lens ($L1$) with 300 mm focal length while the two lenses, $L1$ (200 mm) and $L2$ (250 mm) in the detecting optics assure that the scattered beam is passing in parallel from the interferometer and then is focused in the photocathode of the PMT. A narrow-band interference filter (IF) (1.1 nm) was used in front of the PMT to remove fluorescence.. The samples were put in rectangular cells (Hellma), $1 \times 1 \times 4\ cm$, which was positioned in a electrically heated cell; the temperature was stabilized at 25^0C within $\pm 0.1^0C$.

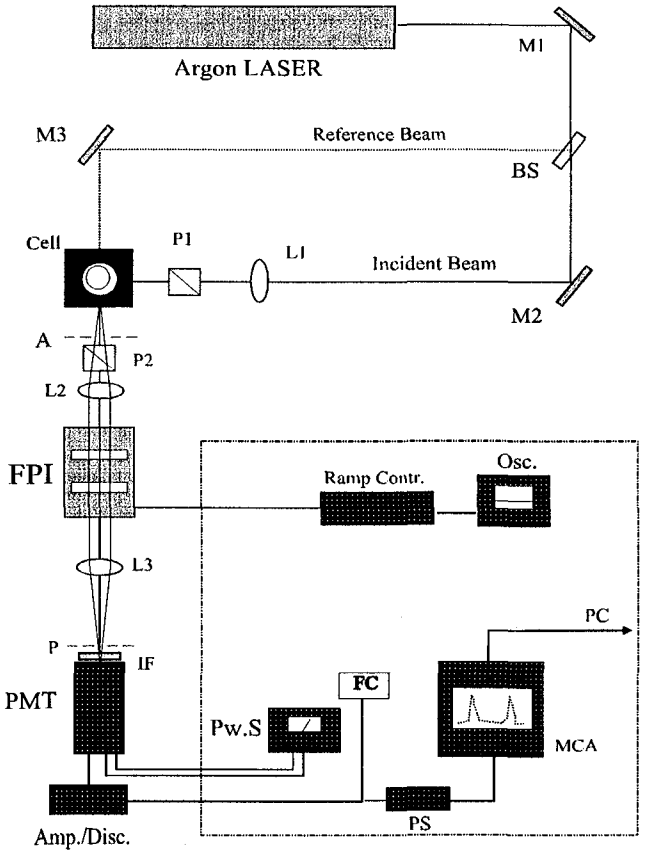

Figure 5.3: Fabry-Perot Interferometry Apparatus

5.3.1 Fabry-Perot Interferometer

The Fabry-Perot interferometer is a frequency scanning device consisting of two parallel (13 *mm* diameter) mirrors which are piezoelectrically driven. The interferometer is driven by a Ramp Generator (Burleigh, CFT controller RC-45); the maximum scan rate of the instrument (about 13 min) is used to have a better signal to noise ratio. A measure of the accuracy of an FPI is the *finesse* which is the ratio of the *Free Spectral Range* (the frequency difference between two successive maximum of the spectrum) and the half-width at the half maximum. In our experiment a finesse of $70 - 75$ is achieved. The sweep generator is regulated so that we detect in a single sweep two Rayleigh peaks of the scattering spectrum (fig. 5.4). The spectra during the experiment are recorded in a 2048 channel multichannel analyzer (Canberra, Series 35+) and after each measurement was transferred to a PC for analysis.

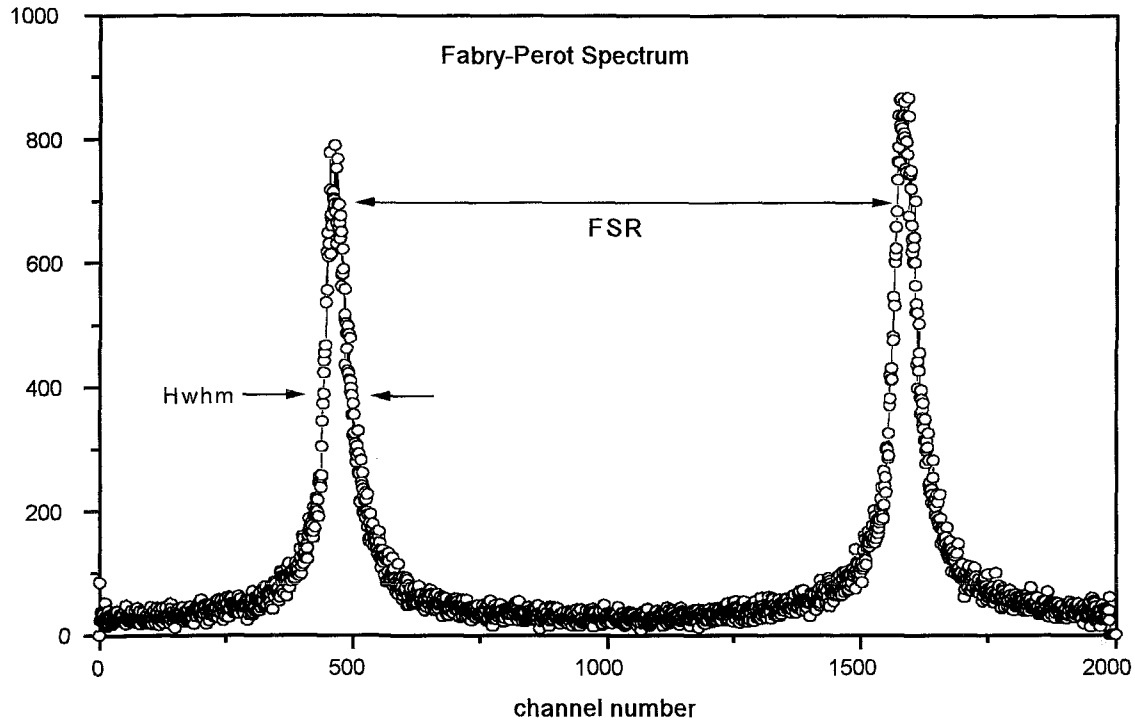

Figure 5.4: A typical Fabry-Perot spectrum of a TPPE polyester solution, as it is recorded in the multichannel analyzer. The Free Spectral Range (FSR) and the half width at half maximum (HwhM) are shown.

5.3.2 Analysis of the spectrum

The analysis of the spectrum involves the fitting of one of the Rayleigh peaks measured; in the case of pure solvent spectra only one Lorentzian can fit very well the spectra, as it is expected, while in the case of the polymer solutions it is clear that we have to use a two Lorentzian fit, since the additional scattering of the polymer molecules involves a much slower characteristic time (and thus narrower Lorentzian peak in the frequency spectrum). The fitting of the Rayleigh peak normally gives both the intensity (as the area under the peak) and the characteristic time (or times) (from the width of the peak) (eq. 3.30). Since, as we explain in chapter 6, in our investigation we are interested only in the total scattering intensity (in the VH geometry) we make use only of the area under the Rayleigh peak calculated by the Lorentzian fit as described above.

5.4 Raman Spectroscopy

The Raman spectra were excited with a Spectra Physics (model 164) Ar^+ laser using typically 100 mW of the 514.5 nm line. The laser beam is directed through an optical train; the latter includes mirrors, iris diaphragms, a narrow band-pass interference filter, a half wave plate, and a cylindrical lens. The specimen is positioned mechanically at a special stage that can rotate by 360^o. The 90^o scattered light is collected with a $F/1.4$ (80 mm diameter) lens at the slit of a monochromator through an analyzer for selecting the appropriate polarization and a quarter wave plate to compensate for grating polarization preference. A Spex model 1403 double monochromator coupled with an RCA model C-31034 photomultiplier tube is used to analyze the scattered radiation. The detection system includes Par photon counting and rate meter electronics. The signal from the PMT and the electronics is recorded and analyzed on a personal computer.

All Raman Scattering experiments were contacted at the laboratory of Prof. G. Papatheodorou at the Institute of Chemical Engineering and High Temperature Chemical Processes in Patras, in collaboration with Dr. G. Voyatzis.

5.5 Pulsed Field Gradient (PFG) NMR

With PFG NMR the time-self-correlation function of the positions of proton bearing segments of polymer chains is measured. When the mean square displacement during the observation time is larger then the radius of gyration, the self diffusion of the centre-of-mass of the chains is determined. The principles of PFG NMR are detailed described in refs. [7]. The basic idea of PFG NMR is tagging of the nucleus with respect to its position in space by a Lamor precession $\omega(z) = \gamma \cdot B(z)$depending on the space coordinate z; γ is the gyromagnetic ratio of nucleus under study, $B(z)$ is the total field applied:

$$B(z) = B_0 + g \cdot z \tag{5.10}$$

The basic experiment is the stimulated echo experiment with a rf-pulse sequence echo $\frac{\pi}{2} - \tau - \frac{\pi}{2} - t - \frac{\pi}{2} - \tau - echo$. During the time intervals 2τ and t transverse and longitudinal nuclear magnetic relaxation occurs, respectively. The measured spin echo attenuation $\frac{A}{A_0}$ due to applied field gradient pulses after the first and second $\frac{\pi}{2}$-rf pulse, respectively, is equivalent to the incoherent intermediate scattering function of neutron scattering [?]:

$$\frac{A}{A_0} = S_{inc}(q,t) = \int \exp(iqz) P(z,t) dz \tag{5.11}$$

where A_0 is the spin echo amplitude without applied field gradients, $P(z,t)$ is the propagator of the self-correlation function of the protons i.e. the probability for a displacement of a polymer segment over the distance z within the diffusion

time t. The term $q = \gamma\delta g$ is a generalized scattering vector with δ denoting the width of the gradient pulse. The use of a Gaussian propagator (free diffusion) in eq. 5.11 leads to

$$\boxed{S_{inc}(q,t) = \exp(-q^2 D_s t)} \tag{5.12}$$

were D_s is the self diffusion coefficient. The PFG NMR experiments were carried with an NMR spectrometer operating at a $1H$-resonance frequency of 400 MHz at room temperature. In one particular experiment δ and t were fixed and g was incremented. The maximum g-value was 25 Tm^{-1}, the maximum δ-value was 1.85 ms. The diffusion times t were typically between 10 and 300 ms.

All the NMR measurements were contacted by Prof. G. Fleisher in the Department of Physics and Geology of the University of Leipzig in Germany.

References

[1] J.B. Berne and R. Pecora. *Dynamic Light Scattering.* Willey Interscience Publications, New York, 1976.

[2] Jr. N.C. Ford. *Dynamic Light Scattering; Applications of Photon Correlation Spectroscopy*, page 7. Plenum Press, 1985.

[3] K. Schatzel. *Dynamic Light Scattering: The Technique and Some Applications*, page 76. Oxford Press, 1993.

[4] S. W. Provencher. *Makromol. Chem.*, 180:201, 1979.

[5] S. W. Provencher. *Computer Physics Communications*, 27:213, 1982.

[6] M. Bender, R.J. Lewis, and R. Pecora. *Macromolecules*, 19:244, 1986.

[7] P.T. Callaghan and E.M. Lifshitz. *Principles of Nuclear Magnetic Resonance Microscopy.* Clarendon Press, Oxford, 1960.

Chapter 6

Chain Conformation of Semirigid Polymers

It is well known that semirigid polymers are characterized by a large persistence length, which is a direct measure of the chain stiffness and is intimately related to the type and stability of the mesophases formed [1, 2]. Accurate knowledge of this property is essential in understanding the mechanical behavior of semistiff polymers, as well as the coupling between translation and rotation, and other features of the dynamic behavior in the isotropic regime and near the nematic transition [3, 4, 5].

Several techniques have been used for the determination of the conformational properties of polymers and oligomers in solution. Among them, magnetic birefringence (Cotton-Mouton effect)[6], polarized dynamic light scattering [7, 8], viscosimetry (Bohdanecky method) [9], electric birefringence (Kerr effect) [10], flow birefringence [11], scattering by X-rays or neutrons [12], intrinsic dynamic viscoelastic moduli [13], whereas for very long biological polymeric filaments fluorescence microscopy appears to be very effective [14]. Of special interest is the technique of depolarized Rayleigh scattering (DRS), which has been successfully utilized for the measurement of the mean square optical anisotropy ($< \gamma^2 >$) of low-molecular weight nematogenic compounds [15, 16], as well as polymeric systems [17].

In this chapter the determination of the persistence length of two different series of stiff polymers by Depolarized Rayleigh Scattering (DRS), will be presented. Moreover, the inherent optical anisotropy of these macromolecules will be used to check the validity of the assumption for the additivity of the bond polarizability tensor [18]. For the calculation of the persistence length we developed a new analysis which relates the experimentally measured depolarized intensity with the conformation of the chain; it accounts for the chain flexibility according to the worm-like chain and for the polydispersity. It has been shown that this analysis applies both for the Depolarized Rayleigh Scattering [19] and the Magnetic Birefringence measurements from a solution of polydisperse worm-

like chains [20]. For the measurement of the depolarized light scattered from the polymer chains we used the technique of Fabry-Perot interferometry (FPI), which produced spectra, that were appropriately analyzed in order to reveal the specific depolarized Rayleigh ratio at infinite dilution and eventually determine the persistence length. The determination of the persistence length by polarized light scattering is based on the measurement R_G for several molecular weights and then fitting the data with the expression relating the R_G with the persinstence length and the contour length (eq. 2.3) similarly to the case of the depolarized intensity. Nevertheless the accurate determination of R_G is not possible for relatively small polymer chains since this is done from the angular dependence of the polarized scattered intensity using eq. 3.50; when $q^2R_G^2/3 \ll 1$ the slope is essentially zero and the radius of gyration cannot be determined. On the contrary, the DRS technique can be used for all polymer chains, from the size of the monomer up the largest molecular weights available. The reason is the fact that the depolarized intensity is related to

$$\sum_{i,j} < \frac{3\cos^2\vartheta_{i,j} - 1}{2} > \tag{6.1}$$

for all elements i and j along the chain, and thus when applying the worm-like model we are led to a quantity which varies in a very similar way to the radius of gyration, but with an apparent persistence length three times smaller [21] (see eqs. 6.10- 6.12). Of course, the use of the DRS method is limited only to macromolecules with significant intrinsic optical anisotropy which can give enough scattering of light in the depolarized geometry even in dilute solutions.

6.1 Depolarized Rayleigh Scattering

The scattering of laser light in the depolarized mode (VH) is induced by orientation fluctuations, which cause fluctuation of the anisotropic part of the polarizability tensor. The main origin of the VH intensity is the intrinsic anisotropy of the scatterer (in our case a polymer chain), which depolarize an incident beam impinging on it. Besides, in a polymer solution there are three other contributions in the depolarized scattering:

a) The VH scattering from the solvent molecules,

b) Collisions, between even optically isotropic scatterers induce anisotropy which contributes to the total depolarized Rayleigh intensity and

c) The interactions between the polymers in nondilute solutions can effect the VH scattering by inducing orientational correlations between the molecules.

As mentioned in Chapter 4, the scattering from a macromolecule is conveniently discussed by considering as a basic scattering element a segment of the polymer rather than the whole molecule. Thus the VH scattering of a poly-

mer chain in solution can be based on the scattering of symmetric top scatterers which, in most cases, resemble the polymer segments.

For a system of symmetric top molecules, the spectrum of the elastically scattered light in the depolarized geometry is given by a Lorentzian distribution around the frequency of the incident beam :

$$\boxed{I_{VH} = Af(n)\frac{1}{n^2}\rho < \gamma^2 > (1+\rho F)\pi^{-1}\frac{1/\tau}{\omega^2+(1/\tau)^2} + I_{CI}(\omega)} \tag{6.2}$$

with ω being the frequency difference of the scattered and incident beam and τ the characteristic time of the relaxation ($= q^2D + 6D_R$, for rotations) [22, 15]. The integrated depolarized intensity at zero scattering wavevector, is then given by:

$$\boxed{I_{VH} = Af(n)\frac{1}{n^2}\rho < \gamma^2 > (1+\rho F) + I_{CI}} \tag{6.3}$$

where A is a constant; $f(n)$ is the local field correction; $1/n^2$ is a geometrical factor (n being the refractive index of the medium); ρ is the number density of the anisotropic scatterers; $< \gamma^2 >$ is the mean square optical anisotropy (averaged over all possible molecular conformations) and I_{CI} is the collision-induced contribution to the scattering intensity. The term $(1+\rho F)$ represents the intermolecular interactions, directly connected with the fluid structure; F_c is a measure of the orientational pair correlations (eq. 3.61), which is concentration-dependent (when no orientational correlation exists, $F = 0$). The molecular optical anisotropy is defined from the traceless part of the polarizability tensor a_0, by [18]:

$$\gamma^2 = \frac{3}{2}trace(\hat{a}_0\hat{a}_0) \tag{6.4}$$

with

$$\hat{a}_0 = a_0 - \frac{1}{3}trace(a_0)\hat{I} \tag{6.5}$$

where $\hat{I} = diag(1,1,1)$. If we further consider cylindrical symmetry around the main axis x of the molecule, then [18] :

$$\gamma^2 = (\Delta a_0)^2 + \frac{3}{4}(\Delta a_0^+)^2 \tag{6.6}$$

with

$$\Delta a_0 = \frac{a_{xx} - (a_{yy} + a_{zz})}{2} \tag{6.7}$$

being the cylindrical term, and

$$\Delta a_0^+ = a_{yy} - a_{zz}$$

the acylindrical term, in which $\hat{a}_0$ decomposes:

$$\hat{a}_0 = \Delta a_0 \hat{J} + \Delta a_0^+ \hat{J}^+ \tag{6.8}$$

where $\hat{J} = diag(2/3, -1/3, -1/3)$ and $\hat{J}^+ = diag(0, 1/2, -1/2)$. In order to deduce the molecular contribution to the depolarized intensity (or the intrinsic molecular anisotropy $< \gamma^2 >$, directly connected with it), the contribution of the collision-induced anisotropy, I_{CI} , should be subtracted from the measured I_{VH} . The optical anisotropy induced by collisions in both atomic and molecular fluids originates from the deformation of their electronic clouds and has a characteristic duration time which is of the order of the duration of the collision [22]. Thus, the characteristic time associated with the collisions between solvent molecules or solvent and polymer molecules is much smaller than the reorientational time of both solvent molecules and polymer molecules and this allows a clear distinction between the two relevant dynamic processes in a DRS experiment. Experimentally this is achieved with the use of the Fabry-Perot interferometer.

The function $f(n)$ entering in the formula for the VH scattering describes the correction in the electric field of the incident light in vacuum, E_0, due to the presence of the liquid dielectric medium. For an internal field which is still open problem in DRS, we used the second power correction to the Lorentz local field, which has been demonstrated experimentally to work reasonably well [15, 17, 23]. Thus,

$$\boxed{f(n) = \left(\frac{n^2+2}{3}\right)^2} \tag{6.9}$$

The second order internal field correction is consistent with the use of Flory's additivity approximation [18] which is actually the Bond Additivity Approximation (BAA) for the polarizability tensor. While a rigorous approach apparently does not favor a correction based on any power law of the Lorentz local field [24], the choice of the appropriate internal field can be essentially by-passed in the actual analysis of chain conformation from DRS for the calculation of the persistence length. Nevertheless it must be mentioned that for the calculation of the molecular optical anisotropy the internal field correction must be used. A brief discussion of the internal field problem in light scattering can be found in Appendix C.

6.2 Analysis of Depolarized Intensity

For the determination of the optical anisotropy, we assume that the macromolecule consists of symmetric top repeating units, each having anisotropy $< \gamma_0^2 >$. Furthermore, by assuming applicability of Flory's group additivity approximation, and by utilizing the wormlike model prediction for the optical anisotropy, we can relate the total optical anisotropy of the polymer with the anisotropy of its monomer unit and the specific characteristics of its conformation by:

$$\boxed{<\gamma^2>=<\gamma_0^2>\sum_{i,j}\frac{3<\cos^2\vartheta_{i,j}>-1}{2}} \tag{6.10}$$

with ϑ_{ij} being the angle between the axes of the optical ellipsoids associated with segments i and j. For the case when the optical ellipsoids are oriented along the segment direction, the following estimation of the polymer's average optical anisotropy is obtained [21] (where only the cylindrical terms are taken into account):

$$\boxed{<\gamma^2>=<\gamma_0^2>lF(L)(\tfrac{2}{3}\tfrac{N}{l_0})} \tag{6.11}$$

where l is the persistence length, l_0 the contour length of the repeating unit, L the contour length, N the number of monomers in the chain, and $F(L)$ is given by:

$$\boxed{F(L)=(1-\tfrac{l}{3L}[1-\exp(-3L/l)])} \tag{6.12}$$

As seen in eq. 6.3, in the limit of zero concentration, the depolarized intensity due to the intrinsic anisotropy is proportional to the average molecular anisotropy of the polymer. To obtain the latter the intensity is converted to absolute Rayleigh ratio by comparison with the depolarized scattering intensity of a solvent used as a reference, according to:

$$R_{VH}=(\frac{I_{VH}}{I_{tol}})(\frac{n}{n_{tol}})^2 R_{VH,tol} \tag{6.13}$$

with I_{VH} being the contribution of the polymer to the VH scattering. The term $(\frac{n}{n_{tol}})^2$ with n and n_{tol} the refractive indexes of the solution and the toluene respectively, is a geometrical correction for the VH intensities in two different solvents [25, 16]. In this work $R_{VH,tol}$ is the Rayleigh ratio of toluene, which was used as reference. Thus in the limit of zero concentration, the contribution of the average molecular anisotropy of the polymer is:

$$\boxed{(\frac{R_{VH}}{\rho})_{\rho\to 0}=\frac{1}{15}(\frac{2\pi}{\lambda})^4(\frac{n^2+3}{2})^2<\gamma^2>} \tag{6.14}$$

λ being the wavelength of the laser light.

From the above analysis, it is now straightforward to use equation eq. 6.14 in order to deduce an expression for the Rayleigh ratio at infinite dilution (normalized by the weight concentration, c, in g/cm^3), which is the quantity directly measured with the DRS technique:

$$\boxed{(\frac{R_{VH}}{c})_{c\to 0}=K_{DRS}lF(L)} \tag{6.15}$$

where K_{DRS} is a constant associated with the DRS technique, given by:

$$\boxed{K_{DRS} = \left(\frac{2\pi}{\lambda}\right)^4 \frac{2}{45} \frac{N_A}{l_0 M_0} \left(\frac{n^2+3}{2}\right)^2 < \gamma_0^2 >} \tag{6.16}$$

with N_A the Avogadro number and M_0 the molecular weight of the repeating unit. This result holds for a *monodisperse sample*, a case which very rarely can be approached in real systems.

For a *polydisperse sample* an average must be contacted over all the different molecular weights present. It is noted, that when dealing with the light scattering intensity R_{VH}, we have to weight the contributions of the respective species of a non-uniform polymer with their weight fraction. This follows from the fact that eq. 6.15 can be also written as $R_{VH} = (K_{DRS}/N_A)\rho M F(L) l$, and for polydisperse samples:

$$R_{VH} \sim \int_0^\infty \rho(M) M F(M) dM = \int_0^\infty \rho(L) L F(L) dL = \int_0^\infty w(L) F(L) dL \tag{6.17}$$

where $\rho(M)$ is the number fraction of species with mass M and $w(L)$ the weight fraction of species with contour length L. Hence, in the generalized analysis of the DRS data for non-uniform polymers, the specific depolarized light intensity can be written as:

$$\boxed{\left(\frac{R_{VH}}{c}\right)_{c\to 0} = K_{DRS} l \int_0^\infty w(L) F(L) dL} \tag{6.18}$$

By *using the Schultz-Zimm distribution* [26]:

$$w(L) = y^{m+1} \frac{L^m}{m!} \exp(-yL) \tag{6.19}$$

where $y = (m+1)/L_w$, $m = (L_w/L_n - 1)^{-1}$ is the polydispersity index, and L_w and L_n are the weight and number average contour lengths, respectively, the integration of eq. 6.18 leads to:

$$\left(\frac{R_{VH}}{c}\right)_{c\to 0} = K_{DRS}\ l\ [1 - \frac{m+1}{m x_w}(1 - (1 + \frac{x_w}{m+1})^{-m})] \tag{6.20}$$

where $x_w = 3L_w/l$ is the reduced contour length. The two limiting cases of interest are the high and the low molecular weights, corresponding to the coil and rod limits, respectively:

(i)

$$\text{for } x_w \gg 1 \text{ we get } \frac{R_{VH}}{c} \to K_{DRS} l \tag{6.21}$$

(ii)

$$\text{for } x_w \ll 1 \text{ we get } \frac{R_{VH}}{c} \to \frac{3}{2} K_{DRS} L_w \tag{6.22}$$

These results suggests that in both limits, the depolarized light scattering intensity (and thus the average optical anisotropy), is independent of the width of the molecular weight distribution (related to the polydispersity index m). Additionally, for very long chains, it is also independent of molecular weight (coil-like behavior), while for short chains, it is directly proportional to L_w (rigid rod-like behavior).

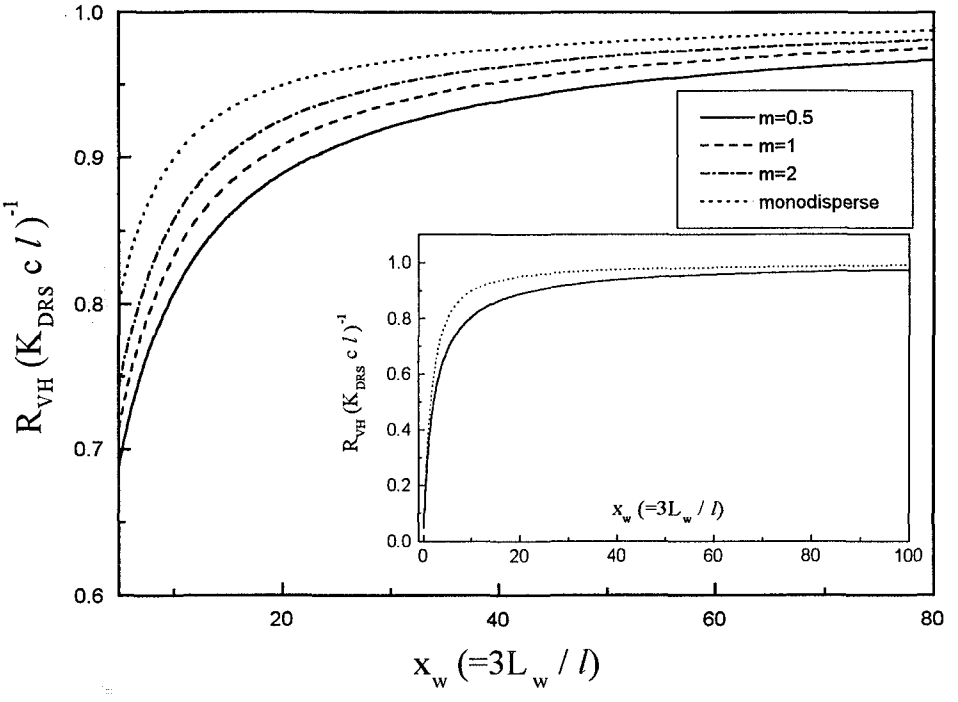

Figure 6.1: $(\frac{R_{VH}}{cK_{DRS}l})$ vs x_w from eqs. 6.20 for $m = 0.5$, 1, 2 and ∞ (decreasing polydispersity). Inset: The same function for a larger range of contour lengths.

This behavior of a wormlike chain is shown in fig. 6.1 where eq. 6.20 is plotted for different values of the polydispersity index. It is easy to show from eq. 6.20, that in the intermediate region the influence of the polydispersity index m is rather limited. This is realized graphically in fig. 6.1. We observe that the for the same x_w the value of $(\frac{R_{VH}}{cK_{DRS}l})$ changes by less than 10% for different values of m, for all molecular weights. The difference is smaller at the high x_w region where the chain has taken a coil conformation. This allows us, also in the view of the uncertainty of the values of the polydispersity, to use the most probable distribution ($m = 1$) [27, 26]. In this way we end-up with a simple equation which relates the persistence length with the depolarized scattering intensity:

$$\boxed{\frac{1}{(R_{VH}/c)_{c\to 0}} = \frac{1}{K_{DRS}\, l} + \frac{2}{3K_{DRS}\, L_w}} \tag{6.23}$$

Eq. 6.23 suggests that it is possible to determine the persistence length of a polydisperse polymer, by simply plotting c/R_{VH} (at $c \to 0$) against $1/L_w$. Thus, the persistence length can be determined from DRS without invoking the IFP, which is incorporated into K_{DRS} and thus independently obtained from the slope of the plot. Further, the effect of the typically high polymer non-uniformity turns out to be nearly insignificant.

The above analysis of the DRS data, accounting for the effects of polydispersity, is also used for the analysis of magnetic birefringence measurements on the same polymer series [20]; actually, the basic physics behind the two techniques is analogous, and both treatments converge to the same scaling predictions. The results of the two experiments will be compared below.

6.3 Experimental Section.

6.3.1 Materials

The polyester TPPE (shown in Fig. 6.2, together with its trimer, a 2',5'-di-n-hexyl-p- terphenyl-4,4"'-diol) and the poly(p-phenylene) PPP (shown in Fig. 6.3, together with its oligomers) used in this work, were synthesized by polycondensation [28, 29, 30]. The molecular characteristics of the various TPPE polyesters and trimer are shown in Table 6.1, whereas those of the various PPP poly(p-phenylenes) and oligomers in Table 6.2. A range of molecular weights M_w from 11,300 to 130,000 and from 31,680 to 47,850, were obtained for the TPPE and the PPP, respectively. The polydispersity of the samples is estimated from the polydispersity index: $m = (L_w/L_n - 1)^{-1}$. M_w was determined by light scattering measurements and M_n by membrane osmometry measurements [29]. The static light scattering determination of M_w for PPP samples were done in a mixed cyclohexane/chloroform solvent, at $25°C$. Furthermore, GPC analysis showed that the all the materials have a unimodal molecular weight distribution [29]. The value in parenthesis for TPPE-1and PPP-1 is an estimation based on the m's and L_w's of the other polymers of the series. The biphenyl (2:0) and terphenyl (3:0) samples were obtained from Aldrich. The DRS measurements were carried out at concentrations ranging from 0.03% up to 4.4% per weight. The upper bound was determined by the solubility of each sample [31]. All measurements were carried out in chloroform solutions for two reasons: a) It was found to be a relatively good solvent for all the samples investigated; and b) its molecular anisotropy is small, although not zero, a fact that allows the measurement of polymer contribution in the total VH intensity for very small polymer concentrations.

TPPE

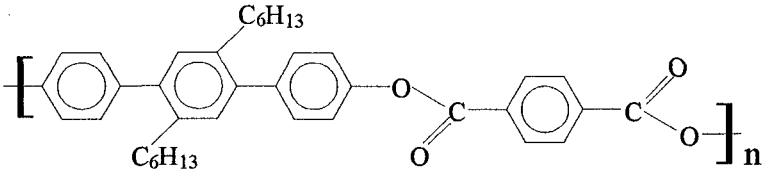

Trimer

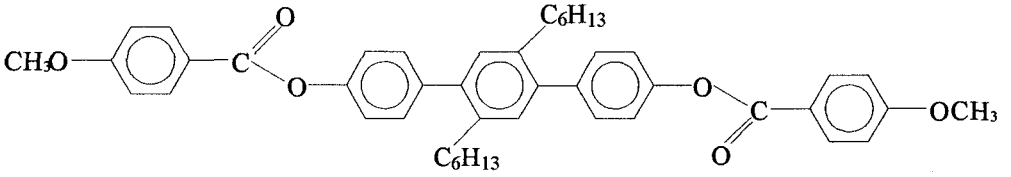

Figure 6.2: Polyester TPPE with hexyl side chains, and its trimer.

Sample	M_w	$L_w(nm)$	m	$R_{VH}/c \times 10^6(cm^2/g)$	$<\gamma^2>/N(\AA^6)$
trimer	699	3.0	∞	62	1601 (N=1)
TPPE-1	11300	44.4	(1.67)	205	5597
TPPE-2	20400	80.2	1.43	224	6115
TPPE-3	31100	122	1.67	249	6798
TPPE-4	47200	185	1.11	251	6853
TPPE-5	130000	511	0.48	256	6990

Table 6.1: Characteristics and data of the polyester TPPE series and the trimer.

Sample	M_w	$L_w(nm)$	m	$R_{VH}/c \times 10^6(cm^2/g)$	$<\gamma^2>/N(\AA^6)$
2:0	154	0.84	∞	24.64	185 (N=1)
3:0	230	1.33	∞	45.23	529 (N=1)
3:6	398	1.33	∞	16.5	319 (N=1)
3:12	566	1.33	∞	16	441 (N=1)
monomer	564	1.48	∞	24.9	686 (N=1)
PPP-1	31680	82.2	(0.45)	241	6650
PPP-2	39060	101.1	0.48	308	8499
PPP-3	43200	117.2	0.45	307	8472
PPP-4	47850	123.2	0.43	342	9438

Table 6.2: Characteristics and data of the poly(p-phenylene) PPP series and the oligomers 2:0, 3:0, 3:6 and 3:12.

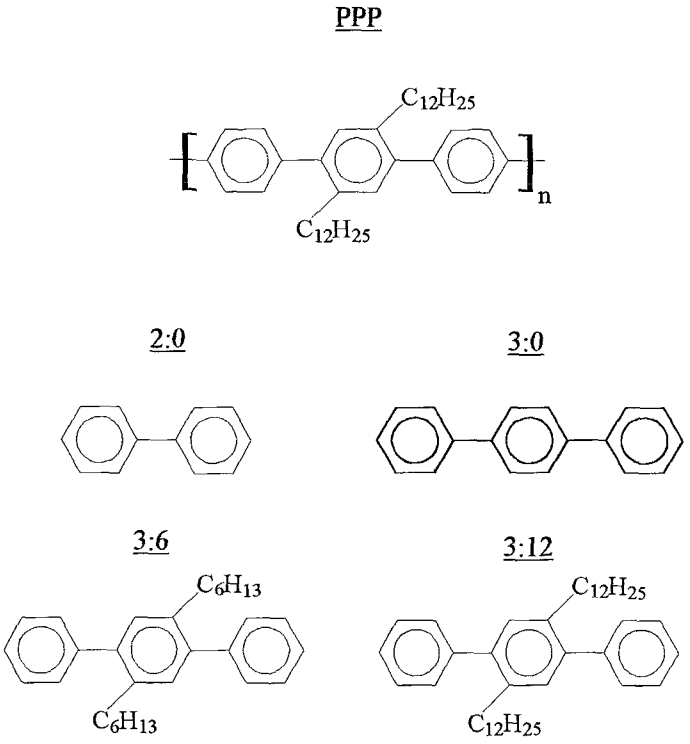

Figure 6.3: Poly(p-phenylene) PPP with dodecyl side chains, and its oligomers 2:0 (no side chains), 3:0 (no side chains), 3:6 (hexyl side chains) and 3:12 (dodecyl side chains).

6.3.2 Measurements

A detailed description of the experimental system used has been presented in chapter 5. At typical depolarized Rayleigh spectrum for the polymer solution and solvent (TPPE-3 in chloroform, concentration 0.1% by weight) along with the corresponding spectrum from pure chloroform is shown in fig. 6.4.

The accurate and reproducible measurement of I_{VH} required proper consideration of the important factors already mentioned above, namely the I_{CI}, F as well as the dependence on the wavevector q. The utilization of a Fabry-Perot interferometer enables us to subtract the contribution of I_{CI}. The latter appears as a broad background in the Rayleigh spectrum since the characteristic time associated with the collision induced anisotropy is much faster than the reorientational motion of all molecules in the solution. Then, the Rayleigh peak is dominated by the significantly slower molecular reorientation. This is the main reason for measuring the spectrum of the Depolarized Intensity instead of directly measuring total depolarized intensity. The obtained intensity spectrum, $I_{VH}(\omega)$, is then integrated in order to get the total intensity I_{VH}. The VH component

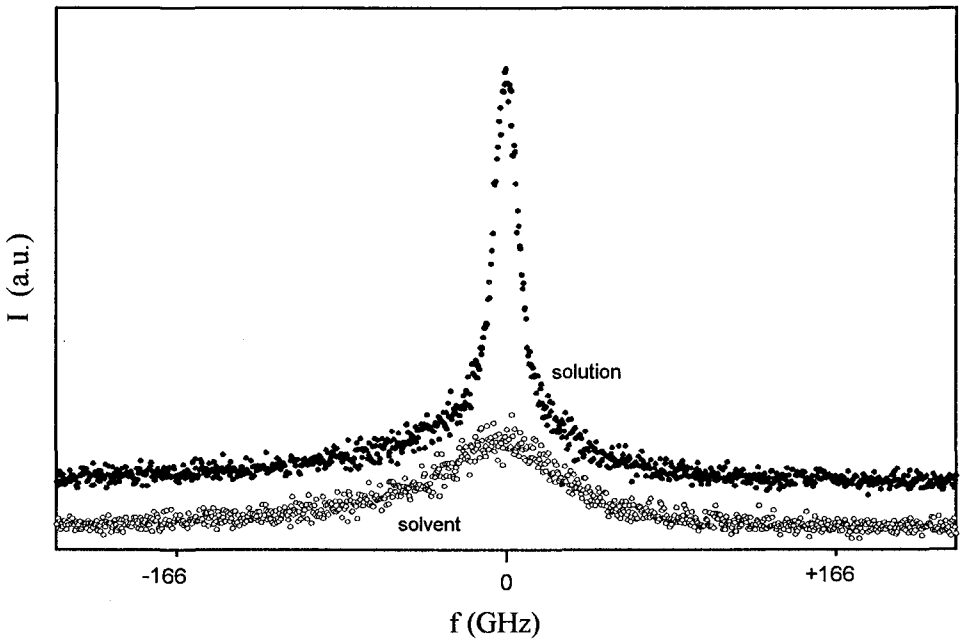

Figure 6.4: Typical depolarized Rayleigh spectrum of a polyester TPPE-3 solution in chloroform (0.1% by weight), at a scattering angle of 90^0, and the corresponding spectrum of the solvent.

of the scattered intensity of the polymer can be isolated from the solvent background and calculated from: $I_{solute} = I_{solution} - (1-\phi)I_{solvent}$, ϕ being the volume fraction, of the solute. Further, the $q-$independence of the intensity I_{VH} was always preserved; this guaranteed the validity of eq. 6.3 above. Finally, in order to avoid intermolecular interactions, the specific depolarization ratio R_{VH}/c was determined at the infinite dilution limit. To accomplish this, it was necessary to undertake numerous careful measurements in a wide range of concentrations, as discussed below.

6.4 Determination of Persinstence Length

Since the analysis presented above is valid for negligible molecular interactions, and even at low concentrations our data exhibit a clear deviation from linearity, we used nonlinear fitting procedure in order to extract the limiting value of c/R_{VH} at $c \to 0$. Fig. 6.5 and fig. 6.6 show the depolarized Rayleigh ratio as a function of concentration for all five TPPE polyester samples and the trimer. It is clear that as the concentration increases, molecular interactions come into

play. A reasonably good nonlinear fitting is obtained for all samples; it should be noted, however, that the slope at vanishing concentration, $(R_{VH}/c)_{c\to 0}$, differs only slightly from sample to sample, and this is explained by the fact that due to the limited range of molecular weights used, there was not much difference in scattering power from the low to the high molecular weight.

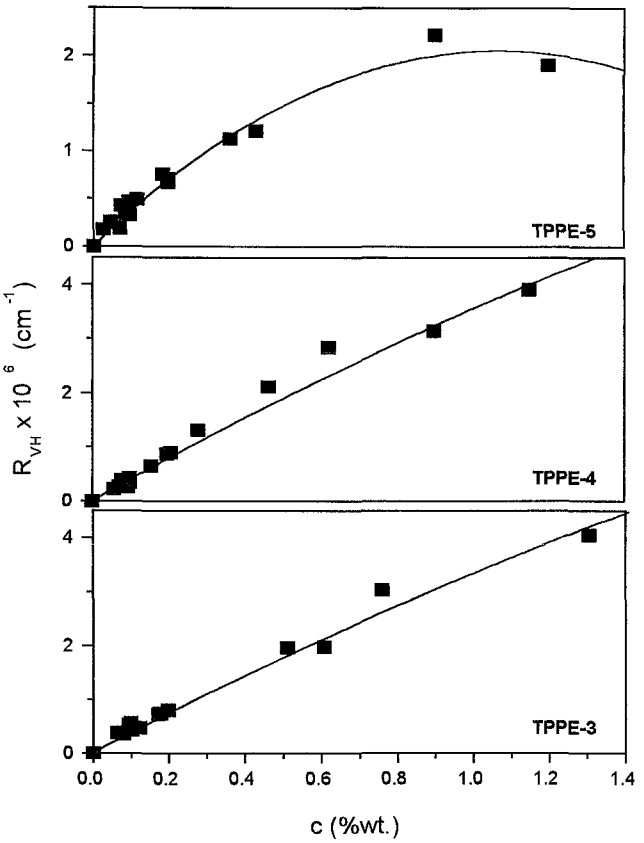

Figure 6.5: Depolarized Rayleigh ratio of the polyester TPPE-1, TPPE-2 and TPPE-3 as a function of concentration, and corresponding nonlinear fits.

A closer look at the data, however, reveals an additional interesting feature: as the molecular weight increases, the second derivative of R_{VH} versus c changes sign. To explain this behavior, we argue that short chains (trimer and maybe TPPE-1) are near the rod limit, whereas the longer chains (TPPE-2, TPPE-3, TPPE-4 and TPPE-5) are near the coil limit. Thus, we expect that in the former case intermolecular interactions dominate at relatively high concentrations, while in the latter one intramolecular interactions might be also involved; these interactions may lead to a slight change in the average segmental pair orientation,

expressed by the second Legendre polynomial, from positive (average orientation angle below 55^o) to negative (average orientation angle above 55^o), which eventually results to the observed change in curvature. Negative curvatures have been reported in the past, with flexible polymers [32, 32, 33].

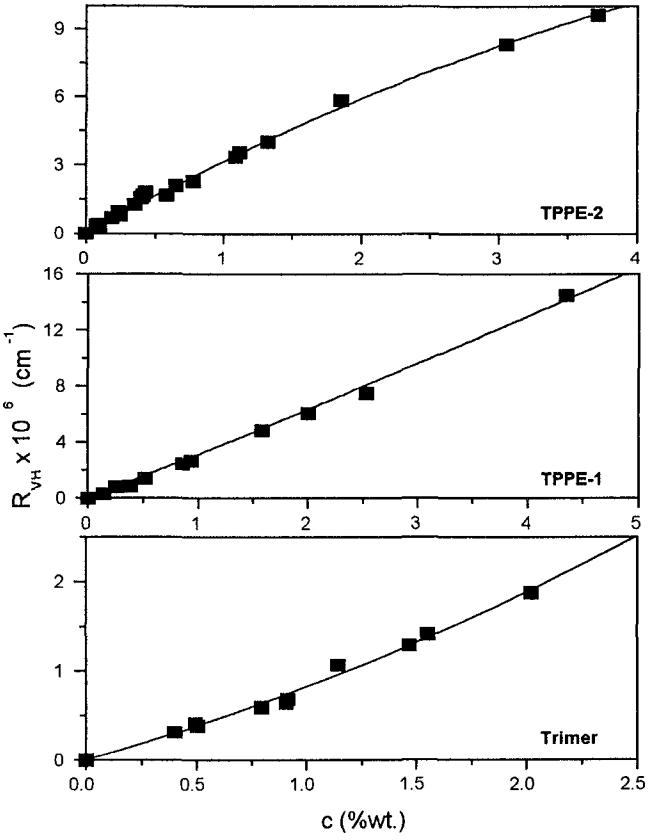

Figure 6.6: Depolarized Rayleigh ratio of the polyester TPPE-4 and TPPE-5 and the trimer, as a function of concentration, and corresponding nonlinear fits.

In the case of the poly(p-phenylene) series, the concentrations used were below 1.2% by weight, and the R_{VH} versus c plots were linear, for all samples PPP-1, PPP-2, PPP-3 and PPP-4, with reasonably good statistics as can be seen in fig. 6.6.

From the R_{VH} versus c plots we determine $(R_{VH}/c)_{c\to 0}$ which is the experimental quantity used to calculate the persistence length of the two series of semistiff polymers. Fig. 6.7 represents the use of eq. 6.23 for the determination of the average conformation of the polyester series. It is also noted that the approximate value of m for the polymers investigated in this work varies from

0.4 to 1.7, as determined by GPC (Tables 6.1, 6.2). Using this information, it is easy to calculate the relative errors from applying eq. 6.23 to polyesters and poly (p-phenylenes) from the plot of fig. 6.1. For the polyester samples TPPE-5, TPPE-4, TPPE-3, TPPE-2 and TPPE-1, the maximum error ranges from 1% to 6% depending on the molecular weight.. For the poly(p-phenylene) samples PPP-1, PPP-2, PPP-3 and PPP-4, with an average $m = 0.45$, the calculated error is around 5%. The least squares line fits the experimental data, with some uncertainty, but given the difficulties and limitations, we argue that fig. 6.7 and 6.8 demonstrate the applicability of eq. 6.23 in determining the persistence length of a wormlike optically anisotropic polymer.

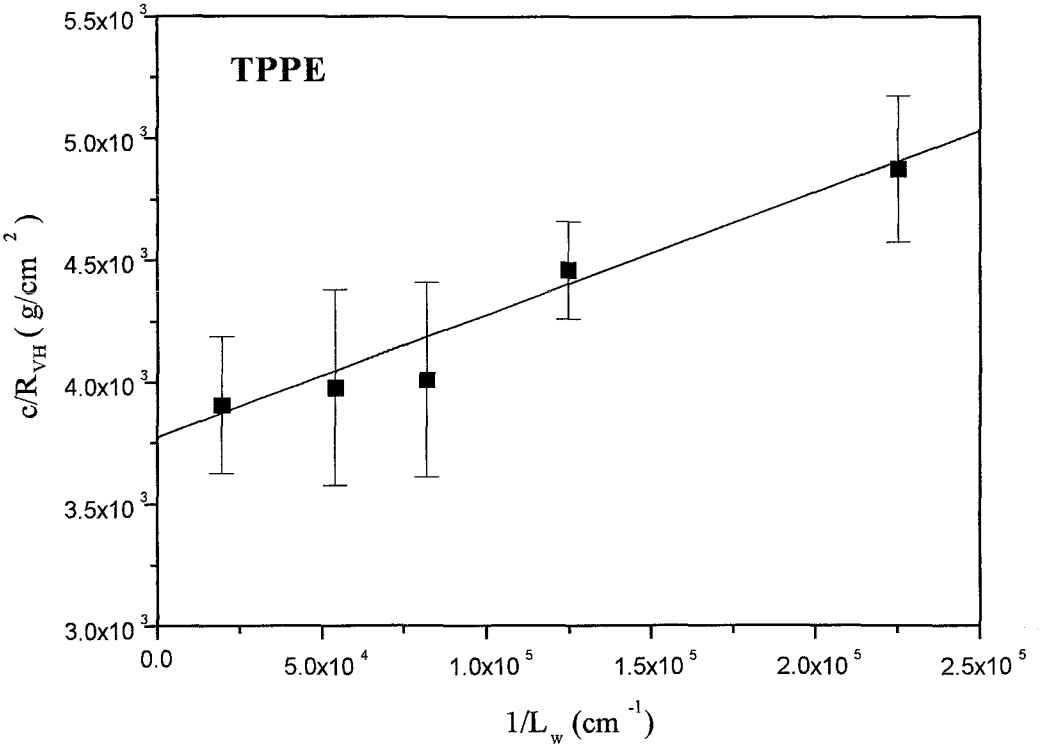

Figure 6.7: Determination of the persistence length of the polyester TPPE, using the linear equation (15), expressing $(c/R_{VH})_{c\to 0}$ as a function of L_w^{-1}. Solid line represents the least squares fit.

The result from the slope and intercept of Figure 6.7 is approximately $l = 19nm$. Further, from the intercept, the value of the DRS constant was determined as $K_{DRS} = 133 \pm 20 cm/g$. This value of l is clearly higher than the corresponding values of the same polyester, measured with different techniques ($11nm$ with magnetic birefringence [20] and $9 - 11nm$ with viscosimetry [29]). It should be noted that the difference in the values of the persistence lengths obtained from

different techniques, reported in the literature, is usually high, much higher than the ones reported here [13, 17]. A wider range of molecular weights would lead to a better fit, and thus l. This is especially true for the low molecular weights, as concluded from Fig. 6.8 (where actually all data points but one are in the coil limit).

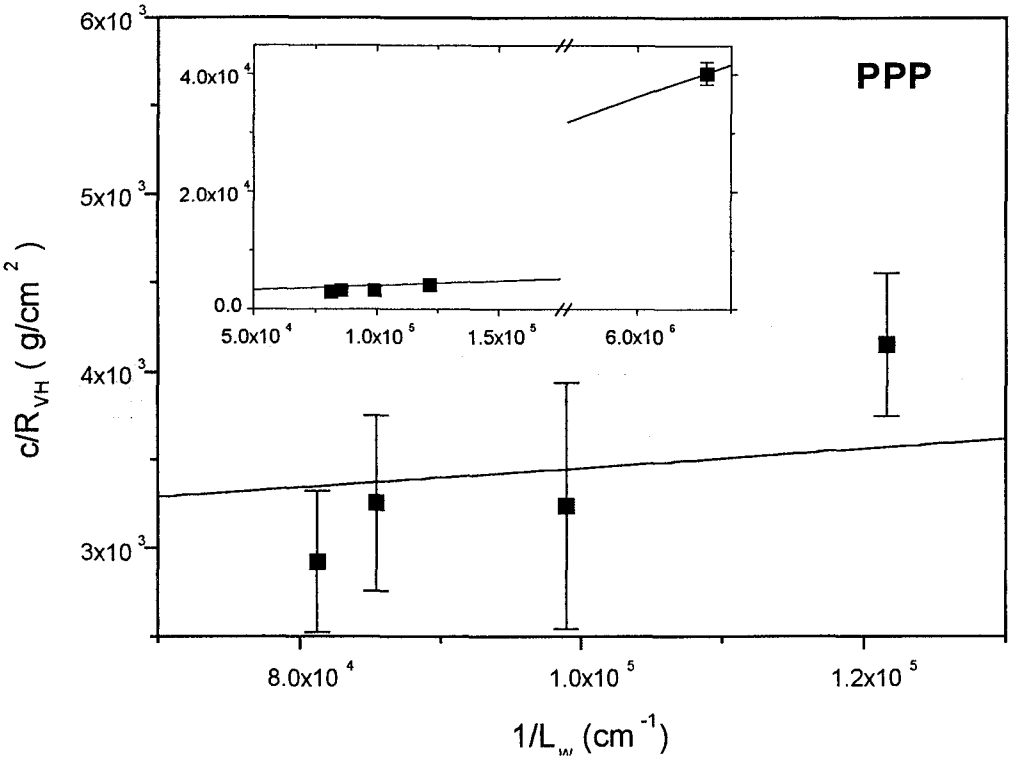

Figure 6.8: Determination of the persistence length of the poly(p-phenylene) PPP, using the linear equation (15), expressing $(c/R_{VH})_{c\to 0}$ as a function of L_w^{-1}. Solid line represents the least squares fit.

The persistence length of the PPP poly(p-phenylene) series was determined in the same way by the data in fig. 6.8. It is found to be approximately $28nm$, while K_{DRS} was found to be $120cm/g$, with similar remarks concerning experimental uncertainty as in the TPPE case. As seen in fig. 6.8, the monomer 3:12 was also used for extracting this value, based on the validity of Flory's incremental scheme (BAA) discussed above; further it served as the low molecular weight limit (all samples appeared to be in the rod limit anyway, thus the l determined was a low bound). It is noted that the value of the specific depolarization ratio for the monomer used in fig. 6.8 was determined from the measurements of the oligomer 3:12 by adding the contribution of substituted phenyls at the ends; the latter is estimated from the 2:0 and 3:0 oligomers. The result is $R_{VH}/c = 24.9\times$

$10^{-6} cm^2/g$. The above results indicate that PPP is a stiffer polymer than TPPE; this is considered reasonable, since due to the differences in the chemical structure of these polymers, as revealed in figures 6.2 and 6.3, in the PPP case the phenyl groups are directly connected in the polymer backbone, resulting in a stiffer molecule. It should be also mentioned that recent computer simulations with such materials (PPP) confirm their large stiffness (compared to polyesters), predicting a persistence length of about $22.0nm$ [34].

6.4.1 Additivity Approximation of the Optical Anisotropy

As already mentioned, the use of the wormlike model in the determination of the optical anisotropy, is based in principal on the validity of the additivity of the monomer anisotropy. We have assumed that the total optical anisotropy can be reproduced from the proper addition of the optical anisotropy of the repeating units. This is an extension of the BAA which assumes that the optical anisotropy is rather a local property and thus the molecular anisotropy is the addition of the anisotropies of the atoms or bonds from which the molecule is made. An other application of this principle aims at predicting the optical anisotropy of oligomers and nematogenic compounds from the values of their constitutive chemical groups [23, 35, 16]. Hence, it is imperative to check this assumption by utilizing K_{DRS} from eq. 6.23. This is done combining the results from the DRS measurements on the polymer samples with that on the oligomers 2:0. 3:0, 3:6, 3:12 and the trimer, as well as values of the optical anisotropies from literature. As mentioned above, the polarizability tensor can be splitted in two contributions: the cylindrical term $\Delta a_0 \widehat{J}$ and acylindrical one $\Delta a_0^+ \widehat{J}^+$. Applying the BAA, the polarizability of an oligomer can be estimated by a tensorial addition of the polarizabilities of its constituting groups [18]:

$$\hat{a}_M = \hat{a}_1 + R_1(\phi_1, \vartheta_1)\hat{a}_2 R_1^T(\phi_1, \vartheta_1) + R_2(\phi_2)R_1(\phi_1)\hat{a}_3 R_1^T(\phi_1)R_2^T(\phi_2) + \ldots \quad (6.24)$$

where the rotation matrices $R_i(\phi_1, \vartheta_1)$ transfer the polarizabilities $\hat{a}_i$ of each group in the frame of the first one by a similarity transformation. The angles ϕ_i, ϑ_j are the internal and valence angles, respectively, between successive groups. In a similar way, the optical anisotropy of a wormlike chain $< \gamma^2 >$, which of course is a scalar quantity, was deduced from the anisotropy of its monomer $< \gamma_0^2 >$ (eqs. 6.10 and 6.11). Usually the acylindrical term is very small compared to the cylindrical one for molecules with cylindrically symmetric monomers.

The value of $< \gamma_0^2 >$ can be calculated from K_{DRS} by using eq. 6.16. For TPPE, the value of K_{DRS} determined experimentally, and also $l_0 = 22$ $\AA$, $m_0 = 560$ and $f(n) = 1.859$, the effective optical anisotropy of the monomer was estimated to be 1196 ± 180 $\AA^6$. By considering only the cylindrical contribution to the optical anisotropy ($< \gamma^2 > \approx \Delta a^2$), the measured Δa of the

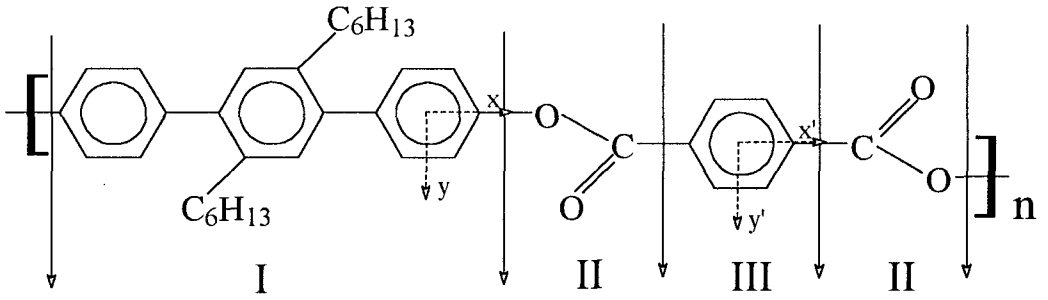

Figure 6.9: Devision of the monomer of TPPE series in groups for the estimation of the optical anisotropy with Flory's Additivity Approximation.

monomer is $34.6 \pm 2.5\AA^3$. On the other hand, with the use of Flory's additivity scheme this can be calculated based on the experimentally determined value of $< \gamma_0^2 >$ of the oligomer, 3:6 (from the measured R_{VH}/c) which amounts to $319\AA^6$ ($\Delta a = 17.86\AA^3$), and values from the literature for the optical anisotropy of the rest of the groups composing the trimer. These are as follows [23, 16]: $\Delta a(OCH_3) = 0.072\AA^3$; Δa(phenyl) $= 7.97\AA^3$; $\Delta a(OCO) = 1.02\AA^3$; and a change of the Δa of the phenyls in the 3:6, when they are substituted in the trimer ($0.097\AA^3$). The TPPE monomer is divided as shown in fig. 6.9 and the polarizabilities of each group were added. This monomeric unit is actually linear besides a small valence angle between x and x' ($\approx 5^o$) [23] induced by the ester group (II) as seen in fig. 6.9. This makes the calculation of the cylindrical part of the polarizability, which has cylindrical symmetry around the x-axis, trivial since for all groups I, II and III: $R_1(\phi_1, 0)\Delta a R_1^T(\phi_1, 0) = \Delta a$. The calculated value of Δa is $32\AA^3$ and the relative error with respect to the experimental is 8% . Including the acylindrical terms of the groups in the calculation does not alter this results since their contribution in the groups II and III are very small, while, it is anyway included in the experimentally determined value of $< \gamma^2 > (3:6)$.

In addition to the above, the trimer was directly measured, yielding a value of $< \gamma^2 >= 1601\AA^6$ (Table 6.1), and thus $\Delta a = 40.01\AA^3$ (if the acylidrical term is ignored). The estimated anisotropy, according to BAA calculations, based on the above values for the various groups is $\Delta a = 37.92\AA^3$; it corresponds to a small error of 5% compared to the experimental value. Thus, the comparison of these estimated values with the direct measurement of the trimer anisotropy as well as the measurement of monomer anisotropy deduced from the DRS analysis of the polydisperse polymer, confirm the validity of the Flory's incremental scheme (or the BAA), with a small error for the effective optical anisotropy of these molecules. Further, they support the utilization of the additivity approximation on a larger scale (that of the whole polymer chain), which is the physical basis

for the use of the wormlike model for the determination of the macromolecular optical anisotropy and the subsequent investigation of the conformation of such semistiff polymers by DRS.

6.5 Conclusions

The chain conformation of a series of polydisperse polyesters and poly(p-phenylenes) has been investigated by means of depolarized Rayleigh scattering in solution. By considering polydisperse wormlike chains, using a Schultz-Zimm distribution, the persistence length, l, was determined from the specific depolarized Rayleigh ratio at infinite dilution and the weight average chain contour length, without involving optical anisotropies or the internal field problem. This general analysis showed that the effect of polymer non-uniformity is nearly negligible. The persistence length, l, was determined by a simple universal plot of the reciprocal of the specific depolarization ratio versus the reciprocal of the weight average chain length. Results for the polyester series TPPE ($l = 19nm$) and the poly(p-phenylene) series PPP ($l = 28nm$) confirm that poly(p-phenylenes) are stiffer molecules than polyesters, but are higher than the ones obtained with different techniques, due to the errors associated with the limited range of molecular weights available. Finally, by determining the effective anisotropy of oligomers, using the second power correction to the internal field, and comparing against the calculated values of the substituent units, it is shown that Flory's group additivity approximation works well for these systems.

References

[1] M. Ballauff. *Materials Science and Technology.* VCH:Weinheim, 1993.

[2] K.F. Wissbrun. *J. Rheol.*, 25:619, 1981.

[3] S.P Russo. *Dynamic Light Scattering: The Technique and Some Applications*, page 512. Oxford Science Publications, 1993.

[4] M.A. Tracy and R. Pecora. *Annu. Rev. Phys. Chem.*, 43:525, 1992.

[5] G. Petekidis, G. Fytas, and H. Witteler. *Colloid Polym. Sci.*, 272:1457, 1994.

[6] K. Fuhrmann, A. Martin, G. Maret, U. Tiesler, and M. Ballauff. *J. Phys. Chem.*, 98:4094, 1994.

[7] R. Sato, T. Norisuye, and H. Fujita. *Macromolecules*, 17:2696, 1984.

[8] T. Coviello, K. Kajiwara, W. Burchard, M. Dentini, and V. Crescenzi. *Macromolecules*, 19:2826, 1986.

[9] M. Bohdanecky. *Macromolecules*, 16:1483, 1983.

[10] H. Watanabe and K. Yoshioka. *Biopolymers*, 4:43, 1966.

[11] V. N. Tsvetkov and L. N. Andreeva. *Adv. Pol. Sci.*, 39:95, 1981.

[12] Kirste R.G. and R.C. Oberthur. *Small angle X-ray scattering.* Academic Press, 1982.

[13] C.J. Carriere, E.J. Amis, and J.D. Schrag, J.L.and Ferry. *J. Rheol.*, 37:469, 1993.

[14] A. Ott, M. Magnasco, A. Simon, and A. Libcharber. *Phys. Rev. E*, 48, 1993.

[15] G. Fytas and A. Patkowski. *Dynamic Light Scattering: The Technique and Some Applications*, page 440. Oxford Press, 1993.

[16] G. Floudas, A. Patkowski, G. Fytas, and M. Ballauff. *J. Phys. Chem.*, 94:3215, 1990.

[17] Y. Takaeda, T. Yoshizaki, and H. Yamakawa. *Macromolecules*, 26:3742, 1993.

[18] P. Flory. *Statistical Mechanics of Chain Molecules, 2nd ed.* Hanser Publishers, Munchen, 1989.

[19] G. Petekidis, D. Vlassopoulos, P. Galda, M. Rehahn, and M. Ballauff. *Macromolecules*, 29:8948, 1996.

[20] U. Tiesler, M. Rehahn, Ballauff M., G. Petekidis, D. Vlassopoulos, G. Maret, and H. Kramer. *Macromolecules*, 29:6832, 1996.

[21] M. Arpin, C. Strazielle, G. Weill, and H. Benoit. *Polymer*, 18:262, 1977.

[22] J.B. Berne and R. Pecora. *Dynamic Light Scattering.* Willey Interscience Publications, New York, 1976.

[23] P.A. Irvine, B. Erman, and P.J. Flory. *J. Phys. Chem.*, 87:2929, 1983.

[24] T. Keyes and B.M. Ladanyi. *Adv. Chem. Phys.*, 56:411, 1986.

[25] A.K. Burnham, G.R. Alms, and W.H. Flygare. *J. Chem. Phys.*, 62:3289, 1975.

[26] Booth C. and R.O. Colclough. *Polymer Engyclopedia.* Academic Press, 1982.

[27] P. Flory. *Principles of Polymer Chemistry.* Cornell Univ. Press, Ithaca,New York, 1953.

[28] M. Rehahn, A.-D. Schluter, and G. Wegner. *Makromol. Chem.*, 191:1991, 1990.

[29] U. Tiesler, T. Pulina, M. Rehahn, and M. Ballauff. 243:299, 1994.

[30] P. Galda and M. Rehahn. *Synthesis*, 1996.

[31] G. Petekidis, D. Vlassopoulos, G. Fytas, N. Kountourakis, and S. Kumar. *Macromolecules*, 30:919, 1997.

[32] Y. Takaeda, T. Yoshizaki, and H. Yamakawa. *Macromolecules*, 28:4167, 1995.

[33] T. Konishi, T. Yoshizaki, J. Shimada, and H. Yamakawa. *Macromolecules*, 22:1921, 1989.

[34] B.L. Farmer, B.R. Chapman, D.S. Dubis, and W.W. Adams. *Polymer*, 34:1588, 1993.

[35] P.J. Flory and P. Navard. *J. Chem. Soc. Faraday Trans.*, 82:3381, 1986.

by electrostatic forces [11], or kinematics [12], aggregation in a stabilized colloidal dispersion is a function of the volume fraction of the suspended particles [13, 14]. Initially, single colloidal particles undergo Brownian motion until small clusters are formed (with increasing concentration); then cluster and particle diffusion results in formation of larger aggregates, and so on. The key factor controlling the formation of aggregate structures is the balance among short-range interparticle forces [1]. The process of cluster growth, when irreversible, has a fractal structure and is characterized by two limiting modes, depending on whether the sticking probability is about one or much smaller than one [15, 16, 17, 18]. Directly related to the aggregation problem is the sedimentation of colloidal particles. This process is controlled by the combined action of the Brownian motion and gravity. The coupling between these two driving forces gives rise to a rich variety of physical phenomena, ranging from cluster formation, to cluster deposition and settling of a gelled suspension [11, 19]. Furthermore, the sedimentation of aggregates can induce further aggregation, controlled by the convective transport of the aggregating material [20]. Thus, in order to understand the mechanism and dynamics of aggregation under these circumstances, it is imperative to control the coupling between cluster diffusion time and cluster settling time [19, 21, 22].

Dynamic light scattering represents a powerful tool for the investigation of the aggregation process, since it provides information on the aggregation dynamics and size of association of the various moieties through a combination of scattered intensity and relaxation rate measurements [23, 24]. Moreover, depending on the system investigated, the measurement of depolarized, in addition to the polarized light scattering, is essential because of its sensitivity and unique information on the structure and shape of the aggregates [25, 26, 27, 28, 29, 30].

It has been known for several years that rod-like polymers in solution aggregate in various solvents [4, 31, 32]. The physical grounds of this process are not clearly understood yet, but it seems that the balance of interparticle forces results in a dominance of van der Waals attractions, leading to aggregation. It is recognized, however, that the nature of interparticle forces cannot be easily determined for solutions of anisotropic particles, since electrostatic and hard-core forces act on the particles positions and orientations in a different way; typically, with increasing concentration hard-core repulsion induces a nematic order of the particles, whereas uniformly charged rods tend towards a perpendicular orientation [1]. There is clear evidence that aggregation can be observed in fresh solutions (within 24 hours from preparation), but the kinetics of this process is characterized by much longer times [33]. Phenomenology suggests that a simple mass-action model [34] can describe the main features of aggregation in terms of cluster formation (dimers and higher-order associations), as shown recently in the case of poly(p-phenylene terephthalamide) solutions [35]. However, it cannot explain the origin of aggregation. The probable relevance of the aggregation of rigid polymers to their phase behavior, and in particular to transitions such as gelation, crystallization, or isotropic-nematic is one of the central questions in this

field. In this direction, recent work [36] on the phase separation of poly(γ-benzyl L-glutamate) in benzyl alcohol, suggests that gelation is due to a combination of crystallization and phase separation via spinodal decomposition. Although molecular aggregation is not explicitly discussed, it is clearly implied that this process is indeed associated with the mechanism of gelation; it is interesting to note in that respect, that two modes of aggregation are considered, namely the binary associations resulting in small clusters, and the associations of the latter into larger aggregates [36, 37, 38].

An attempt to put together the ideas from colloidal aggregation and dynamic light scattering from semidilute solutions of side-chain liquid crystalline polymers was presented in reference [8]. These workers observed cluster formation at a critical concentration independent of the molecular weight, and suggested that it is due to attractive interactions. Clusters were very large and with non-fractal structure, whereas no evidence of long-range liquid crystalline order inside these aggregates was found, from static depolarized light scattering. Similar findings were also reported on the behavior of concentrated colloidal suspensions of anisotropic poly(isobutene)-grafted boehmite rods, using static and dynamic light scattering [39]. At high volume fractions they found an extra relaxation process, attributed to the presence of clusters.

In our opinion the following crucial questions remain open: (i) the deeper understanding of the origin and mechanism of aggregation; (ii) the ordering of the molecules and the characteristic size and shape of the aggregate structures; (iii) the kinetics of aggregation and its relation to sedimentation, which usually accompanies this process; and (iv) the potential relevance of macromolecular self-assembly to polymer-solvent phase separation or transitions such as gelation or isotropic to nematic. These questions will be addressed in this chapter, with the aim to provide some insight into the complex problem of self-assembly in rigid-rod polymers and control molecular dynamics which are discussed in the next chapter.

7.2 Experimental

7.2.1 Materials

In the present study the hairy-rod poly(p-phenylene) PPP-2 with number average molecular weight $M_n = 9,900 g/mol$ was used (table 8.2). The persistence length of these polymer was determined by DRS as described in the previous chapter; it was found to be 28 nm [40], a value which in comparison with other techniques [40, 41] is thought to be an upper bound. The number-average contour length was L_n = 25.7 nm. Thus, the onset of the semidilute region is c^* ($= 1/L_n^3$)$\approx$ 0.11% by weight, and that of the concentrated region c^{**} ($= 1/\ bL_n^2$) is 5.7% by weight. In this calculation we assume b = 1.7 nm taking into account the

side chains as well [42]. We have investigated both dilute and semidilute PPP solutions in toluene, with concentrations in the range $0.1\% - 0.4\%$ and $3.5\% - 5\%$, respectively.

7.2.2 Light Scattering

All light scattering measurements were conducted either with the ALV goniometer set-up or with the fixed angle set-up which are described in chapter 5.

7.2.3 X-Ray Scattering

X-ray diffraction patterns of of various PPP sediment samples were recorded with a curved position-sensitive detector (INEL-CPS 120) using a Guinier focusing camera equipped with a bent quartz monochromator (Cu-Kα_1). PPP powder was measured with a Rigaku D/max-2400 diffractometer, equipped with a graphite monochromator, utilizing a 12 kW rotating anode X-ray generator (Cu-Kα_1).

7.2.4 Experimental Protocol

The studies carried out are divided in two main parts: (a) dilute regime, and (b) semidilute regime. In the former case, the key question is whether one can measure truly molecular transport properties. In the latter case, the main concern is the understanding of the mechanism, nature and kinetics of association, as well as the effects of temperature and sedimentation on the experimental correlation functions. In each case the experimental tool was a combination of static and dynamic (PCS) light scattering, performed on equilibrated systems at various concentrations, temperatures, scattering angles and settling regimes.

7.3 Dilute Regime

Static and dynamic light scattering measurements were carried out in dilute solutions (concentration range $0.07\% - 0.39\%$ by weight), at various temperatures, and in two different solvents (toluene and chloroform).

7.3.1 Statics

Static light scattering measurements were carried out in toluene, at concentrations 0.084% , 0.159% and 0.39% by weight (corresponding to a c/c^* range from 0.8 to 4.4, respectively) and temperatures 25^oC, 50^oC and 80^oC. The purpose of these measurements was to estimate the second virial coefficient A_2 and hence the solvent quality. The data revealed a weak q dependence of the intensity at

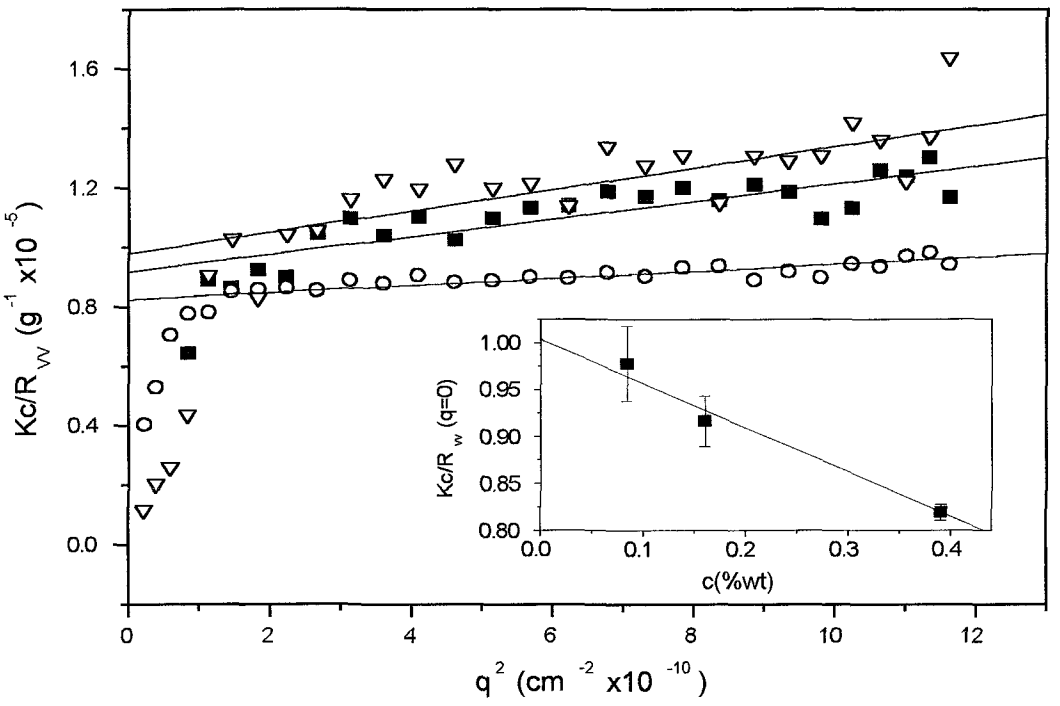

Figure 7.1: Polarized (VV) static light scattering results for PPP in toluene at 25^oC and various concentrations: (○) 0.39 % by weight; (■) 0.16 % ; (▽) 0.084 %. Solid lines represent fits to the high-wavevector (q) region. Inset: Determination of molecular weight by extrapolation of Kc/R_{VV} at $q = 0$ (■), at infinite dilution (solid line).

scattering angles above 30^o, whereas at lower angles an enhanced intensity was observed. Due to the careful way of collecting static data (the trace of the scattered intensity remained constant, without any fluctuations whatsoever), the presence of dust can be excluded as a potential cause of the observed excess intensity at low angles. This sharp intensity deviation at low q's is normally attributed to aggregation [43] and has been reported in several other systems [6, 7, 39].

For all concentrations tested, the VV intensity at $q = 0$ ($I_{VV}(0)$), obtained from the $I_{VV}(q)^{-1}$ versus q^2 plot (a typical such plot is depicted in Figure 7.1, at 25^oC), increases as the temperature decreases. A smaller change is found in the lower concentration. It should be noted that the extrapolation at $q = 0$ for I_{VV} was always done using the data from scattering angles above 30^o, due to the significant scattering at low angles. It is also noted that in contrast to I_{VV}, I_{VH} does not exhibit an upturn at low q's. This behavior can be rationalized as the existence of few isotropic clusters, even at low concentrations. A_2 was estimated

from the dependence of K_c/R_{VV} on q^2, where K is the constant containing the refractive index n and refractive index increment $\partial n/\partial c$, c is the concentration of the polymer, and R_{VV} is the Rayleigh factor, computed from the known R_{VV} of toluene. A_2 was found to be negative at all temperatures investigated, with a nearly unchanged value of $-5 \times 10^{-4}\ cm^2/g$. This result suggests that the solvent quality is not good, and thus aggregates may be formed and the system may eventually phase separate according to the usual phase behavior of a polymer solution under bad solvent conditions (see fig. 2.3).

In addition to A_2 , static measurements revealed that the z-average radius of gyration, $(R_g)_z$, was 22 nm. Using the formula [44, 45, 46] (for a rod of diameter 1.7 nm):

$$(R_g^2)_z = \frac{(m+2)(m+3)}{(m+1)^2}\frac{L_w^2}{12} + \frac{b^2}{8} \tag{7.1}$$

where m is the polydispersity index ($m = (M_w/M_n - 1)^{-1}$), the weight-average contour length L_w was found to vary from 385 to 44 nm, when m varies from 0.5 to 1. It is noted that from Eq. 7.1 b appears insensitive to the calculation of L_w. If the semiflexible conformation of the polymer chains is taken into account (using the wormlike model), the radius of gyration is given by [44, 45]:

$$(R_g^2)_z = \frac{(m+2)}{3(m+1)}lL_w - l^2 + \frac{2l^3}{L_w}\left(1 - \frac{l}{m(m+1)}\left[\left(\frac{m+1}{L_w}\right)^2 - \frac{\left(\frac{m+1}{L_w}\right)^{m+2}}{\left(\frac{m+1}{L_w} + \frac{1}{l}\right)^m}\right]\right) \tag{7.2}$$

From this equation, for a value of the persistence length l between 15 and 28 nm, L_w varies between 74 and 48 nm, leading to similar results as in the rigid-rod case; it is noted that given the polydispersity, the L_w estimated from ref [47] is 77 nm.

Furthermore, the weight average molecular weight M_w was determined from extrapolation of K_c/R_{VV} at infinite dilution (inset of Fig. 7.1), yielding $M_n \approx$ 100,000 at 25^oC, $M_w \approx$ 74,000 at 50^oC, and $M_w \approx$ 52,500 at 80^oC. In chloroform at 20^oC and $c = 0.07\%$ we get $M_w \approx$ 36,900. These results seem to be in disagreement with those reported in a mixed solvent of cyclohexane and chloroform, where it was found that at 25^oC, $M_w \approx$ 29,700 [47], and support the idea that rods are probably aggregated into small units, probably trimers or tetramers under these conditions. Based on the above numbers, the average degree of aggregation amounts to 3.3 for a solution in toluene at 25^oC. We shall term these small aggregates as trimers (typical size) in the rest of this work. Setting aside the slight difference in temperature, which cannot account for the observed deviation, the clear message is that PPP tends to associate in toluene.

7.3.2 Dynamics

PCS measurements were carried out in the same dilute solutions in toluene and chloroform, and in the temperature range $10°C$ to $50°C$, yielding a single relaxation process (translational diffusion). Before use, each solution was heated up at high temperature (about $80°C$), where it was checked that one relaxation process was present; it was subsequently cooled to the test temperature, and left to equilibrate for one hour. Measurements were repeated at several times, during a period of one year, and indicated the same single relaxation process unchanged. This represents a direct demonstration of the time stability of the solution investigated. At this low concentration, the VH dynamics associated with the rotational diffusion of PPP is faster than 10^{-6} sec, and thus falls outside the time window of the correlator, as inferred from the flat correlation functions.

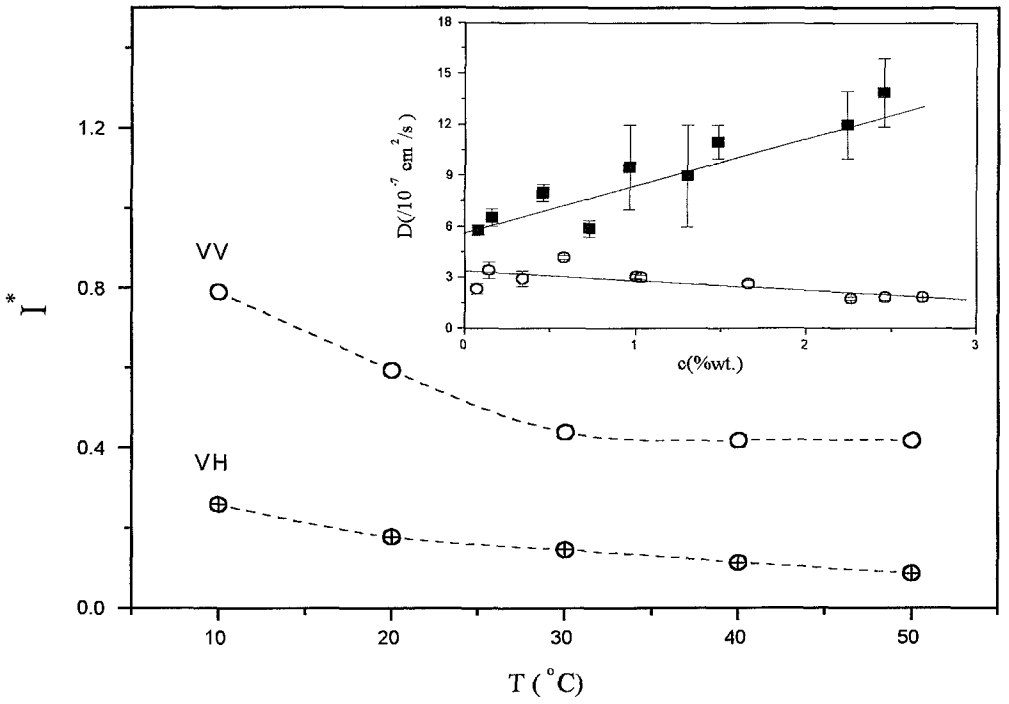

Figure 7.2: Total scattering intensities I^* for polarized (VV) and depolarized (VH) PCS measurements, extrapolated at $q = 0$, for the 0.21% by weight PPP/toluene solution, as a function of temperature; both intensities are normalized to the VV intensity of toluene. Lines are drawn to guide the eye. Inset: Translation diffusion coefficients at various concentrations of PPP/toluene (○) and PPP/chloroform (■) for determination of diffusion, D_0, at infinite dilution. Solid lines represent best fits.

Fig. 7.2 depicts the corresponding VV and VH scattered intensities due to the polymer (normalized to the corresponding VV intensity of toluene), at $q = 0$. An unexpected increase of both intensities as the temperature drops is clearly observed. $I_{VV}(0)$ and $I_{VH}(0)$ exhibit a 90% and 180% increase, respectively, as the temperature is decreased from 50^o to 10^oC. The behavior of I_{VV} represents strong evidence of a decrease of the solvent quality as the temperature is decreased, which suggests that this system becomes more strongly interacting as the temperature is reduced. Further, the behavior of I_{VH} may indicate a strong increase of the orientational pair correlations, even at low concentrations. The intensity information points to the issue of association of the molecules; in such a case I_{VH} is very valuable, since it may suggest potential ways of how the molecules associate to form cluster.

Dynamic measurements at lower concentrations were also carried out in both toluene and chloroform (Fig. 7.2, inset), from which the translational diffusion coefficient D_0 at infinite dilution, extrapolated at $q = 0$, was determined; the latter is assumed to be the self diffusion. By using the relation of Broesma (Appendix B) [48, 49], the contour length L of the rod-like PPP trimers can be determined, by assuming absolute stiffness and a certain value of the rod (trimer) diameter, b. This expression relates D_0 to the geometric characteristics of the trimers:

$$D_0 = \frac{k_B T}{3\pi n L}\left[\ln\left(\frac{2L}{b}\right) - \gamma\right] \tag{7.3}$$

For the toluene solution, the measured diffusion coefficient is $D_0 = (3.41 \pm 0.22) \times 10^{-7} cm^2/s$, while for the chloroform one, $D_0 = (5.65 \pm 0.44) \times 10^{-7} cm^2/s$. Assuming $b = 1.7\ nm$ [42], the corresponding values of L are 87.8 nm and 44.1 nm, respectively. It is noted that for polydisperse samples the z-average diffusion coefficient is actually measured, which for Eq. 7.3 is related to L_w. Further, from the value of L in toluene, which appears large, the rotational diffusion constant [48, 49]

$$D_{R,0} = \frac{3k_B T}{\pi n L^3}\left[\ln\left(\frac{2L}{b}\right) - \zeta\right] \tag{7.4}$$

where ζ is a function of L/b, can be calculated; its value is $D_{R,0} = 33,757 s^{-1}$ for $T = 25^oC$. The relevant characteristic time, $\tau_R = (6D_r)^{-1}$, is then estimated to be $5 \times 10^{-6} s$, indicating that the VH process should be observable inside the time window of the correlator. The fact that we do not get any VH dynamics, strongly suggests that the aspect ratio of the scattering moieties is smaller; the diameter should be larger, and this represents another evidence of aggregation. The assumption of absolute stiffness can be relaxed by considering semi-stiff chains. In such a case, the Hearst-Stockmayer relations [50] are used (Appendix B):

$$D_0 = \frac{k_B T}{3\pi n_0 L}\left[\ln\left(\frac{L}{h}\right) + 0.166\left(\frac{L}{2l}\right) + \frac{h}{b} - 1\right] \quad (7.5)$$

and

$$D_{R,0} = \frac{k_B T}{\pi n_0 L^3}\left[3\ln\left(\frac{L}{h}\right) - 7 + 4\left(\frac{h}{b}\right) + \frac{L}{2l}\left(2.25\ln\left(\frac{L}{h}\right) - 6.66 + 2\left(\frac{L}{b}\right)\right)\right] \quad (7.6)$$

where h is the length of the repeating unit (1.49 nm), l taken typically as 25 nm and $b = 1.7$ nm. Application of Eq. 7.5 in the case of the solution in toluene leads to $L = 105$ nm. Then, from Eq. 7.6 $D_{R,0} = 41,837$ s^{-1} and $\tau_R = 4 \times 10^{-6} s$, which is similar to the stiff rod results above. Therefore, it can be concluded that chain flexibility (or rigidity) should not be the reason for the observed effects, or the lack of VH dynamics in the time window available. Furthermore, from the measured diffusion constant in toluene and for an average $L_w = 65$ nm (as determined from static light scattering, using the wormlike model) we get a hydrodynamic diameter of $b = 6$ nm. Compared to the value of $b = 1.7$ nm considered above, this result is in agreement of the static results above, suggesting that the scattering moieties (in toluene) are rather small aggregates (typically trimers, as discussed before) lying parallel to each other; the actual number of molecules forming these small aggregates depends on the conformation of the molecules, and mainly the side chains, but based on the above numbers, as well as the wormlike conformation of the macromolecules, the static and dynamic information on aggregation is consistent; but again, typically they are trimers. This parallel alignment is not surprising, since this orientation is necessary for the van der Waals forces to dominate and aggregation to take place [1, 51], and is also consistent with the VH intensity behavior (Fig. 7.2).

7.3.3 Semidilute Regime

Phenomenology

We now turn to the higher concentrations with the aim of investigating the dynamics of self-assembly of the hairy rods. We start with a semidilute solution of concentration 3.9% ($c/c^* \approx 35$), which was measured 6 days after preparation at three successive temperatures, namely 25 , 50 and 80^oC, respectively. It is noted that, before each measurement, the samples were always left to equilibrate, as already mentioned. Results in terms of $g_{VV}(q,t)$ and the distributions $L(ln\tau)$ are depicted in Fig. 7.3. It is noted that all $g_{VV}(q,t)$ shown have been corrected for the instrumental factor f^*, and hence represent net normalized intensity time correlation functions. At the end of the measurements, the sample was left at 80^oC overnight and measured again the 2nd day after cooling at the same temperature.

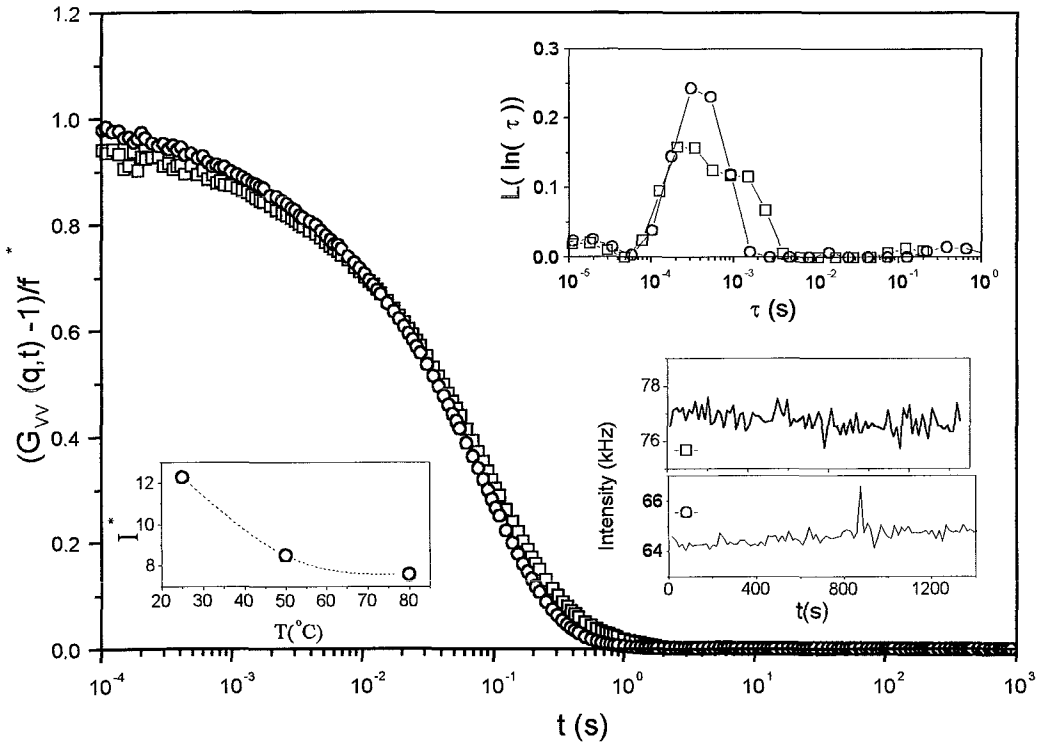

Figure 7.3: Polarized (VV) intensity correlation functions for a 3.9% by weight PPP solution in toluene, at a scattering angle of 45^o and a temperature of 25^oC, before (□) and after (○) a temperature treatment at 80^oC. Corresponding distribution of relaxation times and intensity profiles during the experiments, are depicted in the upper and lower right insets, respectively. The mean total polarized intensity normalized to that of toluene, I^*, is shown at different temperatures in the lower left inset.

It is clear that on the first day there is a second process at 25^oC, slower than the main one; the latter is attributed to cooperative diffusion of the polymer. This extra process seems to be an induced one, since it disappears with increasing temperature. Further, it does not reappear on the second day, when cooling down to 25^oC, and keeping the solution at that temperature for 24 hours. The corresponding total intensity for the second day increases (by about 60%) as the temperature drops from 80^oC to 25^oC, and is depicted in the lower left inset of Fig. 7.3. Further, in the temperature range studied (25^oC to 80^oC) the dynamics of the main process scales with the solvent viscosity. This suggests that, besides the disappearance of the extra slow process, no break-up of the original scattering moieties, i.e. trimers (in the "entangled" state), takes place at the specific concentration, as the temperature increases.

The presence of the extra slow process originally at 25^oC, together with its

disappearance at 80^oC and the corresponding intensity behavior, represents an evidence of the significance of the role of the thermodynamic interactions in this phenomenon, which appears to be time-dependent. Further, it is noted that the temperature treatment described in Fig. 7.3 leads to a $g_{VV}(q,t)$ at 25^oC with no extra process within at least 24 hours, indicating a way to obtain a semidilute solution without additional intermolecular processes (among trimers, as discussed in the dilute regime section) within a certain time; this is important for studying molecular (rather trimer in this case) dynamics under such conditions. The above information suggests that interactions in the system are increased at lower temperatures (while dynamics still probes only one molecular -rather trimer- relaxation process), and this of course brings up the issue of phase separation, which will be discussed below.

Kinetics of aggregate formation

Using the information from Figs. 7.2 and 7.3, it was decided to perform these investigations at 10^oC and a concentration of 5% ($c/c^* \approx 45$), since under these conditions the observed effects are anticipated to be more dramatic. The solution was left for at least one day at 80^oC to break-up any potential intermolecular aggregates, as confirmed by the single relaxation process at that temperature. It was then cooled down to 10^oC, where successive static and dynamic light scattering measurements were carried out for a period of about three weeks. Fig. 7.4 shows the time evolution of $g_{VV}(q,t)$ for this solution at a scattering angle of 45^o. The first day corresponds to the fresh solution, pretreated at 80^oC as already described, and measured within 24 hours after reaching the final temperature of 10^oC. Only one relaxation process appears, which is attributed to the cooperative diffusion of the molecules (trimers) in the semidilute solution. This process has a characteristic time which remains constant at about $0.5ms$, from the first to the 15th day. However, with elapsed time we observe an additional slow process (third day), which appears to be more pronounced as time evolves, and comprises actually of two separate relaxation modes (15th day). Meanwhile, the total intensity (inset of Fig. 7.4) increases and exhibits significantly larger fluctuations. On the 15th day, the second process, which we call "slow", has a characteristic time in the range of $20ms$, while the third one, which we call "ultraslow", has a characteristic time of about $350ms$.

From this discussion, it follows that the time of the evolution of these processes is of the order of two weeks. The $g_{VV}(q,t)$ of the 1st day indicates that the first process is a stretched exponential, with a typical value of the shape parameter $\beta = 0.7$. This is expected, since in semidilute solution the coupling between rotation and translation or other relaxation mechanisms, may interfere with the cooperative diffusion, in addition to polydispersity effects. The dynamics of both concentration and orientation fluctuations, without the interference of the cluster formation with time (as measured soon after preparation) will be discussed in

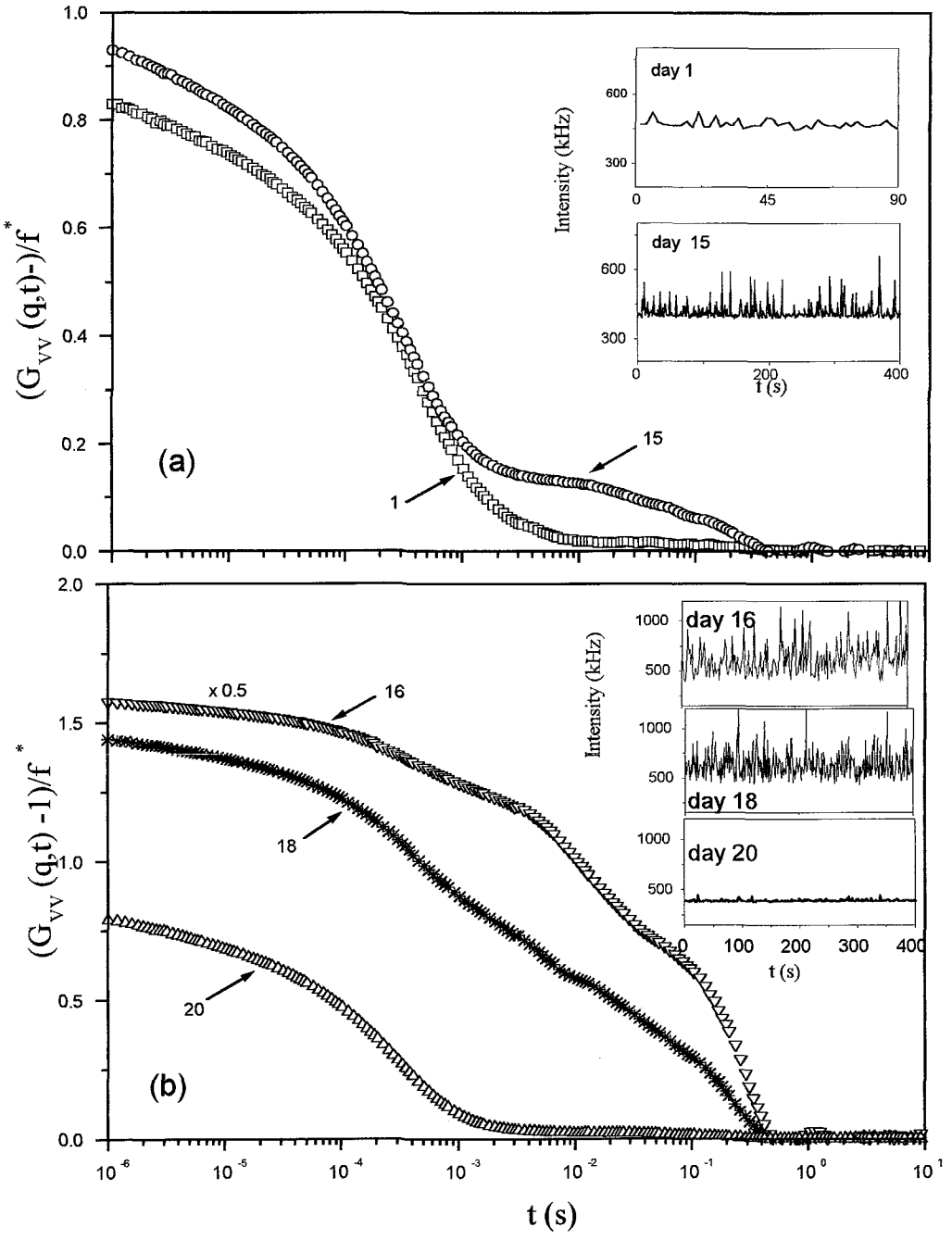

Figure 7.4: Polarized intensity correlation functions for a 4% by weight PPP solution in toluene, at a scattering angle of 45^o and a temperature of 10^oC, at various elapsed times: (a) 1st and 15th day from solution preparation, (b) after the disterbance: 16th, 18th, and 20th days (indicated by the arrows) from solution preparation. The correlation function of the 16th day exhibits a pronounced contrast, and is divided by 2 (x0.5) for clarity. Inset: Traces of the corresponding total scattering

the next chapter.

The slower processes can be characterized either from the $g_{VV}(q,t)$ of the 15th day or from the corresponding one right after the disturbance (e.g., 16th day), as discussed below. The second slow process is typically nearly single exponential or slightly steeper ($\beta = 1.1$), while the main characteristic of the third ultraslow mode is its clearly steeper than single exponential shape; when fitted with a KWW function it gives a shape parameter with typical value of $\beta = 1.4$. Further, the relaxation times of the three processes, exhibit different q-dependencies, as discussed in section 7.3.4 below.

The formation of clusters, related to the slow and ultraslow processes, was accompanied by sedimentation. This was observed visually; a cloudy off-white sediment was apparent in the bottom of the sample cell, filling a small volume fraction of the solution. When the sample was examined by PCS after 1 hour, the amplitude of the two slow processes, as well as the total intensity and its fluctuation increased substantially, as can be seen in Figs. 7.4 and 7.5 and their insets. Meanwhile, the amplitude of the main process is apparently decreased. Note that in Fig. 7.4 one correlation function (16th day) is divided by 2, since its contrast is very high, as discussed below (section 7.3.4). This dramatic effect is certainly due to the slight disturbance of the sample, associated with the removal of the sample cell from the goniometer set-up and its subsequent return. As a result of that, some clusters, mostly from the top surface of the sediment, break apart from it and are redispersed to the top solution giving rise to additional intensity fluctuations, as well as enhanced average intensity and contrast. Eventually, at steady state these dispersed clusters will settle down, as it will be discussed below.

An additional feature associated with the extreme sensitivity of the correlation functions to mechanical disturbance, is the fact that the increased contrast of the slow modes now provides a means to characterize them systematically; this was a rather difficult task to do before this disturbance, as can be inferred from the correlation function of the 15th day (Fig. 7.4). From Figs. 7.4 and 7.5, it is apparent that during the 16th day the slow and ultraslow processes are very pronounced, but they decrease with time rather significantly; for instance, on the 18th day, their contrast has dropped. Finally, on the 20th day, i.e., 5 days after the sample disturbance, the fast main process dominates the correlation function, whereas the total intensity is decreased and becomes smooth (no fluctuations). This behavior is clearly a result of the sedimentation of aggregates and any potential larger formations, which appear as the off-white cloud, dispersed in the solution. The q-dependence of the dynamics of the various processes is unaffected: the fast process is q^2-dependent, the slow is weakly q-dependent, and the ultraslow one is almost q-independent. It should be mentioned however, that it is difficult to determine the characteristic times with high accuracy, due to the uncertainty involved in the experimental procedure. In this context, it must be noted that although it is widely recognized that the optimum way to

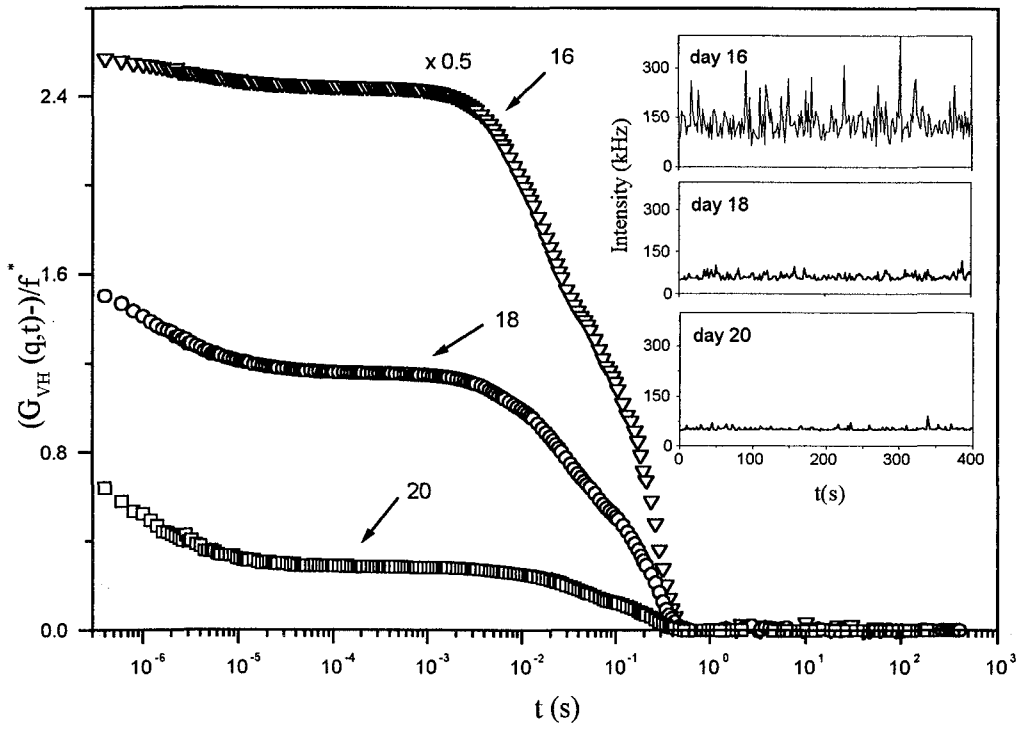

Figure 7.5: Depolarized intensity correlation functions for the 4% by weight PPP solution in toluene, at 45° and 10°C, at the 16th, 18th, and 20th days (indicated by the arrows), from solution preparation. The correlation function of the 16th day exhibits a pronounced contrast, and is divided by 2 (x0.5) for clarity. Inset: Traces of the corresponding total scattering intensities.

analyze the experimental $g(q,t)$ is by means of the ILT analysis, the treatment of the $g(q,t)$ exhibiting cluster modes was carried out using a double or triple KWW fit, and not ILT, since the correlation functions of the slow processes are sharper than single exponential. The characterization of the slow and ultraslow modes is completed by measuring the dynamics in the VH geometry, as seen in Fig. 7.5. The tail just seen in Fig. 7.5, at the fast edge of the time window of the correlator, is real and represents the fast VH process due to molecular reorientation, which slows down significantly with increasing concentration of the rod-like chains [42, 52]. Setting this mode aside, we clearly see two slow VH processes, with intriguing similarities with the respective VV relaxation functions: they loose amplitude from the 16th to the 20th day; their times are the same in magnitude as the corresponding VV times, within experimental error. The fact that both slow and ultraslow processes are VH active indicates that they are anisotropic; this suggests possible ways of formation of the clusters and larger

associations. As already mentioned, when the slow and ultraslow processes were dominant in the period between 16th and 18th days, both in VV and VH (Figs. 7.4 and 7.5), the total contrast exceeded the full contrast of our set up. The only explanation that can be given at this point is the statistical bias due to the presence of large and sudden fluctuations of the scattered intensity; this breaks up the translational time invariance of the scattered intensity, and as a result the process is no longer "stationary stochastic" [53]. Under these circumstances, the Siegert relation (Eq. 3.12) may not hold anymore. This problem makes the calculation of the amplitudes of the relaxation processes somehow ambiguous. To hadle this difficulty, we assume that the contrast of the fast well-resolved (in the polarized geometry) process is true, and that the rest of the contrast needed to reach full contrast is split into the two extra processes according to their apparent contrasts. Results of the amplitude analysis are discussed in section 7.3.4.

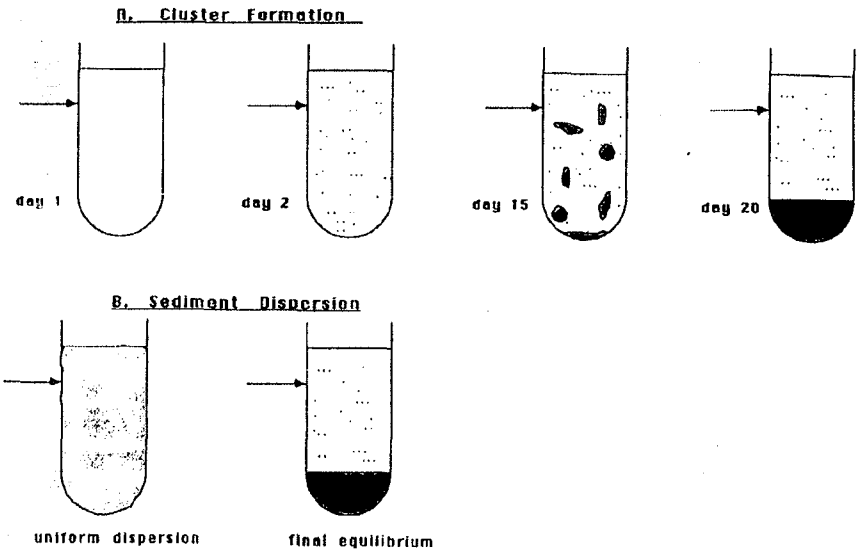

Figure 7.6: Schematic of the measured PPP sample, illustrating the position of measurement and formation and sedimentation of the cloud (a), or the dispersion of the sediment and settling of a uniform suspension (b). Arrows indicate position of PCS measurement. (a) Cluster formation: day 1: homogeneous solution; day 2: aggregation nuclei formed; day 15: cloud formation; day 20: final equilibrium between sediment and top clear solution. (b) Sediment dispersion: uniform dispersion: immediately following shaking; final equilibrium: sediment with top clear solution, after about 1-2 hours, depending on shaking.

Before proceeding with the detailed discussion of the nature of the aggregation modes, the heating cycle and sedimentation studies, it is illustrative to explain

the physical layout of these investigations. As can be seen schematically in Fig. 7.6, the static and dynamic experiments on cluster formation "look" at a fixed position of the sample cell, near the top surface (indicated by the horizontal arrow). At the beginning of the kinetic experiment, the sample is homogeneous, as in day 1, for instance (see also Fig. 7.4). Then, with time some aggregation nuclei are formed, which may cross the probe volume, on day 3 for example. Later, on day 15, some clouds are formed, which seem to be in equilibrium with smaller moieties. Finally, sedimentation of the various associations (also clouds) takes place; there is a large concentration gradient toward the bottom of the sample, and eventually at steady state there is a top clear solution in equilibrium with the sediment, at day 20.

The intervention of sedimentation

It is now clear that since the associations settle under gravity once they grow beyond a certain size, understanding the sedimentation process is a crucial task. To this end, the behavior of the semidilute phase-separated system (with the sediment, at the end of the 20th day) was studied systematically at various temperatures, in order to determine the "onset-of-melting" temperature, corresponding to a single relaxation process, as discussed below. The first temperature examined was 25^oC. The situation is illustrated schematically in Fig. 7.6, where the two-phase system was agitated manually in order to obtain a macroscopically uniform suspension. Due to the extreme sensitivity of the system under investigation to mechanical disturbance, it is obvious that these shaking experiments are not quantitatively reproducible. This means that the characteristic times for the beginning and end of the transient settling regime are not reproducible, but vary depending on the shaking. Nevertheless, the physical picture remains unchanged. A typical sedimentation kinetics experiment is illustrated in Fig. 7.7, which depicts the total scattered VV intensity, normalized to the polarized intensity of toluene at 45^o, as a function of time. Initially, the sample is uniformly dispersed and the intensity is constant. After about one hour settling has started and becomes evident through the sharp decrease of intensity. Eventually, after about 200 minutes the intensity reaches a lower plateau, indicative of steady state. From this experiment, we can determine when steady (upper and lower plateau) or transient conditions have been reached. Further, the upper plateau corresponds to multiple scattering, as will be discussed in next section, since the sample is opaque, due to the dispersed clusters which form a macroscopically uniform dispersion. The lower plateau corresponds to a homogeneous solution, more dilute than the original 5% one, in equilibrium with the sediment, where practically one main relaxation process is observed. Finally, in the transitional regime the settling of the aggregates gives rise to large intensity fluctuations. These aspects are addressed in the following sections.

The real time behavior of the dispersed sediment in terms of sedimentation is

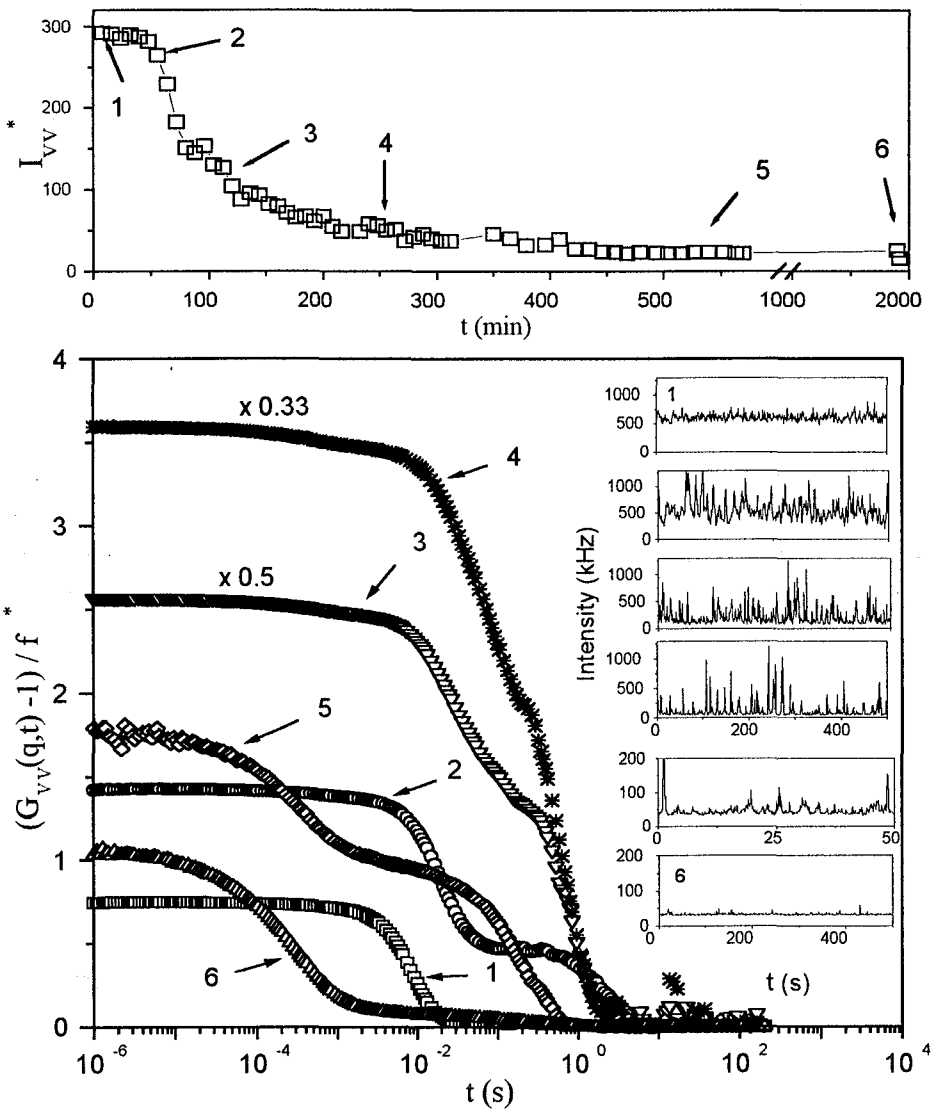

Figure 7.7: (upper): Normalized Polarized light scattering intensity, as a function of time, after a macroscopically uniform suspension was obtained through sediment dispersion (Fig. 7.5). The arrows indicate the times at which correlation functions were recorded: (1) 10 minutes; (2) 45 minutes; (3) 2 hours; (4) 4 hours; (5) 9 hours; (6) 32 hours. Measurements were carried out at a scattering angle of 45^o and a temperature of 25^oC. Lower part (lower): Relevant correlation functions along with their corresponding traces of the total scattering intensity. The correlation function of the 2nd and 4th hours exhibit a pronounced contrast, and are divided by 2 (x0.5) and 3 (x0.33) for clarity. Arrows indicating times correspond to those of the upper part (a).

described in Fig. 7.7a, discussed above. Characteristic results from PCS measurements of VV dynamics are depicted in Fig. 7.7b. The first intensity correlation function, taken from the uniform dispersion corresponds to the upper intensity plateau, at about 50 minutes, (referring to Fig. 7.7). The nearly opaque dispersion gives rise to multiple scattering, as confirmed by the low transmitted intensity (about 8%), the identical VV and VH correlograms, as well as visual observation. The relevant intensity trace was rather smooth and stable. The correlation function exhibits one dominant relaxation process, which is clearly sharper than single exponential (β varies between 1.6 and 1.9), and a rather weak slow process (Fig. 7.7). For the first hour, the intensity decreases only slightly with time (nearly constant), but there is a significant increase of fluctuations (insets of Fig. 7.7b). After 55 minutes this increase becomes dramatic and the correlation function exhibits clearly a slow process with significant amplitude, while the process seen under multiple scattering conditions is slowed down with respect to the first measurement. After the first hour the intensity starts decreasing sharply, and at the end of the third hour it drops to the 1/6 of its initial value.

The polarized intensity correlation functions after 2 and 4 hours (Fig. 7.7) consist of three processes: the fast cooperative diffusion of the trimers, which can be barely observed due to its relatively low contrast, and the slow and ultraslow processes, both with very large contrasts. The second slow process has a shape parameter of $\beta \approx 1.1$, whereas the third ultraslow one is even steeper, with $\beta \approx 1.4$. The corresponding intensity has dropped, due to sedimentation, and the intensity fluctuations are high. These fluctuations can be seen by eye as large spikes in the scattering volume (and may be due to the large moieties which are translating or reorienting in and out of the illuminated volume). After 9 hours the intensity has dropped substantially, and the large fluctuations are more rare. The two slow processes loose amplitude and are not easily discriminated anymore, whereas the fast diffusive process becomes now dominant. After 32 hours, the intensity is almost constant and the correlation function reveals the main fast process ($\beta \approx 0.7$) and an extra very small slow relaxation, which comprises of the slow and ultraslow processes.

Heating and cluster break-up

We have repeated the above experiment (statics and dynamics) at various temperatures above $25°C$, in order to determine the temperature corresponding to the melting of the associations. At $40°C$ and $50°C$ the solution was observed for a few days. The decrease of the intensity occurred just after the first day (corresponding to the uniform dispersion of Fig. 7.6), and the correlation functions revealed the same dynamics as in the case of $25°C$, suggesting that on the average the clusters did not break-up. At $65°C$ the solution became clear immediately, but a further decrease of the intensity, accompanied by a decrease of the amplitude of the slow process was observed. The corresponding VH corre-

lation function also exhibits a decrease of the amplitude of the slow processes. No sediment was apparent visually at the bottom of the sample cell. This can be explained both by a melting of most of the last aggregates and/or their sedimentation (which is minimal, and thus does not produce any visually observed sediment). Finally, the solution was agitated and put at 75^oC. There was a slow process (small in amplitude) apparent in the VV and the VH function which disappeared after 3 days. It is important once again to note the sensitivity of the VH dynamics to these experiments. This heating-dissolution experiment is better illustrated in Fig. 7.8, which depicts the total polarized intensity of the scattering moieties, normalized by that of toluene, as a function of temperature and time.

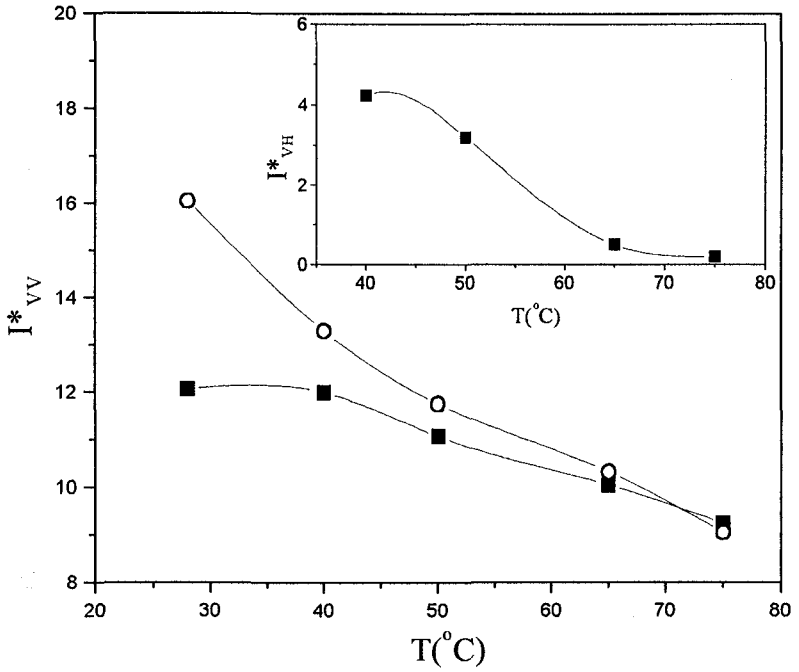

Figure 7.8: Total, normalized, polarized scattering intensity from a 5% PPP solution in toluene, as a function of temperature and time. (○) refer to the first and (■) to the last (5th or 6th) days of measurement at each temperature. Inset: Total depolarized scattering intensity (I^*_{VH}) from the 5% PPP solution in toluene, normalized to the corresponding intensity of toluene, as a function of temperature, at the last day. Solid lines are drawn to guide the eye.

Actually, by time we refer to the first and last measurements; the latter were undertaken between the 3rd and 6th day, depending on the temperature. It can be clearly observed, that above 65^oC steady state was reached immediately, suggesting that this temperature corresponds to dissolution (complete break-

up of the aggregates). Further, from the intensity ratio of the first and last measurements, we can obtain the change of concentration of the upper phase (referring to 7.6) with temperature. As the temperature rises from $28°C$ to $75°C$, the concentration increases from 3.8 to 5% by weight. The inset of Fig. 7.8 depicts the total steady state (in final equilibrium) VH intensity as a function of temperature. This plot represents an unambiguous way to determine the melting temperature, where all aggregates are broken apart, and we are back to the homogeneous solution of trimers.

7.3.4 The aggregation modes

In order to characterize the slow and ultraslow relaxation modes, their q-dependence was investigated at the three extreme cases: (a) at $t = 0$, corresponding to the cloudy dispersion, where multiple scattering dominates; (b) at $t = 3$ hours, corresponding to transient settling regime, where the contrast is pronounced; and (c) at $t = 30$ hours, corresponding to the lower intensity plateau, where the usual single scattering conditions are recovered . It is noted that the measurements in the transient regime were carried out at a different time than those of Fig. 7.7, and hence the corresponding relaxation rates of the slow and ultraslow modes are different. Nevertheless, the underlying physics behind these processes is the same, as already discussed and will be seen below.

Initial regime - Multiple Scattering

In this regime, the dynamics is practically q-independent, and nearly the same, both in the VV and the VH geometry. The sample is opaque and the transmission, $T = I/I_{tol}$, measured with a power meter (with a sensitive area of radius 1 cm, in a distance of about 12 cm from the sample cell) in the forward direction is about 8% in case (a) and about 60% in case (c). It is thus apparent that light is scattered multiply from our sample, and that the single scattering formalism cannot be applied here. On the other hand, the sample although opaque, is not milky, allowing thus the path of light to be observed; this suggests that in this situation we have not yet reached the limit of light diffusion in the sample, which can be treated quantitatively using the theory of *Diffusive Wave Spectroscopy* (DWS) [54, 55]. Furthermore, although the transmission from a multiply scattered sample in a slab geometry is $T = (5l^*/3L)/(1 + 4l^*/3L)$ (where l^* is the transport mean free path , i.e. the length scale at which the direction of light is randomized [54, 55, 56]) would yield $l^* = 0.05L$, which is a reasonable number for applying DWS, this is not the case in the present experiment. The reason has to do with the geometry of the scattering cell used (cylindrical), as well as the way the actual transmission measurement was carried out, which did not measure the light transmitted and scattered by the last scatterer in a solid angle of 2π in the forward direction, but rather only a part of it.

Given the above complications, in lack of other alternative, we try to assess the experimental observations qualitatively, and start from the theory of DWS. In DWS the light is assumed to follow a random walk inside the scattering medium, and the scattered field autocorrelation function is given by [54, 55]:

$$C(t) = \left\langle \sum_p \frac{|E_p|^2}{\langle I \rangle} \exp(-i\Delta\phi_p(t)) \right\rangle \tag{7.7}$$

where E_p is the amplitude of the scattered electric field along a path with p scattering events, $< I >$ the average total scattered intensity at the detector, and $\Delta\phi_p(t)$ is the phase shift of light along the path p.

In the case of independent successive scattering events, caused by scatterers undergoing Brownian motion, and independence of the scattering wavevector q_i from the displacement of the scatterer $\Delta r_i(t)$, we get:

$$C(t) = \int P(s) \exp\left(-\frac{1}{3}k_0^2 \left\langle \Delta R^2(t) \right\rangle \frac{s}{l^*}\right) ds \tag{7.8}$$

where s is the length of the path of the light, $P(s)$ is the probability that light will follow this path, k_0 is the scattering wavevector at an angle $\theta = 180^o$, and $\langle \Delta R^2(t) \rangle$ is the mean square displacement of the scattering particle, which in the diffusion limit here is given by $6Dt$ (see also chapter 3).

In the case of a scatterer in a velocity field (here, due to sedimentation) we have [55, 57]:

$$\Delta\phi_p(t) = kt \sum_{\upsilon=1}^{p} \widehat{e}_\upsilon \left[\overline{V}(\overline{R}_\upsilon - \overline{V}(\overline{R}_{\upsilon+1})\right] \tag{7.9}$$

where $\widehat{e}_\upsilon$ stands for the unit vector corresponding to the light beam which emerges after the υth scattering event, and $\overline{V}$ is the velocity of a scatterer at position $\overline{R}_\upsilon$. It is thus evident from eq. 7.8, that only a velocity gradient, Γ, within the probe volume can produce a phase change; in other words, in this case we detect the velocity gradient of moving particles. The corresponding correlation function is then:

$$C(t) = \int P(s) \exp\left(-\frac{sl^*}{30}k_0^2\Gamma^2 t^2\right) ds \tag{7.10}$$

Comparing eqs. 7.8 and 7.10, it is important to note the t^2-dependence in the case of velocity gradient detection, which in a sense relates to a deterministic motion, as opposed to the t-dependence in the case of random Brownian motion. Further, we emphasize again that the quantity related to the phase shift in the former case is the velocity gradient and not the diffusion coefficient (which is associated to the Brownian motion).

From Eq. 7.8 it is apparent that the decay of the correlation function is faster, the larger the path s is. This happens because in multiple scattering each particle in the light path has to move only a small distance in order for the entire path length to change by one wavelength. Thus longer light paths give shorter decay times. Further, the decay rate depends on the scattering geometry (at different scattering angles the light paths are different), rather than the scattering wavevector directly. Thus, DWS predicts a decrease of the characteristic time of a relaxation process under multiple scattering conditions, compared to the same process in the single scattering limit. This behavior conforms with our experiments, as judged from the correlation functions of Fig. 7.7b. As the sedimentation proceeds with time, and the single scattering conditions are approached, the relaxation process of multiple scattering case becomes significantly slower. In addition, the shape of the correlation function becomes less steep, approaching a single exponential decay (Fig. 7.7 and 7.9); this can be explained by the fact that during the initial stage (a) we observe the motion of clusters in a flow field (sedimentation), whereas in the late stage (c) we mainly observe clusters undergoing Brownian motion in the clear phase (single scattering; sedimentation is absent).

The experimental data at various angles between 15^o and 150^o reveal a nearly q-independent dynamics; the characteristic relaxation rate at $q = 0$ is found to be about $500s^{-1}$. From the fitting of the correlation function we obtain the shape parameter $\beta = 1.9$, which practically suggests that we are in the velocity gradient limit (ballistic motion).

Intermediate regime -Single Scattering limit

The main findings are depicted in Fig. 7.10b. Referring to the dynamics, depicted in Fig. 7.10a and 7.10b, the slow mode exhibits a very weak q-dependence in the relaxation rates, both in the VV and VH scattering, whereas the ultraslow mode is characterized by q-independent relaxation rates, both in the VV and VH geometries. In terms of the static picture, and referring to Fig. 7.10b, the intensity of both the slow and the ultraslow process is strongly q-dependent, both in the VV and the VH, especially at low q's. Moreover, it is apparent that nearly all polarized light scattering intensity is due to the anisotropy of the scattering moieties. The former arises from both concentration fluctuations, which are isotropic (I_{iso}) and orientation fluctuations which are anisotropic (I_{VH}).

For independently moving particles in an orientationally isotropic environment, in the absence of translation-to-rotation coupling and in the single scattering limit, the usual expression for the polarized scattered intensity is (eq. 3.22):

$$I_{VV}(q) = I_{iso}(q) + 4/3 I_{VH}(q) \tag{7.11}$$

For large scatterers, where intramolecular interference is important, the above relation does not hold always. Instead, as discussed in chapter 3, there is an ad-

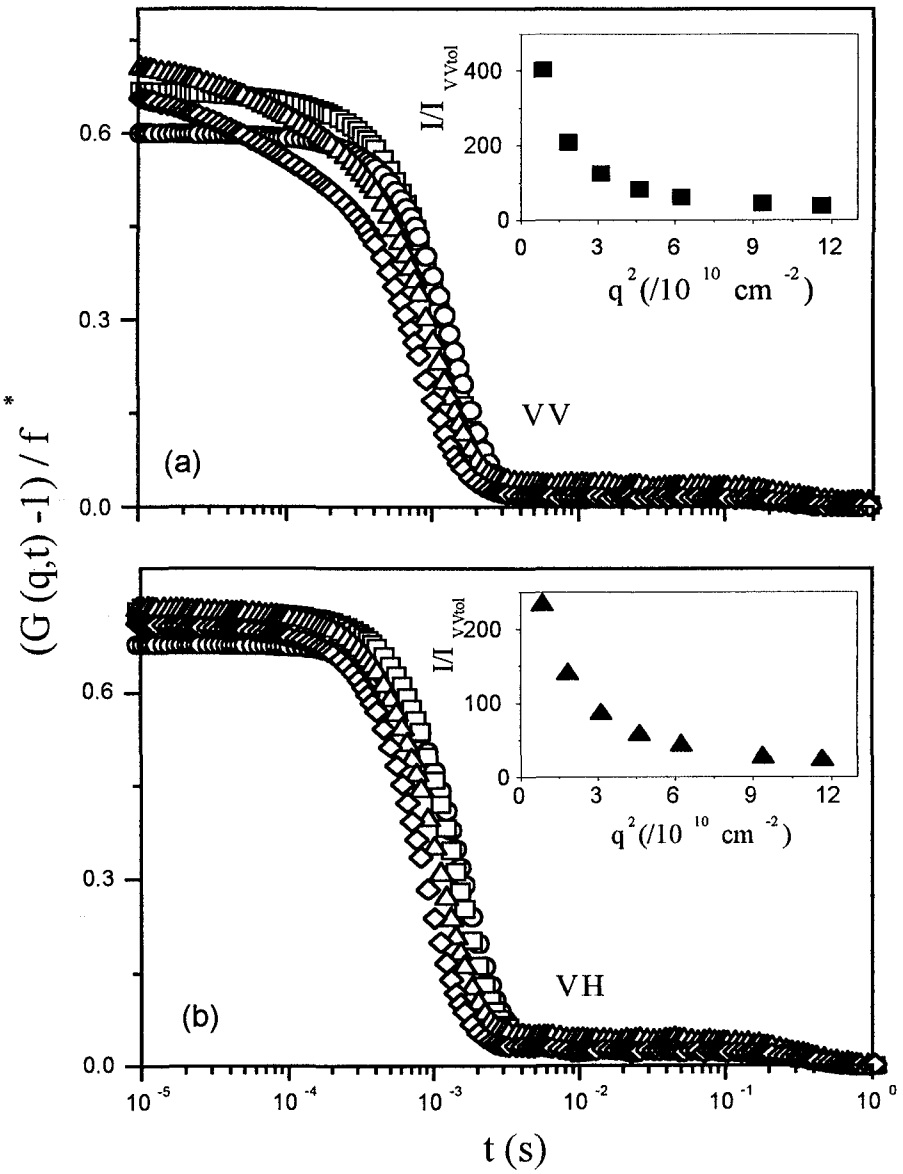

Figure 7.9: VV (a) and VH (b) correlation functions for the initial stage (opaque solution) for several scattering angles: 45° (◯); 60° (□); 120° (△); 150° (◇). Insets: The q-dependence of the corresponding scattering intensity normalized with the VV intensity of toluene.

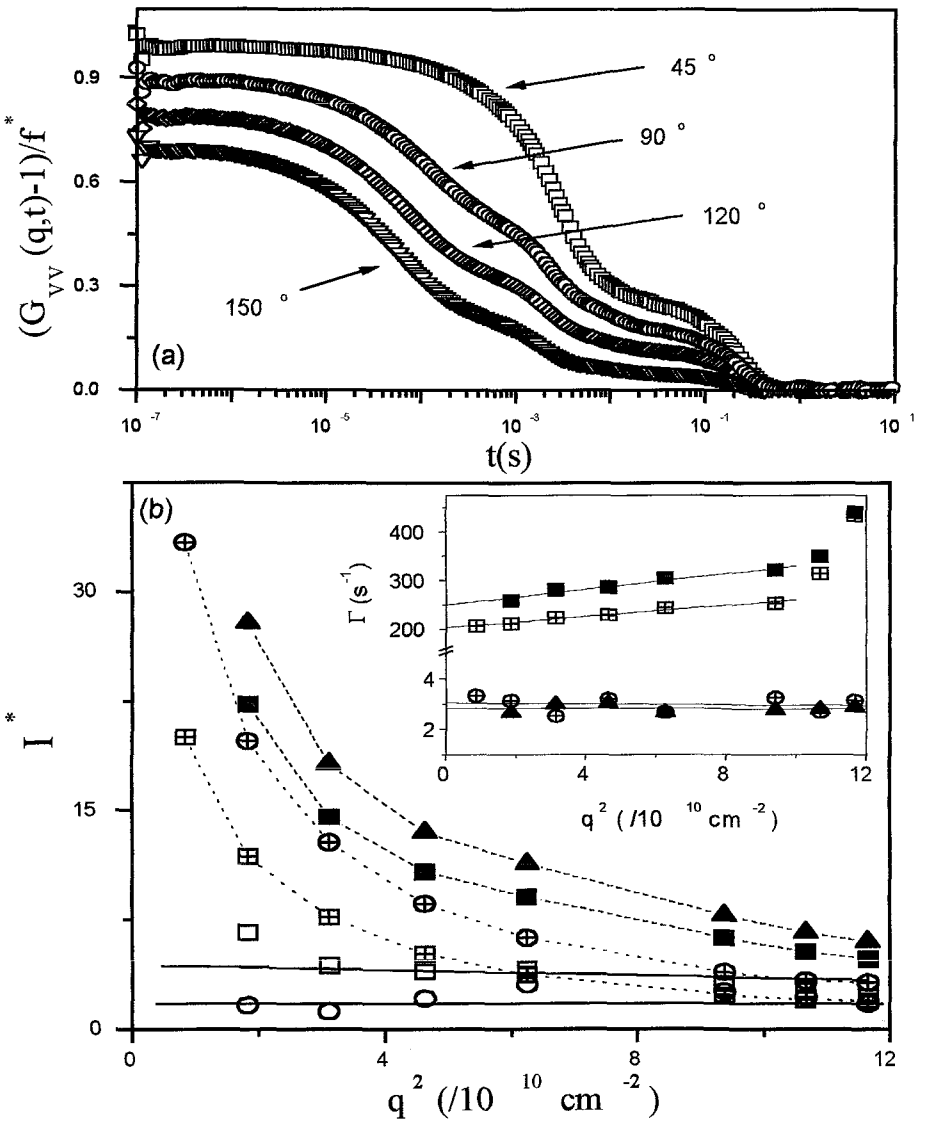

Figure 7.10: Upper part (a): VV intensity correlation functions in the intermediate single scattering regime (corresponding to transient settling in Fig. 7a), at various scattering angles θ: 45° (□); 75° (○); 120° (◇); and 150° (▽). Lower part (b): Polarized and depolarized intensities,normalized by the VV intensity of toluene, for both slow modes in the transient settling regime, following sediment dispersion, as functions of q^2. VV slow: (■); VV ultraslow: (▲) ; VH slow: (▽); VH ultraslow: (△); Isotropic contributions to VV intensity, I_{iso}: slow (□) and ultraslow (○). Inset: Corresponding relaxation rates Γ for the slow and ultraslow, measured in the polarized and depolarized geometries as a function of the scattering wavevector, q.

ditional term, I_{coupl}, originating from a coupling of concentration and orientation fluctuations (eq. 3.33) [58]:

$$I_{coupl} \sim N\alpha\beta \left\langle \sum_{i,j}^{n} (3cos^2\theta_i - 1) \exp\left[iq(r_i - r_j)\right] \right\rangle \tag{7.12}$$

This term always vanishes at $q = 0$, or for scatterers with completely randomly orientated segments.

The isotropic contribution estimated by substracting only the 4/3rds of the VH intensity (according to Eq. 7.11) is small for both the slow and ultraslow process (Fig. 7.10b, inset); actually it amounts to about 15% of the VV intensity, except in the high q's where it can reach 30%. In our experiments the extra term I_{coupl} (Eq. 7.12) is probably also important, making thus the actual contribution of the isotropic intensity even smaller. This strongly suggests that the two aggregate processes originate essentially from the anisotropic part of the scattering intensity. Further, it is noted that the amplitude ratio of the two processes ($\alpha_{slow}/\alpha_{ultraslow}$, where α is the amplitude of a particular relaxation process) remains nearly constant. More specifically, in the VV geometry it is about 0.8, whereas in the VH geometry it is about 0.6, for all scattering angles between 30^o and 150^o. Moreover, this ratio does not change with time, within the same sedimentation regime (transient or plateau).

The combined information on intensities and rates provides the following picture of the light scattering mechanism of the aggregate processes (slow and ultra slow): Both have the same origin (due to the same amplitudes), which is the orientational fluctuations of the scattering moieties. The slow mode has a shape parameter only slightly above 1 (Fig. 7.10a), and thus it can be attributed to rotational diffusion; it is treated as a single exponential relaxation. From the measured rates for the slow mode in the intermediate regime, and using the classical relation for the depolarized field correlation function (chapter 2):

$$C_{VH}(q,t) \approx N\beta_i^2 exp\left[-(6D_R + Dq^2)t\right]$$

we get $D_R = 34s^{-1}$ (from the intercept of Γ_{VH} vs q^2 at $q = 0$) and $D = 5 \times 10^{-10} cm^2/s$ (from the slope of Γ_{VH} vs q^2) (Fig. 7.10b). A single size R_H cannot account for these values through the usual expressions (for stick boundary conditions), namely $D_R = 3k_BT/4\pi\eta R_H^3$ and $D = k_BT/6\pi\eta R_H$, respectively. Thus, in order to rationalize these findings, we consider the diffusion coefficients for ellipsoids [58, 59, 60, 61]. In particular, for an oblate ellipsoid with large axis b and small axis a, the translational and rotational diffusion coefficients are given by:

$$D = \frac{k_BT}{6\pi na} G(\rho) \text{ and } D_R = \frac{k_BT}{16\pi na^3} \left(\frac{(2-\rho)G(\rho) - 1}{(1-\rho^2)} \right) \tag{7.13}$$

with $G(\rho) = (\rho^2 - 1)^{1/2}\rho\arctan[(\rho^2 - 1)^{1/2}]$ and $\rho = b/a$. Using the above experimental values of D_R and D, we get $a = 559\ nm$ and $b = 578.5\ nm$. This result suggests that scattering originates from slightly deformed spherical clusters with a hydrodynamic radius of about 570 nm. For a moiety of such a size, qR_g in the light scattering range is between 2.7 and 19.6, and therefore the form factor, independent of the shape, is already vanishingly small (below 0.2) [58]. Thus, it is expected that the anisotropic contribution in the intensity dominates over the isotropic one.

The ultra slow process is clearly steeper than single exponential; this situation actually corresponds to an intermediate regime between the diffusion limit and the free translation limit. In such a case, quantitative evaluation of the data is presently not possible. By taking into consideration the presence of sedimentation, as already discussed, we propose that this process is due to sedimentation-induced number fluctuations [58, 62], which give an extra term $< \delta N(0)\delta N(t) >$ in the intensity correlation function $G^{(2)}(q,t)$ i.e., large associations entering and leaving the probe volume which give an extra term $< \delta N(0)\delta N(t) >$ in the intensity correlation function $G^{(2)}(q,t)$. These moieties must be large associations entering and leaving the probe volume. It can be some network of anisotropic clusters settling under gravity, rather than diffusing randomly. Further, the number fluctuations are related to non-Gaussian concentration fluctuations, associated with a small number of particles in the scattering volume (also responsible for the increased contrast). We believe that the latter is indeed the case in our experiments, because the ultraslow process was observed after the settling process was in progress (roughly in day 15, corresponding to the intermediate regime, and referring to Fig. 7.6a), meaning that the concentration in the area of the measuring point was already reduced. Further, number fluctuations can be VH active as well, simply due to the anisotropy of the clusters. This picture is in agreement with the strong q-dependence of the scattering intensity, which implies that clusters are large.

Finally, case (c) corresponding to the time after complete phase separation and sediment formation exhibits the same dynamic characteristics a semidilute solution with smaller than the overall concentration in the sample before phase separation, simply due to the smaller concentration of the polymer molecules in the upper clear phase.

7.4 A tentative interpretation of the aggregation process.

In order to obtain a better understanding of the structure of the aggregates, we performed X-ray scattering studies of the sediment. Typical results are depicted in Fig. 7.11. It is interesting to note that the peak observed at low scattering

angles is clearly sharper than what is usually expected in the nematic phase, whereas in contrast to the expected amorphous hallow at higher angles, a extra structure in that range is also observed. This is also in contrast to direct powder diffraction measurements with the original material, which showed the sharp peak at low angles and the amorphous hallow at high angles. From these measurements it can be stated that the aggregates do not form a nematic, but rather a crystalline phase, characterized by two length scales: the distance between macromolecular backbones ($d_1 = 2.7\ nm$) and the distance between side chains ($d_2 = 0.6\ nm$). Thus the conformation of side chains in the solvent seems responsible for the formation of crystallites. These findings are in harmony with the strong anisotropy of the slow aggregation modes discussed before. Further, it is noted that the fact that the PPP powder does not exhibit any side chain crystallinity, implies that during the slow nucleation process resulting from aggregation, the side chains have time to arrange in a crystalline phase, in contrast to the situation of (quick) solvent casting, from which the powder was obtained.

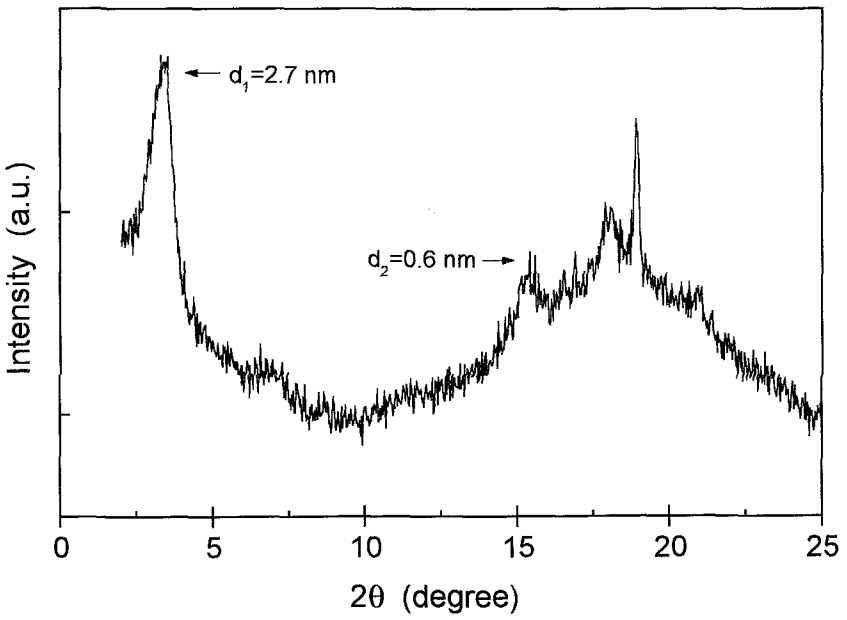

Figure 7.11: Scattered X-ray intensity from PPP sediment in toluene (produced from a 5% solution), as function of scattering angle (2θ), indicating crystallined structure. Values of d_1 and d_2 represent characteristic distances between macromolecular backbones and side chains, respectively.

A remaining question emerging from the above discussion is whether the structures inferred by the relaxation processes conform to the standard thermodynamic picture of polymer solutions. To answer this question, let's for simplicity assume that the hairy-rod macromolecules (each of length L) "like" to form clusters; each cluster is of length L and has a square front surface of side $\sim N^{1/2}$, N being the number of rods in a cluster. If γ_s and γ_f denote the surface tension of the side (with dimension $LN^{1/2}$) and front of the cluster, respectively, we have $\gamma_f \geq \gamma_s$. Then, the free energy gain ΔF of the cluster, relative to a homogeneous state of isolated rods, can be written as:

$$\Delta F = N\left(-\Delta G_{melt}(\phi) + 2\gamma_f\sigma^2\right) + 4L\sqrt{N}\left(\gamma_s\sigma^2\right) \tag{7.14}$$

where $-\Delta G_{melt}$ is the free energy gain per rod on aggregating and σ is the rod diameter. Eq. 7.14 suggests that when $2\gamma_f\sigma^2 > \Delta G_{melt}$, there exists a metastable region where nuclei of any size are unfavorable, i.e. $\Delta F > 0$, independent of N . This result represents a clear departure from the conventional picture for flexible macromolecules, for which there is always a critical size N, beyond which $\Delta F < 0$ inside the two-phase region. The implication of this is that nucleation only happens for deep quenches. By considering now the situation where nucleation can occur, we can calculate the activation energy ΔF_{act} required to form a stable nucleus, from Eq. 7.14 by considering $\partial(\Delta F)/\partial N = 0$. In the case $\Delta G_{melt} >> 2\gamma_f\sigma^2$, this leads to:

$$\Delta F_{act} = \frac{\left(2L\gamma_s\sigma^2\right)^2}{\Delta G_{melt}} \tag{7.15}$$

By assuming $\Delta G_{melt} = L\Delta G^{seg}_{melt}$, where ΔG^{seg}_{melt} is the melting (or association) energy per segment, the above equation reduces to:

$$\Delta F_{act} = L\frac{\left(2\gamma_s\sigma^2\right)^2}{\Delta G^{seg}_{melt}} \tag{7.16}$$

The above analysis indicates that the nucleation probability of rod-like polymers is lowered when compared to their flexible counterparts, and most importantly that the activation barrier for rod-like polymers is larger than for their flexible counterparts, since it increases with rod length. This in turn suggests a slow rate of nucleation, which is indeed observed experimentally. Furthermore, the above assumption of cluster length L can be reconsidered. It is now clear that nucleation cannot proceed with individual rods lined up end to end, since there is no free energy gain in such a process. On the other hand, two clusters (of length L) can come together end-to-end, since this will minimize the front surface energy. The question is whether it is possible to form clusters of one-rod length or not. To resolve this, we have to decide whether a typical cluster is of size L or $L_c >> L$. When two rods, each of length L, are coming together, they are approximately in parallel configuration, as already discussed [51, 63, 1]. The

time for the rods to line-up is L^2/D, where D is the diffusion coefficient. If this time is shorter than the average time between collisions, we have formation of clusters of size L, otherwise of size L_c. The latter time is aproximately $c^{-2/3}/D$, where c is the average number concentration of rods per volume. Thus, for $L^2/D < c^{-2/3}/D$, or $c < 1/L^3 = c^*$, clusters of one-rod length will be formed; this is of course not favorable due to side surface free energy barrier (Eq. 7.15), as already discussed. However, for $c > c^*$, clusters of length L_c will be formed. This is the typical case of aggregation proceeding by nucleation-and-growth, which has been observed in our experiments. Thus, in the dilute regime, no aggregation takes place. As the concentration increases, in the semidilute regime, aggregation is possible with slow growth, leading to formation of large clusters with nearly parallel association, and/or networks of clusters associating end-to-end. This thermodynamic analysis, which captures the main features of the association dynamics, observed experimentally, is actually consistent with the formation of large aggregates (more than 30 associating molecules); it cannot account for the trimers formation [64, 65].

7.5 Concluding remarks

The association dynamics of toluene solutions of a hairy rod-like poly(*p*-phenylene) with flexible dodecyl side chains has been investigated thoroughly by using photon correlation spectroscopy in the polarized (VV) and depolarized (VH) modes, and static light scattering. Toluene was found to be not a good solvent. In the dilute regime, molecules are assembled into small aggregates consisting of about three to four molecules in parallel configuration, termed trimers. In the semidilute regime, two new relaxation processes were found, which appeared at room temperature after about a week from the preparation of the solution, and disappeared with heating at about 65°C. They are attributed to the formation of clusters, of typical size 570 nm. The substantial VH sensitivity indicates strong anisotropy of the aggregates, which are crystallized, as revealed by X-ray scattering. Both in the VV and VH, the slow process is characterized by weakly q-dependent dynamics and strongly q-dependent intensity, and the ultraslow one exhibits q-independent dynamics and strongly q-dependent intensity, whereas the amplitude ratio of the two processes is essentially constant. These processes are steeper than single exponential decay with $\beta \approx 1.1$ and 1.4 for the slow and ultraslow, respectively. They are related to the orientational fluctuations of the clusters, giving rise to slow reorientational motion with negligible isotropic contribution, and ultraslow number fluctuations of the anisotropic aggregates. A simple thermodynamic analysis suggests that rodlike macromolecules exhibit a larger activation energy barrier compared to their flexible counterparts, in agreement with the experimental evidence. Furthermore, the first stages of sediment redispersion exhibit multiple scattering with a steeper than exponential relax-

ation process ($\beta \approx 1.9$), associated with sedimentation-induced velocity gradient in a transient pseudo-network formed by the dispersed clusters. Finally, it is noted that the association processes described here are reversible, since a heating cycle to 65°C leads to cluster break-up and a single relaxation process of the trimers in semi-dilute solution.

References

[1] P. van der Schoot and T. Odijk. *J. Chem. Phys.*, 97:515, 1992.

[2] G. Wegner and K. Mathauer. *Mat. Res. Soc. Symp. Proc.*, 247:767, 1992.

[3] M. Ballauff. *Angew. Chem.*, 28:253, 1989.

[4] A.M. Jamieson, J.G. Southwick, and J. Blackwell. *Journal of Polymer Science:Polymer Physics Edition*, 20:1513, 1982.

[5] M.E. Ferrari and V. Bloomfield. *Macromolecules*, 25:5266, 1992.

[6] P. Weissenburg, T. Odijk, P. Cirkel, and M. Mandel. *Macromolecules*, 27:306, 1995.

[7] P. Weissenburg, T. Odijk, P. Cirkel, and M. Mandel. *Macromolecules*, 28:2315, 1995.

[8] W. Richtering, W. Gleim, and Burchard W. *Macromolecules*, 25:3795, 1992.

[9] E.L. Meyer, G.G. Fuller, R.C. Clark, and W.-M. Kulicke. *Macromolecules*, 26:504, 1993.

[10] Y. Gatziotis, S.K. Siddiquee, and J.W.van Egmond. *Macromolecules*, 30:7253, 1997.

[11] W.B. Russel, D.A. Saville, and W.R. Schowalter. *Colloidal Dispersions.* Cambridge University Press, Cambridge, 1989.

[12] P. D'Hene, J. Mewis, and G.G. Fuller. *J. Colloid Interface Sci.*, 143:356, 1993.

[13] D.A. Weitz and M. Oliveria. *Phys. Rev. Letters*, 52:1433, 1984.

[14] J.E. Martin. *Phys. Rev. A*, 36:3415, 1987.

[15] M. Carpineti and M. Giglio. *Phys. Rev. Letters*, 68:3327, 1992.

[16] M. Carpineti and M. Giglio. *J. Phys.: Condens. Matter*, 6, 1994.

[17] P.W. Roux, A.T.J.M. Woutersen, B.J. Ackerson, and C.G.D. Kruif. *Physica A*, 156:876, 1989.

[18] M.Y. Lin, H.M. Lindsay, D.A. Weitz, R.C. Ball, R. Klein, and P. Meakin. *Phys. Rev. A*, 41:2005, 1990.

[19] C. Allain, M. Cloitre, and M. Wafra. *Phys. Rev. Letters*, 74:1478, 1995.

[20] P.B. Warren, R.C. Ball, and A. Boelle. *Europhysics Letters*, 29:339, 1995.

[21] M. Carpineti, F. Ferri, M. Giglio, E. Paganini, and U. Perini. *Phys. Rev. A*, 42:7347, 1990.

[22] R. Piazza, T. Bellini, and V. Degiorgio. *Phys. Rev. Letters*, 71:4267, 1993.

[23] D.A. Weitz, J.S. Huang, M.Y. Lin, and J. Sung. *Phys. Rev. Letters*, 54:1416, 1985.

[24] Q. Ying, J. Marecek, and B. Chu. *J. Chem. Phys.*, 101:2665, 1994.

[25] A. Vailati, D. Asnaghi, M. Giglio, and R. Piazza. *Phys. Rev. E*, 48, 1993.

[26] R. Piazza and V. Degiorgio. *Physica A*, 182:576, 1992.

[27] D. Asnaghi, M. Carpineti, M. Giglio, and A. Vailati. *Physica A*, 213:148, 1995.

[28] B.U. Felderhof and R.B. Jones. *Phys. Rev. E*, 48:1084, 1993.

[29] B.U. Felderhof and R.B. Jones. *Phys. Rev. E*, 48:1142, 1993.

[30] B.U. Felderhof and R.B. Jones. *J. Phys.: Condens. Matter*, 6, 1994.

[31] P. Doty, J.H. Bradbury, and A.M. Holtzer. *J. Am. Chem. Soc.*, 78:947, 1956.

[32] W.E. Rockefort and S. Middleman. *J. Rheol.*, 31:337, 1987.

[33] P. Weissenburg, T. Odijk, Kuil M., and M. Mandel. *Polymer Comm.*, 33:5328, 1992.

[34] C. Wolff, A. Silberberg, Z. Priel, and M.N. Layec-Raphalen. *Polymer*, 20:281, 1979.

[35] E.Y. Chu, S.C. Xu, Z.M. Lee, C.K.F. Sek, E.M. Okamoto, Y.and Pearce, and T.K. Kwei. *Polym. Sci.: B: Polym. Phys.*, 33:71, 1995.

[36] J.C. Horton and A.M. Donald. *Polymer*, 32:2418, 1991.

[37] S.P Russo. *Reversible Polymeric Gels and Related Topics*, volume 350. ACS Symposium Series, 1987.

[38] A.H. Russo, P.S. Howdhury and M. Mustafa. *Mat. Res. Soc. Symp. Proc.*, 134:207, 1989.

[39] J. Buitenhuis, J.K.G. Dhont, and H.N.W. Lekkerkerker. *Macromolecules*, 27:7267, 1994.

[40] G. Petekidis, D. Vlassopoulos, P. Galda, M. Rehahn, and M. Ballauff. *Macromolecules*, 29:8948, 1996.

[41] U. Tiesler, M. Rehahn, Ballauff M., G. Petekidis, D. Vlassopoulos, G. Maret, and H. Kramer. *Macromolecules*, 29:6832, 1996.

[42] G. Petekidis, G. Fytas, and H. Witteler. *Colloid Polym. Sci.*, 272:1457, 1994.

[43] M. Carpineti and M. Giglio. *Phys. Rev. Letters*, 70:3828, 1993.

[44] H. Benoit and P.J. Doty. *J. Phys. Chem.*, 57:958, 1953.

[45] H. Benoit and J.S. Higgins. *Polymers and Neutron Scattering.* Oxford Science Publications, Oxford, 1994.

[46] M. Schmidt. *Macromolecules*, 17:553, 1984.

[47] P. Galda and M. Rehahn. *Synthesis*, 1996.

[48] S. Broesma. *J. Chem. Phys.*, 74:6989, 1981.

[49] S. Broesma. *J. Chem. Phys.*, 32:1626, 1960.

[50] J.E. Hearst and W.H. Stockmayer. *J. Chem. Phys.*, 7:1425, 1962.

[51] M. Warner. *J. Chem. Phys.*, 73:5874, 1980.

[52] T. Sato and A. Teramoto. *Adv. Pol. Sci.*, 126:85, 1996.

[53] K. Schatzel. *Dynamic Light Scattering: The Technique and Some Applications*, page 76. Oxford Press, 1993.

[54] D.A. Weitz and D.J. Pine. *Dynamic Light Scattering: The Technique and Some Applications*, page 653. Oxford Press, 1993.

[55] G. Maret. *Mesoscopic Quantum Physics.* Elsevier Science B. V, 1995.

[56] P.D. Kaplan, A.G. Yodh, and D.J. Pine. *Appl. Opt.*, 32:3828, 1993.

[57] D. Bicout, E. Akkermans, and R.J. Maynard. *J. Phys. I*, 1:471, 1991.

[58] J.B. Berne and R. Pecora. *Dynamic Light Scattering.* Willey Interscience Publications, New York, 1976.

[59] C.-M. Hu and R. Zwanzig. *J. Chem. Phys.*, 60:4354, 1974.

[60] F. Perrin. *J. Phys. Rad.*, page 497, 1934.

[61] F. Perrin. *J. Phys. Rad.*, page 1, 1936.

[62] D.W. Schaefer and B.J. Berne. *Phys. Rev. Letters*, 28:475, 1972.

[63] M. Warner. *Phil. Trans. R. Soc. Lond. A*, 344:403, 1980.

[64] P. van der Schoot. *J. Phys. Chem.*, 96:6083, 1992.

[65] G. Petekidis, J.D. Weinhold, S. Kumar, D. Vlassopoulos, and G. Fytas. 1997.

Chapter 8

Dynamics of Solutions of Stiff Polymers

In this chapter we present the investigation of the dynamic behavior of stiff polymers in solutions. Three different series of polymer samples were used; they all belong in the general family of poly-(p-phenylene)s (PPP) with flexible side chains (Hairy-Rod Polymers). The main advantage of these kind of stiff polymers is their inherent molecular optical anisotropy which enables the use of the powerful technique of depolarized light scattering for the investigation of orientation fluctuations, together with polarized dynamics light scattering for the study of concentration fluctuations. A main concern in choosing a model system for this study is also the good solubility, which enables the study in a large concentration regime.

Typically, the collective dynamics of polymers in solution is probed experimentally by photon correlation spectroscopy (PCS), which in the polarized geometry (VV) reveals the isotropic concentration fluctuations, and in the depolarized geometry (VH) the orientational fluctuations. The theoretical studies and the experimental investigations on systems of rodlike polymers have been discussed in chapter 4. The results from these studies are not fully conclusive concerning three aspects:

(A) The mechanisms for relaxing concentration fluctuations in solution, especially in the concentrated region, where a coupling of translational to rotational diffusion is expected and the concentration dependence of the cooperative diffusion coefficient,

(B) The dynamics of orientation fluctuations and the concentration dependence of the rotational diffusion.

(C) The dependence of the self-diffusion on molecular parameters and concentration.

(D) The effect of the flexibility in the above aspects and of the approach to a transition to an anisotropic phase on the above aspects.

This chapter is organized in three parts were we discuss the results in the three different series of PPP's in the dilute and semidilute regime and concentrated region. In all these studies the main experimental techniques are PCS in the VV and the VH geometry and static light scattering. The topics that are addressed in this part are:

(i) The characterization of the molecular dimensions and the determination of the solvent quality in the dilute regime from both dynamic and static light scattering. The comparison with, known by other studies and in different solvents, molecular characteristics of the macromolecules used reveals the character of the scattering particles probed by light scattering.

(ii) The origin and character of the relaxation modes in the polarized (VV) correlation functions and the concentration dependence of the resulting diffusion coefficients (in the case of diffusive modes) or relaxation times. More specifically the determination of the molecular originating modes like the cooperative diffusion and the distinction from the modes originating from association.

(iii) The origin of the processes in the depolarized scattering, and a discussion in relation with relevant theories.

(iv) The concentration and molecular weight dependence of the translational and rotational diffusion coefficients and the comparison with existing theoretical models.

(v) The concentration and molecular weight dependence of other quantities deduced from light scattering such as scattering intensities, and osmotic modulus.

In addition we present supplementary measurements of self-diffusion by PFG-NMR and also viscosity measurements in some of the samples studied.

8.1 Materials

In these study we have used three different series of poly-(p-phenylenes) kindly provided by Prof. G. Wegner (MPI-P, Mainz, Germany) and Prof. M. Ballauff (Polymer-Institute, University of Karlsruhe, Germany). The formulas and the molecular characteristics of the three series of poly-(p-phenylenes) with flexible side chains which are used in this work are presented below:

A) Poly($p-2,5$-di-n-dodecyl-1,4-phenylene) (MPI-P)

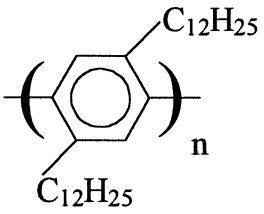

P-12

The characteristics of this macromolecule shown in Table 8.1 were determined by GPC. It must be noted that the determination of the absolute values was done using as a reference molecule a flexible polystyrene polymer and these is expected to introduce an error in the determination of M_n of rodlike polymers. The synthesis of P-12 [1] occurred at 65^oC by polymerization of bis (1,3-propanediol)ester of 2,5-di-n-dodecyl-benzene-1,4-bisboronic acid with 1,4-dibromo-2,5-di-n-dodecylbenzene in the presence of 6 meq catalyst $[Pd(PPh_3)_4]$ in a reaction vessel for 8 days. The polymer was precipitated into acetone, filtered, washed in boiling water and dried. The polymer was additionally dissolved in toluene, precipitated into acetone collected and vacuum-dried.

Sample	$M_n(g/mol)$	$L_n(nm)$	L_w/L_n	$L_e(nm)$
P-12	25190	30.2	2.4	25.2

Table 8.1: Molecular characteristics of sample P-12

Solutions of P-12 in toluene suitable for homodyne photon correlation spectroscopic measurements in the range of $1.4 - 33\ mg/cm^3$ were prepared by slow evaporation of the solvent from a dilute solution. A dust free solution of the latter was obtained by slow filtration through a $0.45\ \mu m$ teflon millipore filter into the light scattering round cell ($10\ mm$ o.d.). The solutions were maintained at 80^oC between measurements and equilibrated at the temperature of the experiment (20^oC or 40^oC) for about 1 hour before measurements.

B) Poly($p-2,5$-di-n-dodecyl-1,4-terphenylene) (Univ. Karlsruhe)

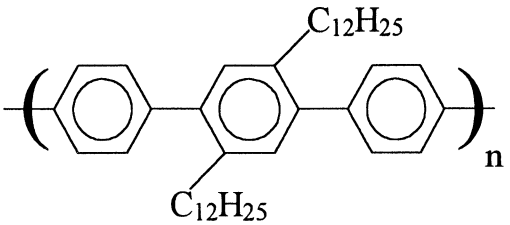

PPP-12

The synthesis of these series of hairy-rods, PPP-12, with dodecyl side chains (the hairs), as for all poly(p-phenylenes), was done by polycondensation [2, 3]. In the present work, a series of PPP's with different molecular weights was utilized. The molecular characteristics are summarized in Table 8.2 (L represents

the length of the macromolecular backbone, whereas the subscripts w , n and e refer to weight average, number average and the effective, respectively). Due to the synthesis method used, PPP-12 are rather polydisperse as can be seen in table 8.2. As it is discussed in chapter 6, depolarized Rayleigh scattering measurements were carried out in order to determine the persistence length, utilizing the wormlike model and taking into account the polydispersity . The persistence length was found to be about 28 nm [4]; this value is determined as an upper limit due to a comparison of the results on a semistiff polyester series (see chapter 6) by depolarized light scattering, viscosimetry and magnetic birefringence measurements. Moreover, the investigation of the aggregation behavior of these molecules in two different organic solvents (toluene and chloroform) which is presented in chapter 7, has led to the separation of the molecular (trimer in the case of toluene) and aggregate contribution to the polarized light scattering spectrum [5].

Sample	$M_n(g/mol)$	$L_n(nm)$	L_w/L_n	$L_e(nm)$
PPP-2	9900	25.7	3.2	22.3
PPP-3	12600	32.6	3.1	27.3
PPP-5	14800	38.5	3.2	31.4

Table 8.2: Molecular characteristics of PPP-12 series.

Dust-free samples were obtained by careful filtration of the dilute solutions through a $0.22\mu m$ teflon Millipore filter into a dust-free light scattering cell. Higher concentrations were obtained by slow evaporation. The solutions were measured at 25°C, after heating them at about 80°C overnight, to avoid aggregation for few days [5].

C) Sulfonated Poly(p-terphenylene) (MPI-P)

The third series of poly-(p-phenylenes) studied were the sulfonated PPP's and was proven to be the most soluble of all. The molecular characteristics of the samples used are summarized in Table 8.3.

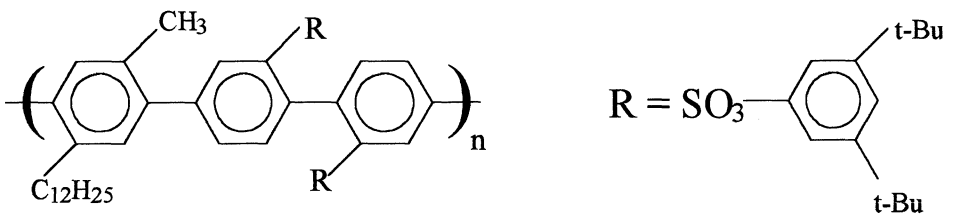

PPP/S

Sample	$M_n(g/mol)$	$L_n(nm)$	L_w/L_n	$L_e(nm)$
PPP/S-1	99900	133.8	1.91	73.8
PPP/S-3	54000	73	2.09	49.7
PPP/S-7	22000	29.7	1.82	24.8
PPP/S-9	16500	22.3	1.64	19.4
PPP/S-10	8150	11	1.42	10.2

Table 8.3: Molecular characteristics of PPP/S series.

8.2 General Features

Before discussing the results of our study on each sample, a general overview of their basic characteristics and dynamic behavior is presented.

In principle, for solutions of rod-like polymers the overlap concentration, c^*, above which interparticle interactions start becoming important, is very small, and thus PCS measurements in the dilute regime are rather difficult. For rods with significant flexibility, c^* can be estimated either from the radius of gyration of the polymer chain or from its end to end distance. In the former case $\rho^* = (4/3\pi R_g^3)^{-1}$ and the macromolecule assumes a coil conformation , which can be true for chains with contour length much higher than their persistence length. On the other hand, molecules with contour length close to the persinstence length, like the present PPP's, resemble more a bended rod which has an overall cylindrical rather than spherical shape, characterized by the end to end distance ($L_e =< R^2 >^{1/2}$), and an effective diameter b_e larger than the molecular diameter b [6]. In the latter case, the overlap concentration can be approximated by $c^* = 1/L_e^3$.

Since all the molecules that we have used have a persistence length around 25 nm (chapter 6) the polymer chain exhibits significant flexibility and the conformation for most of the samples is far from a rigid rod. Thus we have calculated the end-to-end vector L_e according to the wormlike model (eqs. 2.10) and using the known number average contour length L_n and a persistence length of 25 nm (Table 8.1, 8.2, 8.3). From these values we can then determine the number concentrations, $\rho^* = 1/L_e^3$ and $\rho^{**} = 1/bL_e^2$. In any case for polydisperse samples we believe that the right average of the contour length, for the calculation of ρ^* is the number average.

P-12 sample

The P-12 sample was the first one used; solutions of this macromolecule in toluene were utilized for a study mainly of orientation fluctuations. The main problem of this molecule is the low solubility in toluene (as well as $CHCl_3$) solutions which did not allowed the study for concentrations larger than 35 mg/cm^3 (4% by weight). At higher concentrations the solutions phase separate even at $40°C$ were the measurements were contacted in an effort to minimize aggregation and

with the hope to avoid phase separation. This was also the reason that we chose toluene, instead of $CHCl_3$ (which was considered to be equally good solvent). Moreover the nematic to isotropic transition was not reached since classical phase separation preceded (to a rich and a poor polymer phase). In fact P-12 exhibits a similar with PPP-12 behavior in terms of aggregation and phase separation; the latter was discussed in details in chapter 6. Nevertheless the dynamics of this stiff and highly optically anisotropic macromolecule enables us to measure good VH correlation functions and investigate the orientational fluctuations; such good VH data are actually very rare if not absent in literature.

PPP-12 sample

The solubility problems of P-12 led us to the use of another PPP based macromolecule, which was also available in different molecular weights. The molecular weight dependence of both the transport coefficients and their concentration dependence, as well as its effect on relaxation modes of concentration and orientation fluctuations are of great interest and importance. The difference of PPP-12 from P-12 is only at the degree of substitution of the flexible side chains and thus it is not surprising that PPP-12 is not very soluble either. Nevertheless we were able to reach concentrations up to 56 mg/cm^3 (6.5% by weight) in toluene (see also chapter 6) and up to 6 mg/cm^3 (4% by weight) in $CHCl_3$. At relatively low concentrations (less than 5% by weight) solutions of these hairy-rod polymers in both toluene and chloroform undergo a transition, which is characterized by the formation of large clusters, eventually settling with time (if the polymer-solvent density difference allows). This phenomenon was found to relate to association, driven by Van der Waals forces, and a subsequent crystallization of the flexible side chains inside the clusters [5] as discussed in chapter 7. In chapter 7 we have investigated the association of these molecules; the time and temperature dependence of both small (formation of "trimers") and large scale association which leads to phase separation and precipitation.

In this chapter we present the dynamics of the molecularly dispersed single or unimer (trimer) scatterers since we have avoided the large scale clustering. The utilization of VV and VH light scattering data (dynamic and static) as well as PFG-NMR self diffusion data in two different solvents enables us to separate the relaxation processes which originate from small molecular aggregates (unimers) from those due to single molecules. As in the P-12 case, PPP-12 phase separates, as discussed in chapter 7, without showing an isotropic to nematic transition, although as we discuss in chapter 7 the dense phase formed after the phase separation in toluene solutions is composed of large clusters with high orientational order of the chain backbone and some crystalline order of the side chains. Another finding of our study of PPP-12 solutions is the absence of any significant molecular weight dependence of diffusion coefficients and scattering intensities probably due to the small differences in the molecular weights and the large polydispersity

of the samples. Finally the results in $CHCl_3$ show that it is better solvent than toluene; this is reflected in the dynamics of concentration fluctuations where the cooperative diffusion of single molecules can be detected. It is noted than due to the high polydispersity and small range of molecular weights of the polymers of Table 8.2, it is not possible to examine the effects of molecular weight.

PPP/S sample

The last series of PPP's that we used in our study is also the most promising for the investigation of single molecule dynamics. The macromolecular structure of PPP/s shows that the side chains are irregular, consisting of both flexible alkyl chains and sulfonated phenylene groups, while the chain backbone is the same with the other series. These difference in the side chains, has a drastic effect on the solubility of the polymer; in three different organic solvents that we have used the solubility is excellent. Maximum concentrations of 20% up to 66% were reached in solutions of toluene, chloroform and trichloroethylene depending on the sample. Only for some molecular weights did we obtain opaque phases at high concentrations (S-3 at 20%, S-7 at 40%, S-10 at 40%) indicating a phase separation; nevertheless no precipitation was observed.

8.3 Dynamics of P-12

Here the study of orientation and concentration fluctuations, utilizing P-12 toluene solutions, is discussed in a limited concentration range.

8.3.1 Dilute Region-Characterization

In this investigation the molecular weight determined by GPC despite the reservations mentioned above will be used, nevertheless a critical comparison of our results will be made concerning this point. For P-12 in toluene L_e values (Table 8.1) give the following characteristic concentrations:

- $c^* = 0.303\%$ and $c^{**} = 4.48\%$ (by weight)

Hence the examined concentrations are in the dilute and semidilute regime; the concentration varies from $c/c^* = 0.5$ to 13. ($c = 1.4\ mg/cm^3$ to $33.3\ mg/cm^3$). In the dilute and early semidilute solutions ($c/c^* \leq 4.6$) both polarized and depolarized time correlations functions were recorded at different scattering wave vectors q. The polarize correlation function which reveal the concentration fluctuations can be fitted by one main diffusive process. On the other hand, two distinct relaxation modes contribute to the orientation relaxation function with q and c dependent amplitudes. Both the polarized and depolarized correlation function display a non diffusive slow process (mode C) whose amplitude increase

with concentration and decreasing angle. This is attributed to some large clusters (few in number) which cause number fluctuations when that enter in the scattering volume resulting to an apparently non-diffusive VV and VH mode of the same nature with the ultra slow modes observed and discussed in the association study (Chapter 7). We will not discuss this mode further in the chapter.

Before presenting the results of the VH and VV static and dynamic experiments it is useful to calculate the transport coefficients (D_0 and $D_{R,0}$) for the polymer molecules in the zero concentration limit according to the expressions given in Appendix B.

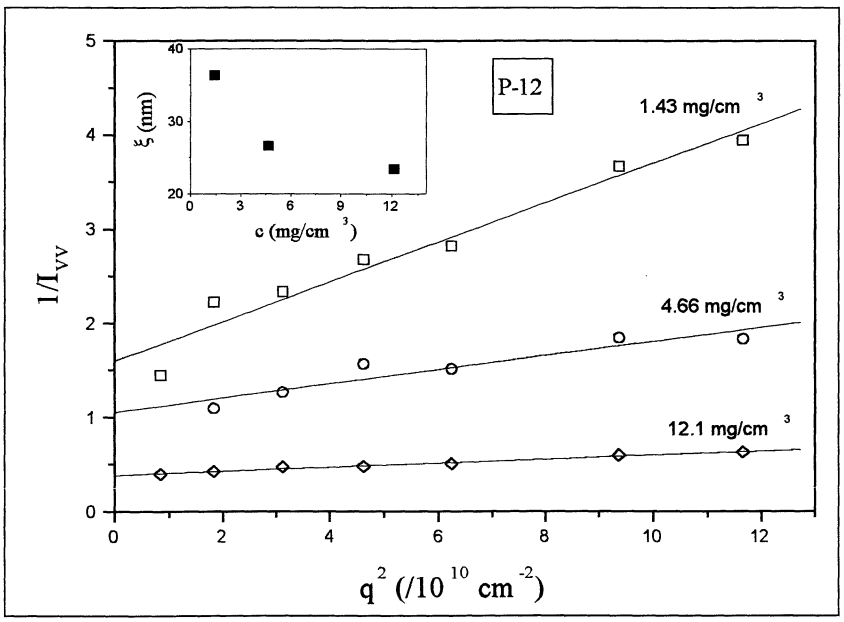

Figure 8.1: Angular dependence of the inverse of the scattering polarized intensity at three different angles. Inset: the concentration dependence of the correlation length ξ.

- The use of Yamakawa-Fujii relation for a wormlike chain (eq. B.13) with $L_n = 30.2\ nm$ and $l = 25\ nm$ leads to a translational diffusion $D_0 = 8.06 \times 10^{-7}\ cm^2/s$, while for $L_w = 72.5\ nm$ leads to a $D_0 = 4.43 \times 10^{-7}\ cm^2/s$.

  The rotational diffusion calculated from the relations of Hearst and Stockmayer for stiff chains (eq. B.9) for $L_n = 30.2\ nm$ and $l = 25$ gives $D_{R,0} = 664120\ s^{-1}$, while for $L_w = 72.5\ nm$ we get (eq. B.11) $D_{R,0} = 63400\ s^{-1}$.

The above values, are quite larger than the experimentally found indicating the existence of larger than molecular, scattering moieties..

Statics

Additional evidence for the existence of larger than the one macromolecule scatterers besides the dynamics comes from both M_w, and the radius of gyration, R_G. The scattered intensity, extrapolated to zero concentration and scattering wavevector (thermodynamic limit), yields the molecular weight, M_w and also the radius of gyration, R_g (from the q-dependence) and the second virial coefficient, A_2 (from the c-dependence) according to (eq. 3.53, Zimm Plot):

$$\frac{Kc}{R_{VV}} = \frac{1}{M_w}(1 + \frac{q^2 < R_g^2 >_z}{3} + ..) + 2A_2c \tag{8.1}$$

The angular dependence of the scattered intensity due to the polymer molecules in the polarized geometry is shown in fig. 8.1 for three different concentrations.

The correlation length ξ ($= R_G/\sqrt{3}$ at $c \rightarrow 0$) can then be directly calculated according to:

$$I(0)/I(q) = 1 + q^2\xi^2 + ... \tag{8.2}$$

The correlation length is seen to decrease with increased concentration, as expected due the interpenetration of polymer chains. This shows that already at 0.5% we are above the overlap concentration. Extrapolation to $c \rightarrow 0$ results to a z-average (since we are dealing with a polydisperse solution) radius of gyration $(R_G)_z = \sqrt{3}\xi = 62 \pm 4$ nm. For a a polydisperse solution of wormlike chains $(R_G)_z$ is given by eq. 7.2, which for $l = 25$ nm and $m = 0.7$ yields a weight average contour length $L_w \simeq 300$ nm. In this estimation a wormlike shape of the scatterer is assumed. Since the size found is much larger than the molecular dimensions, the above assumption implies an end to end molecular association which results to a wormlike supramolecular moiety..

The calculation of M_w we used (see eq. 3.53) the same refractive index increment, $\partial n/\partial c = 0.08$ cm^3/gr, with that of PPP-12 measured in toluene. The molecular weight is then estimated according to eq. 8.1 to be $M_w = 1.05 \times 10^5$ gr/mol, corresponding to contour length $L_w \simeq 126$ nm. This value is 1.7 times larger than the value in Table 1 suggesting again some association of the P-12 molecules; smaller though, from what R_G suggests. Note that in the estimation of M_w the only uncertainty is that of $\partial n/\partial c$ and there is no model for the shape of the scatterer involved in the calculation.

Dynamics

The polarized PCS measurements show one main process which is clearly of diffusive nature (q^2 dependent decay rate Γ) and which slows down as the concentration increases. The VV correlation function is shown in figure 8.2 for three different concentrations together with the diffusion coefficient D_c deduced from these measurements according to the procedure described in chapter 5. This

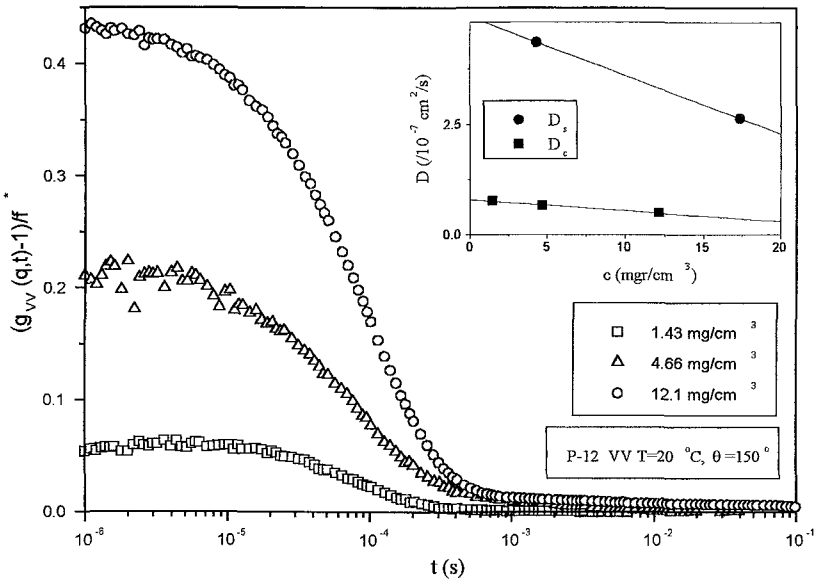

Figure 8.2: VV correlation functions for P-12 toluene solutions in three different concentrations at $\theta = 150^o$. Inset: The concentration dependence of D_c (from polarized PCS) and D_s (from PFG-NMR).

process originates from the cooperative diffusion of the polymer chains, which in the dilute region (at $c \to 0$) is identical with the translational self diffusion of the center of mass of the chain. The latter was measured for two concentrations by PFG-NMR and is also shown together with light scattering D_c in the inset of fig. 8.2. In nonzero concentrations light scattering is measuring, D_c, (see chapter 2 and 3) which in the virial regime is related to the thermodynamics of the solution through eq. 2.13.

There is a clear difference between the experimental self diffusion (NMR) and cooperative diffusion (PCS); the extrapolated to zero values of the two diffusion coefficients are

- $(D_c(0))_z = 0.79 \times 10^{-7}\ cm^2/s$ and $D_s(0) = 4.93 \times 10^{-7}\ cm^2/s$

This difference can be partly attributed to the different averages of the diffusion coefficient that the two experiments measure. Light scattering is measuring the z-average [7] while NMR the n-average of the diffusion coefficient; the former is related with the $1/L_w$ and the later with $(1/L)_n$, in the case of polydisperse rods. The above values are significantly smaller than the calculated above from $L_n = 30.2\ nm$, and can be rationalized by a much larger chain. If eq. B.12 is used (for $b = 1.7\ nm$), $(D_c(0))_z$ gives an $L_w \simeq 900\ nm$ while $D_s(0)$gives $L_n \simeq 63$

nm which are respectively 12 and 2 times larger than the expected. Another difference between the NMR D_s and light scattering D_c is that the later includes thermodynamic interactions (according to eqs. 2.10, 2.12) which in the case of a polymer in a bad solvent will slow down the diffusion in excess to the increased, with c, friction. Thus, it is most probable that with light scattering we have to go to very dilute solutions to measure the real self diffusion of the scatterers.

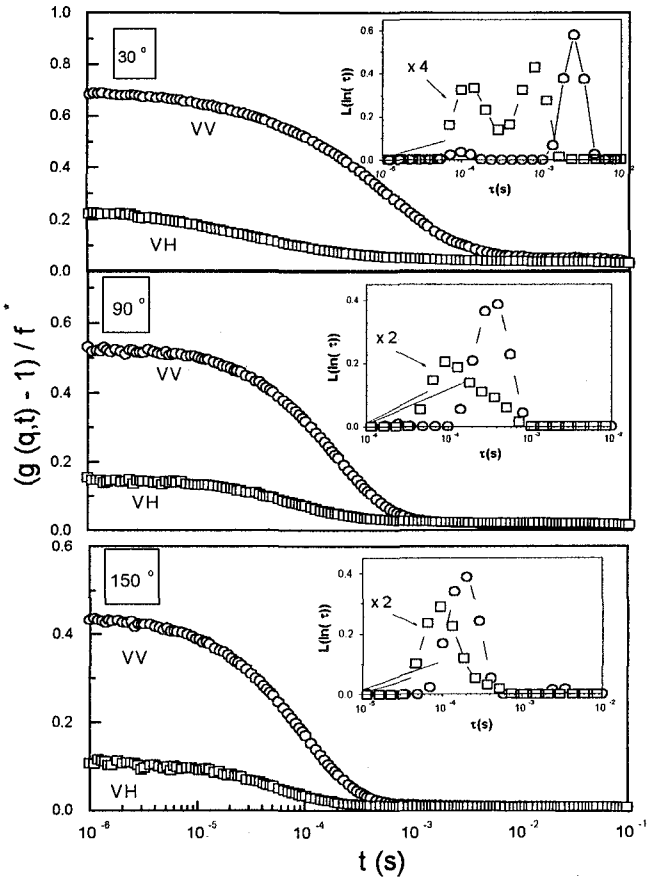

Figure 8.3: Experimental net polarized and depolarized correlation functions of 12 mg/cm^3 solution of P-12 at three different scattering angles (θ) at 20^oC. The inverse Laplace transform of these functions are shown in the inset.

In the case of the rotational diffusion of a rod the related to $D_{R,z}$ length scale is $(1/L^3)_z$ which is approximately $(L_w/L_n)^{-1}/L_n^3$. The measured correlation time for orientation fluctuations of our polydisperse system of molecules with $L_n = 30.2\ nm$, in the limit of zero c, should be $\tau_{R,0} = (6D_{R,0})^{-1} \simeq 6 \times 10^{-7}$ s . This is very close to the shortest time of PCS and thus it the rotational diffusion dynamics should not be observed in the depolarized measurements of

our smaller concentrations. Nevertheless, in aggreement with the translational diffusion measurement, the rotational diffusion coefficient measured by depolarized light scattering is much smaller (the time is slower) again suggesting a large scatterer (of the order of $L_w \simeq 900\ nm$) as we show below.

To conclude the characterization of the scattering moiety we can say the following:

A) Both static and dynamic measurements suggest a larger scatterer than the molecular dimensions given by GPC.

B) The M_w determined by static light scattering, and $D_s(0)$ measured by NMR, suggest a dimer associating end-to-end (with $L_n \simeq 60\ nm$)

C) The translational and rotational coefficients determined by dynamic light scattering suggest a much larger scattering moiety; a wormlike chain with $L_w \simeq 900\ nm$ can rationalize these findings.

D) In view of the above we will not attempt any definite characterization of the scatterers, and we will use the c^* calculated using $L_n = 30.2\ nm$ bearing in mind that we are dealing most probably with a wormlike scatterer made of few polymer chains associating end-to-end.

8.3.2 Results of depolarized scattering

For concentrations less than 4 mg/cm^3, the depolarized intensity was very weak to allow the measurement of $g_{VH}(q,t)$ within reasonable accumulation time (few hours). The high depolarization ratio (~ 0.2) of the solutions justifies the choice of the poly(p-phenylene) for depolarized light scattering studies. Hence, the quality of the experimental $g_{VH}(q,t)$ allows a detailed analysis of the shape of the orientation relaxation function.

Figure 8.3 shows experimental net correlation functions $(g(q,t)-1)/f^*$ for the 12 mg/cm^3 ($c/c^* = 4.6$) solution at three different scattering angles at $T = 20^oC$ for both the polarized and the depolarized geometry together with the corresponding distributions of relaxation times (insets). In contrast to the polarized intensity correlation functions, $g_{VV}(q,t)$, arising from concentration fluctuation, the somewhat faster $g_{VH}(q,t)$ display a bimodal distribution relaxation function $L(\ln\tau)$. The intensity I_{VH} increases at small q's as indicated also by the increase of the amplitude $\alpha = g_{VH}(q,0)$ of the VH correlation function (fig. 8.3), and it suggests long chains i.e. $qL_e > 1$.

Moreover at constant q, the increase of polymer concentration is expected, on the ground of topological and thermodynamic reasons, to affect the orientational dynamics. An example of these dependences is presented in Fig. 8.4, where for $c/c^* = 9.37$ and at $q = 0.034\ nm^{-1}$ we show how the VH correlation function varies with q and c respectively. Besides the increase in the amplitude α with

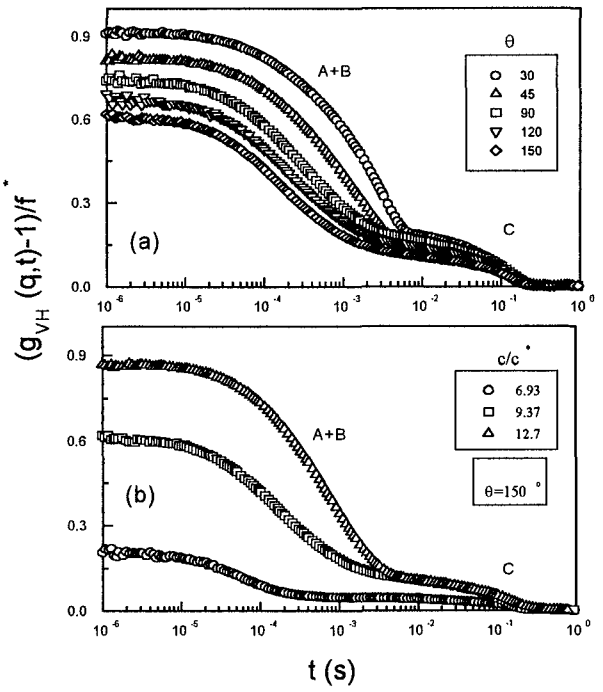

Figure 8.4: Depolarized time correlation functions for P-12 toluene solutions at 40^oC and (a) at $c = 18\ mg/cm^3$ and at different scattering angles and (b) at $q = 0.034\ nm^{-1}$ for three different concentrations. The main modes A and B as well as the ultra slow are indicated.

increasing $1/q$ and c, there is a concurrent narrowing of the shape of $g_{VH}(q,t)$. This modification becomes evident in the form of $L(\ln \tau)$, that displays a bimodal shape with increasing domination of the slow mode (B) as the polymer concentration increases and q decreases (fig. 8.5). The enhancement of the slow mode (B) relates to the concurrent increase of the I_{VH} intensity with solute concentration beyond the expected linear c-dependence (see fig. **??**). The rate of increase of the most probable (slow (B) VH mode) relaxation rate Γ_s of the distribution with q decreases at high q's (fig. 8.6).

8.3.3 Discussion

The shape of the experimental orientation relaxation function $g_{VH}(q,t)$ (Fig. 8.3 and 8.4) is represented by a bimodal relaxation distribution function (Fig. 8.5) (besides the ultraslow mode). There are theoretical models [8] as well as simulation studies [9] that predict the existence of two channels for the relaxation

of rodlike polymers or even a multiexponential decay of the correlation function [10] (see also chapter 4). Nevertheless the strong indication of association that we have for the P-12 sample makes the discussion in terms of such models rather unsafe. As mentioned in the next sections, for the other two samples studied (PPP-12 and PPP/Su) we were able to distinguish quite clearly the molecular from the aggregation modes when the later were present. Thus based on the discussion we had in the previous section, the slow mode is assigned to the collective reorientational motion of the polymer aggregates, already seen from the dilute regime. A very similar situation is met for solutions of the smallest molecular weight S-10 of the much more soluble PPP/S series.

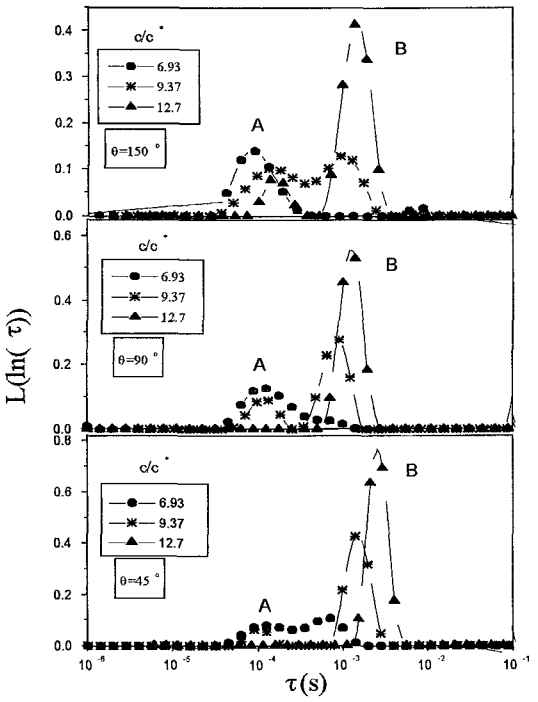

Figure 8.5: Distribution of $L(\ln\tau)$, of orientation relaxation times obtained from the experimental $g(q,t)$ of fig. 4 at three scattering angles for three concentrations. The main modes A and B are indicated.

On the other hand neither the fast VH mode conform with the rotational diffusion time expected for a free polymer chain which is given above and is two orders of magnitude larger (see the calculated D and D_R for the individual molecules, in the characterization section). Another information that is important for the determination of the origin of the two VH modes is the amount of the depolarized scattered intensity which is in the time window of the correlator. From

the total contrast of the VH intensity we can conclude that in all concentrations measured almost all the intensity originating from the polymer molecules is contributing in the observed VH processes i.e. the two main modes that we discuss and the ultra slow q-independent mode that we have just mentioned above (see fig. 8.3 and 8.4). Thus the vast majority of the polymer molecules are involved in the two relaxation processes we observe and very few are free. Hence, all scatterers are wormlike aggregates.. Then for the present polydisperse and associating sample, the fast process might be attributed either to the rotational motion of shorter associates confined in cages formed by the longer ones or to the faster rotational motion in the cage that is suggested for monodisperse rodlike solutions (see chapter 4). This assignment can rationalize the insensitivity of the rate Γ_f to q and c variations expected and found for fast rotational motion since

$$C_{VH}(q,t) \sim \exp[-(Dq^2 + 6D_R)t] \tag{8.3}$$

and $\Gamma_f = 6D_{R,f} \gg Dq^2$.

The slow rate, Γ_s, for $c/c^* < 5$ displays a linear q^2 dependence with a non-zero intercept as expected for diffusing particles large enough so that $6D_{R,s} \sim Dq^2$. The value Γ_s (at $q = 0$) defines D_R, that slows down significantly with increasing c as discussed below. Moreover, Γ_s for $c/c^* > 5$ is found to exhibit a peculiar q-dependence depicted in fig. 8.6. For the two highest concentrations, Γ_s becomes virtually q-independent at high q's as can also be seen in fig. ??. The depolarized light scattering intensity $I^*_{VH} = \alpha_s I_{VH}/I_{tol}$, associated with the slow process, is shown as a function of q in the inset of Fig. 8.6. This plot displays angular asymmetry over the accessible range of q's that can be described by a correlation length $\xi = 57\ nm$ for the orientation fluctuations according to eqs. 8.2. The change in the q-dependence of the dynamics (Γ_s) at high concentration ($c/c^* > 5$) but not of the anisotropic intensity might reflect a different mechanism for orientation relaxation at high qL. At this q range, the smaller than expected Γ_s reflects to a local relaxation (q-independent) character of the orientation fluctuations.

A downward curvature has been reported for the q^2-dependence of the relaxation rate Γ_{VV} for the concentration fluctuations (polarized light scattering) in PBLG nondilute solutions [11] while low optical anisotropy has precluded dynamic depolarized experiments. It is accounted in the framework of the random phase approximation theory for rod like polymers [12] in isotropic solutions and by introducing a qL dependent osmotic virial coefficient [13, 14] (see also chapter 4). Nevertheless the RPA predictions for the depolarized dynamics do not suggest a similar behavior for Γ_{VH}, as discussed in chapter 4. Qualitatively, eq. ?? for rigid rods would capture this feature provided the excluded volume factor $A^*(qL, c, \vartheta)$ and/or the weight factors f_1^* and f_2^* were decreasing functions of qL at high c.

Alternatively, it is conceivable that the presence of the long (hexyl) sub-

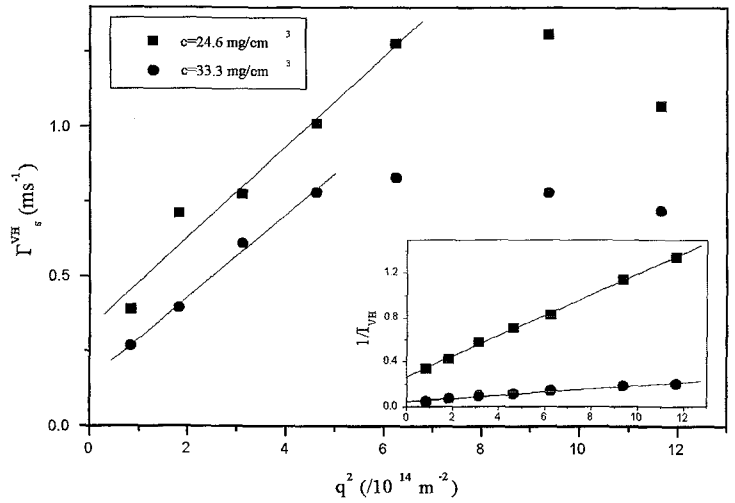

Figure 8.6: Variation of the orientation relaxation rate Γ_s, obtained from the slow peak of $L(\ln \tau)$, with the scattering wavevector for the two larger concentrations at 40^oC. Inset: The variation of the inverse of the depolarized intensity with q^2 for these solutions.

stituents in this hairy rod system might modify the hydrodynamic conditions. We will show, however, that a more pronounces slowing down of VH dynamics in the high q-range is revealed in the other two samples (PPP-12 and PPP/Su) studied and where we are able to detect orientation fluctuations of single polymer chains and not of associates. These strong findings are discussed in details in the following sections (mainly in section 8.6).

The concentration dependence of the rotational diffusivity D_R, given by the limiting low q value of Γ_s and Γ_f are shown in fig. 8.7 together with the data from the simulation study of rigid rods by Bitsanis et al. [9]. According to simulation [9] and dynamic electric birefringence [15] results of PBLG, the crossover to the c^{-2} dependence occurs at $c/c^* > 100$. In contrast, the present hairy rod system appears to approach this limit at $c/c^* > 10$ (fig. 8.6); note however that this is due to the fact that we probe the reorientation of larger than one molecule moieties, while the c^* was calculated from the molecular dimensions. It is important to note that the concentration dependence of the rotational diffusion coefficient of the molecular aggregates follow a very similar curve with the expected for rodlike systems; while only at the larger concentrations it is following the c^{-2} DE prediction. The rotational diffusion coefficient corresponding to the fast process is found to be c-independent (fig. 8.7). The present data are also used in comparison with data of PPP/S-10 (section 8.6).

The depolarized light scattering intensity normalized to the anisotropic in-

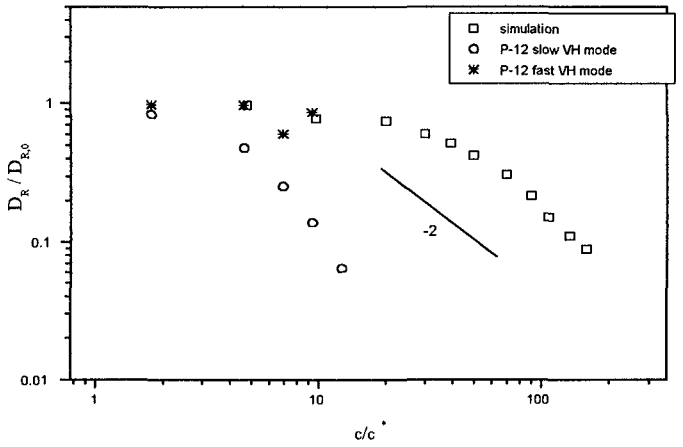

Figure 8.7: Concentration dependence of the rotational diffusivity D_R of both VH modes in P-12/toluene solutions at 40^oC. The scaling prediction of DE theory is indicated by the slope of the solid line. For comparison simulation results of rigid rods are shown.

tensity $I^*_{VH} = \alpha_s I_{VH}/I_{tol}$ normalized to the anisotropic intensity of the toluene increases linearly with concentration at low c. Strong positive deviations from the linear dependence are observed as the concentration increases towards to a critical concentration c_{cr}. Such an increase is expected for solutions of stiff molecules which approach the isotropic to nematic transition; however, in the present sample as in the case of PPP-12 discussed in chapter 7, we are dealing rather with a phase separation due to bad solvent conditions and not with an I-N transition (see chapter 2). The strong rise in the intensity at high c especially at low q's, indicates pronounced orientational order. For the present system, the intensity at two scattering angles are shown as a function of c/c^{**} at 40^oC. For $c/c^{**} < 0.5$ that corresponds to $c/c^* < 7.5$, I^*_{VH} is still proportional to the polymer number concentration (inset in Fig. 6).

The clear kink in the concentration dependence of indicates the crossover from the linear to the strong nonlinear rise in the depolarized intensity and occurs at $c/c^{**} \simeq 0.5$ for both q's. The I^*_{VH} deviates at $c/c^{**} \simeq 1$; for comparison we mention that the Onsager prediction for an isotropic to nematic transition for a completely dispersed system of rods with $L = 30\ nm$ would be $c_n \simeq 5c^{**} \simeq 15\%$. In Maeda's calculation of the depolarized light scattering , the intensity at low angles is predicted to diverge at $c = c_n$. Qualitatively similar increase in the total depolarized intensity with increasing concentration was reported for PBLG solutions [11]. Deviations from the linear dependences were observed for $c/c^{**} > 0.5$ which in phenomenological agreement with the present data.

To investigate relaxation mechanism of molecular orientation fluctuations it

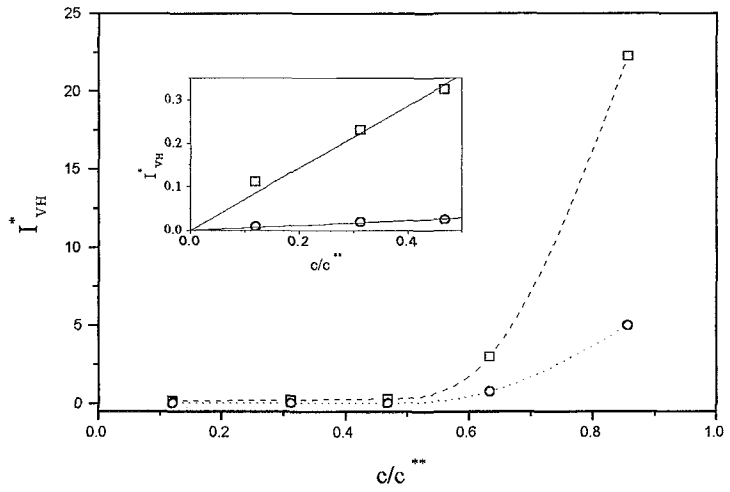

Figure 8.8: Depolarized light scattering intensity normalized to the anisotropic intensity of the the solvent for the slow process (B) in P-12/toluene solutions vs concentration at two scattering angles ($\theta = 30^o$ and 150^o) and 40^oC. The inset show the I_{VH} vs c/c^* in the linear regime.

will be crucial to study PPP samples with narrower molecular weight distribution and with better solubility. This will be done with PPP-12 but mainly with the PPP/S sample.

8.3.4 Summary of P-12 results

The orientation relaxation function $g_{VH}(q,t)$ of poly(p-phenylene) (P-12) hairy rods in solutions can be recorded by PCS due to the significant molecular optical anisotropy. For rod concentrations c/c^* in the range 0.5 to 13, $g_{VH}(q,t)$ displays a bimodal relaxation distribution function with increasing contribution of the slow mode as the concentration increases. Both these modes are related with the formation of rather larger and anisotropic (probably wormlike) aggregates due to an association of the polymer chains (end-to-end). The mechanisms for relaxing the orientation fluctuations are attributed to a slow reorientation of the aggregate which follows a DE concentration dependence at the higher c's and a faster local rotation with c-independent behavior. The depolarized intensity deviates from a linear c-dependence at the higher of the concentrations reached indicating some increased orientational order; however a I-N order is not reached due to phase separation.

8.4 Dynamics of PPP-12

The overlapping concentration, c^*, for these samples in toluene, calculated from an effective L_e, as we mention above are:

- $c^* = 0.180\%$ and $c^{**} = 2.31\%$ (PPP-2),
  $c^* = 0.125\%$ and $c^{**} = 1.97\%$ (PPP-3),
  $c^* = 0.098\%$ and $c^{**} = 1.77\%$ (PPP-5),

These values are about 10 times smaller than those based on R_g. The lowest concentrations studied in this work ($c = 0.07\%$, ($0.6\ mgr/cm^3$) for PPP-2) were determined by the ability of the PCS technique to resolve good VV correlation functions within a few hours. As in the case of P-12 we used the static and dynamic information in the dilute region to characterize the dimensions and molecular weight of the scatterers. Solutions of all molecular weights in toluene reveal bad solvent conditions as the second virial coefficient, A_2 deduced from the polarized scattering intensity according to eq. 8.1, was found to be negative ($\simeq -6 \times 10^{-4} cm^3/g^2$). At the same time solutions in chloroform exhibit good solvent behavior ($A_2 \simeq 1 \times 10^{-3} cm^3/g^2$) for PPP-5 sample and close to θ conditions for PPP-2. In toluene, the molecular weight of PPP-2 was found to be significantly higher than in chloroform, in agreement with the values of the translational diffusion coefficient at zero concentration, D_0. As we discussed in chapter 7, based on the values of molecular weight and D_0 in the two solvents, small clusters (aggregates), consisting on the average of three chains, are formed in toluene, even in dilute solutions [5]. Somewhat surprisingly, for the larger PPP-5, the values of the molecular weight in both solvents were quite close, in agreement with the values D_0, implying a smaller degree of aggregation than in PPP-2. For all samples, D_0 assumes larger values in chloroform than in toluene (the larger difference was observed for PPP-2). Based on these findings, we can conclude that there is evidence of aggregation in the toluene solutions (more pronounced in PPP-2), whereas association is negligible in chloroform, at low concentrations.

8.4.1 Cooperative diffusion

In the dilute regime, a single nearly molecular translational diffusion process can be detected, irrespectively of the solvent quality. However, this relaxation process is rather broad. In the KWW analysis (see eq. 5.9), β typically varies between 0.7 and 0.9, for concentrations up to about 5 mg/cm^3 ; this may be attributed to the large polydispersity of the samples (Table 8.2). A typical VV intensity autocorrelation function in the dilute region at $\theta = 150^o$ ($q = 0.037 nm^{-1}$), is shown in Fig. 8.9 (for PPP-5, $c = 3\ mg/cm^3$, $c/c^* = 3.8$, in toluene and $c = 2.9\ mg/cm^3$, $c/c^* = 3.5$, in chloroform). It is a single diffusive relaxation, as also

confirmed by the relaxation spectrum, obtained by CONTIN analysis (shown in this figure as well) and the q^2-dependence of the decay rate (inset of Fig. 8.9); it is attributed to the translational diffusion of the PPP's. As the concentration increases above about 8 mg/cm^3, the VV correlation function becomes broader for both solvents. Moreover, for chloroform solutions, two relaxation modes can be resolved by the CONTIN analysis. In Fig. 8.9b, the VV intensity autocorrelation function of a semidilute chloroform solution of PPP-5 ($c = 41.4\ mg/cm^3$, $c/c^* = 50.2$) at $\theta = 150^o$ clearly reveals these two relaxation modes which are both diffusive (inset of Fig. 8.9b). While the fast process is identified with the cooperative diffusion, based on the concentration dependence of the diffusion coefficient and the scattered intensity, the slow mode is new and its origin will be discussed in the next section.

From the q-dependence of the scattered intensity the correlation length ξ, can be calculated. If we use the total scattering intensity this is found to be nearly independent of concentration, about $15nm$, for all samples. The correlation length is expected to drop from its dilute region value, where it represents the geometric characteristics of the macromolecule (radius of gyration), to some average mesh size of the network that the polymer chains form when they start to overlap in the semidilute region. The correlation length is dropping as $c^{-3/4}$ in solutions of flexible polymers [16], whereas for rods it is expected to drop, as the transition to the nematic state (at c_n) is approached, as $\xi \sim (1 + 8c/c_n)^{-1/2}$ resulting from Onsager theory [17] and the classical light scattering theory and in accordance to mean field predictions of DSO [18] (Chapter 4). The smaller decrease compared to that of flexible molecules in solution has been observed [19], but also even weaker decrease than the predicted $c^{-1/2}$ has been found [11] in solutions of stiff macromolecules. The correlation length calculated from the total scattered intensity in solutions of chloroform do not show any decrease with concentration due to the existence of the slow mode which gains intensity.

Fig. 8.10 depicts the concentration dependence of the scattered intensities and the distribution relaxation function $L(ln\tau)$ of PPP solutions in chloroform. The scattered intensities at $q \to 0$ are shown for PPP-2 and PPP-5 solutions. The concentration is normalized with c^* (estimated from L_e) and the intensity of each mode is normalized relative to toluene, i.e., $I_i = a_i I/I_{tol}$. It is noted here that the PCS technique offers the unique advantage of isolating various contributions (such as slow modes) from the total scattering intensity, and thus accurately determining parameters such as osmotic modulus, friction coefficients, and of course identifying the origin of relaxation modes other than the cooperative diffusion. The intensity I_c associated with the cooperative diffusion mode increases with concentration only in the dilute regime, whereas this increase ceases as intermolecular interactions become significant, signifying the transition to the semidilute regime. The broad peak of I_c versus c occurs around $c \approx 10c^*$; above this concentration, negative interference lead to the decrease of the total scattered intensity. This rather extended transition is common in rodlike polymer

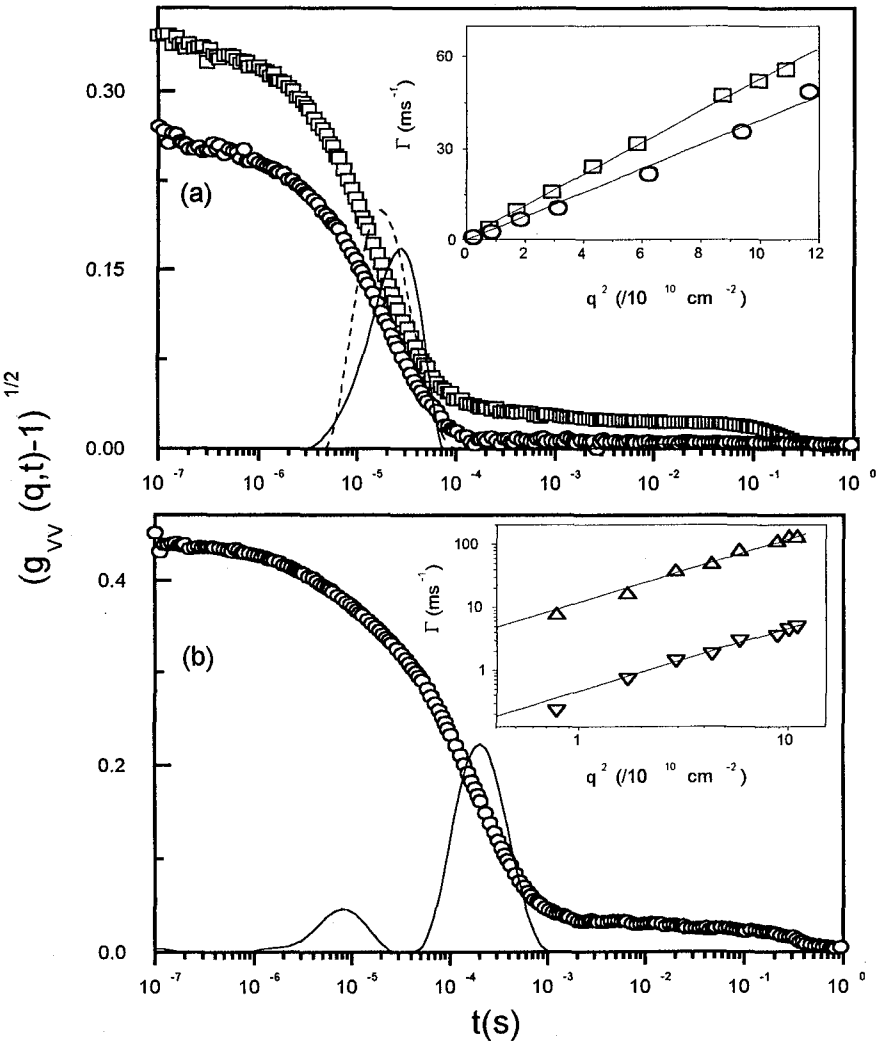

Figure 8.9: (a) Net polarized field autocorrelation functions $C(q,t)$ for dilute solutions of PPP-5 in toluene ($c = 3.03\ mgr/cm^3$; ◯) and chloroform ($c = 2.85\ mgr/cm^3$; □) at $25°C$ and a scattering angle $\theta = 150°$ ($q = 0.034\ nm^{-1}$ and $0.033 nm^{-1}$ respectively), along with their corresponding distributions of relaxation times, obtained from ILT analysis (solid and dashed lines, respectively). Inset: q^2-dependence of the corresponding decay rates, Γ. (b) Net normalized polarized field autocorrelation function for a 41.4 mgr/cm^3 solution of PPP-5 in chloroform (◯) , along with the respective distribution of relaxation times. Inset: q^2-dependence of the corresponding two decay rates, fast (△) and slow (▽).

solutions, where the onset of the semidilute region occurs at $c \approx O(10\ c^*)$ [20, 21] and not at $c \approx c^*$; this difference matches the disparity between the volumes L^3 and $4/3\ \pi R_g^3$ for rods and flexible coils, respectively. For $c > 10\ c^*$, I_c decreases weakly, whereas the intensity I_s associated with the slow mode, increases strongly, with concentration; this is also evident from the distribution of relaxation times (eq.), of PPP-2 solutions in chloroform, shown in the inset of Fig. 8.10, at $\theta = 45^o$ ($q = 0.013 nm^{-1}$). It is noted that for $c \approx 10\ c^*$ the separation of the two processes is not sufficient, and hence the intensities are subject to larger error. However, the mode resolution increases with c since the two diffusion coefficients have opposite c-dependence.

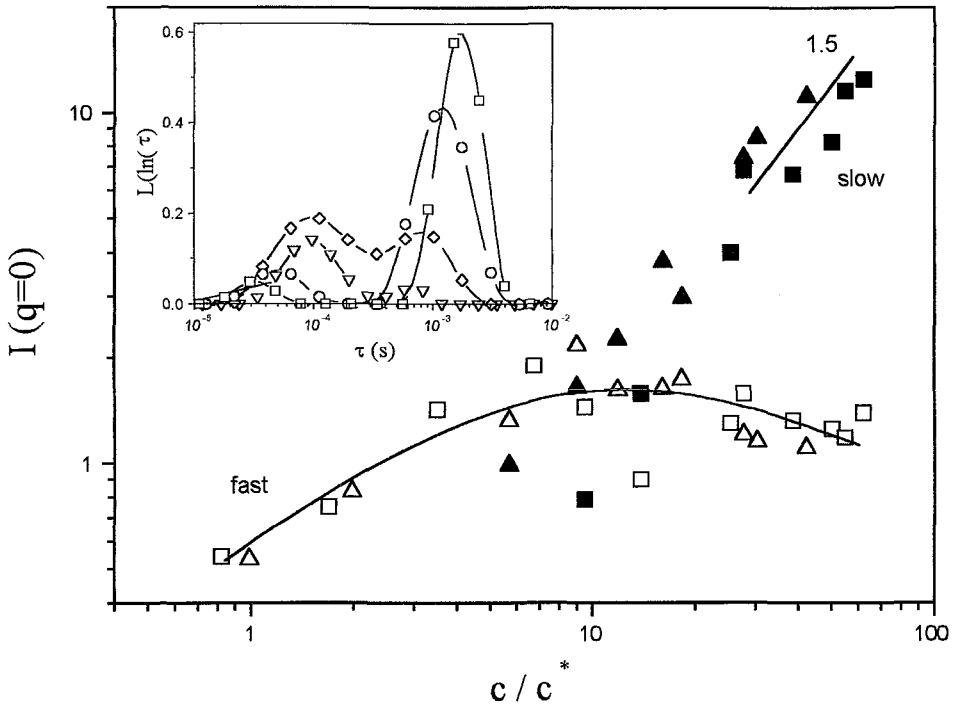

Figure 8.10: Concentration dependence of the scattering intensities of the two dynamic modes, extrapolated to $q \rightarrow 0$, and normalized with the polarized toluene intensity, for various PPP's: open sympols correspond to the cooperative mode and solid ones to the slow mode. Lines are drawn to guide the eye or indicate slopes. Inset: Distribution of relaxation times from $L(\ln \tau)$, for PPP-2 in chloroform at $\theta = 45^o$ ($q = 0.013\ nm^{-1}$) and various concentrations: $c/c^* = 0.99$: $\bigtriangledown$; 9.01 : $\diamond$; 30.3 : $\bigcirc$; 42.1 : $\square$.

The angular dependence of the relaxation processes determining the concentration correlation function $C(q,t)$, are depicted in Fig. 8.11, for a PPP-5 solution

in chloroform at $c/c^* = 50.2$. The distribution of relaxation times is multiplied by the total intensity (Fig. 8.11a) for a better comparison of the intensities associated with the two processes. As expected for a cooperative diffusive process with small correlation length ($q\xi \ll 1$), I_c is virtually q-independent (Fig. 8.11b). On the other, I_s increases weakly at low q's and becomes q-independent at even higher c's. The apparent slight intensity increase at low q's suggests the presence of larger than molecular scatterers, but it is clearly different from the scattering intensity of the large clusters in toluene after two weeks, at similar concentrations (Chapter 7).

In order to resolve relaxation modes of molecular origin we performed measurements in a solvent of reduced quality, i.e. toluene. In such a case, one main relaxation process which is related to isotropic fluctuations, can be unambiguously distinguished, in the polarized correlation function. Like in chloroform solutions this mode is clearly diffusive and for all molecular weights is slower than the cooperative diffusion process in chloroform. In contrast to the cooperative diffusion in the latter, the diffusion coefficient in toluene is decreasing with concentration for the PPP's. Moreover, the intensity $I_s(q = 0)$ increases monotonically with concentration, in contrast to the behavior of I_c, and hence the signature of the crossover to the semidilute regime is unclear for the toluene solutions. The reference value of c^* used for solutions in toluene is the same as that for chloroform solutions. The concentration dependence of I_s of PPP-2 solutions in toluene is depicted in Fig. 8.11. The different behavior of both the intensity and the dynamics of the main mode in toluene solutions, as compared to the cooperative diffusion (Fig. 8.10) in chloroform, suggests that the origin of this mode is not the mutual diffusion of the polymer chains in semidilute solutions. As will be discussed below, this process is related to the self-diffusion of small aggregates. On the other hand, the distribution of relaxation times, shown in the inset of Fig. 8.11 for different concentrations at $\theta = 45^o$ ($q = 0.013nm^{-1}$), suggests that at least one faster process with relatively low-intensity is present in toluene solutions; this could relate to cooperative diffusion, but it is overwhelmed by the slow mode. Based on the comparison between this fast process and the depolarized correlation function (section 8.5.3), the former originates from orientation rather than concentration fluctuations.

In the virial regime, the cooperative diffusion should vary linearly with c (eq. 2.9),

$$D_c = D_o(1 + k_D c + ...) \tag{8.4}$$

In chloroform solutions, k_D is found to be positive, in qualitative agreement with the static light scattering result, i.e., chloroform is a good solvent for these PPP's. In this regime, the experimental data give $k_D = 67cm^3/g$ for PPP-2 and $k_D = 39cm^3/g$ for PPP-5. The calculated value of $k_D = 2A_2M_n$ ($= 2(\pi f N_{AV} d^2 L_n/M_n^2)M_n$), neglecting the effect of friction and excluded volume and

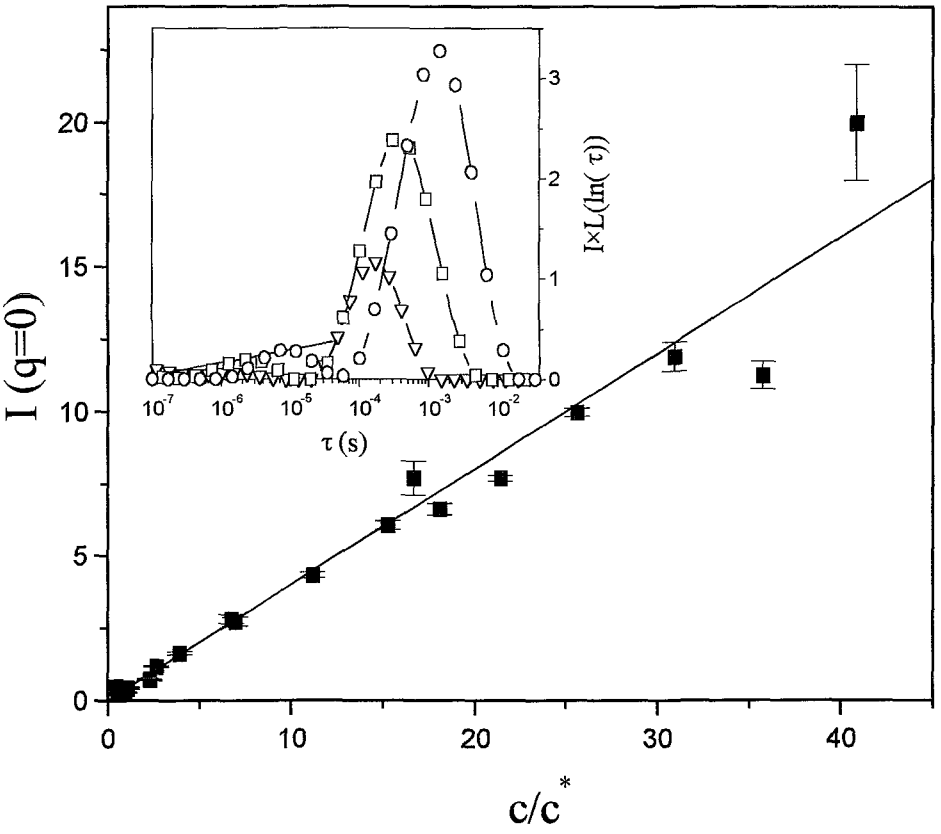

Figure 8.11: Concentration (c/c^*) dependence of the scattering intensity, extrapolated to $q \rightarrow 0$, for PPP-2 in toluene (■). Solid line represents the linear fit. Inset: Corresponding distribution of relaxation times $L(\ln\tau)$, at $q = 0.014\ nm^{-1}$ and various concentrations: $c/c^* = 6.8$: ▽ ; 21.4 : ■ ; 40.9: ○. The fitting procedure can resolve fast low-intensity modes as well (see text).

using the experimental A_2 value for PPP-5, is $36cm^3/g$. The computed value is significantly larger ($129cm^3/g$), if the Ishihara-Hayashida [22] expression for the thermodynamic second virial coefficient is used. For solutions in toluene, k_D is expected to be negative, since both the thermodynamic ($A_2 < 0$) and friction factors slow down the diffusion. This is qualitatively confirmed by experiments since there is no relaxation mode with increasing decay rate in toluene solutions.

Fig. 8.12a shows the osmotic modulus reduced by the molecular weight for solutions of PPP-2 and PPP-5 in both solvents; it can be calculated either from the total scattered intensity or from the intensity, I_c, of the cooperative mode (in the case of chloroform solutions); we recall that the average total intensity includes contributions from the slow mode as well. The osmotic modulus represents the resistance of the polymer solution to concentration fluctuations and

is expected to increase with concentration, suppressing the scattered intensity due to concentration fluctuations. In chloroform, total intensity data lead to a small increase of the osmotic modulus $(\partial\pi/\partial c)$ at low concentrations and a final level off above 22.7 mg/cm^3. Over the examined concentration range, solutions in toluene reveal a practically constant osmotic modulus, being about 3 times smaller than in chloroform. This finding corroborates with the notion that there are more aggregates (trimers) in toluene than in chloroform, manifested also in the VH dynamics (section 8.5.3). The presence of an additional slow process, however, can strongly alter the values and the c-dependence of the osmotic pressure, estimated from static light scattering data. Knowledge of the dynamics, on the other hand, makes the assessment of the intensity I_c of the cooperative mode, which is necessary to calculate the osmotic modulus, possible. The latter clearly reveals the expected behavior for all samples used (PPP-2 and PPP-5, Fig. 8.12b). In the semidilute region ($c > 10c^*$) $(M_w/N_A)(\partial\pi/\partial c) \sim c^{1.1\pm0.1}$ whereas in the virial regime ($c < 10c^*$) the dependence is weaker ($\sim c^{0.4}$) (Fig. 8.12a). The mean-field DSO prediction for the osmotic modulus of rod-like polymer solutions is a linear increase with c, $(M/RT)(\partial\pi/\partial c) = 1 + 8c/c_n$. For comparison, in semidilute solutions of flexible linear chains the osmotic modulus scales with $c^{1.3}$ [16] for good solvents. In the present investigation, neither the correlation length nor the osmotic modulus, deduced from total intensity data, exhibit the behavior of a rod-like solution (Fig. 8.12a). A linear concentration dependence for the osmotic modulus would assume the slope of 1.7 ± 0.3, which in the light of the DSO theory would suggest that $c_n \approx 4c^*$. This prediction, however, could not be verified, since the present PPP's phase separate before they form a nematic phase. The osmotic moduli of solutions of these semiflexible PPP's in the semidilute regime exhibit therefore a behavior intermediate between rigid-rod and flexible homopolymers. The weaker compared to the flexible polymers increase of the osmotic modulus can be rationalized by the fact that a semistiff chain has a much more loose structure than a flexible coil, facilitating interparticle mixing in the semidilute and concentrated regimes. Experiments on PBLG and xanthan solutions have shown a c^1 behavior for the osmotic modulus [11, 23]. In the other extreme of reduced interparticle mixing, a sharp osmotic modulus increase with concentration is reported for multiarm star polymers and hard colloidal particles [24, 25].

The speed-up of D_c above c^*, shown in Fig. 5b, is due to increasing intermolecular interactions and excluded volume effects, which surpass the increase of the friction with concentration. It is worth mentioning that in semidilute solutions of flexible polymers, it is the reduction of the blob size, which is responsible for the increase of D_c with c. In the case of rodlike polymers, all the segments are correlated moving in phase, and thus the motion of a part similar in size with the correlation length, follows the motion of the whole molecule. In the wormlike molecular picture, the statistical segment is twice the persinstence length and hence again molecules with contour length of about 2 to 3 times their

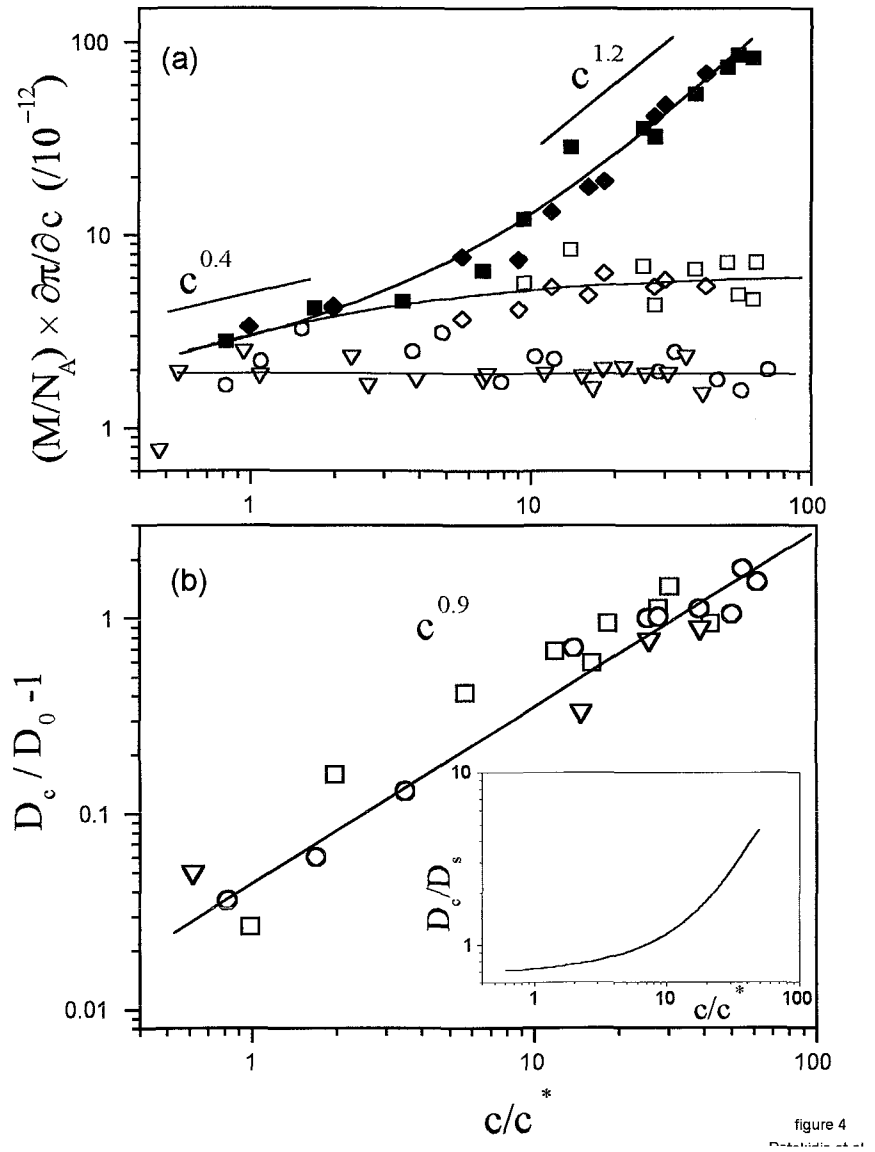

Figure 8.12: (a) Concentration dependence (c/c^*) of the osmotic modulus (normalized with molecular weight), as deduced from the cooperative and total intensities, for PPP's in two solvents: chloroform (cooperative: PPP-2 (♦); PPP-5 (■); total: PPP-2 (◇); PPP-5 (□)); and toluene (total: PPP-2 (▽); PPP-5 (○)). Solid lines are drawn to guide the eye. (b) Concentration dependence (c/c^*) of the cooperative diffusion coefficient in chloroform: PPP-2 (□) ; PPP-3 (▽) ; PPP-5 (○). Inset: Concentration dependence of D_c/D_s.

persinstence length should move much more correlated than flexible chains even in concentrated solutions. DSO theory suggests that $D_c = \frac{D_0}{2}[1 + 8c/c_n]$ varies linearly with c, assuming that the self-diffusion coefficients behave as DE theory predicted ($D_{\parallel} = D_{\parallel,0}$, $D_{\perp} = 0$). From Fig. 8.12b it can be seen that $D_c/D_0 - 1$ scales with $(c/c^*)^{0.9}$. This is closer with the prediction for the rods (baring also in mind the scattering of the data), compared to that for flexible coils ($\sim c^{0.75}$). If on the other hand, we assume a linear with c/c^* dependence according to DSO, we get a slope which implies that $c_n \approx 100c^*$. This is certainly an overestimation and in contradiction with the estimation of c_n based on the comparison of the osmotic modulus data with DSO predictions. Thus DSO predictions does not conform with our experimental findings. Moreover DSO predicts two relaxation modes for the decay of concentration fluctuations as the isotropic to nematic is approached; this modes as we shall show later can not explain our experimental findings.

8.4.2 Slow mode-Self diffusion

The slow mode appears in chloroform solutions in the semidilute regime, whereas in toluene it is always dominant, overwhelming the cooperative diffusion (Figs. 8.12, 8.14, 8.15). From the increase of the intensity with concentration, it is clear that this mode is not related with the slow mode of the DSO model of isotropic solutions of rodlike molecules in the vicinity the nematic transition [11]. The diffusion coefficient D_s related to the slow mode in chloroform, as well as the main one in toluene, decrease with concentration, as seen in Fig. 8.14. Slow modes were found in several dynamic investigations of both stiff and flexible polymer solutions and in most cases they were attributed to clusters [26, 27, 28].

For polydisperse particles, it has been predicted that not only concentration fluctuations (relaxing through collective motions) give rise to refractive index variations but also exchange fluctuations from particles of different refractive index or/and size enabling the observation of the self-diffusion of the molecules by dynamic light scattering measurements. This has been observed in different systems; colloidal spheres and rods [29, 30], multiarm star polymers [24] and block copolymers [31]. For rods polydisperse in size, the dynamic structure factor is predicted to split into two terms [30]:

$$C_{VV}(q,t) = A_c \exp^{-q^2 D_c t} + A_s \exp^{-q^2 D_s t} \tag{8.5}$$

where A_c and A_s are the amplitudes, and D_s is associated with the long-time self-diffusion coefficient.

In order to find the origin of the slow mode, we also carried out pulsed-field gradient NMR measurements, probing directly D_s, for PPP-3 at different concentrations, as seen in Fig. 8.13. The same procedure as in PCS measurements was used, in order to prevent clustering. A third cummulant analysis fit [32] was

chosen for the incoherent structure factors:

$$ln(S_{inc}) = a - \overline{D}q^2t + 1/2\mu_2(q^2t)^2 - 1/6\mu_3(q^2t)^3 \qquad (8.6)$$

where $\overline{D} = \overline{\Gamma}/q^2$ is the diffusion coefficient related to the initial decay rate, and $\mu_2 \equiv \int(\Gamma - \overline{\Gamma})G(\Gamma)d\Gamma$, $\mu_3 \equiv \int(\Gamma - \overline{\Gamma})^2G(\Gamma)d\Gamma$ are the second and third moments of the decay rate distribution $G(\Gamma)$. The fact that a cummulant analysis can fit well the data means that there is a distribution of self-diffusivities., rather than a double exponential decay. The second moment of the distribution increases with concentration; a measure of the breadth of the distribution is the ratio $\mu_2/\overline{\Gamma}^2$ ($\equiv [\overline{(D^2)}_Z - \overline{D}_{Z^2}]/\overline{D}_{Z^2}$ is the z-average normalized variance of the D distribution), which increases with c from 0.18 to 0.4 for the data in toluene. In the highest concentrations also the third distribution is found to be important ($\mu_3/\overline{\Gamma}^3 \simeq 0.12$). We also estimated the long time diffusion from the slope of the $ln(S_{inc})$ at long times. From these data, it is clear that self-diffusion coefficients decrease with concentration, as seen in the inset of Fig. 8.13. For nearly the same concentrations in the two solvents, the tail of the distribution is more pronounced in toluene, resulting in a larger $\mu_2/\overline{\Gamma}^2$. Furthermore, the characteristic times of the long-time decay are essentially the same in both solvents, whereas for the short-time decay, the times in toluene are slower, the difference being larger at higher concentrations (see also inset of Fig. 8.13).

The NMR self-diffusion data, obtained from the long-time decay, compare favorably with the slow diffusion PCS data for chloroform, or the main diffusion for toluene. The self-diffusion coefficient from the cummulant analysis are in both solvents larger than the light scattering slow diffusivities. (Figs. 8.13, 8.14). A compilation of the diffusion coefficients is presented in Fig. 8.14, for all molecular weights and concentrations investigated. In the case of chloroform (Fig. 8.14a), the dramatic difference of cooperative and slow diffusion coefficients, is a manifestation of the different origin of these two mechanisms of relaxation of isotropic fluctuations; moreover, it confirms the assignment of the slow mode detected by PCS to a self-diffusion, in both solvents (see also Fig. 8.14b). The question is whether we detect the self diffusion of single molecules or that of clusters. We believe that the slow mode seen in light scattering and the long time diffusion measured by PFG-NMR originate from the self-diffusion of small clusters in the solution of the single polymer chains. In addition PFG-NMR also measures the self-diffusion of single molecules, which is represented by the initial decay or first cummulant diffusion coefficient and as expected is faster than the self-diffusion of clusters but decreases with a similar trend. The reason for detecting with PCS the motion of individual clusters and thus we measure their self-diffusion is due to a refractive index difference that they have relative to the average refractive index of the solution. This can be the result of the higher local concentration of polymers inside a cluster. This justifies the contrast needed to have scattering of light due to spatial composition fluctuations, which relax

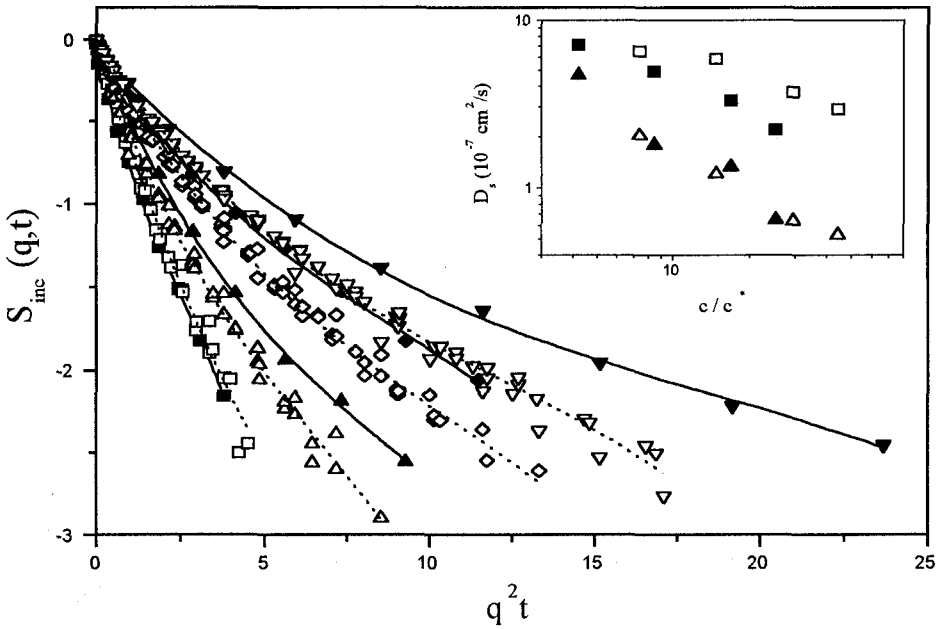

Figure 8.13: Pulse field gradient NMR measurements on various PPP-3 solutions in two solvents, showing the measured decay functions of the incoherent structure factor, $S_{inc}(q,t)$: Open sympols represent measurements in chloroform at concentrations (7.5, 15, 30 and 45 mgr/cm^3 respectively) ; solid sympols correspond to mesurements in toluene ($c = 4.34$, 8.67, 17.3 and 26 mgr/cm^3 respectively). Solid and dashed lines represent cumulant fits (see text). Inset: Concentration dependence of the corresponding diffusion coefficients: short-time: □ and ■; long-time: △ and ▲.

through the self-diffusion of the clusters. It is clear, however, from the dynamics and the q-dependence of the intensity, that we do not have large clusters in the solution, even in toluene, such as the ones investigated in chapter 7. Also we must mention that the system is in equilibrium during the time of the measurements and that both the dynamic and static results were in all cases reproducible. From another point of view the situation resembles the interdiffusion in a ternary mixture of two homopolymers and a solvent were the refractive index difference between the two species results in the observation of the diffusion of one species relative to the other [33, 34].

The intensity of the slow mode in chloroform is shown in Fig. 8.10; it increases with concentration as $c^{1.5}$. In toluene the total scattering intensity which increases almost linearly with concentration is probably a result of two opposing factors, the increase of the slow mode intensity and the decrease of that of the cooperative; this is also the case for the total intensity in solutions of chloroform.

In both solvents, the diffusion coefficient of the slow mode decreases as c^{-1}, within experimental error. The slowing down of the dynamics is not accompanied with an increase of the correlation length, which as was mentioned, is found to be nearly constant with concentration. These findings suggest that the origin of this mode is molecular associates which do not increase in size. Further, in chloroform the scatterers do not become larger but rather they increase in number. We believe that, although we cannot separate the scattering intensity of cluster mode in toluene, this should have similar behavior with the one in chloroform i.e., faster than linear increase, which is due to the increasing number of clusters formed while their size is almost constant. Another interesting feature can be seen by comparing the osmotic modulus, calculated from the total scattering intensities in the two solvents. The osmotic modulus in chloroform is almost three times higher than that in toluene solutions and thus the scattering power is higher in toluene than in chloroform. This, in connection with the similar correlation lengths found in the two solvents, suggests that the clusters which are the main contribution in the scattering intensity, at the higher concentrations, are about three times more in toluene than in chloroform.

The self-diffusion of the single molecules is represented by the initial decay of the incoherent structure factor measured in PFG-NMR. This is decreasing with concentration as $c^{-0.5}$ in both solvents, within experimental error. The concentration dependence of the self-diffusion of the polymer chains is smaller than the predictions of all theoretical treatments that predict decrease of the chain mobility with concentration; both the scaling ideas by Tinland, Maret, and Rinaudo [35] and the Green function approach by Edward and Evans [36] or Sato and Teramoto [37] predict much sharper decrease of the self-diffusion in the semidilute region.

The self-diffusion measured by NMR can also be used together with the cooperative diffusion of the single polymer chains measured by light scattering to find the osmotic modulus since $D_c/D_s = (\partial\pi/\partial c)f_s/f_c$ where f_s and f_c are the self and mutual friction coefficient respectively. The self-friction is related to the motion of a single particle while the mutual-friction represents the resistance of the solution to a concentration gradient imposed by thermal fluctuations.. In the inset of figure 8.12b the ratio of the cooperative to the self diffusion coefficients is shown for PPP-3 sample. Comparing D_c/D_s with $(M_w/N_A)(\partial\pi/\partial c)$ shown in figure 8.12a we see that the osmotic modulus determined directly form the scattered intensity of the cooperative mode increases faster with concentration, than the ratio D_c/D_s. This means that $f_s/f_c < 1$; the mutual friction coefficient is larger than the self friction. This behavior can be related to negative velocity cross-correlation of polymer chains in a semidilute solution which can be visualized as movement of the polymer chains away from each other in an effort to relax concentration fluctuations. This has been found also for PBLG solutions for a similar concentration regime whereas for higher concentrations an opposite relations was found [35].

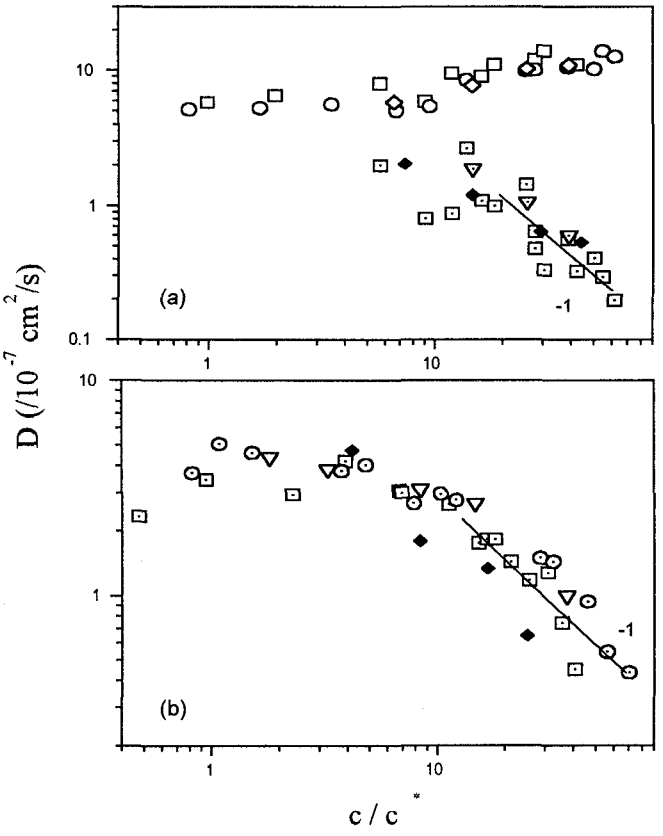

Figure 8.14: Concentration dependence (c/c^*) of the diffusion coefficients for all samples in chloroform (a), and toluene (b). PPP-2: □ cooperative mode ; ⊡ slow mode (both solvents); PPP-3: ◇ cooperative ; ▽ slow mode (both solvents); PPP-5: ◯ cooperative mode ; ⊙ slow mode (both solvents). The long time self diffusion coefficient for PPP-3 solutions in both solvents (♦) is also shown for comparison.

8.4.3 Rotational Diffusion

As mentioned previously, orientational dynamics are observed mainly in toluene solutions, while for similar concentrations in chloroform solutions the relaxation times of the orientation fluctuations are too fast to be detected in the PCS time window. The VV measurements in toluene in dilute and semi-dilute solutions revealed one main diffusion process, associated with the self-diffusion of the clusters, as already mentioned above (Figs. 8.9a and 8.11). In concentrations above $\phi = 25\ mg/cm^3$, well into the semi-dilute regime, a faster relaxation process is also detected (Fig. 8.11); it can be better resolved at low scattering angles due to its q-independent decay rate, in contrast to the diffusive main mode. Fig. 8.15 demonstrates the existence of this fast process unambiguously, for PPP-5 at a

concentration of $\phi = 36.9\ mg/cm^3$ ($c/c^* = 46.3$) and $q = 0.009nm^{-1}$. This non-diffusive mode is attributed to the rotational dynamics of the scatterers (trimers), through the contribution of the depolarized intensity (I_{VH}), to the polarized intensity (I_{VV}); for scatterers in an orientationally isotropic environment and in the single scattering limit, the polarized scattered intensity is given by (eq. 3.22) [38]:

$$I_{VV}(q) = I_{iso}(q) + 4/3I_{VH}(q) \tag{8.7}$$

where the subscript *iso* refers to the isotropic part of the intensity originating from isotropic concentration fluctuations. The corresponding VH correlation function is also depicted in Fig. 8.15, along with the distributions of relaxation times and the intensities of the two VV modes, as well as the $4/3I_{VH}$ (inset of Fig. 8.15). From both intensity and dynamics, it is evident that the fast mode detected in toluene solutions in the VV correlation function originates from the orientational fluctuations of the system. This information, which is necessary for avoiding misinterpretation, could be obtained only through the ability to measure VH dynamics, and the combination of VV and VH measurements.

It is noted that the VH dynamics were detected only in toluene solutions and concentrations above about $\phi = 25\ mg/cm^3$, since at lower concentrations the molecular orientation time appeared to be faster than $10^{-7}s$. However, at higher concentrations, it is possible to measure the dynamics of orientation fluctuations. A typical example is shown in Fig. 8.16a (PPP-5, $c/c^* = 70$). A ILT analysis reveals two relaxation modes (inset of Fig. 8.16a); the q-dependence of the fast process cannot be truly assessed, since its dynamics fall into the short time limit of the correlator's window. The VH correlation function appears to be much broader ($\beta_{KWW} \approx 0.4$) than the VV one. The large polydispersity of the samples can only partly explain a broader distribution of the orientation relaxation spectrum compared to the isotropic one, due to the corresponding stronger L-dependence of D_R (see chapter 4 and Appendix B).

The main mode becomes slower with increasing q, as is also evident from the correlation functions of Fig. 8.16a, which at larger q's relax within the time range of PCS. This unusual behavior has neither been theoretically predicted nor unambiguously observed experimentally; a seemingly similar observation has been briefly reported for PBLG solutions [21]. It is not trivial to rationalize physically speeding-up of rotational diffusion at large length scales. The actual negative q^2-dependence of the slow reorientational rate is depicted in Fig. 8.16b, at different concentrations in the semidilute regime. The larger the concentration, the more pronounced this slowing down of the dynamics at large q's is, while the total depolarized intensity is q-independent for all concentrations. However, the VH intensity associated with the slow mode, exhibits a small increase with q at the highest c; extending the measurements to even higher c's is precluded due to limited solubility. An increase of the VH intensity with q might imply

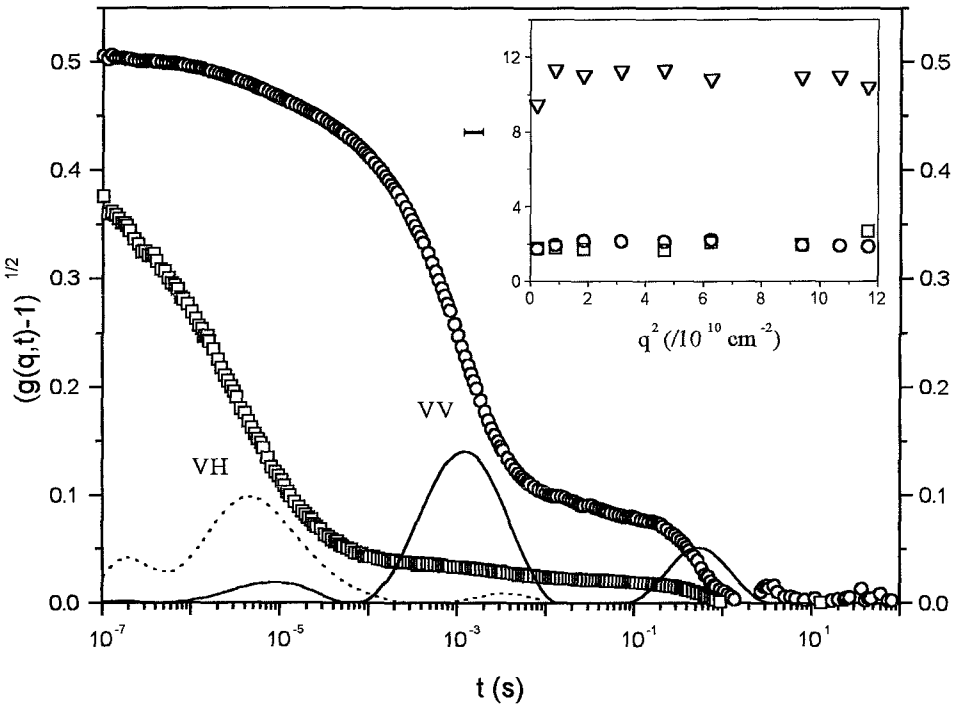

Figure 8.15: (a) Net normalized scattered VV (○) and VH (□) field autocorrelation functions for a 36.9 mgr/cm^3 solution of PPP-5 in toluene, along with the corresponding distributions of relaxation times. The correspondence of fast VV (solid line) and VH (dotted line) modes is demonstrated. Inset: q^2-dependence of the respective scattered intensities: slow VV mode (○); fast VV mode (▽); 4/3 of VH mode, as described in text (■)

some local ordering of parts of these semistiff polymers, which can slow down the orientational dynamics. Such a peak of the VH intensity at finite q, was found to relate with correlated anisotropic scattering disclination lines in nematic liquid crystalline polymers [39, 40].

Fig. 8.17 depicts the concentration dependence of the depolarized correlation functions for various PPP-5 solutions at $\theta = 150^\circ$ ($qL \approx 2.5$). The total scattered VH intensity, in both solvents, is shown as a function of the reduced c in the upper inset of Fig. 8.17, whereas the lower inset depicts the weak reduction of the relaxation rate ($\Gamma_{VH} = 6D_R$) with concentration (in the limit $q \to 0$). The total VH scattering intensity, in the thermodynamic limit ($q = 0$) and in both solvents, increases linearly with c, assuming also the same values. This finding suggests negligible pair orientation correlations, as the depolarized intensity is proportional to the number density and the intrinsic molecular anisotropy, ex-

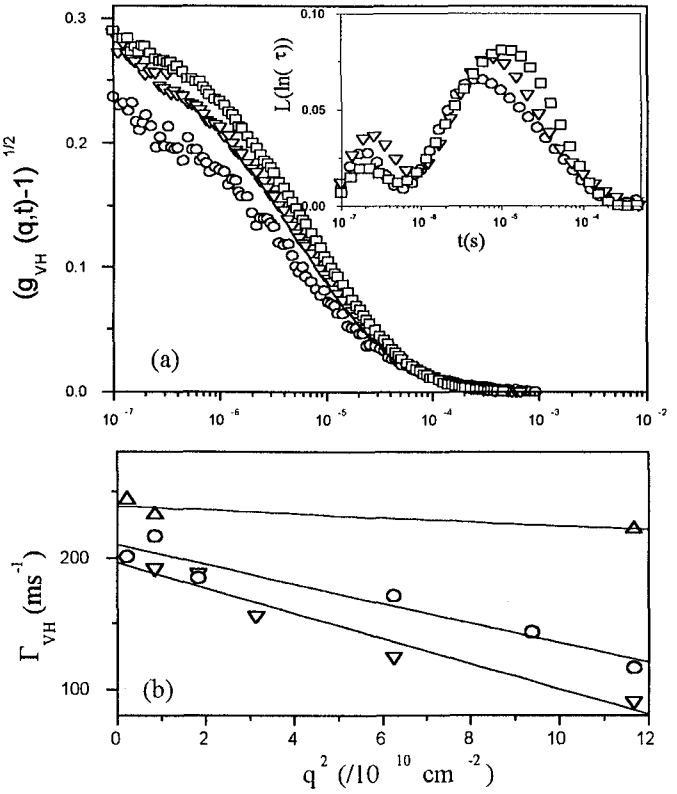

Figure 8.16: (a) Orientation time correlation functions for a semi-dilute solution of PPP-5 in toluene ($c/c^* = 70$), for different scattering angles ($\theta = 30^o$: ◯ ; $\theta = 90^o$:▽ ; $\theta = 150^o$: □) . Inset: Corresponding relaxation spectra $L(\ln \tau)$. (b) Reduction of the rotational relaxation rates, Γ_{VH} , with q at different concentrations of PPP-5 in toluene ($c/c^* = 29$:△ ; 46 ◯ ; 70: ▽); solid lines represents best linear fits.

cluding the possibility of excess VH scattering from cluster anisotropy; in the latter case, I_{VH} should be different in the two solvents. Further, the ratio translational diffusion (which is identified with the self-diffusion of the clusters) and slow rotational diffusion, D_s/D_R , decreases with concentration, as can be seen in from fig. 8.14 and 8.17 (their c dependence are clearly different) suggesting that in toluene we do not observe the translation and the rotations of the same scatterer. In such a case this ratio would riter stay constant and approximately equal to the square of the fydrodynamic radius of the cluster, R_H^2 (if the diffusion constant of a sphere is used), or incresing if equations for the c dependence of D_s and D_R of wormlike (or fuzzy) cylinders (such as 4.21 and 4.28) are used to describe the diffusion of the cluster. Thus, although the slow mode in VV originates from the translational diffusion of the clusters which relax composition

fluctuations, the reorientational dynamics are controlled both inside and outside of the clusters by the rotation or the change of shape of each polymer chain, which causes polarizability anisotropy fluctuations.

The significantly different orientational dynamics of PPP's in the two solvents needs justification. In toluene scattering from regions of some orientational ordering of the polymer chains dominates, leading to a slowing down of the rotational dynamics, with the peculiar q-dependence of the slow decay rate. In this picture, the fast VH mode can be attributed to the average reorientation of the polymer chains; these chains reorient as they would in a semidilute completely isotropic solution of semistiff chains. In chloroform solutions we mainly see this rotational relaxation since the number of areas with local orientation are not enough to affect the VH dynamics.

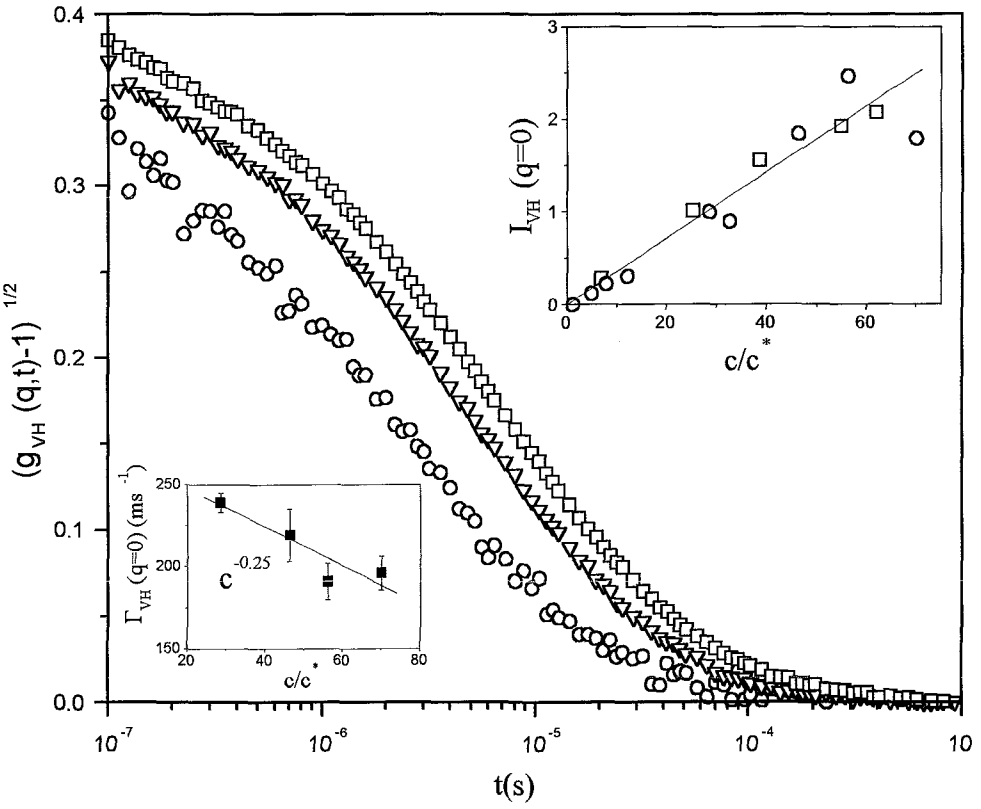

Figure 8.17: Orientation time correlation function for PPP-5 solutions in toluene at $q = 0.034nm^{-1}$ ($c/c^* = 26$: ○ ; 46: ▽ ; 56: □). Upper inset: Concentration dependence (c/c^*) of the total VH intensity from solutions of PPP-5 in toluene (○) and chloroform (□). Solid line denotes a linear fit. Lower inset: Concentration dependence of the rotational relaxation rate, Γ_{VH} , at $q \rightarrow 0$ for PPP-5 solutions in toluene (■).

The rotational diffusion at $q = 0$ decreases as $c^{-0.25}$ over the rather narrow concentration range of our measurements (lower inset of Fig. 8.17). We should mention that even for rod-like particles the rate is not expected to follow the c^{-2} behavior of the Doi-Edwards model in the whole semidilute and concentrated regime; but rather a weaker c-dependence (c^{-1}) at low concentrations and only for highly entangled solutions the DE behavior is reached. [41, 15, 9]. In the next sections, where we study the orientation fluctuations of PPP/S solutions in a much broader concetration regime with minimal aggregation, we observe the same behavior of the VH correlation function more pronounced. As discussed there, it does not relate with the existence of clusters.

8.4.4 Summary of PPP-12

The dynamics of concentration and orientation fluctuations of model hairy-rod poly(p-phenylenes) was probed with photon correlation spectroscopy, both in the polarized (VV) and depolarized (VH) geometries, in the semidilute regime. In VV, in addition to the cooperative diffusion, we detected the self-diffusion of small stable aggregates ($D_{slow} \sim c^{-1}$) (the trimers which are discussed in chapter 7), as confirmed by independent pulse field gradient-NMR measurements. Thus, the Doi-Shimada-Okano description of the relaxation of concentration fluctuations was not confirmed. The dynamics helped significantly in obtaining the correct static information by isolating individual contributions to relaxation of concentration fluctuations. Up to $c/c^* \simeq 70$, which was the highest concentration reached before dissolution took place, the cooperative diffusion depended on $c^{0.9}$, a behavior intermediate to the flexible and rodlike predictions. Similarily, the osmotic modulus revealed a $c^{1.2}$ increase in the semidilute region, which is closer to the flexible chain behavior. The molecular self-diffusion coefficient scaled with $c^{-0.5}$, in qualitative agreement with the perturbation approaches in the early semidilute regime. Reorientational (VH) correlation functions were obtained at high concentrations in toluene, and were dominated by a broad process exhibiting a slowing down at high q's and concentrations ($c^{-0.25}$). It was assigned to the molecular reorientation in the presence of some orientational correlations in space, due to local order of parts of the chains. These results reveal the need for more depolarized measurements in a wider concentration range.

8.5 Dynamics of concentration fluctuations in PPP/S solutions

The sulfonated poly-(p-phenylenes) (PPP/S) (Table 8.3) were the most soluble molecules from all three PPP series used, allowing the investigation of both orientation and concentration fluctuations by DLS at very high concentrations (up to 66% by weight). This was also achieved due to the absence of a transition to a nematic phase. The latter, although desirable for investigating the dynamic and static pretransitional effects, inhibits the study of highly concentrated isotropic solutions of stiff polymers; moreover since solutions in the a liquid crystalline phase become opaque, studies in the single scattering limit are not possible.

Sample	c^* (%wt.)	c^{**} (%wt.)	c/c^*	c/c^{**}
PPP/S-1	0.047	2.05	4.9-1400	0.11-32
PPP/S-3	0.084	2.47	3.45-226	0.12-7.69
PPP/S-7	0.276	4.02	3.7-107	0.26-7.3
PPP/S-9	0.431	4.93	0.1-90	0.01-7.82
PPP/S-10	1.45	8.74	0.65-26	0.11-4.31

Table 8.4: Characteristic concentrations of PPP/S samples

In the study of PPP/S solutions besides, the VV and VH dynamic light scattering measurements, we also carried out NMR experiments on S-3 in order to measure the self diffusion as well as shear rheology experiments on S-1 and S-7 samples, in order to measure both the viscosity and the dynamic storage (G') and loss (G'') moduli of the solutions.

The dynamics in the dilute region and early semidilute regime can be used to characterize the samples by utilizing the relations of Appendix B to calculate the contour length of the polymer chain from the measured translational diffusion coefficients. The overlap concentration, c^*, and the onset of excluded volume effects, c^{**}, are calculated using the characteristic length L_e, and are shown in Table 8.4 along with the concentration regime studied.

Five different molecular weights (S-1, S-3, S-7, S-9, S-10) were investigated in toluene solutions, while S-3 was also studied in solutions of chloroform and trichloroethylene (TCE). Solutions of S-1 and S-9 were concentrated up to 66% and 40%, respectively, without any sign of phase separation whatsoever. On the other hand, both chloroform and TCE solutions of S-3 become opaque above about 20%, whereas toluene solutions of S-7 and S-10 become opaque above 25% and 40% respectively. This is a sign of phase separation similar to the one observed in solutions of P-12 and PPP-12 in much smaller concentrations. This phase separation seems to lead to two isotropic phases, as in the case of the flexible polymer solutions (or other two component systems), rather than to nematic-isotropic coexisting phases, which are characteristic of rodlike systems. This was concluded by the absence of a pretransitional increase of the depolarized intensity,

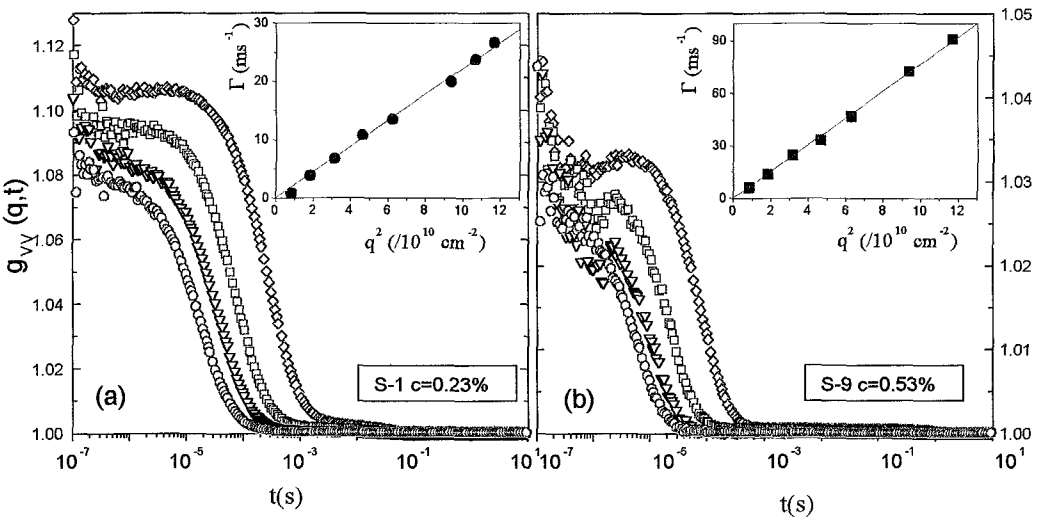

Figure 8.18: Normalized intensity correlation functions $g_{VV}(q,t)$in dilute toluene solutions and the corresponding decay rates (insets) at several scattering angles: (○): 150°, (▽): 90°, (□): 60°, (◇): 30°, for S-1 at c=0.23% (a) and S-9 at c=0.23% (b).

as well as by observing virtually no birefringence of the sample between cross polarizers. The lack of a transition to a nematic phase in these highly anisotropic, stiff polymers was not known. A possible reason might be a steric effect of the topologically irregular side chains, which may not allow proper packing so that the backbones of the chains form a nematic phase. This unexpected finding, although originally disappointing proved to be very fortuitous concerning the investigation of the dynamics of highly concentrated isotropic solutions of stiff chains.

In fig. 8.18 we show the normalized intensity correlation functions $g_{VV}(q,t)$ as measured in a PCS experiment in the VV geometry for two dilute solutions of S-1 (a) and S-9 (b) at four different scattering angles. In this concentration region only one relaxation process is detected and represents the translational diffusion of the polymer chains (or their cooperative diffusion at concentrations above c^*). Their diffusive character is evident from the q^2-dependence of the relaxation rate Γ, shown in the insets of fig. 8.18.

At low concentrations ($c/c^* \lesssim 10$), concentration fluctuations are found to relax only through one process which corresponds to the cooperative diffusion of the molecules (fig. 8.18 and 8.29). The cooperative mode becomes faster as the concentration is increased, due to excluded volume and thermodynamic interactions, while at the limit of zero concentration it represents the translational diffusion of single molecules. As concentration increases we observe additional relaxation modes (figs. 8.19,8.20,8.29 and 8.28) for all molecular weights investigated.

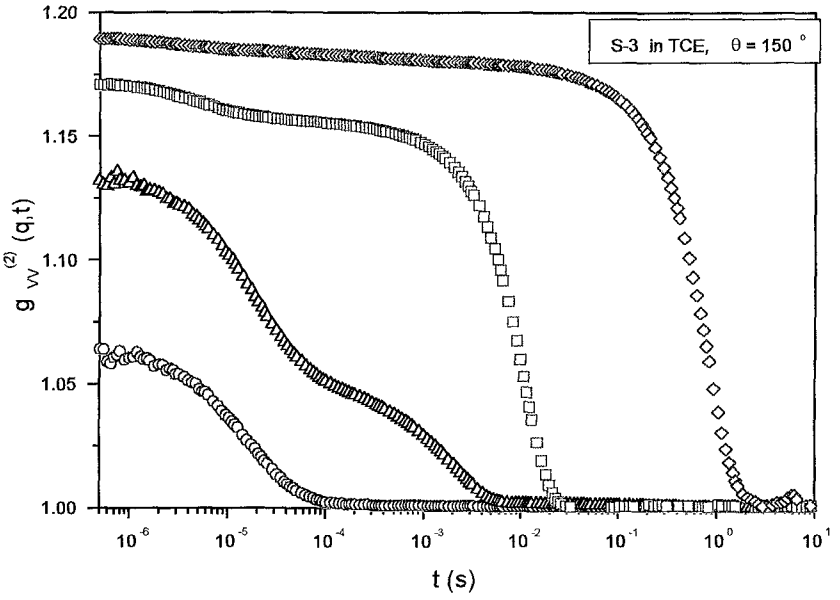

Figure 8.19: Normalized intenstity correlation functions for four solutions of S-3 in TCE: (○): 0.087%, (△): 1.42%, (□): 5%, (◇): 12%.

In fig. 8.19 the polarized intensity correlation function for S-3 solutions in TCE reveal a slower than the cooperative diffusion mode, which gains amplitude and becomes slower with increasing concentration. This mode, although possessing the same concentration behavior, is less pronounced in chloroform (fig. 8.20) and even less in toluene (fig. 8.21) solutions. In chloroform and toluene solutions the fact that the slow mode, which is attributed to clusters, has smaller amplitude and slows down significantly allows the observation of both the cooperative diffusion and also of an additional intermediate process as seen in fig. 8.20 and 8.21. In these figures the intensity, $g_{VV}(q,t)$, or the field, $C_{VV}(q,t)$, correlation functions are depicted for the S-3 solutions in chloroform and S-7 solutions in toluene, respectively; in the latter case, the modes can be better seen. In fig. 8.20b, the distribution of relaxation times $L(ln\tau)$ multiplied by the normalized scattered intensity, I/I_{tol}, is depicted. At least one intermediate mode, between the cooperative and the slow one, is found, which is of diffusive character. In fig. 8.21, the same modes are also seen for S-7 solutions; the slow mode is clearly smaller in amplitude whereas the diffusive character of all three decay rates is shown in the inset of fig. 8.21a while the virtually q-independent intensities are shown in the inset of fig. 8.21b.

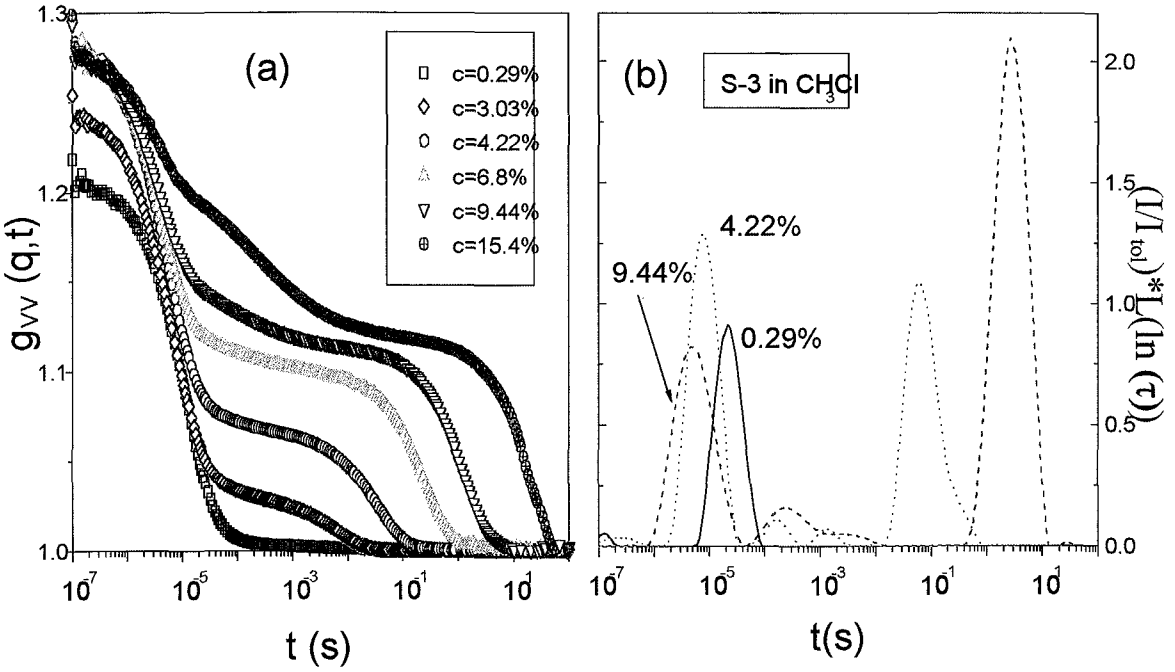

Figure 8.20: (a) Normalized intensity correlation function for several concentrations of S-3 solutions in chloroform at 150°. (b) Distributions of relaxation times $L(ln\tau)$ from the inverse Laplace transform of three concentrations multiplied by the normalized intensities I/I_{tol}.

8.5.1 Cooperative diffusion

Dynamics

The cooperative diffusion is the main mechanism for the relaxation of concentration fluctuations; in the dilute region where individual molecular motions can be observed it is reduced to the translational diffusion of a single molecule. As discussed before, there are two opposing factors in collective diffusion,

$$D_c = (\frac{M}{N_A})(1-\phi)^2(\partial\pi/\partial c)_{T,P} \ / \ f_m \tag{8.8}$$

namely the osmotic modulus, which in good solvent conditions speeds up the diffusion and the hydrodynamic friction, which slows it down. In the limit of zero concentration $(\partial\pi/\partial c)_{T,P} = RT/M$ and thus the translational diffusion $D_s = kT / f_s$ is measured.

In fig. 8.22 we show the concentration dependence of the cooperative diffusion coefficient for PPP/S at different molecular weights. The concentration is normalized with the overlap concentration c^* calculated using L_e (table 8.3) to

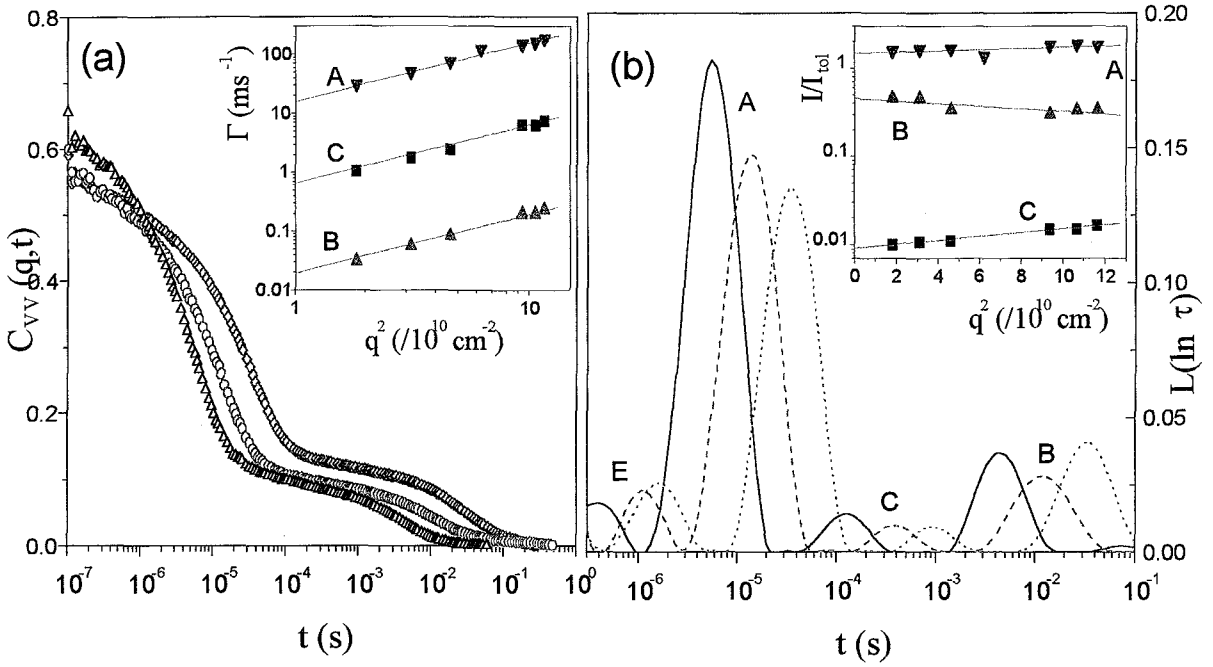

Figure 8.21: (a) Polarized intensity correlation functions for a 7.83% S-7 solution in toluene at three scattering angles: (△) 150°, (○) 75°, (◇) 45°. Inset: Decay rate of the three relaxation modes (A,B,C) (b) Distribution of relaxation times for the three angles: solid line (150°), dashed line (75°) dotted line (45°). Inset: q-dependence of the intensities of the modes.

reveal the degree of enmeshment of the different molecular weight samples. In this figure the molecular weight dependence of the cooperative diffusion is evident in both the dilute regime and in high concentrations. In both the semidilute and concentrated regime, it is in contrast to what is expected from the flexible polymer chains were the cooperative diffusion, corresponding to the diffusion of the blobs, is molecular weight independent. We note that in the PPP-12 case the cooperative diffusion was apparently not depending on the molecular weight but that was due to the high polydispersity and the proximity of the molecular weights. This molecular weight dependence can be attributed to the highly correlated motion of a large part of a wormlike chain (of the order of $2l$); in the limit of rodlike chains the whole molecule moves in phase, and thus even above the overlap concentration, we can see a molecular weight dependence in contrast to the flexible chains were we see the diffusion of the blobs. To avoid any misunderstanding we should note that still the relaxation of concentration fluctuations in nondilute solutions of rodlike particles are of collective nature and involve the cooperative motion of a collection of molecules. This is why the cooperative dif-

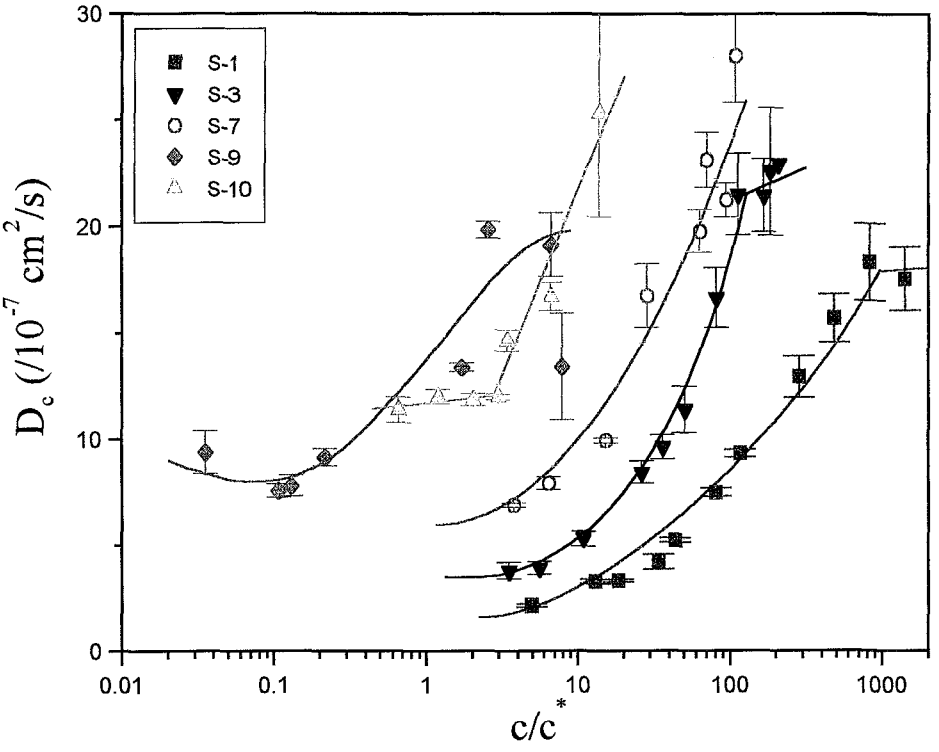

Figure 8.22: Concentration dependence of the cooperative diffusion coefficient of the PPP/S samples in toluene. The lines are drawn to guide the eye.

fusion of all polymers, including rods, speed-up in good solvents under the effect of the thermodynamics.

Another observation is that at high concentration the cooperative diffusion tends to a plateau region or even decreases weakly, as observed in the smaller molecular weight S-9 (fig. 8.22). This should imply the increase of the frictional effect or even its complete domination over the thermodynamic (osmotic pressure) tendency to speed up the relaxation of concentration fluctuations. Nevertheless, this change is molecular weight dependent since it does not appear at the same c/c^* for all samples. It is seems that in smaller molecular weights (with exception of S-10 which exhibits aggregation from low concentrations) the friction in the cooperative diffusion overcomes the osmotic pressure effect in smaller concentrations.

In fig. 8.23 the concentration dependence of D_c is shown at the lower concentrations; extrapolation in this region to zero concentration yields the translational diffusion, D_0, of the molecule. These values are shown in table 8.5

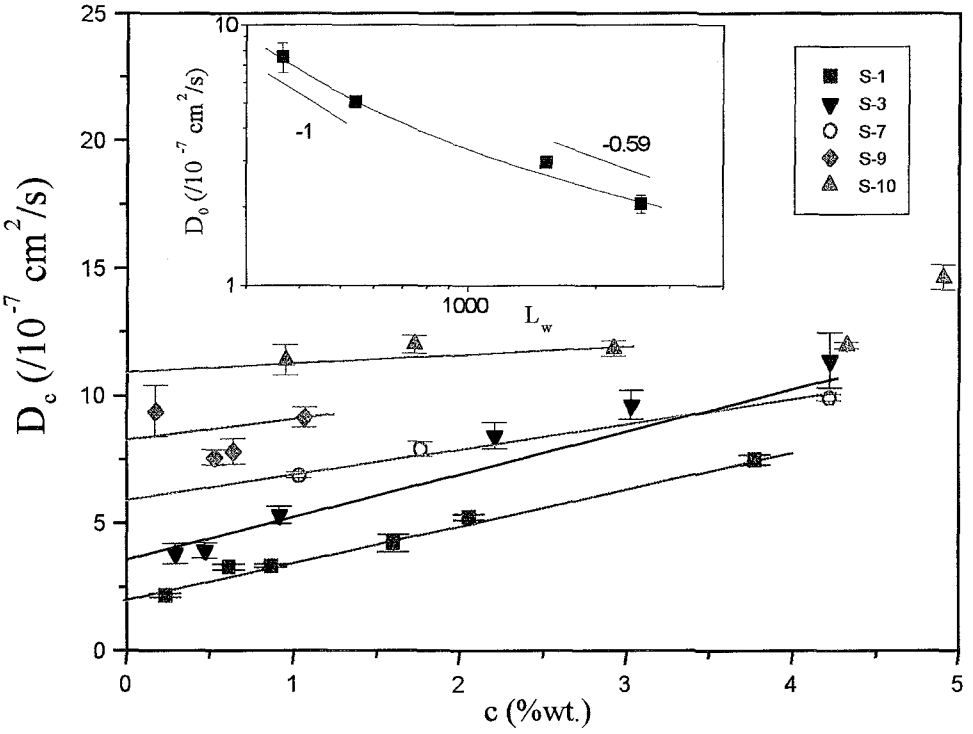

Figure 8.23: Diffusion coefficients in the dilute and early semidilute regimes for PPP/S samples in toluene. Lines are fits to get D_0. Inset: The molecular weigth dependence of the zero concentration diffusion coefficient D_0.

Sample	$D_0(/10^{-7}\ cm^2/s)$	$L_w(nm)$	L_w(from M_w)	$D_{R,0}(s^{-1})$
PPP/S-1	2.06±0.16	245±15	256	36600
PPP/S-3	3.02±0.15	144.4±10	152.7	120551
PPP/S-7	5.06±0.08	67.6±2	54.1	580000
PPP/S-9	7.53±1	38.1±	36.5	1100000
PPP/S-10	11.68±0.3	14.1±1	15.7	6500000

Table 8.5: D_0 and calculated values of L_w. Also L_w from M_w is given for comparison, and estimated $D_{R,0}$.

With these values of D_0 we can calculate the contour length L_w using the proper formulas for the translational diffusion of wormlike chains or rodlike chains given in Appendix B. For the two larger molecular weights S-1 and S-3 the relation of Yamakawa and Fujii [42] for $L > 4.556l$ was used (eq. B.12) while for the smaller molecular weights the relation for stiff chains with $L < 4.556l$ (eq. B.11) or the rodlike expression of Broesma [43, 44, 45] (eq. B.3) give similar lengths. For all PPP/S samples, a diameter $b = 1.7$ nm and a persistence length $l = 25$ nm is used. We see (Table 8.5) that the values of L_w from the translational

diffusion data are in very good agreement with the values corresponding to the known molecular weights M_w. This confirms both the validity of these expressions for these semiflexible polymer molecules as well as the absence of aggregation in the dilute toluene solution and chloroform solutions. The latter finding is not valid for the smallest molecular weight S-10, since in this sample there is a slower mode present even from the dilute solutions (fig. 8.34); this mode is attributed to clusters. Its behavior will be discussed below. Measurements in TCE, although not as extensive as in toluene conform with the above picture, as shown in fig. 8.24. In the insets of fig. 8.23 and 8.24 the molecular weight (or contour length) dependence of the translational diffusion D_0 is shown. A fit of all data points with a straight line yields a dependence $L^{-\nu}$ with $\nu \simeq 0.65$, clearly higher than the $\nu \simeq 0.5 - 0.59$ prediction for the flexible chains. In the limit of rigid rods $D_0 \propto L^{-1}\ln(L/2b)$. A closer look of the data shows that the two smaller molecular weights in both TCE and toluene have a sharper L-dependence than the larger molecules conforming with the idea of a gradual transition from an $L^{-1}\ln(L/2b)$ to an $L^{-0.5}$ dependence, as the shape changes from a rodlike to a coil with increasing L.

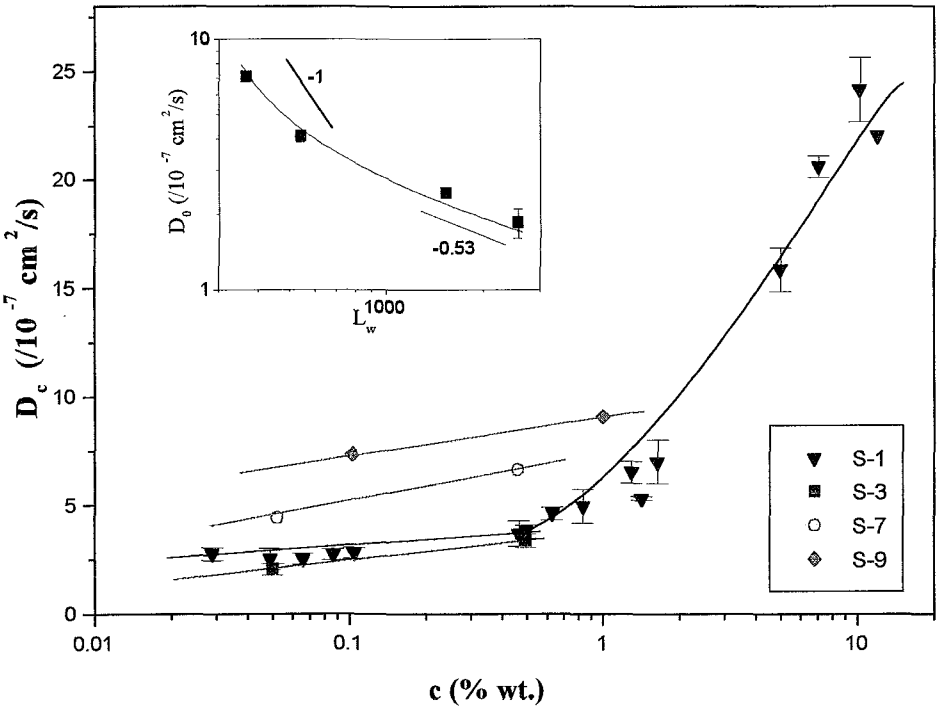

Figure 8.24: Diffusion coefficients in the dilute and early semidiute regime for PPP/S samples in TCE. Inset: The molecular weigth dependence of the zero concentration diffusion coefficient D_0.

A log-log plot of D_c with c would reveal the scaling behavior of the cooperative diffusion coefficient with concentration but it may be applied only in nondilute concentrations otherwise an unphysical zero D_c at $c = 0$ would be implied. A better description of D_c is by determining the scaling behavior of $D_c/D_0 - 1$, as we did for the PPP-12 samples. In this case the general relation,

$$D_c = D_0(1 + \kappa c^v) \tag{8.9}$$

is assumed to describe the behavior of D_c and to account for both the thermodynamic and the frictional effects on eq. 8.8. In this respect eq. 8.9 is a phenomenological description of the data which might be supported by some theoretical approaches like the mean-field approach of DSO theory (eq. 4.39) which we also discussed with the PPP-12 data. This theory however, which describes rodlike chains, does not take into account the slowing down of the parallel diffusion of the rods and assumes that the cooperative friction coefficient f_c follows the behavior of the self-diffusion friction in the oversimplified form ($D_s = \frac{1}{2}D_0$) of the DE theory.. A more realistic approach would be to incorporate in the relation for D_c the fuzzy cylinder model predictions for the self-diffusion D_S (eq. 4.21, 4.27) for semistiff chains, with a prediction for the osmotic modulus (for example from the DSO-Onsager approach or from the scaling particle theory (SPT) for wormlike hard spherocylinders [46]). Combining eq. 4.21 and 4.30 gives:

$$D_c = \frac{1}{2}D_0[(1 - aL^2b\rho)^2 + (1 + \varepsilon L^3\rho)^{-2}](1 - \phi)^2(1 + \frac{\pi}{2}bL^2\rho) \tag{8.10}$$

where the decrease of D_c due to friction is stronger than its increase due to thermodynamics. A sharper increase of the osmotic modulus is predicted by the SPT theory, which may allow the increase of the cooperative diffusion coefficient if a concentration dependent parallel self diffusion is allowed. Combining SPT predictions [46] with 4.21 we get:

$$D_c = \frac{1}{2}D_0[(1 - aL^2b\rho)^2 + (1 + \varepsilon L^3\rho)^{-2}](1 - \phi)^2[1 + \frac{B\rho}{1 - v\rho} + \frac{2C\rho^2}{(1 - v\rho)^2}] \tag{8.11}$$

with B, C functions of the geometrical characteristics of the spherocylinder and the their orientational distribution and v its molecular volume [46].

Fig. 8.25 depicts a log-log plot of $D_c/D_0 - 1$ vs c/c^* (similar to fig. 8.12b for PPP-12). For concentrations between 5 and $300c^*$ we find that a scaling exponent between 0.9 and 0.7. The larger molecular weights exhibit the higher exponents: for S-1 in toluene we get $v = 0.9$ while for S-3 in TCE and chloroform we get $v = 0.92$. At the same time S-7 and S-9 in toluene give $v = 0.78$ and 0.72, respectively. This slope changes at higher concentrations reflecting the dominance of friction as discussed above. Note that for flexible chains the scaling

prediction for the concentration dependence in of the cooperative diffusion in the semidilute region is $c^{0.75}$. The fact that the flexible chain exponent is approached for the smaller molecular weight which resembles more to a rod than a coil is counterintuitive at first sight. However, we will see that this behavior is due to the different concentration dependence of the osmotic modulus $\frac{M}{N_A}(\partial\pi/\partial c)_{T,P}$.

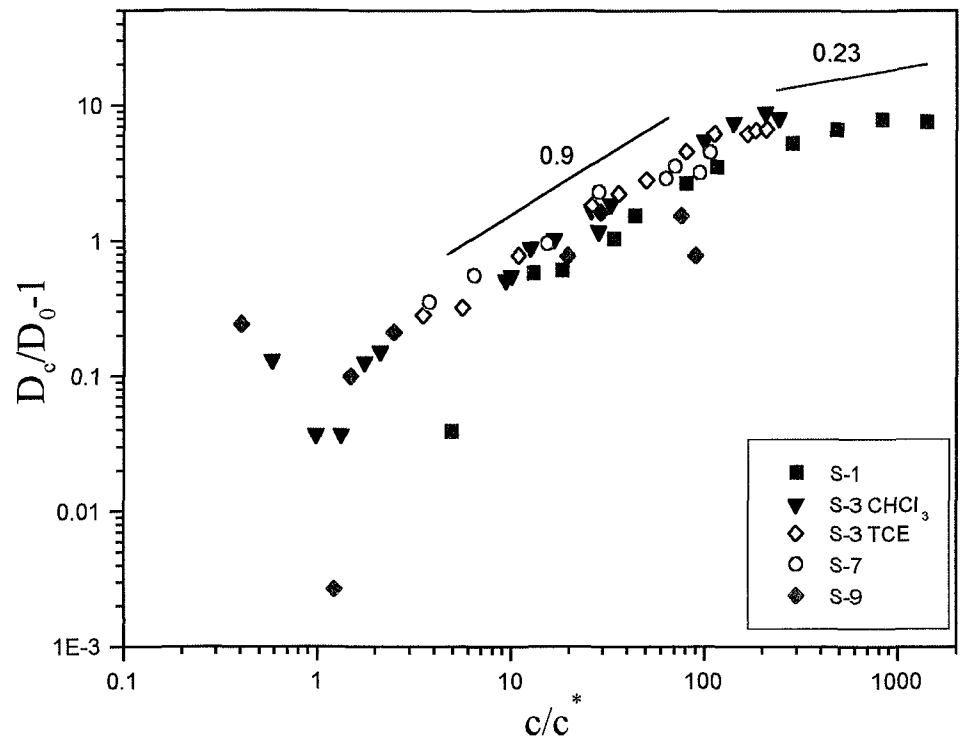

Figure 8.25: Concentration dependence of D_c/D_0-1 in a log-log plot with the reduced concentration c/c^*, for all PPP/S samples. The solid lines indicate the c-dependence in the intermediate and high concentration region of the S-1 sample.

Scattering Intensity-Osmotic Modulus

In fig. 8.26 we show the intensity of the cooperative process I_c (a) and the osmotic modulus normalized with the molecular weight (b). The latter is calculated from the intensity:

$$(\frac{M}{N_A})(\partial\pi/\partial c)_{T,P} = A\frac{c}{I_c/I_{tol}} \tag{8.12}$$

with $A = \frac{4\pi^2 kT}{N_A\lambda_0^4 R_{tol}}\rho_{tol}M_w n^2(\partial n/\partial c)^2$, according to (eq. 3.57). The cooperative intensity exhibits the expected behavior; it increases linearly with concentration

at the dilute (or low concentration) regime, whereas above the overlap concentration the rate of increase becomes smaller and at high concentrations it decreases. In general, in aggreement with the findings in the PPP-12 sample, the cooperative intensity shows a rather broad plateau or a weak decrease in the semidilute region (above the c^*) and drops at much higher concentrations, in contrast to the much faster drop that is found for flexible chains.

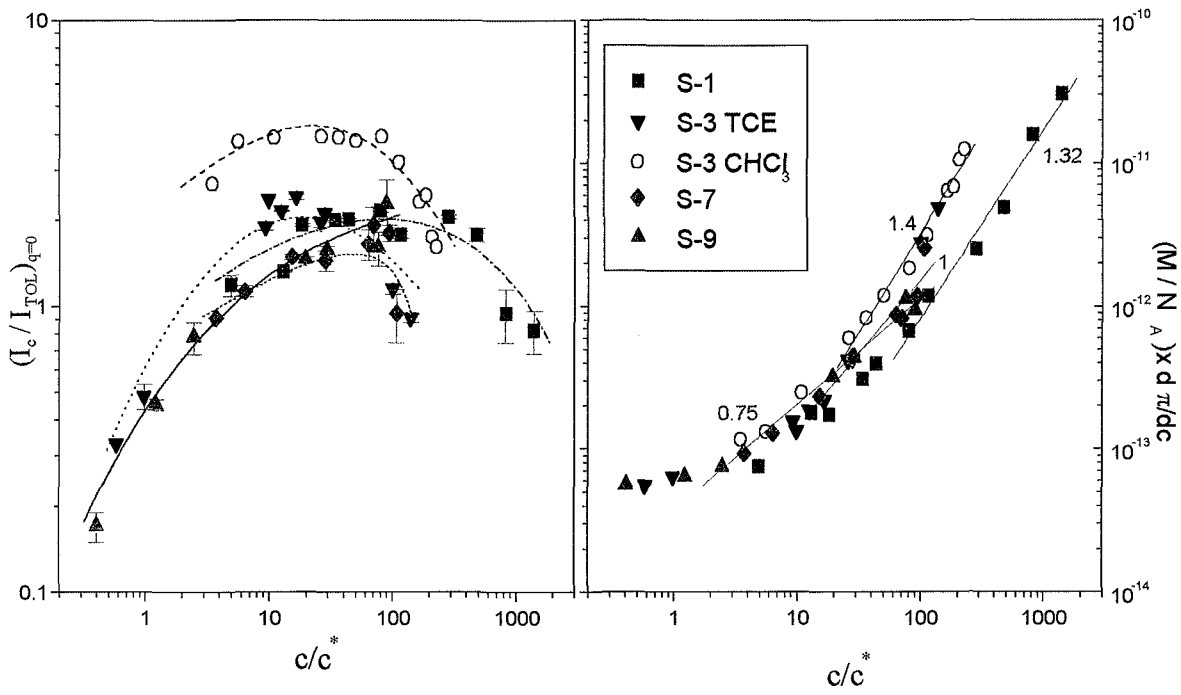

Figure 8.26: (a) Normalized to toluene intensity of the cooperative process for S-1, S-7 and S-9 in toluene and S-3 in TCE and chloroform vs c/c^*. Lines are drawn to guide the eye. (b) Corresponding concentration dependence of the osmotic modulus (normalized with the molecular weight).

The behavior of scattering intensity of the cooperative mode in semidilute and concentrated polymer solutions can be supported by the negative interference of scattered light from a system of overlapping chains or in a thermodynamic language, by the increase of the osmotic pressure as concentration increases, which tends to suppress the concentration fluctuations giving rise to light scattering. Thus, the different concentration dependence of I_c in flexible and rodlike (or wormlike) chains can be discussed in terms of concentration dependence of the osmotic modulus $(\partial\pi/\partial c)_{T,P}$. Fig. 8.26b reveals the differences between the large and small molecular weights i.e., polymer chains which look more like a coil and a rod respectively. In this log-log plot, $(\frac{M}{N_A})(\partial\pi/\partial c)_{T,P}$ is found to scale with

c with an exponent: 1.4±0.1 (S-3) , 1.32±0.1 (S-1) , 1±0.1 (S-7) and 0.75±0.1 (S-9). We note that for the PPP-12 sample we found an exponent of 1.2 at high concentrations. For flexible chains the scaling prediction for good solvents in the semidilute region is $c^{1.3}$ [16], while for rodlike polymers the DSO-Onsager theories predict a linear increase of $(\partial\pi/\partial c)_{T,P}$ with c. The weaker increase of the osmotic pressure with concentration for rodlike chains is reasonable as already discussed for PPP-12 and reflects further the weaker decrease of the scattering intensity of stiff polymers, above the overlap concentration. However, the SPT theory for wormlike spherocylinders predicts a much stronger increase in $(\partial\pi/\partial c)_{T,P}$ with c according to [46]:

$$(\partial\pi/\partial c)_{T,P} = \frac{RT}{M(1-\upsilon\rho)^2}[1 + \frac{B\rho}{1-\upsilon\rho} + \frac{2C\rho^2}{(1-\upsilon\rho)^2}] \tag{8.13}$$

which is a relation used for deriving eq. 8.11. Such a strong is concentration dependence is certainly not observed in our systems, neither in the case of PPP/S nor for PPP-12.

In conclusion, $(\partial\pi/\partial c)_{T,P}$ for the PPP/S samples at that in high concentrations scales with an exponent ($\sim$ 1.35 for S-3 and S-1) close to the one predicted for flexible coils (1.3) while for the smaller it scales with the exponent predicted for rodlike polymers by DSO (1 for S-7), or smaller (0.75 for S-9).

8.5.2 Self Diffusion-Friction coefficients

Comparing the dynamic (D_c) with the static information ($(\partial\pi/\partial c)_{T,P}$), one can deduce the cooperative friction f_s of the system which then can be compared with the self-friction f_c from the self-diffusion coefficient D_c measured by NMR. In fig. 8.27a we show the normalized with the viscosity of the solvent and the contour length cooperative friction coefficient, calculated from the intensity of the cooperative mode and D_c, according to

$$f_c = (\frac{M}{N_A})(\partial\pi/\partial c)_{T,P}(1-\phi)^2/D_c$$

This friction per unit length exhibits an increase with concentration with a scaling exponent between 0.5 and 0.3 (the smaller molecules S-7 and S-9 have the weaker increase). The friction of the larger molecular weight S-1 is seen to be smaller than that of the other samples, a finding that might be attributed to a relatively larger dynamic flexibility due to its more coiled shape. However, we should note that it might be also due to some discrepancy of the actual value of the overlapping concentration from the c^* that we calculated.

In fig. 8.27b the self friction coefficient, $f_s = kT/D_s$ for the S-3 solutions is depicted. The incoherent structure factor, $S_{inc}(q,t)$ measured by PFG-NMR was used to get D_s, both from the initial decay rate according to a cummulant fit and from the long-time decay rate, since $S_{inc}(q,t)$exhibits a broader than a

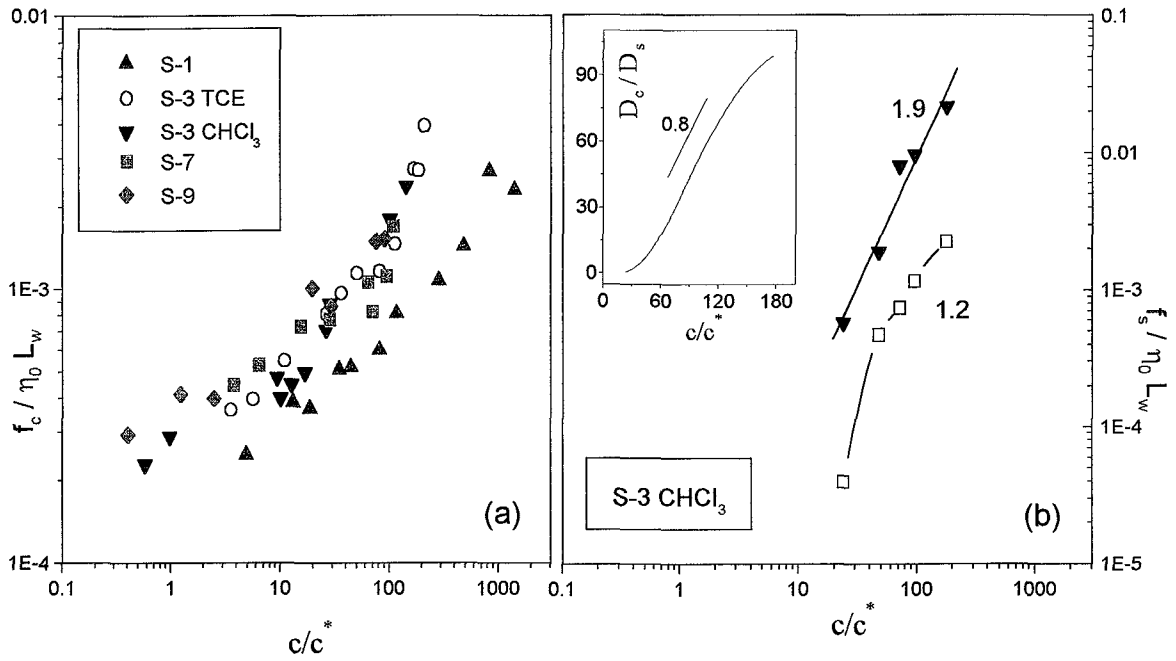

Figure 8.27: (a) Cooperative friction coefficient deduced by combining static and dynamic light scattering data, normalized with the viscosity of the solvent and the contour length of the polymer, for all PPP/S samples. (b) Self-friction coefficient for S-3 in chloroform, from the NMR measurements as deduced from the initial (□) and the long-time (▼) decay rate. Inset: Concenration dependence of the ratio of the cooperative and the self-diffusion coefficient.

single exponential decay much like in PPP-12. Both the short and the long time self-diffusion coefficients show a much stronger concentration dependence ($c^{1.2-1.9}$), compared to f_c ($c^{0.5}$), implying that these two quantities are different. Moreover, the ratio of the ratio of the corresponding diffusion coefficients, D_c/D_s, shown in the inset of fig. 8.27b exhibits a weaker concentration dependence than $(\frac{M}{N_A})(\partial\pi/\partial c)$(fig. 8.26b), in aggreement with the above. Note that the latter finding was also used for the PPP-12 data to conclude for the difference of the two frictions.

8.5.3 Intermediate mode

As we mentioned above an additional diffusive mode is found to contribute in the VV correlation function between the cooperative and the slow, in the semidilute regime. Fig. 8.28 and 8.29 depict the field correlation functions $C(q,t)$, together with the respective distributions of relaxation times $L(ln\tau)$ multiplied with the

normalized scattered intensity, I/I_{tol}, for several concentrations of S-1 and S-7 samples, at 120°and 90° scattering angle respectively.

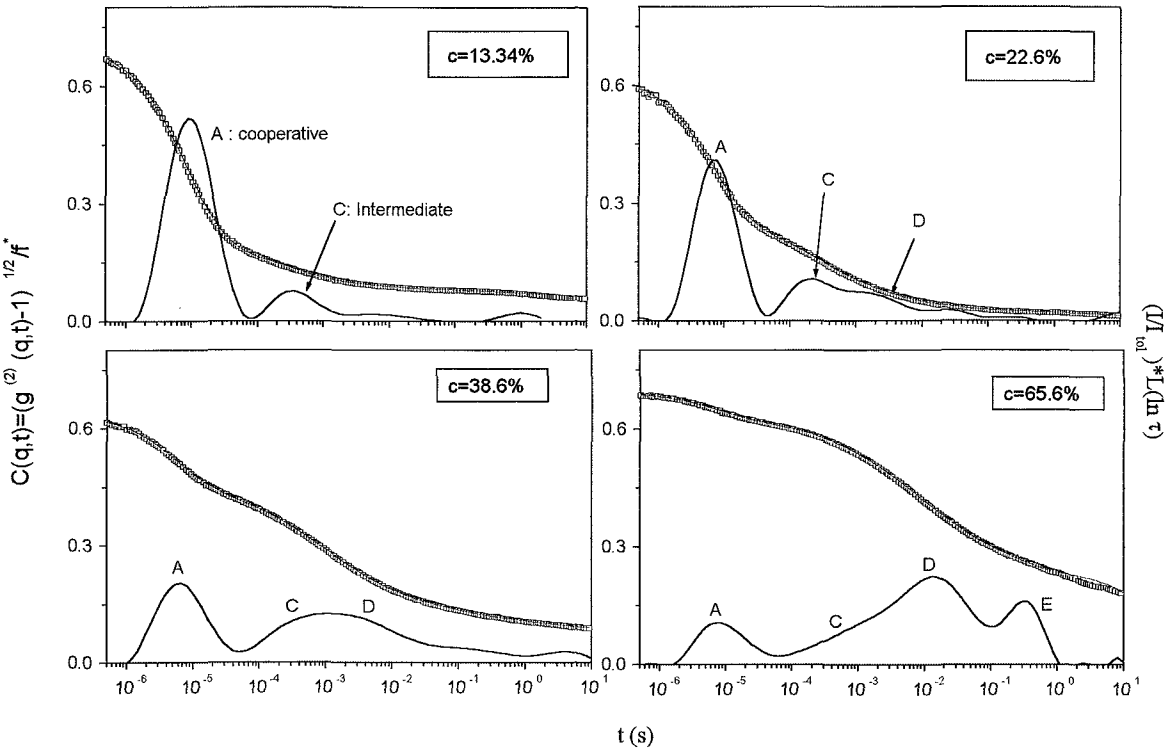

Figure 8.28: Normalized field correlation functions $C_{VV}(q,t)$ of S-1 solutions in toluene, at 120° for four different concentrations (c=13.34%, 22.6%, 38.6%, 65.6%). The distributions of relaxation times, multiplied by the normalized scattering intensity, are also shown (solid lines). The letters A to E denote the varius relaxation modes detected which are discussed in the text.

Between the cooperative process (A) and the slow mode (B) we observe the intermediate mode (C) and at higher concentrations a fourth mode (D). A careful analysis of both the VV and the VH correlation functions reveals that when the VH intensity is significant and the corresponding dynamics are in the time window of the correlator, the VH dynamics are seen in the VV correlation function through the $4/3I_{VH}$ term (eq. 3.22) as we also found for the PPP-12 sample. In fig. 8.30 we show $C_{VV}(q,t)$ and $C_{VH}(q,t)$for two cases:

(a) The VH dynamics are much faster than the intermediate VV mode and are revealed in the VV correlation function as a faster than the cooperative mode and

(b) The VH dynamics are in the same time as the intermediate VV mode which now appears much more pronounced. In the latter case the angular de-

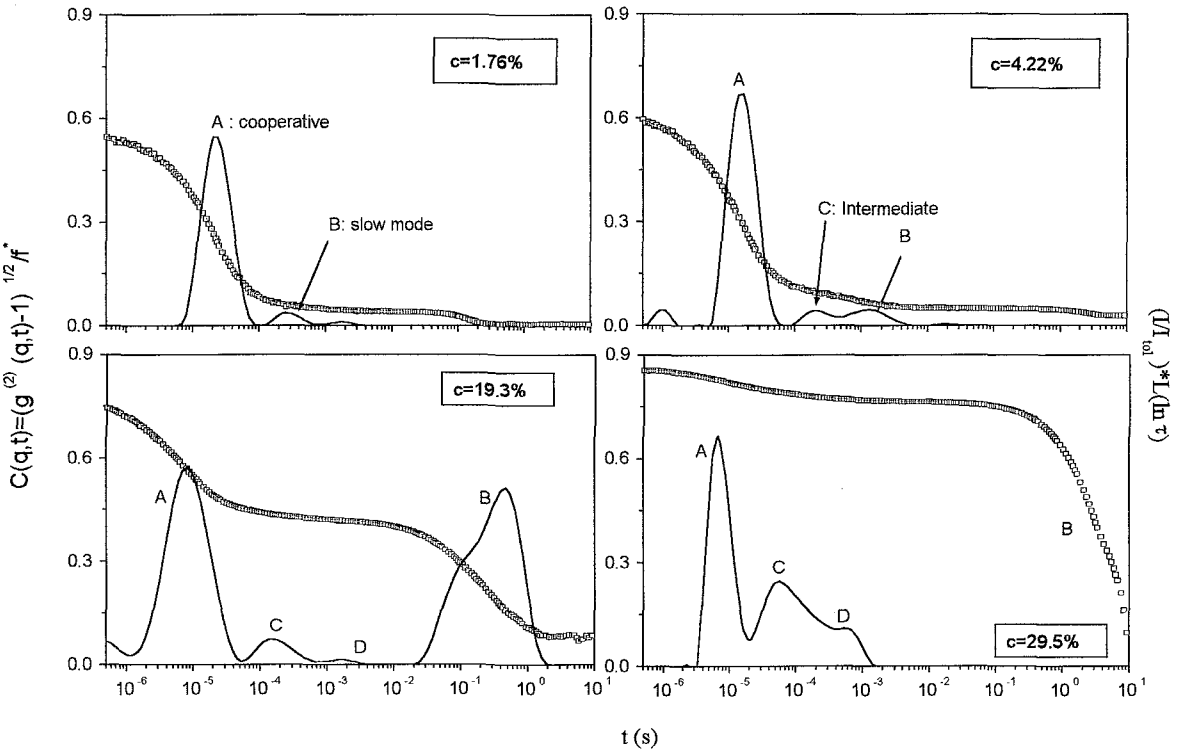

Figure 8.29: Normalized field correlation functions $C_{VV}(q,t)$ of S-7 solutions in toluene, at 90^o and for four different concentrations (c=1.76%, 4.22%, 19.3%, 29.5%) The distributions of relaxation times, multiplied by the normalized scattering intensity, are also shown (solid lines).

pendence of the decay rate, Γ of the intermediate mode may appear altered so that an apparent non-diffusive character is found.

Due to the complication that orientational fluctuations introduce in the resolution of the intermediate mode in the higher concentrations we will discuss its dynamics only in the case where the decay rate is clearly proportional to q^2.

The facts that all PPP/S samples are quite polydisperse (see table 8.1) and that D_s values from NMR, are very close to the values of D_{int} , make the self diffusion a good candidate for the intermediate diffusive mode; in such a case it is the polydispersity-induced contrast which enables light to distinguish between chemically identical molecules. This kind of mechanism has been identified in several systems such as diblock copolymers [31], colloidal spheres [29] and rods [30], and most recently in multiarm star polymers [24]. To examine this possibility we enhanced the molecular polydispersity of the system by preparing an equimolar mixture of the larger (S-1) with the smaller (S-9) molecular weight. If the intermediate mode originated from the self-diffusion of the molecules, we

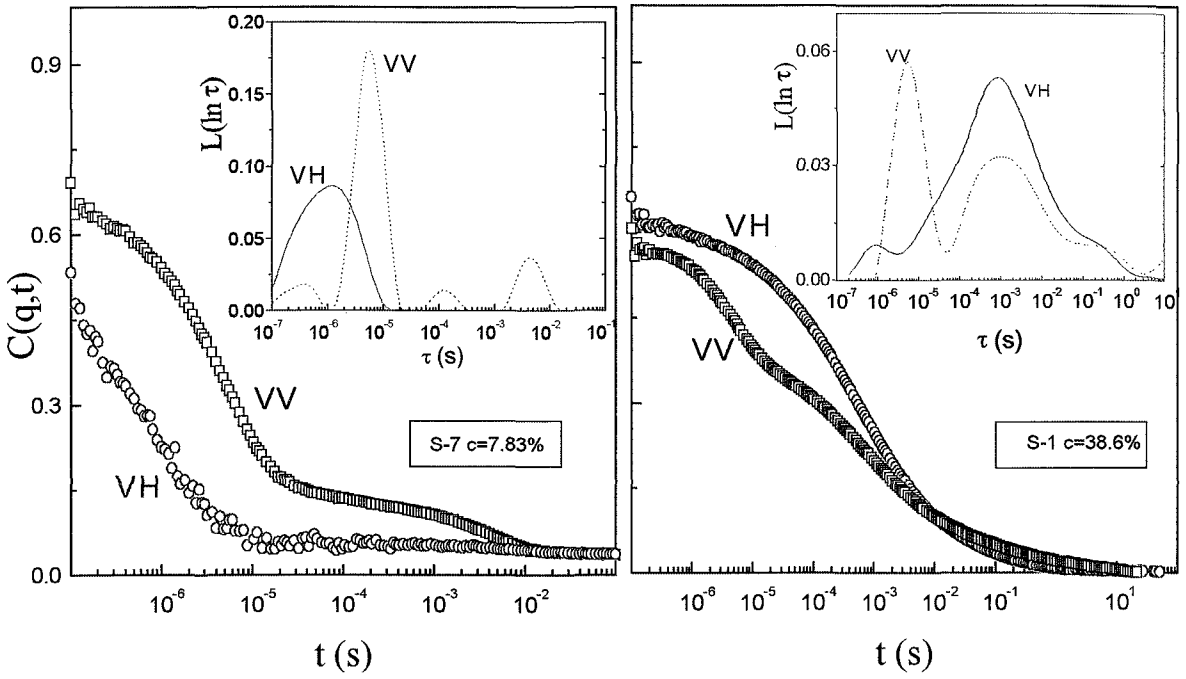

Figure 8.30: VV and VH field correlation functions at 150°, along with their corresponding distributions of relaxation rates (insets) for: (a) a c=7.83% solution of S-7 and (b) a c=38.6% solution of S-1 in toluene.

would expect a large increase of its intensity in the mixture (S-1+S-9). In fig. 8.31 we show concentration dependence of both the diffusion coefficient (a) and the scattered intensity (b) of the intermediate mode for all molecular weights as well as for the mixture.

It is clear that the intensity of the mixture is very similar with that of S-1 and S-9 solutions. This finding actually excludes the possibility of the a "polydispersity" self-diffusion mode. Moreover, the D_{int} is found to be essentially c-independent or increase weakly with c, whereas a self diffusion constant is expected and found (S-3 by NMR) to decrease with concentration, reflecting the increase of the friction in the absence of any thermodynamic effect. Note also that since the increase of the I_{int} at high concentrations is possibly due to the intervention of the VH dynamics, the intensity seems to be c-independent; a polydispersity mode in general gains intensity at high concentrations. The above findings may characterize the intermediate mode as a second cooperative mode, mainly due to its weak speed up with concentration and its diffusive character. In a two-component system it is difficult to predict or even visualize a second cooperative mode and thus only speculations can be made at present on the nature of the intermediate process.

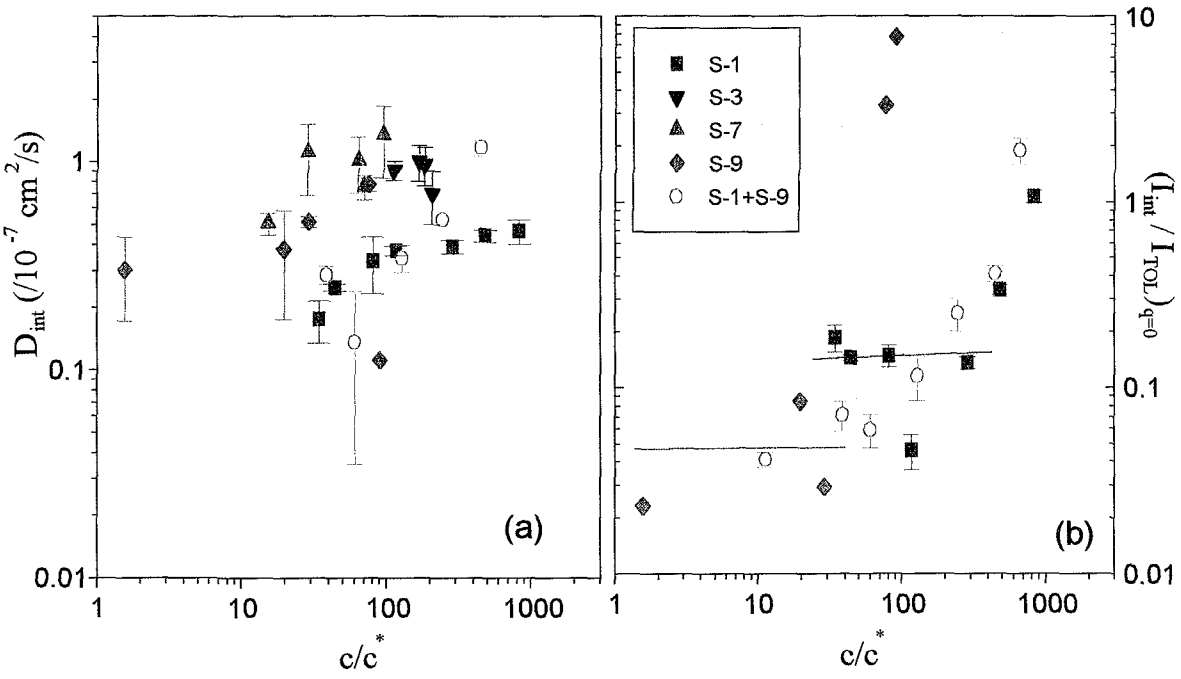

Figure 8.31: Concentration dependence of (a) the diffusion coefficient of the intermediate VV mode for all molecular weights and for the equimolar mixture of S-1 and S-9 (○) and (b) the intensity of the process for S-1, S-9 and the mixture.

As discussed in chapter 4, DSO theory predicts a bimodal relaxation of concentration fluctuations as a solution of rodlike molecules approach the nematic order. In this model the fast cooperative process is expected to dominate as the concentration is increased, over the slow one, which reflect the usual relaxation of concentration fluctuations in the isotropic regime, through both translation and rotational cooperative motions of the rods. In our study though, it is a slower than the normal cooperative mode that is observed at nondilute solutions, rather than a faster. Of course a very important differentiation from DSO considerations is the absence of a transition to a nematic phase in the PPP/S solutions, even at very high concentrations. However, in the presence of correlated local orientations found in this system (see discussion of VH scattering below), one may speculate that coupling of orientation with concentration fluctuations could result in a relaxation of concentration fluctuations through two different cooperative mechanisms of similar character with the predicted by DSO.

8.5.4 Slow mode -Clusters

Although PPP/S samples are very soluble up to high concentrations, some limited aggregation can not be avoided in the semidilute and concentrated regimes. As we have seen in all samples particular in chloroform or TCE, a slow diffusive mode appears above c^*, which gains intensity with concentration and becomes significantly slower. This cluster mode in the VV correlation function represents the relaxation of concentration fluctuations by the diffusive motion of a group of molecules with higher local concentration and thus different refractive index from the rest of the polymer solution as explained in PPP-12. This difference in the refractive index enables the observation of the cluster diffusion in the medium of the polymer solution. Note that in the VH correlation function we either do not observe any slow mode related to the cluster mode in VV (as in S-1 solutions) or when such a mode is observed it is found to decrease with equilibration time (in contrast to the one observed in VV) indicating that only some non-equilibrium clusters possess orientational order and thus different from the average optical anisotropy. These findings suggest that in this system the observed clusters are rather optically isotropic structures.

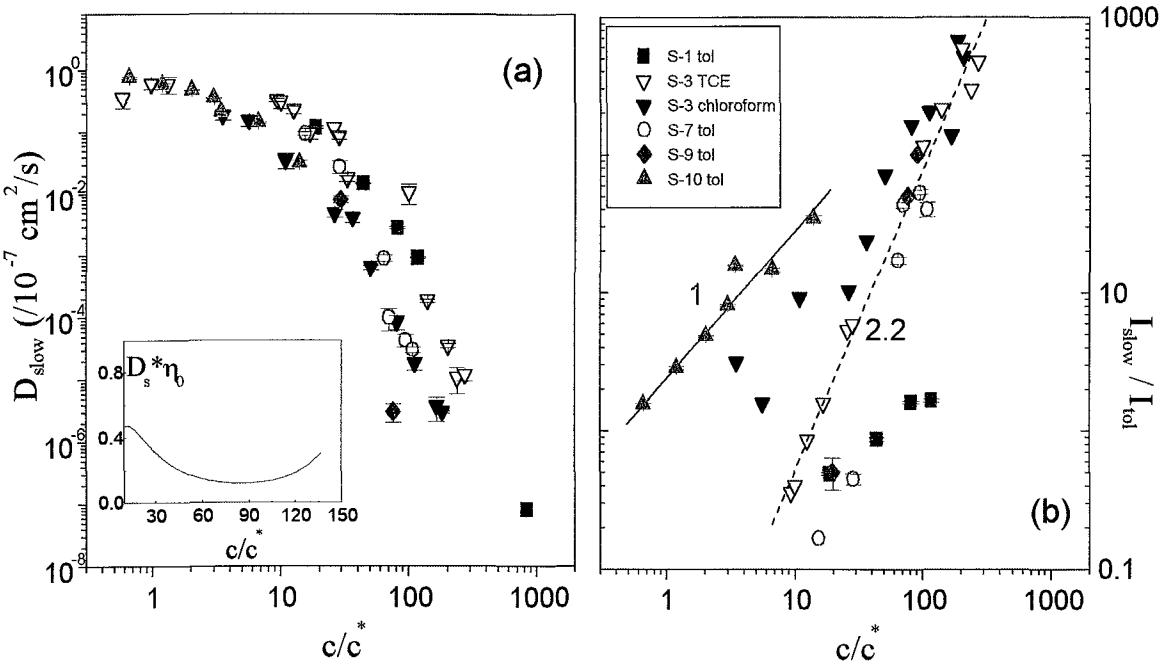

Figure 8.32: Concentration dependence of the slow mode: (a) Diffusion coefficient for all samples measured. Inset: D_s multiplied with the zero shear viscosity for the S-7 saample. (b) Intensity of the slow mode relative to that of toluene, vs c/c^*.

In fig. 8.32 we show the concentration dependence of the slow mode diffusion coefficient (a), as well as that of its intensity for all molecular weights investigated in toluene, chloroform and TCE. A strong slowing down of the diffusion is mainly due to the strong increase of the viscosity of the solution with concentration, as revealed by the product of D_{slow} with η_0 shown in the inset of 8.32a. The zero shear viscosity η_0 was measured for S-1 and S-7 samples (in the latter up to $c = 40\%$) by shear rheology measurements discussed below. For a compact object of size R, diffusing in a medium with viscosity η_0, the product $D_{slow}\,\eta_0$ is $kT/6\pi R$; thus the decrease observed in the inset of 8.32a suggests an increase of the size of the cluster with concentration. For S-7 these clusters have an estimated average radius of 55 nm, which increases up to 220 nm at high concentration. In aggreement with this increase the intensity of the cluster mode increases more than linearly with c (8.32b), except for S-10 which we discuss below.

The size of the clusters can also be estimated from the angular dependence of their intensity. In fig. 8.33 we show this dependence for several concentrations of S-3 in chloroform. An interesting finding is that in most our data the angular dependence of the I_{slow} cannot adequately be fitted by an Ornstein-Zernicke relation (eq. 8.2), but rather by a Debye-Bueche expression

$$I(q)^{-1/2} = I(0)^{-1/2}(1 + q^2\xi^2) \tag{8.14}$$

which implies a pair distribution function $f(r) = exp(r/\xi)$; the latter corresponds to a medium where two species (in our case clusters and single molecules) are randomly distributed, but with a sharp interfaces between each other [47]. The characteristic size calculated from eq. 8.14 is shown in the inset of fig. 8.33; it is found to increase with concentration from about 50 to 100 nm, similarly to what we found above.

Concerning this cluster mode the smallest molecular weight S-10 exhibits a different behavior which has some similarities with the behavior of P-12 and PPP-12. In this sample two modes are present in the VV correlation function even in the dilute regime and are attributed to free molecules and small clusters. In fig. 8.34a the concentration dependence of the cooperative and cluster mode are shown. The latter which even in the dilute region is also seen in the VH correlation function as a slow rotational relaxation (see also fig. 8.36), has an intensity which increases in proportion to c (fig. 8.32). These findings suggest that the slow mode in S-10 sample originates from a wormlike anisotropic cluster produced mainly by an end-to-end aggregation of the rodlike molecules, so that it has both large optical anisotropy and large size to be seen in the VH correlation function in the dilute regime. Moreover, it does not increase in size since its intensity is proportional to the number of scatterers. This description is very similar with that for the P-12 sample discussed above. For this reason we present for both samples the VH decay rates in fig. 8.32b. The concentration dependence of the slow VH modes, which is are the dominant one, are very similar in the two

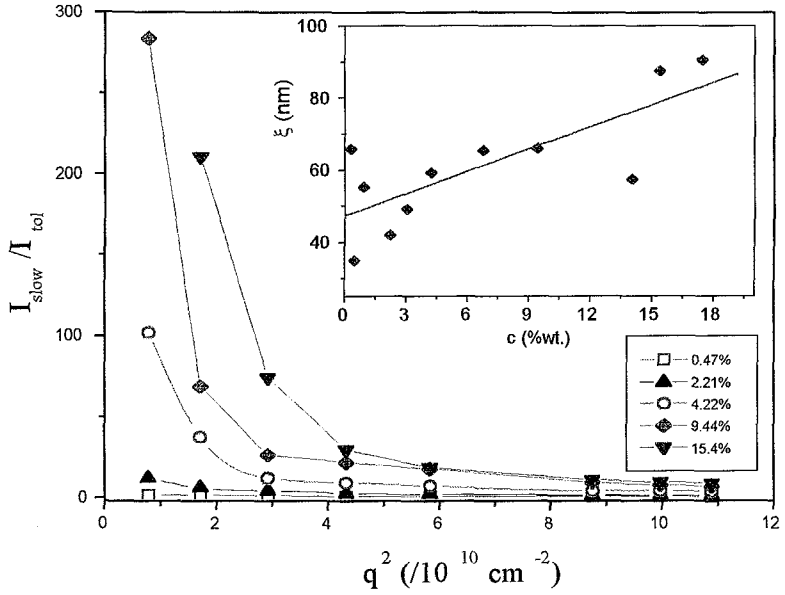

Figure 8.33: Angular dependence of the intensity of the slow mode at several concentrations of S-3 chloroform solutions. Inset: Correlation length as calculated from a fitting of data with a Debye-Buche expression vs concentration.

systems. In addition, in S-10 we have an indication of a faster VH mode as well, similarly with the fast VH mode in P-12 with a c-independent decay rate.

We observe in both of this samples that the rotational diffusion coefficient, D_R of the dominant slow mode follows a concentration dependence very similar to the predicted from most theories of rodlike and wormlike chains (see eq. 4.11, 4.14, 4.19, 4.28). Qualitatively this is described by a gradual increase of the concentration dependence according to

$$D_R = D_{R,0}[1 + \frac{C\rho}{(1 - D\rho)}]^{-2} \tag{8.15}$$

which for large concentration follows or slightly exceeds the Doi-Edwards scaling prediction. Nevertheless, this systems are not molecularly dispersed wormlike or rods but rather associates of similar shape. In P-12 we have concluded that the are almost no free molecules (all take part in aggregates) while in PPP-12 there is clear indication of free molecules together with stable aggregates in equilibrium.

The rotational and the translational diffusion coefficients of the S-10 clusters extrapolated at zero concentration can be used to calculate their average size. Assuming a wormlike shape we can calculate (using the expressions in Appendix B) a contour length $L = 584$ nm and a diameter $b = 5.6$ nm assuming a persistence length equal to that of the free molecules ($l = 25$ nm). The tendency for an

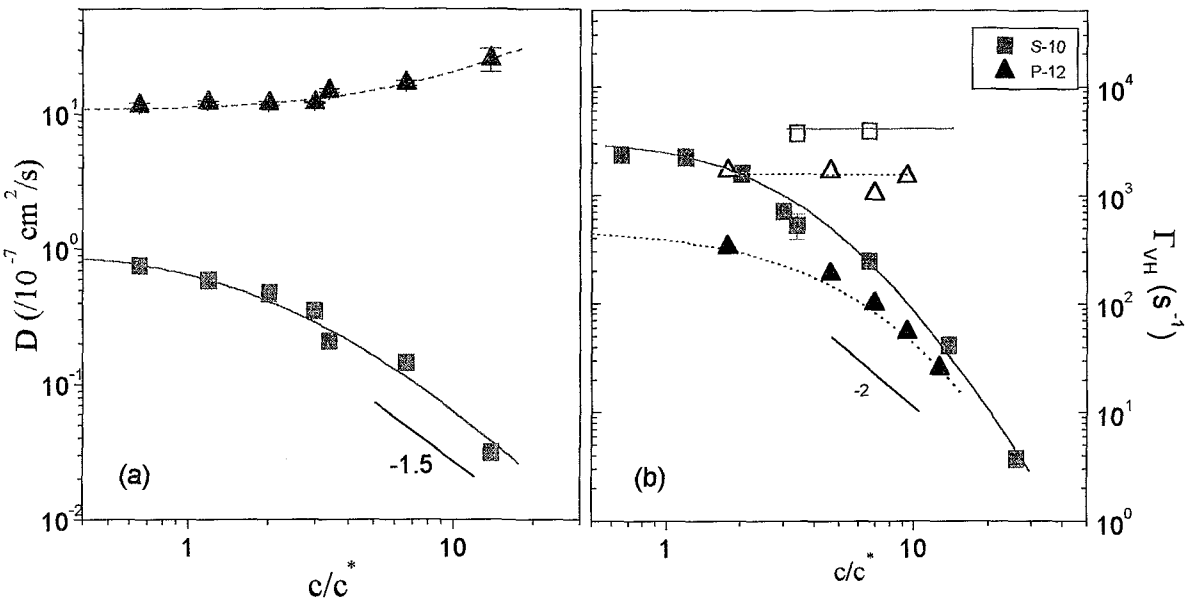

Figure 8.34: (a) Concentration dependence of the cooperative (▲) and cluster (■) diffusion coefficients of S-10 in toluene (b) The rotational decay rates for the two modes observed in the VH correlation function in solutions of S-10 and P-12 ; open sympols: fast mode, solid sympols: slow mode.

end-to-end aggregation in the low M_w S-10 compared to the other samples might be due to the concentration of the chain ends and/or the reduced solubility due to low chain flexibility.

8.5.5 Shear Rheology

The dynamic storage (G') and loss (G'') moduli of solutions of S-1 and S-7 at various concentrations, ranging from the dilute to the concentrated regimes, were measured using small-amplitude oscillatory shear experiments. A Rheometric Scientific constant strain rheometer (model ARES with a very sensitive dual-range force rebalance transducer and a high-resolution actuator) was utilized. Measurements were carried out in the cone-and-plate geometry (25 mm diameter, 0.04 rad cone angle) at room temperature, and in an atmosphere saturated in solvent (toluene) in order to eliminate solvent evaporation during measurements (the latter was realized with a vapor barrier system). Dynamic strain sweep (at constant frequency, from 1 to 100%) and frequency sweep (at constant strain, from 500 to 0.05 rad/s) tests were carried out in order to determine the regime of linear viscoelasticity and obtain the frequency-dependent shear mechanical moduli.

8.6 Depolarized Dynamics and Correlations of PPP/S sample

Figure 8.35 shows the experimental time orientational correlation function $C_{VH}(q,t)$ for two PPP/S solutions in two different solvents at $25°C$ and scattering angle $30°$. A two-step relaxation is clearly evident from the $C_{VH}(q,t)$ of S-1 and the distribution of relaxation times $L(ln\tau)$ of the two solutions irrespectively of M_w and solvent (toluene, chloroform and/or tetrachloroethylene). For all examined samples, $C_{VH}(q,t)$ conforms to this bimodal relaxation scheme for solute concentration above about 10% in three different solvents. The insensitivity of the shape of $C_{VH}(q,t)$ to the solvent quality, the distinctly different isotropic light scattering (from concentration fluctuations) over the same time range and the similar bimodal orientation relaxation in the chemically dissimilar PPP-12 favor the molecular origin of this behavior.

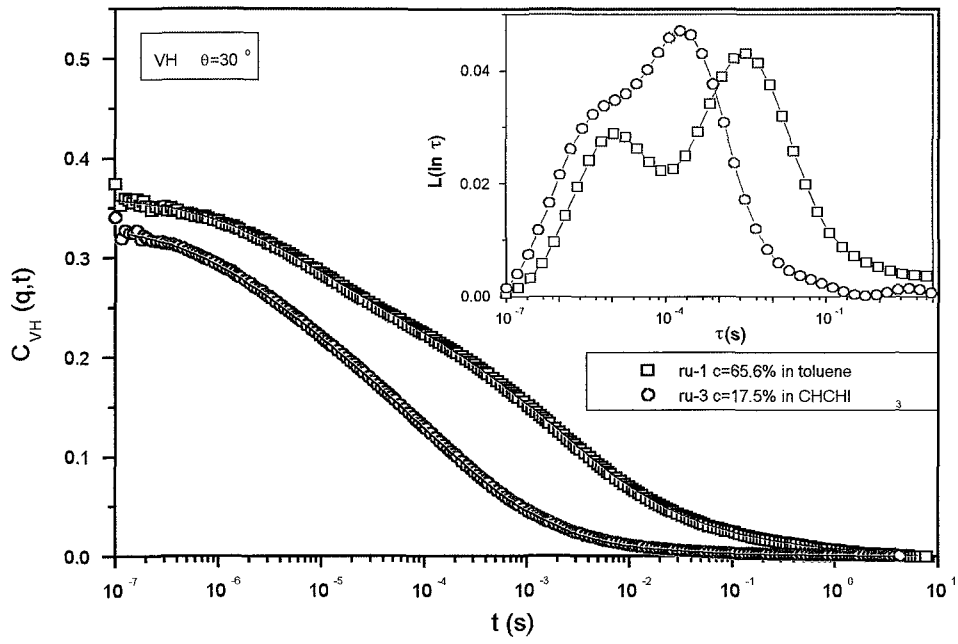

Figure 8.35: Experimental orientational relaxation functions at $q^2 \simeq 9 \times 10^{-3}\ nm^{-1}$ for S-1 (65.6%) and S-3 (17.5%) in toluene and chloroform respectively. The two distributions $L(ln\tau)$ of relaxation times which represent well (solid lines) the experimental $C_{VH}(q,t)$are shown in the inset.

Alternatively, non molecular factors, such as aggregation, would lead to unique isotropic and anisotropic scattering displayed by the low M_w S-10 solutions in

toluene in Figs. 8.36 and 8.34 and also by the chemically different P-12, as discussed above (sect. 3.5.4). The slow process in the concentration and orientation relaxation functions assumes similar dynamics with q-dependent rates characteristic of optically anisotropic clusters with translational and rotational diffusion. Like in all other samples (Fig. 8.35), the fast process of $C_{VH}(q,t)$, which is just entering the PCS time window in Fig. 8.36 relates to the molecular orientation dynamics.

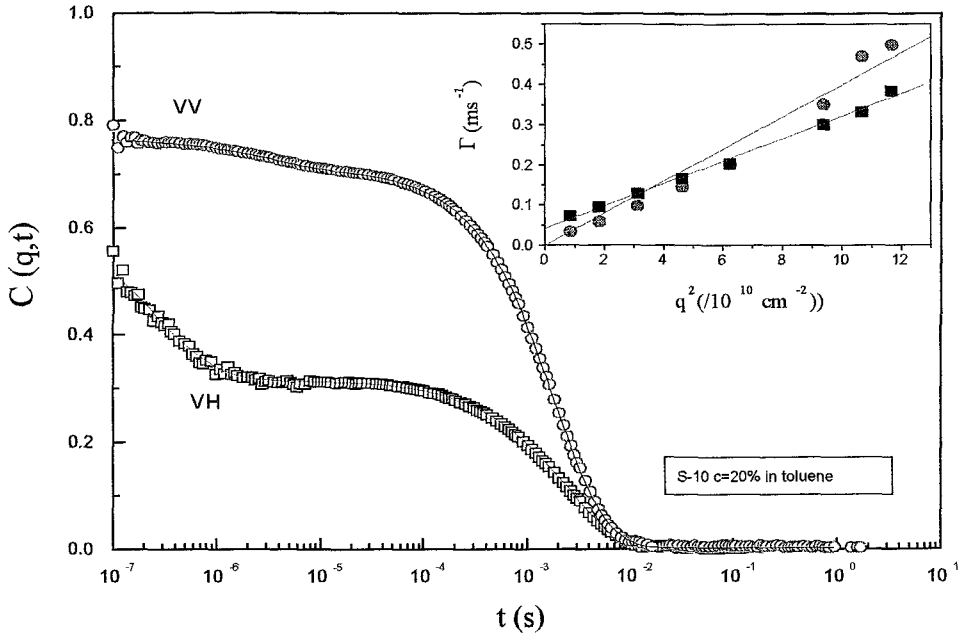

Figure 8.36: Experimental concentration and orientation correlation functions for 20% solution of S-10 in toluene at $q = 0.034nm^{-1}$ and 25^oC. The inset shows the variation of the relaxation rate for the slow process in the two functions with q.

An additional support of the molecular origin of the relaxation functions in Fig. 8.35 is provided by the presence of enhanced short range orientation fluctuations in the system. The contribution of the peak at long times in $L(ln\tau)$ of Fig. 8.35 increases at high q's as shown in the inset of Fig. 8.37a and 8.38a for 13.3% and 38.6% S-1 solutions in toluene respectively. Aggregation would lead to stronger forward (low q's) light scattering. Figure 8.37a and 8.38a reveals, for the first time, spatial correlations in the orientation fluctuations associated with the second (slow) process of the $C_{VH}(q,t)$ providing evidence of the presence of local ordering (see below).

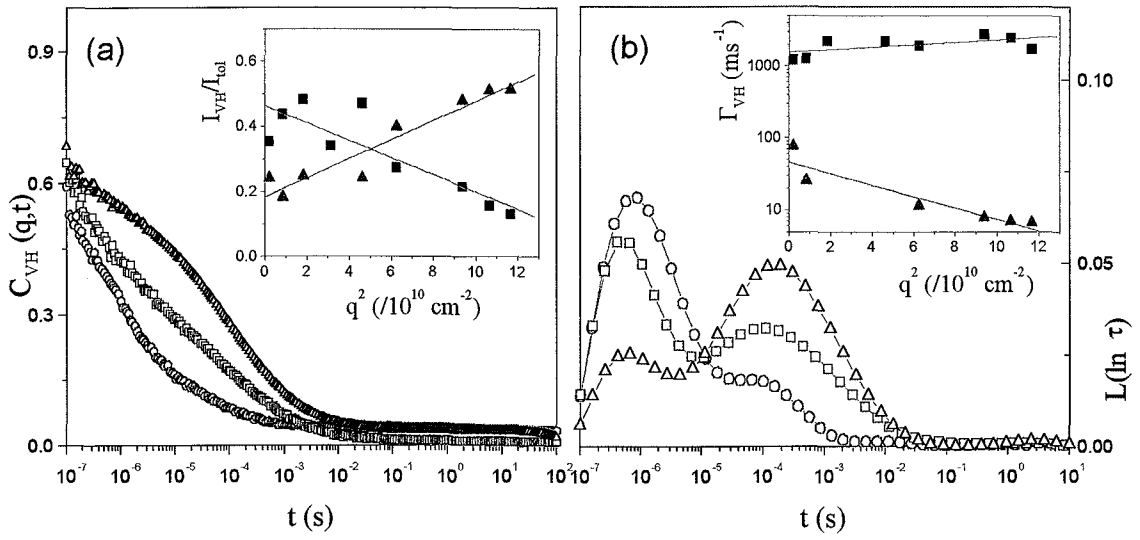

Figure 8.37: (a) Experimental orientational relaxation functions for 13.3% S-1 at three wave vectors (between 0.009 nm^{-1}(○) and 0.034 nm^{-1}(△)) and 25°C. Inset: q-dependence of the normalized intensities I_{VH}/I_{tol} of the fast (■) and slow (▲) modes. (b) Distribution of orientation relaxation times for the same q's. Inset: q-dependence of the decay rates Γ_{VH} of the fast (■) and slow (▲) modes.

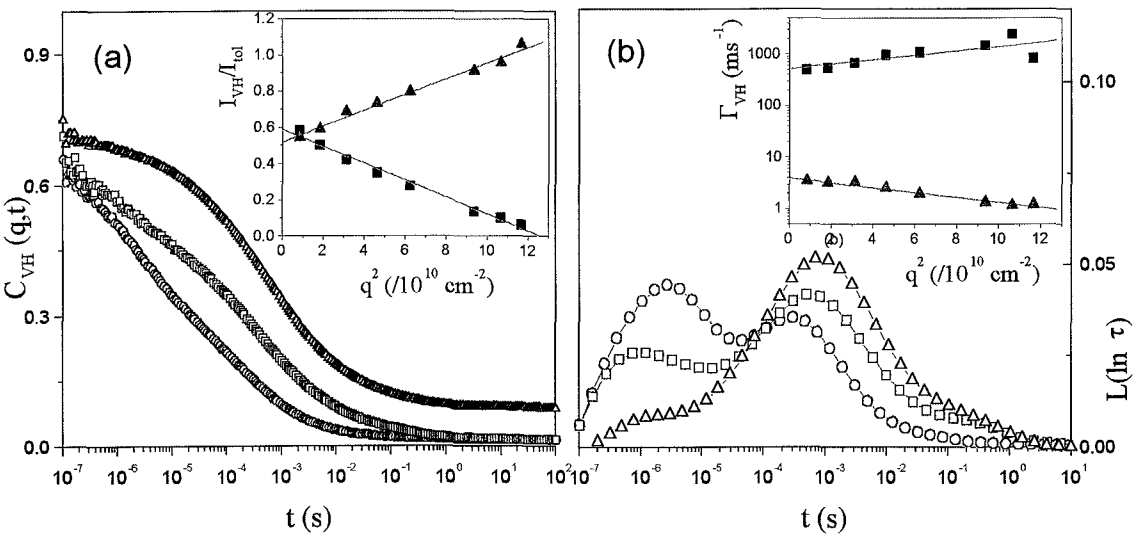

Figure 8.38: (a) Experimental orientational relaxation functions for 38% S-1 at three wave vectors (between 0.009 nm^{-1}(○) and 0.034 nm^{-1}(△)) and 25°C. Inset: q-dependence of the normalized intensities I_{VH}/I_{tol} of the fast (■) and slow (▲) modes. (b) Distribution of orientation relaxation times for the same q's. Inset: q-dependence of the decay rates Γ_{VH} of the fast (■) and slow (▲) modes.

The slow process exhibits a distribution of relaxation times as indicated by the broad (more than two decades in time) width of $L(ln\tau)$; a representation of the second process of $C_{VH}(q,t)$ by a KWW function (eq. 5.9) yields values of β between 0.3 and 0.4 for the high q's of Fig. 8.38 at which the slow relaxation dominates. For comparison the fast process of $C_{VH}(q,t)$ appears to display narrower distribution as reflected in the higher $\beta(= 0.65 \pm 0.05)$ obtained from the representation of the experimental $C_{VH}(q,t)$ at low q's by a double KWW equation. In view of the relation for the rotational diffusion of rodlike molecules, $D_R \sim L^{-9}$ (eq. 4.11) the polydisperse nature (distribution of chain length) of the samples (Table 8.3) might account for the non-exponential shape of the fast process. The most probable relaxation rates (at the peak maxima of $L(ln\tau)$) display reciprocal relationships to q; the fast rate Γ_f increases while the slow Γ_s decreases with q (fig. 8.37 and 8.38). These main findings for the bimodal $C_{VH}(q,t)$ will be discussed in the next section.

We complement the dynamic depolarized light scattering data, with information on the dynamic shear moduli for two PPP/S samples at different concentrations. As seen in Fig. 8.39, the linear viscoelastic data of a concentrated entangled 8% S-1 solution in toluene, at room temperature, exhibit the standard terminal regime scaling behavior for $G'(\sim \omega^2)$ and $G''(\sim \omega)$, which allows the straightforward estimation of the longest chain relaxation time τ and the zero-shear viscosity η_0 $(= G''/\omega$, at low frequencies). The single terminal process of Fig. 8.39 conforms to the picture of molecularly dispersed polymers, since any presence of aggregates or permanent network would yield an extra terminal relaxation or enhanced (plateau-like) elastic modulus, respectively. The inset of Fig. 8.39 depicts the (strong) concentration dependence of η_0 for S-1 and S-7.

8.6.1 Orientation relaxation function

The insensitivity of the orientation dynamics to the choice of nominally good solvents was thoroughly examined for S-3 in toluene, $CHCl_3$ and TCE for solute concentrations up to 20%; higher concentrations led to opaque solutions. As mentioned in the preceding section, the bimodal shape of $C_{VH}(q,t)$ resolved above $\sim 6\%$ is present in all three solvents. The normalized scattered depolarized intensity, I_{VH}/I_{tol}, associated with the two processes for $c > 6\%$ and the solute contribution for $c < 6\%$, where dynamic resolution was not possible, is compared among the solutions in the three solvents in Fig. 8.40a. The same figure (b) includes the relaxation rates of the two processes in the limit $q = 0$ at different S-3 concentrations in the three solvents. The observed good agreement, within experimental error, for both static and dynamic data clearly supports unchanged chain conformation and interactions in the three solvents; up to about 20% the total I_{VH}/I_{tol} increases linearly with the concentration of the anisotropic molecular scatterers. Moreover, in the inset of Fig. 8.40a the distribution of relaxation times $L(ln\tau)$of solutions in $CHCl_3$ ($c = 17.4\%$) and TCE ($c = 18\%$) also reveal

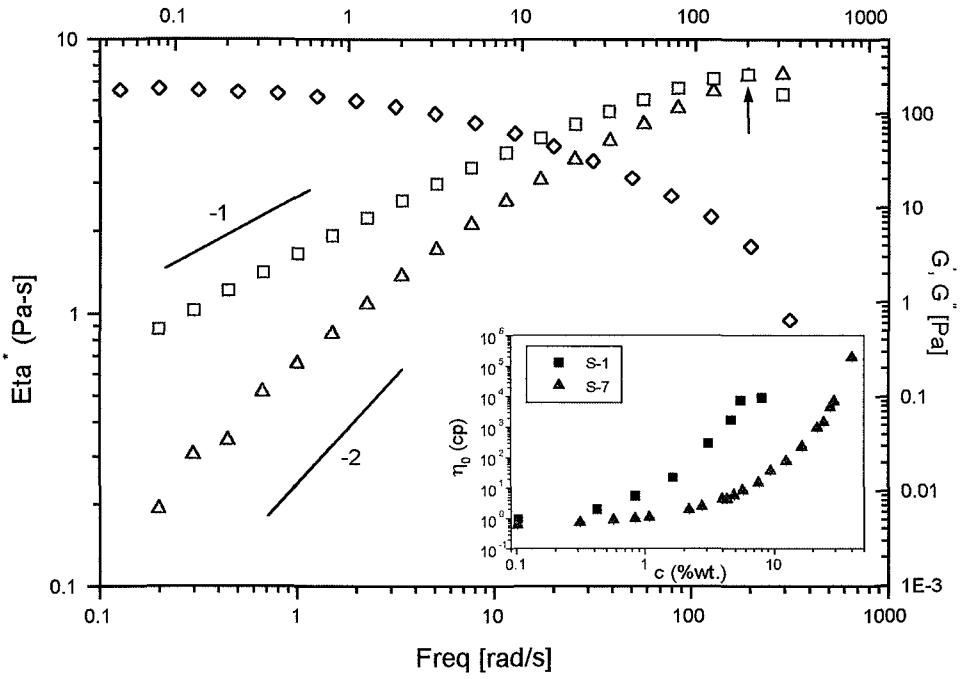

Figure 8.39: Frequency dependence of the dynamic shear moduli (storage, G' (□); loss, G''(△)) for a typical semidilute S-1 solution in toluene (8%) at room temperature. The $G' - G''$ crossover identifies the longest relaxation time. The dynamic shear viscosity, yielding the solution's zero-shear viscosity, η_0, is also shown in the plot (◇). Inset: Concentration dependence of η_0 for S-1 (■) and S-7 (▲).

identical VH dynamics in both solvents. Note that these solvents do not possess the same quality as judged from the intensity of a slow process in the isotropic light scattering.

This bimodal shape of $C_{VH}(q,t)$, which does not relate to aggregation phenomena, has not been predicted theoretically for either rigid or semiflexible polymers (chapter 4) and although was not characterized experimentally in wide concentration regime (owing to limited solubility) was also seen in the depolarized experiments of PPP-12 (see previous sections). To establish the phenomenology of this unusual orientation relaxation behavior, the variation of $C_{VH}(q,t)$ with the wavelength (q^{-1}) of the fluctuations and solute concentration was thoroughly examined for five PPP/S samples. The relaxation rates and intensities were obtained respectively from the position and integration of the peaks in $L(ln\tau)$.

In fig. 8.41and 8.42 we show the angular dependence of the correlation function $C_{VH}(q,t)$ and the distribution of relaxation times $L(ln\tau)$, together with the corresponding intensities and relaxation rates of the fast and slow mode for two different concentrations (c = 17.34% and c = 29.5%) of S-7 in toluene. This

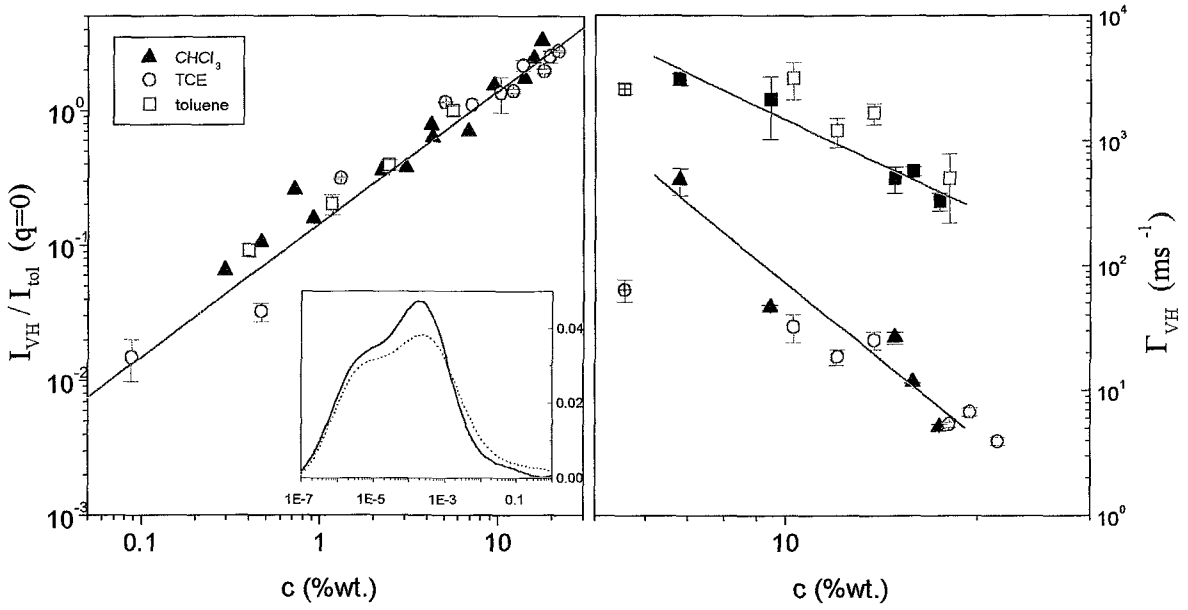

Figure 8.40: (a) Depolarized light scattering intensity (normalized to the polarized intensity of toluene) in the thermodynamic limit $q = 0$ for S-3 solutions in three solvents: TCE (◯), $CHCl_3$ (▲) and toluene (□); inset: distrinution of relaxation times for a 17.4% solution in $CHCl_3$ (solid line) and 18% in TCE (dotted line). (b) Rate of the two processes of $C_{VH}(q,t)$ in the thermodynamic limit $q = 0$ for S-3 solutions in three solvents: TCE (□: fast, ◯: slow), $CHCl_3$ (■: fast, ▲: slow) and toluene (⊞: fast, ⊕: slow).

figures should be compared with figs. 8.37 and 8.38 which present data from the highest molecular weight S-1. It is seen that the two relaxation modes are better separated in time in the larger molecular weight (S-1) while the variation of $I_s(q)$ and $\Gamma_s(q)$ with q is more evident, than in the smaller (S-7). These behavior is systematic for all samples of the PPP/S series.

In fig. 8.43 and 8.44 we show the concentration dependence of the $C_{VH}(q,t)$ and of the respective $L(ln\tau)$ for S-1, S-3, S-7 and S-9 samples. For the larger molecular weights S-1 and S-3 the data are shown for an intermediate scattering angle (60°) while for the two smaller S-7 and S-9 in the highest scattering angle (150°), so that they can be better resolved. It is again clear that the time separation of the modes is larger in S-1 and S-3 compared to S-7 and S-9. Moreover, the slowing down of both of these modes is evident as well as the domination of the slower mode as concentration increases.

It must be noted that in these figures and for all except the S-1 data the contribution of an ultra-slow mode (slower than $10s$) was substracted, so that the field correlation functions $C_{VH}(q,t)$ from different concentrations can be bet-

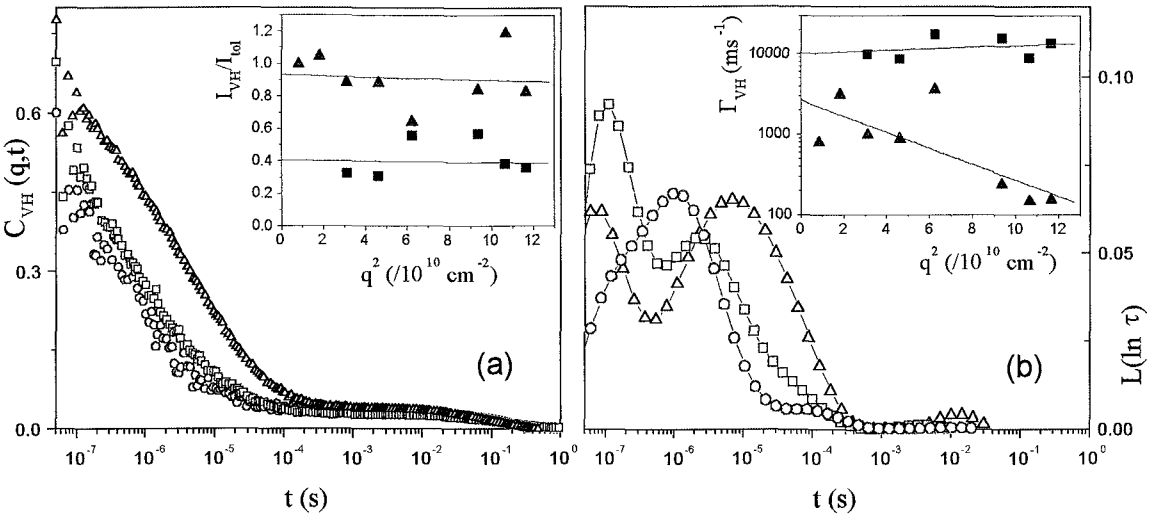

Figure 8.41: (a) Experimental orientational relaxation functions from an S-7 solution (17.34% in toluene), at three wave vectors (between 0.009 nm^{-1}(○) and 0.034 nm^{-1}(△)). Inset: q-dependence of the normalized intensities I_{VH}/I_{tol} of the fast (■) and slow (▲) modes. (b) Distribution of orientation relaxation times for the same q's. Inset: q-dependence of the decay rates Γ_{VH} of the fast (■) and slow (▲) modes.

ter compared. It has been observed that such slow modes in the VH scattering are result from non equilibrium ultra slow structures, possibly related with the ultra-slow processes that is observed in polarized correlation functions and are attributed to clusters. In any case, these slow modes are not affecting the molecular (much faster) dynamics and loose amplitude with time (a full equilibration, though, might take few weeks in highly concentrated samples). Thus, care has been taken to avoid such structures by slowly evaporating the solutions between successive measurements at different concentrations and also equilibrating the samples for at least few days before measuring. In this sense the most successful sample was S-1 where the slow mode in the VH was actually absent (even in the very sensitive $C_{VH}(q,t)$) as seen in fig. 8.43a.

The contribution of the main (slow) mode, with broad distribution of relaxation times, increases while it becomes slower with increasing q for all PPP/S samples as demonstrated in Fig. 8.45 for three solutions of S-1 in toluene. Short range (and hence high q) orientation fluctuations are more probable and decay slower than long wavelength fluctuations, as indicated by the variation of $I_s(q)$ and $\Gamma_s(q)$ with q, for the slow process (Fig. 8.45) of $C_{VH}(q,t)$. This interplay is reminiscent of the effect of interactions on collective dynamics exclusively, so far, observed for composition fluctuations in systems exhibiting an ordering transition with macroscopic length scales [48].

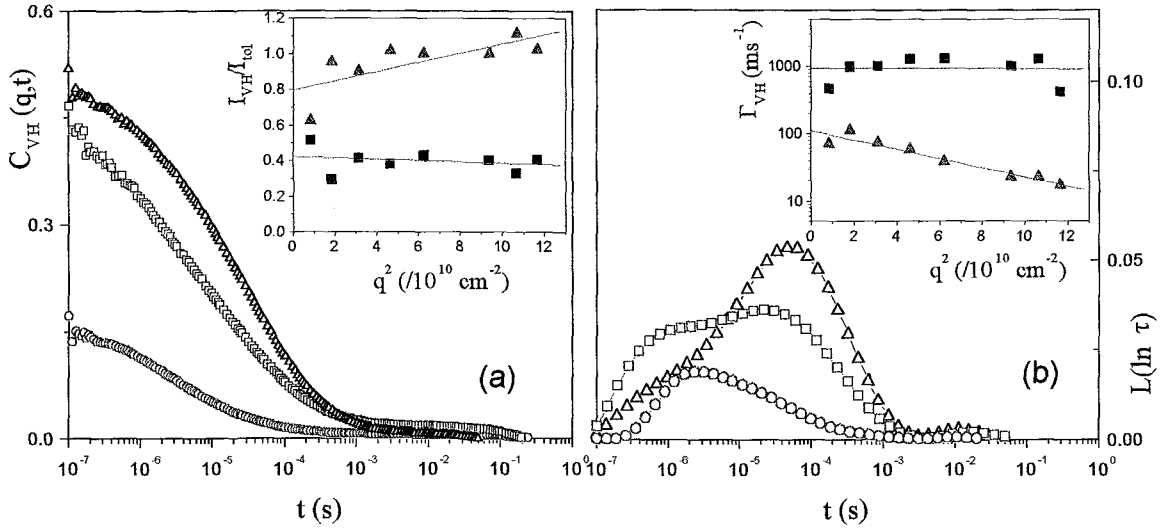

Figure 8.42: (a) Experimental orientational relaxation functions from an S-7 solution (29.5% in toluene), at three wave vectors (between 0.009 nm^{-1}(○) and 0.034 nm^{-1}(△)). Inset: q-dependence of the normalized intensities I_{VH}/I_{tol} of the fast (■) and slow (▲) modes. (b) Distribution of orientation relaxation times for the same q's. Inset: q-dependence of the decay rates Γ_{VH} of the fast (■) and slow (▲) modes.

On the other hand, the fast I_f (Fig. 8.45) is found to increase moderately with q as expected for optically anisotropic scatterers undergoing rotational and translational diffusion (eq. 8.3) with $\Gamma_{VH}(q) = 6D_R + q^2D$. The intensity, I_f associated with this process should either be virtually q-independent for $q\xi < 1$ or decrease with q for larger characteristic length (or size). The latter is unlike if the characteristic size is the persistence length ($l \sim 25nm$). An alternative possibility would be the increase of the coherence length ξ of orientational fluctuation correlations in the isotropic region approaching the nematic phase transition in molecular liquid crystals [49]. The observed decrease of I_f with q for all samples was found to compensate roughly the corresponding increase of I_s as indicated by the insensitivity of the total $I_{VH}(= I_f + I_s)$ to q variations. In the same context, the intensity I_{VH} was found to scale linearly with c (Fig. 8.40 and 7 below) that implies overall negligible orientation correlations. The apparently different interpretations of $I_{VH}(q, c)$ and $I_f(q)$ can be reconciled by a partitioning of the anisotropic segments of PPP/S in the two processes. The static I_{VH} alone could therefore lead to misinterpretation of its q- and c-dependence without the ability to measure the dynamics of the orientation fluctuations.

The concentration dependence of I_{VH} and its contributions, I_f, I_s, which is a sensitive index of static orientation correlations is visualized for all samples in Fig. 8.46 and its inset respectively. Pertinent information is included in this Figure.

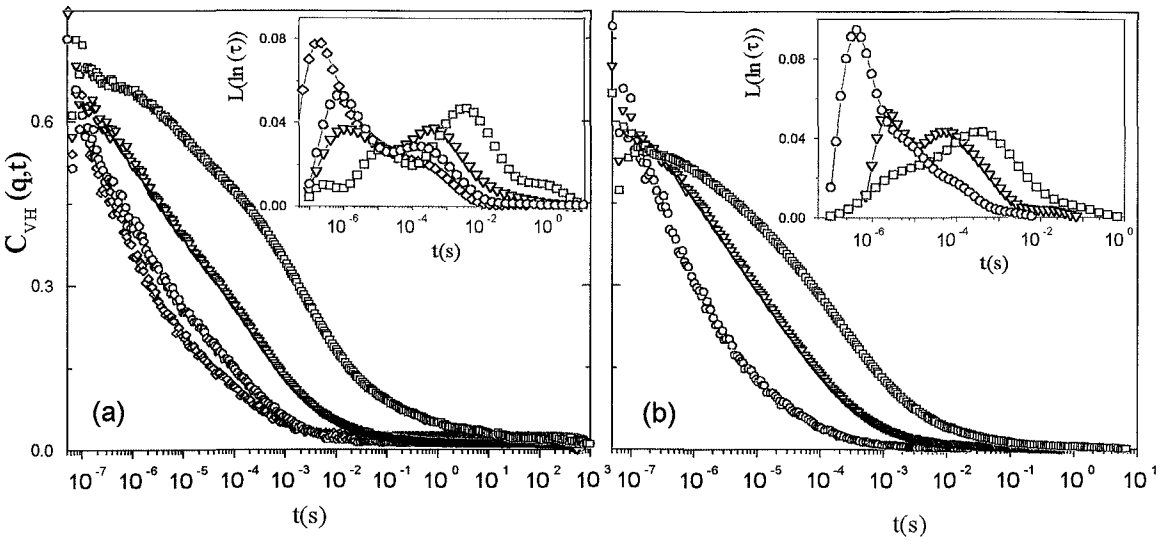

Figure 8.43: VH field correlation functions at $\theta = 60^o$ for: (a) four different concentrations of S-1 in toluene; (◇)13.3%, (○) 22.6%, (▽) 38.6% and (□) 65.6% and (b) three concentration of S-3 in chloroform; (○) 6.8%, (▽) 14% and (□) 17.4%. Insets: The respective distributions of relaxation times.

Below about 10%, all samples but S-3 (c.f. Fig. 8.40) display experimentally the same I_{VH} indicating the semiflexible nature of PPP/S already above S–9, i.e. the optical molecular anisotropy $< \gamma^2 > \sim L$ (see also chapter 6). The virtually linear increase of I_{VH} with c implies isotropic solution of orientationally uncorrelated Kuhn segments of size $2l$. For $c \geq 10\%$, the dynamics of orientation fluctuations fall into the PCS time window and the resolution of the two processes (Figs 8.35,8.37,8.38,8.41,8.42) allows the estimation of I_f and I_s (inset of Fig. 8.46). The linear relationship $I \propto c$ persists up to the highest c for S-1, S-3 and S-7 with exception the less flexible S-9 ($L \sim l$) for which I_{VH} increases stronger than c. The two intensity contributions show different c-dependence with I_s varying stronger than I_f, due probably to enhanced orientational pair interactions. The latter should also affect the variation of the collective rate Γ_s with c as opposed to $\Gamma_f(c)$ which is examined next.

Since both I_f and I_s depend on q (Fig. 8.45), Fig. 8.47 depicts the c-dependence of these quantities at $q = 0$. At first glance, the separation of the two relaxation rates increases with c reflecting the stronger c-dependence of I_s. The variation with c is stronger than the DE prediction c^{-2} (eq. 4.11) and any other relevant expressions (eq. 8.15) for both rates, which much like the bimodality of $C_{VH}(q,t)$, does not conform to the mean field theoretical predictions for rigid-rod polymers (chapter 4). In the same context, an estimation of the rotational diffusion rate, $6D_R$, in the dilute regime for semistiff worm-like chains (eq. B.9

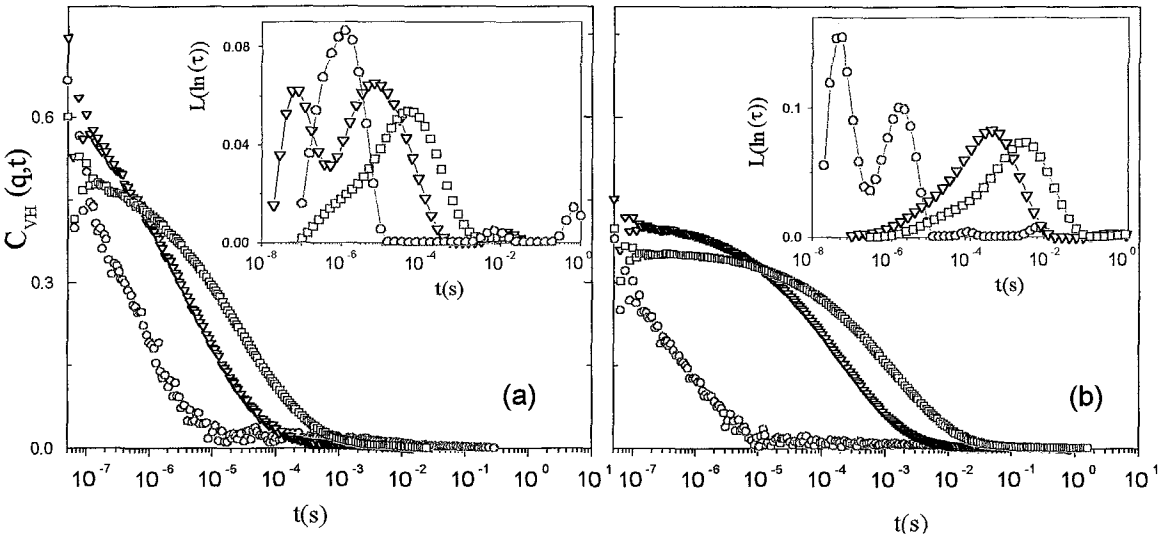

Figure 8.44: VH field correlation functions at $\theta = 150^o$ for: (a) for S-7 in toluene; (○) 7.8%, (▽) 17.43% and (□) 29.5% and (b) for S-9 in toluene; (○) 12.5%, (▽) 32.6% and (□) 38.6%. Insets: The respective distributions of relaxation times.

or B.11), considering the uncertainty of the persistence length leads to systematically slower values (arrows in Fig. 8.47) (see also Table 8.5) than anticipated from the experimental Γ_f rates.

It is further noted, that the measured solution viscosities also exhibit a much stronger that c^2 dependence (inset of Fig. 8.39). From Figs. 8.39 and 8.47 it is clear that the measured longest viscoelastic relaxation rate ($0.2\ ms^{-1}$ for a $c = 8\%$ solution of S-1) is much slower (by nearly 2 decades) than the slowest orientational relaxation rates. This can be explained by the fact that the longest viscoelastic relaxation in the present experiments is actually the disentanglement time for the transient physical networks formed at the high concentrations investigated, whereas on the other hand the detected VH rates relate to molecular reorientations of Kuhn chain segments (as discussed below), and are of inter-, rather than intrachain origin; the latter speculative argument could explain why we do not see the disentanglement process (related to end-to-end chain orientational motion) in the orientational correlation function, in agreement with other dynamic results from entangled flexible polymer chains. The fast VH rates correspond to the Rouse-like transition regime at much higher frequencies in the viscoelastic measurements, and are accessible only by employing the time-temperature superposition principle. However, that was not attempted, since lowering the temperature would result in reduced solvent quality, with potential implications to the phase state of the solutions and molecular processes. On the other hand, a comparison of the data in the inset of Fig. 8.39 and Fig. 8.47 for S-1 and S-7,

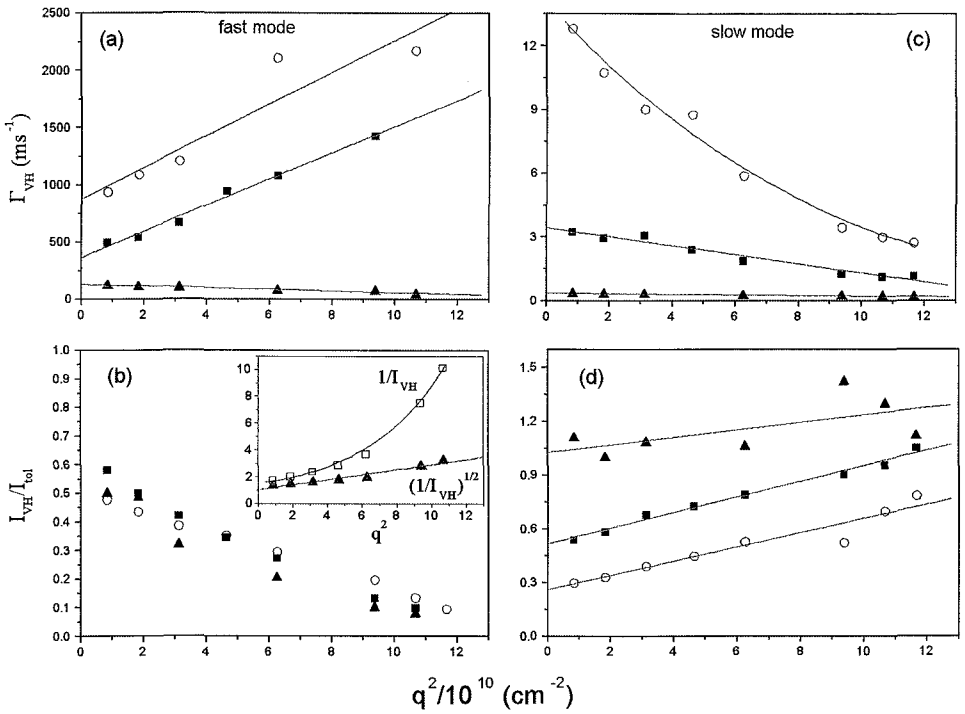

Figure 8.45: q-dependence of I_{VH} and Γ_{VH} for the two processes of $C_{VH}(q,t)$(fast: (a) and (b), slow: (c) and (d)) for three concentrations of S-1 in toluene: (◯) 22.6, (■) 38.6 and (▲) 65.6%. Inset b: Fits of Debye and Ornstein-Zernicke orientational correlation fluctuations to the I_{VH} for the fast process at $c = 38.6\%$.

based on the fact that the zero-shear solution viscosity (Fig. 8.39) relates to the chain end-to-end reorientational motion and the difference in magnitudes of the relaxation rates, provides a further strong evidence that with PCS we do detect orientational correlations of Kuhn segments, i.e., length scales shorter than the chain length.

Aside from the disagreement with the theory of rigid rod-like polymers, the slowing down of Γ_f and Γ_s with c becomes systematically stronger with decreasing L/l. Hence at high c, orientation fluctuations relax faster in S-1 than in S-9 despite the fact that S-1 is about 9 times more concentrated (the ratio of c^* for S-9 and S-1). Since the PPP/S samples possess the same static flexibility (l =const) (Fig. 8.46) this unexpected result might reflect the cooperative nature of the dynamics of the contour fluctuations in agreement with the broad $L(ln\tau)$ distribution of the slow process. To verify this conjecture, we examine how the orientation dynamics of the equimolar S-1/S-9 mixture above 10% compare to the relaxation function of the individual components.

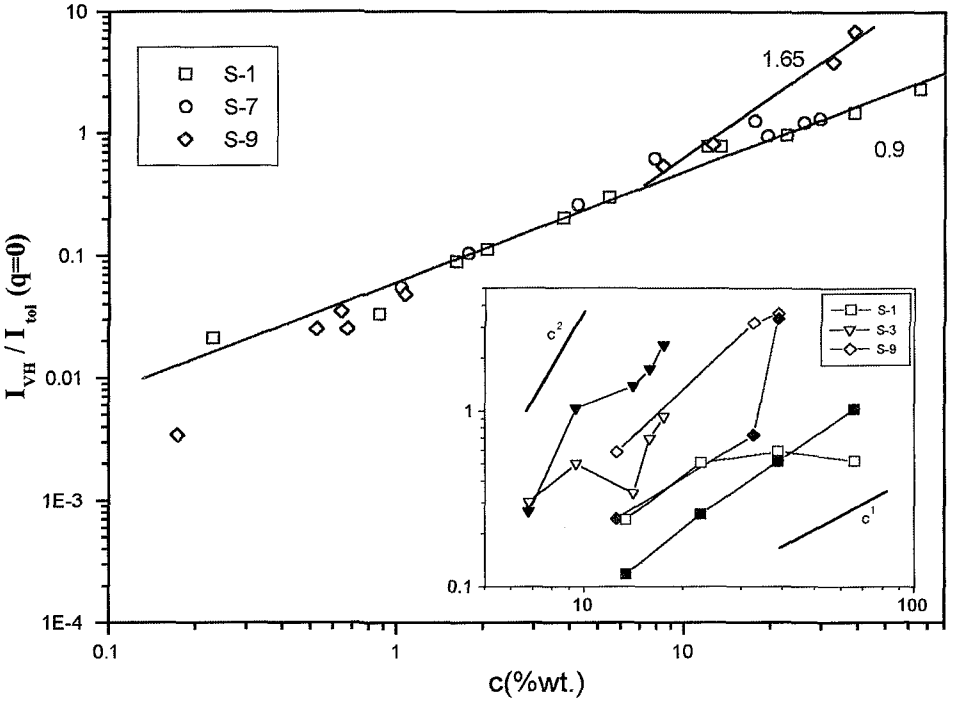

Figure 8.46: Concentration dependence of the total depolarized I_{VH} and I_f (open sympols) , I_s (solid sympols) separately for the fast and slow process (inset) in all samples. SloAll intensities refer to the thermodynamic limit ($q = 0$).

Despite the fact that the two components have quite different orientational dynamics at low (~10%) and high ($\sim$ 40%) concentrations (Fig. 8.47), two processes still contribute to the experimental $C_{VH}(q,t)$ of the equimolar S-1/S-9 solution in toluene and the two rates are shown in Fig. 8.47. In a miscible system this provides strong evidence of dynamic cooperativity which is moreover, supported by the domination of the slow component in the mixed ternary solution; Γ_f and Γ_s are close to the corresponding rates of S-9 and S-1 respectively at about 10% and 30%, i.e., the slow component determines the mixture orientational dynamics. The depolarized intensities I_{VH}, I_f and I_s show no measurable changes in the S-1/S-9 solution and are expectably similar to these in S-1 with the higher weight concentration. It appears therefore that the strong c-dependence of Γ_f and Γ_s results from the increased cooperativity with c that is reminiscent to the glass dynamics. The good solubility and the absence of mesophases in the PPP/S enables the investigation of the isotropic phase in the concentrated regime.

In general the very sharp decrease of the rotational diffusion coefficient of both the fast and the slow VH process can only be accounted by a very strong

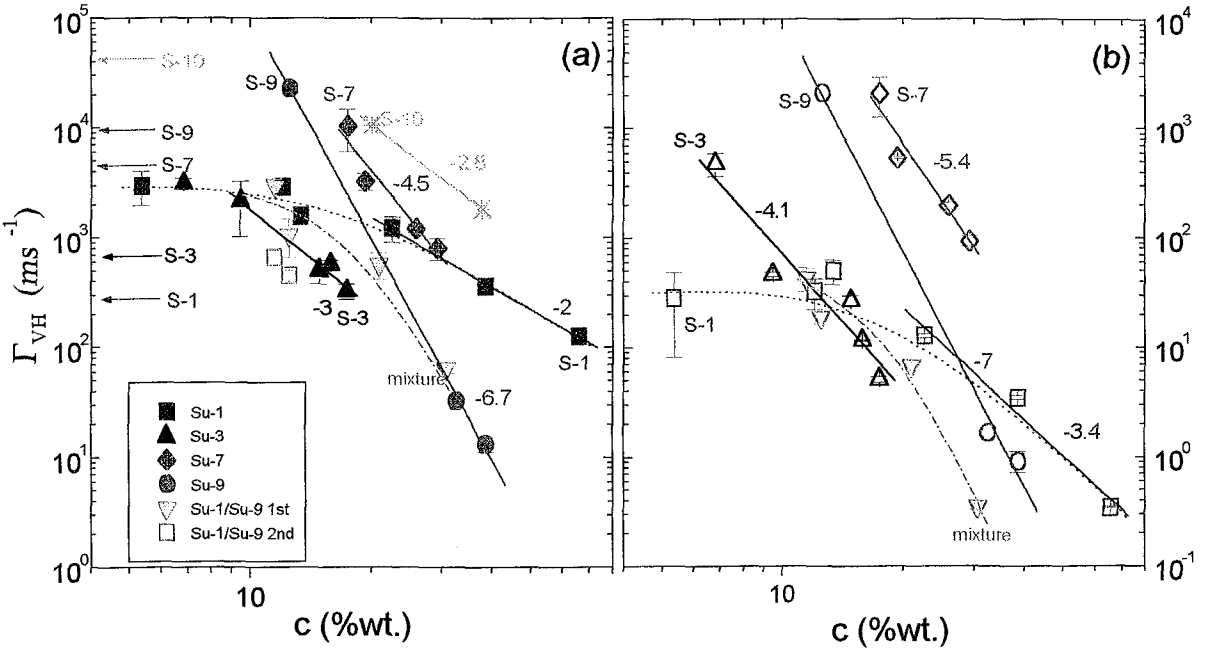

Figure 8.47: Concentration dependence of the two relaxation rates Γ_f (a) and Γ_s (b) obtained from the inversion of the orientation correlation functions. The arrows indicate estimates of the rotational diffusion rate, $6D_{R,0}$ for semistiff chains and -2 is the theoretical prediction for the c-dependence of rigid-rods.

decrease of the parallel translational diffusion which in all models for the rotational diffusion of both rodlike and stiff polymers governs the behavior of the rotational diffusion (see chapter 4). As we discussed in chapter 4, the jamming effect caused by end-to-end collisions predicts a stronger than the DE prediction for D_R, which usually is thought to be small and is described by the term $(1 - D\rho)$in eq. 8.15. The only approach describing this phenomenon that can predict a very strong concentration dependence is the "Hole" theory [46], which predicts an exponential slow down of the longitudinal diffusion of a rodlike (or wormlike) chain with increasing concentration, according to:

$$D_{\parallel} = D_{\parallel,0} \exp(-V_{ex}^{*}\rho) \tag{8.16}$$

where V_{ex}^{*} is the mutual excluded volume between a critical, for the translational movement, hole and one surrounding chain. Such an expression can be used also for describing the sharp increase with concentration of the viscosity.

8.6.2 Fast orientation fluctuations

Based on the q-dependence (Fig. 8.45) of Γ_f and its relationship to η_0, the fast decay in $C_{VH}(q,t)$ can be assigned to the collective rotational motion of the Kuhn segments of the persistent PPP/S chains. In the concentrated regime, this motion is strongly restricted as reflected in the strong c-dependence of Γ_f (Fig. 8.47). The time average correlation between the orientations of neighboring Kuhn segments can persist over a certain distance i.e., the coherence length ξ defining the size of "swarms" [49, 50]. The orientational ordering in the isotropic phase is usually local and I_f is virtually q-independent since $q\xi << 1$. For the present systems, however, Fig. 8.45 reveals a q-dependence for I_f at high concentrations, which cannot adequately be represented by the Ornstein-Zernicke type of orientation correlations [49, 47] $f(r) = \frac{1}{r}\exp(r/\xi)$ predicting $I(q)^{-1} = I(0)^{-1}(1 + q^2\xi^2)$. Instead, $I(q)^{-1/2} = I(0)^{-1/2}(1 + q^2\xi^2)$ which implies Debye-Bueche [47] orientation correlation function $f(r) = exp(r/\xi)$ provides a better description of the experimental I_f (inset of Fig. 8.45).

Among the samples, S-1 and S-3 with the largest length L/l values, as well as the equimolar S-1/S-9 ternary solution, display the strongest q-dependence for I_f which moreover increases with c; for S-1, ξ varies between 30 and 45 nm over the concentration range 11.6 to 66%, whereas for S-3, $\xi = 35$ nm at $c = 17.5\%$. For S-7 and S-9, the rate of decrease of I_f with q is significantly weaker and rather insensitive to concentration variations over the range 15 to 40%. It appears, therefore, that the dynamically more flexible S-1 and S-3 chains (Γ_f in Fig. 8.47a) exhibit orientational fluctuation correlations on the average over a longer distance ($\xi \approx$O(50 nm)) than the shorter S-7 and S-9 with local scale ($\xi < 20$ nm). The orientation fluctuations associated with the fast mode are randomly correlated (in all directions) in space and hence the orientation correlated regions are on the average spherical in space leading to a maximum I_f in the forward ($q = 0$) direction.

The collective orientation fluctuations in dense semiflexible polymer systems (chapter 4) [38]:

$$I_{if}(\mathbf{q},t) =< \sum_{P,Q}^{N} \sum_{l,m}^{n} \boldsymbol{\alpha}_P^l(0)\boldsymbol{\alpha}_Q^m(t) \exp i\mathbf{q} \cdot (\mathbf{r}_Q^m(t) - \mathbf{r}_P^l(0)) > \tag{8.17}$$

appear to decay mainly via rotational motions of the Kuhn segments, and should therefore be insensitive to L variations. The much slower overall rotational motion of the chain, with a rate $D_R(c)$, does not appreciably modify the orientational part of $C_{VH}(q,t)$ (preexponential part of Eq. 8.17), and hence the decay of $C_{VH}(q,t)$ is an insensitive probe of D_R. In fact, the viscoelastic longest relaxation time (e.g., Fig. 8.39) $\tau \approx D_R^{-1}$ is much slower than Γ_f, as already discussed.

8.6.3 Slow orientation fluctuations

The unusual increase of I_s with q indicates another sort of orientation correlations in the nm length scales in concentrated isotropic stiff polymer solutions. A 4-fold clover leaf depolarized light scattering pattern with an off-axis intensity peaks has been reported for crystalline polymers [51, 52, 53], nematic liquid crystalline polymers [39] and more recently in microphase separated diblock copolymers [54]. Suppression of the forward scattering with a peak of the depolarized intensity at finite q_{max} is possible if the optic axis is allowed to vary within two correlated regions i.e. for non random orientation correlations. The average domain size e.g. spherulites [51, 52, 53] distances between disclination lines [39] and ordered grains [54] relates to q_{max} and for these systems is of the order of microns i.e., I_{VH} peaks at very low scattering angle θ_{max} $(0.5 - 2)$.

For the present isotropic PPP/S solutions, I_s (Fig. 8.45) attains no maximum value up to the highest light scattering q ($\approx 0.034\ nm^{-1}$) indicative of the involvement of short sizes, $O(nm)$. Such orientational ordering was inferred from small neutron scattering measurement of the structure factor of isotropic solutions of rigid poly(γ-benzyl-L glutamate) [55]. If we associate I_s with orientationally correlated Kuhn-segment-pairs, the intersegmental distance should determine $q_{max} \approx 2\pi(c/M)^{1/3}$. In this oversimplified picture, the increase of I_s with q should be more pronounced in S-1 than S-9 at similar concentrations and less evident at high c, as for both cases q_{max} shifts to higher values. In fact, these trends are supported by the experimental $I_s(q)$ of the PPP/S solutions (Fig. 8.45).

The reciprocal q-dependences of I_f and I_s (Fig. 8.45) indicate according to the preceding discussion, the presence of preferred local orientational ordering (size $\sim q_{max}^{-1}$) which persists over the coherence length ξ ($> q_{max}^{-1}$). The much slower rate Γ_s reflects the cooperative motion of the correlated Kuhn-segment-pairs. In this structural picture, the unexpected and unusual slowing down of Γ_s with q corroborates the notion that the most probable short wavelength fluctuations are long-lived.

In principle, this effect of interactions is foreseen by the mean field prediction for the dynamic structure factor of concentrated rodlike polymers [14] (see also chapter 4):

$$\begin{aligned} C_{VH}(\mathbf{q},t) &= \frac{1}{\rho LV} < E_{VH}(\mathbf{q},t)E^*_{VH}(\mathbf{q},0) > \qquad (8.18) \\ &= \frac{L}{4\pi}\int_t^\infty dt' \int d\mathbf{u} E_{VH}(\mathbf{q},t)\exp[-\Omega(\mathbf{q})t']\Theta(\mathbf{q}))E^*_{VH}(\mathbf{q},0) \end{aligned}$$

where $s(\mathbf{q},\mathbf{u})$ expresses the intramolecular interference, $E_{VH}(\mathbf{q},t) = \alpha_{VH}(\mathbf{u})s(\mathbf{q},\mathbf{u})$ and $\Omega(\mathbf{q}) = \Theta(\mathbf{q})\Phi(\mathbf{q})$, with $\Theta(\mathbf{q})$and $\Phi(\mathbf{q})$ operators for the translation-rotation

diffusion of the rod and the rod-rod interaction. Thus, since the collective rate $\Omega(q) \sim \Phi(q)$, it appears that the decrease of $\Gamma_s(q)$ with q (Fig. 8.45) is roughly compensated by the increase of $I_s(q)(\propto \Phi(q)^{-1})$. The slower rate Γ_s, as compared to Γ_f, is rationalized by the larger size of the correlated Kuhn-segment pairs, whereas its steeper c-dependence (Fig. 8.47) resembles the disparity in the variation of the associated intensities I_s and I_f (inset of Fig. 8.46) with c. This relationship is dictated by the collective nature of both processes and is more pronounced for the shortest S-9.

8.7 Conclusions on the Dynamics

The dynamics of concentration and orientation fluctuations of three series of PPP's was probed with polarized and depolarized PCS from dilute to highly concentrated regime ($c = 0.5-1400c^*$) in different solvents [41, 56, 57, 58]. The fact that in PPP/S which was highly soluble no nematic transition was observed enabled us to investigate the dynamics of these stiff molecules in unreachable, so far, high concentrations of isotropic solutions. In these samples, the cooperative diffusion $D_{c=0}$ identifies with the translational diffusion of the molecules and conforms with theoretical predictions while the rotational diffusion $D_{R,c=0}$ (extrapolated from the semidilute region) conforms with chains of smaller size, revealing the importance of internal bending motions in the depolarized light scattering. In addition in the PPP/S series with samples in a broad range of molecular weights, D_c is found to depend on M_w in both the dilute regime (revealing the stiff nature of the chain) and in the semidilute and concentrated regime in contrast to the observed behavior of flexible polymers.

The cooperative diffusion coefficient is found to increase in all samples studied while its intensity reveals a broad maximum with concentration. Quantitatively these reflects to a $(D_c/D_0 - 1) \sim c^{0.72-0.9}$ at the semidilute regime (depending on the molecular weight) a result intermediate between the prediction for flexible ($c^{0.75}$) and rodlike (c^1) polymers; the latter however involves unsafe assumptions which we discuss. Moreover in the concentrated regime ($c/c^{**} > 5$) D_c increases less strongly with c revealing strong frictional effects. At the same time the osmotic modulus $(\partial\pi/\partial c)_{T,p}$ is found to scale with $c^{0.75-1.4}$ depending on M_w. The cooperative friction coefficient deduced from light scattering I_c and D_c is found to be different from the self-diffusion friction deduced from NMR data. The latter reveals a self-diffusion coefficient D_s which decreases with concentration.

In PPP/S samples where aggregation is minimum an second, weaker, diffusive process is found in the polarized correlation function. It has a weakly increasing diffusion coefficient and a constant intensity with concentration. We have excluded the possibility of a polydispersity induced self-diffusion mode by measurements in a mixture of molecular weights. Moreover these two cooperative relaxation modes does not seem to conform with the mean field predictions for

rigid rods near the nematic transition, although they might be of the same nature.

The VH correlation functions revealed rich orientational dynamics with some highly unusual findings. Two distinct VH process are found systematically related with the molecular orientational fluctuations in PPP/S and PPP-12 samples. The fast process is related with the cooperative reorientational movements of the parts of the stiff chain of the size of the Kuhn segments and reveals an increasing with concentration correlation length ξ for the decay of orientation fluctuations. The slow mechanism is characterized by a decay rate which slows down unusually at high q and posses an increasing with q intensity. In view of the absence of any theory for the depolarized light scattering of semistiff polymers in the concentrated regime, and based on the phenomenology of the slow VH mode as well as similar findings in other systems we may relate this mode with the correlated reorientation of Kuhn-segment-pairs with preferred local orientational ordering (size $\sim q_{max}^{-1}$) which persists over the coherence length ξ ($> q_{max}^{-1}$). In this structural picture, the unexpected and unusual slowing down of Γ_s with q corroborates the notion that the most probable short wavelength fluctuations are long-lived. Another important finding is the very strong concentration dependence of the rotational diffusion coefficients of both the fast and the slow mode. The fast rotational diffusion, $D_{R,f}$ is found systematically to decrease weaker than the slow mode $D_{R,s}$, both of them scale with c^{-x} much faster than the Doi-Edwards scaling prediction ($x = 2$) or the slightly steeper concentration dependence that theories which take into account end-to-end collision and finite diameter effects predict. In our experiments x ranges from 2 to 7 at high concentrations ($20 < c/c^* < 1400$) and prove how much the rotational diffusion can be slowed down in solutions of stiff polymers. Moreover, the larger M_w samples systematically exhibit weaker concentration dependence, implying that flexibility is more of dynamic rather than static nature. These strong concentration dependence of the rotational diffusion, which is also consistent with a high concentration dependence of the zero-shear viscosity in aggreement with theories relating the two quantities, can be only rationalized with the prediction of "hole" theory for an exponentially decreasing parallel diffusion $D_{\parallel}$ which is reflected to both the rotational diffusion and the zero-shear viscosity. These results provide important hints for the formulation of theories on the dynamics of such anisotropic systems.

References

[1] H. Witteler. PhD thesis, Mainz, Germany, 1993.

[2] P. Galda and M. Rehahn. *Synthesis*, page 614, 1996.

[3] M. Rehahn, A.D. Schluter, and G. Wegner. *Makromol. Chem.*, 191:1991, 1990.

[4] G. Petekidis, D. Vlassopoulos, P. Galda, M. Rehahn, and M. Ballauff. *Macromolecules*, 29:8948, 1996.

[5] G. Petekidis, D. Vlassopoulos, G. Fytas, N. Kountourakis, and S. Kumar. *Macromolecules*, 30:919, 1997.

[6] T. Sato, Y. Takada, and A. Teramoto. *Macromolecules*, 24:6262, 1991.

[7] K.S. Schmitz. *Dynamic Light Scattering by Macromolecules.* Academic Press, London, 1990.

[8] M. Fixman. *Phys. Rev. Letters*, 55:2429, 1985.

[9] I. Bitsanis, H.T. Davis, and M. Tirrell. *Macromolecules*, 23:1157, 1990.

[10] K. Zero and R. Pecora. *Macromolecules*, 15:87, 1982.

[11] L. M. DeLong and P. S. Russo. *Macromolecules*, 24:6139, 1991.

[12] M. Doi, T. Shimada, and K. Okano. *J. Chem. Phys.*, 88:4070, 1988.

[13] T. Maeda. *Macromolecules*, 22:1881, 1989.

[14] T. Maeda. *Macromolecules*, 23:1464, 1990.

[15] Y. Mori, N. Ookubo, R. Hayakawa, and Y. Wada. *Journal of Polymer Science:Polymer Physics Edition*, 20:2111, 1982.

[16] P.G. de Gennes. *Scaling Concepts in Polymer Physics.* Cornell University Press, Ithaca, 1979.

[17] L.S. Onsager. *Ann. N.Y. Acad. Sci.*, 51:627, 1949.

[18] T. Shimada, M. Doi, and K. Okano. *J. Chem. Phys.*, 88:2815, 1988.

[19] Y. Jinbo, T. Sato, and A. Teramoto. *Macromolecules*, 27:6080, 1994.

[20] M.A. Tracy and R. Pecora. *Annu. Rev. Phys. Chem.*, 43:525, 1992.

[21] S.P Russo. *Dynamic Light Scattering: The Technique and Some Applications*, page 512. Oxford Science Publications, 1993.

[22] A. Ishihara and T. Hayashida. *J. Phys. Soc. Japan.*, 6:40, 1951.

[23] T. Coviello, W. Burchard, M. Dentini, and V. Crescenzi. *Macromolecules*, 20:1102, 1987.

[24] R. Seghroushni, G. Petekidis, D. Vlassopoulos, G. Fytas, A.N. Semenov, J. Roovers, and G. Fleisher. *submitted to Europhysics Lett.*, 1997.

[25] G. Merkle, W. Burchard, K.F. Freed, and J. Gai. *Macromolecules*, 26:2736, 1995.

[26] J. Seils and R. Pecora. *Macromolecules*, 28:661, 1995.

[27] L. Wang, M. M. Garner, and H. Yu. *Macromolecules*, 24:2368, 1991.

[28] W. Richtering, W. Gleim, and Burchard W. *Macromolecules*, 25:3795, 1992.

[29] P.N. Pusey and R.J.A. Tough. *Dynamic Light Scattering, Applications of Photon Correlation Spectroscopy*, page 85. Plenum Press:New York and London, 1985.

[30] J. Buitenhuis, J.K.G. Dhont, and H.N.W. Lekkerkerker. *Macromolecules*, 27:7267, 1994.

[31] T. Jian, S.H. Anastasiadis, A.N. Semenov, G. Fytas, G. Fleisher, and A.D. VIlesov. *Macromolecules*, 28:2439, 1995.

[32] B. Chu. *The Scattering of Light and Other Electromagnetic Radiation.* Academic Press, New York, 1969.

[33] M. Benmouna, Duval M. Benoit, H., and Z. Akcasu. *Macromolecules*, 20:1107, 1987.

[34] P. Zhou and Brown W. *Macromolecules*, 23:1131, 1990.

[35] Z. Bu, P.S. Russo, D.L. Tipton, and I.I. Negulescu. *Macromolecules*, 27:6871, 1994.

[36] S.F. Edwards and K.E. Evans. *Trans.Faraday Soc.*, 78:113, 1982.

[37] T. Sato and A. Teramoto. *Macromolecules*, 24:193, 1991.

[38] J.B. Berne and R. Pecora. *Dynamic Light Scattering.* Willey Interscience Publications, New York, 1976.

[39] T. Hashimoto, A. Nakai, T. Hasegawa, S. Rogaczer, and R.S. Stein. *Macromolecules*, 22:422, 1989.

[40] F. Greco. *Macromolecules*, 22:4622, 1989.

[41] G. Petekidis, G. Fytas, and H. Witteler. *Colloid Polym. Sci.*, 272:1457, 1994.

[42] H. Yamakawa and M. Fujii. *Macromolecules*, 6:407, 1973.

[43] S. Broesma. *J. Chem. Phys.*, 32:1626, 1960.

[44] S. Broesma. *J. Chem. Phys.*, 74:6989, 1981.

[45] M.M. Tirado, C.L. Martinez, and J.G. de la Torre. *J. Chem. Phys.*, 81:2047, 1984.

[46] T. Sato and A. Teramoto. *Adv. Pol. Sci.*, 126:85, 1996.

[47] H. Benoit and J.S. Higgins. *Polymers and Neutron Scattering.* Oxford Science Publications, Oxford, 1994.

[48] N.B. Boudenne, S.H. Anastasiadis, G. Fytas, M. Xenidou, N. Hadjichristidis, A.N. Semenov, and G. Fleisher. *Phys. Rev. Letters*, 77:506, 1996.

[49] P.G. de Gennes. *The Physics of Liquid Crystals.* Clarendon Press, Oxford, 1974.

[50] T.W. Stinson and J.D. Lister. *Phys. Rev. Letters*, 30:668, 1973.

[51] R.S. Stein and S.N. Stidham. *J. App. Phys.*, 35:42, 1964.

[52] P. Debye and S.N. Stidham. *J. App. Phys.*, 30:518, 1949.

[53] R.S. Stein, P.F. Ehardt, S.B. Clough, and G. Adams. *J. App. Phys.*, 37:3980, 1966.

[54] M.C. Newstein, B.A. Garetz, H.J. Dai, and N.P. Balsara. *Macromolecules*, 28:4587, 1995.

[55] N. J. Wagner, L. M. Walker, and B. Hammouda. *Macromolecules*, 28:5075, 1995.

[56] G. Petekidis, D. Vlassopoulos, G. Fytas, and G. Fleischer. *Macromolecules in press*, 1997.

[57] G. Petekidis, D. Vlassopoulos, G. Fytas, R. Rulkens, and G. Wegner. *in preparation*, 1997.

[58] G. Petekidis, D. Vlassopoulos, G. Fytas, R. Rulkens, G. Wegner, and G. Fleisher. *in preparation*, 1997.

Chapter 9

Molecular Orientation in Films of Stiff Polyesters

It is well known that molecular orientation in polymers, induced for example by drawing, results in ultra-high modulus materials (usually fibers or films) [1]. This important and highly desired property is a manifestation of the intrinsic stiffness of polymer chains, and is therefore particularly pronounced in semi-crystalline and liquid crystalline polymers [2]. The latter, in particular, exhibit significant chain rigidity and might lead to specific moduli comparable to that of steel; consequently, they are extremely interesting materials in terms of industrial applications [3]. This enormous potential of oriented polymers has created the need to accurately characterize the degree of molecular orientation in both the bulk and films, under various processing conditions. Several experimental techniques have been applied to this end [2, 4, 5], including birefringence, X-ray diffraction and scattering [6, 7], infra-red dichroism [8, 9], fluorescence polarization, NMR, dynamic mechanical thermal analysis (DMTA), Raman scattering [10], and more recently polarization-modulation methods (infra-red dichroism [11] or Raman [12, 13]). These techniques have been applied extensively to a number of flexible polymers such as polyethylene [14], polypropylene [6, 7, 15], poly(vinyl chloride) [16, 17, 18], poly(ethylene terephthalate) [19], polystyrene [20], poly(methyl methacrylate) [10], as well as flexible polymer blends [21, 22]. The key message from these investigations is that molecular orientation in flexible polymers (amorphous or semicrystalline) can be determined unambiguously, and thus the effects of deformation (e.g. drawing) on the material's final properties can be assessed.

A special note should be made for the Raman spectroscopy; in addition to its potential (like other techniques) to provide independent information on the average molecular orientation of both amorphous and crystalline phases in a semicrystalline polymer, it enables independent determination of the second as well as the fourth moments of the orientation distribution function; the former is defined as $< P_2(cos\theta) >= [3 < cos^2\theta > -1]/2$ and will be referred to as

P_2 , whereas the latter is defined as $< P_4(cos\theta) >= [35 < cos^4\theta > -30 < cos^2\theta > +3]/8$ and will be referred to as P_4. Both parameters are necessary in order to fully determine the orientation distribution function and to understand the mechanical properties of oriented polymers in terms of molecular models. Moreover, Raman scattering does not impose any geometrical restrictions on the test specimens (as for example, infra-red dichroism does). On the other hand, the analysis of the Raman data is somehow ambiguous and certainly requires a good knowledge of the molecular structure of the system under investigation, and a large number of experiments for each orientation (P_2,P_4) data point. In that respect Fourier transform infra-red (FTIR) spectroscopy and wide angle X-ray diffraction (WAXD) are quite useful. Both are more straightforward in the analysis and require much less experimental effort, as it will become evident later; but FTIR provides information only on P_2, whereas the determination of P_4 from WAXD is rather cumbersome.

Orientation phenomena in liquid crystalline polymers have also received a great deal of attention, due to their great potential for industrial applications, mainly the ones associated with fibers and films. Infrared spectroscopy, X-ray diffraction and DMTA have been the techniques of choice for these materials [23, 24]. It is clear that these materials orient much more effectively than their flexible counterparts, but again two types of oriented areas, namely liquid crystalline and isotropic may be present, depending on the material's liquid crystalline phase behavior. Several investigators have addressed the effects of draw ratio and geometry. Most of the literature data refer to film or bulk measurements; the former were performed in order to assess the surface-induced orientation [25]. However, no complete analysis of the distribution of molecular orientation has been carried out to date. This is striking, especially if one considers the widespread applicability of these materials. Further, it should be noted that a complete and detailed quantitative analysis of the molecular orientation of low-molecular weight liquid crystalline phases, based on Raman scattering measurements, has been performed several years ago [26]; however, Raman scattering has not been used to date to the study of polymeric liquid crystals.

In this study, laser Raman spectroscopy, FTIR spectroscopy and WAXD have been utilized in order to quantitatively determine the degree of molecular orientation in uniaxially oriented liquid crystalline films of polyesters a function of the draw ratio. The films were produced by solution casting of the polyester in chloroform at room temperature, and subsequent drawing at high temperatures and various draw ratios. Results of the combined information concerning the second and fourth terms of the expansion of the orientation distribution function is very important for the understanding the film's molecular orientation. Moreover, it can serve as an important ingredient of theoretical approaches addressing the effect of draw ratio on the polymer orientability. It is shown that both P_2 and P_4 increase with draw ratio, but with a rapidly decreasing slope leading towards a plateau. The analysis leading to the determination of these moments,

as well as the components of the Raman tensor, is based on the theory of Bower for uniaxially oriented polymers, and results in a system of five nonlinear algebraic equations, which is rather ambiguous to solve, leading to several alternative physically meaningful values of P_2 and P_4. In order to avoid these difficulties, an effort had been made to better understand the molecular system under investigation. This led to the choice of a specific Raman frequency for the investigation of the bond orientation. The latter was accomplished by introducing some important assumptions concerning the Raman tensor and the system under study, and resulted in a simple and straightforward method to determine the orientation distribution functions. Results and their ramifications are discussed both qualitatively and quantitatively in view of the corresponding FTIR and WAXD data on the same polyesteric films, their practical applicability, as well as the existing evidence in the literature. The two latter techniques provide valuable information and help determining the effect of liquid crystallinity on chain orientation, and distinguishing between large-scale domain orientation and molecular-level orientation. It is shown that the polyesteric films orient very effectively at relatively low draw ratios (compared to the flexible polymers). The combination of the techniques used represents a very powerful tool for a complete quantitative characterization of the molecular orientation in liquid crystalline polymers.

This chapter is organized as follows: Section 2 describes the materials and the three experimental techniques utilized. The results and a thorough analysis and discussion are presented in section 3. Finally, the main conclusions are summarized in section 4.

9.1 Experimental Section

9.1.1 Materials

In this study a model polyester with hexyl side chains similar to the one used in the conformation study (chapter 5) [27] was used and coded as PES 3:3/C6.Its chemical structure is shown schematically in figure 9.1. Its molecular weight was determined to be about 35000, based on intrinsic viscosity measurements [28]. The polymer was dissolved in chloroform, at concentrations in the range of 3% to 6% by weight. Prior to film casting, the solution was filtered on a Teflon filter ($5\mu m$ pore size) to remove dust particles. Solutions were then cast on a glass plate at room temperature with $1000\mu m$ blades [28]. Films of nearly uniform thickness (of about $30 \pm 2\mu m$) were obtained after evaporation of the solvent. Uniaxially oriented films were obtained by drawing the PES 3:3 / C6 cast films in an oven at a temperature of about $270°C$. The temperature was controlled by passing preheated dry nitrogen gas through the oven. The standard drawing speed was $2cm/min$, and the specimen length and width before drawing were $5cm$ and $1cm$, respectively. The draw ratios achieved were between 1.5 and 3.1.

Even by varying the temperature and drawing speed, it was not possible to obtain films at higher draw ratio, due to breaking [24].

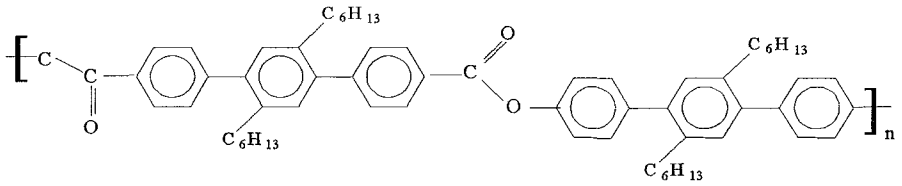

Figure 9.1: Molecular structure of polyester PES 3:3/C6.

9.1.2 Laser Raman Scattering

The Raman scattering set up is described in chapter 5. The polymer film specimen is positioned mechanically at a special stage that can rotate by 360°. Measurements were carried out at three different geometries of the incident laser beam with respect to the drawing direction of the film specimens and the polarization direction (fig. 9.2). In the first geometry, the drawing direction was perpendicular (90°) to the direction of the incident laser beam; in the second one, it was parallel (0°); and finally, in the last one it was at 45° with respect to the incident laser beam. The reason for choosing this variety of geometries is related to the need to obtain specific values of the scattered radiation (as function of the above angle and polarization direction), as dictated by the theoretical requirements for the quantitative determination of the molecular orientation; this will become apparent below, and has been addressed in the literature as well [29, 30].

9.1.3 FTIR Spectroscopy

Infrared spectra were measured in the transmission mode on a Bruker vacuum spectrometer (IFS 113v). The sample was mounted with its plane perpendicular to the incident infrared beam. A KRS-5 wire-grid polarizer was positioned before the sample to polarize the infrared radiation. The polarizer remained fixed and the sample was rotated by 90° in order to obtain transmission spectra with different polarization directions. The transmission spectrum of the polarizer was measured using the same instrument settings, and was employed as the reference spectrum. All spectra were measured at room temperature and represent the average of 200 scans at 2 cm^{-1} resolution.

The FTIR measurements were contacted by Dr. E.I. Kamitsos in the Institute of Theoretical and Physical Chemistry of the National Hellenic Research Foundation in Athens.

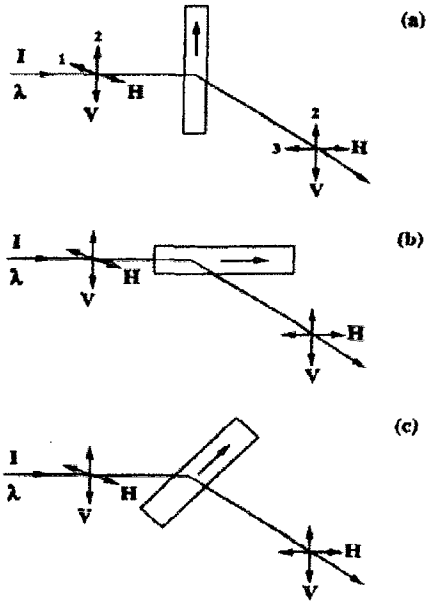

Figure 9.2: Characteristic scattering geometries for the Raman spectroscopic measurements: (a): perpendicular position of specimen, corresponding to 90^o angle between incident laser beam and macroscopic drawing direction; (b) horizontal position of specimen, corresponding to 0^o angle between incident laser beam and macroscopic drawing direction; (c): diagonal position of specimen, corresponding to 45^o angle between incident laser beam and macroscopic drawing direction. V and H represent the vertical and horizontal polarization to the scattering plane, respectively, of the incident or scattered laser radiation. Numbers $1-3$ refer to the coordinate system of the Raman tensor.

9.1.4 WAXD

Oriented film diffractograms were recorded in transmission mode using Ni-filtered radiation (flat film, sample to film distance 6 cm). For determining the degree of orientation, a procedure according to Crevecoeur23 was used. The azimuthal intensity distribution $I(\theta)$ of the most intense (100) equatorial reflection was established with an ENRAF-Nonius densitometer, via radial scans with a varying step size of 1 to 5 degrees. Air scattering was substracted after recording a blank diffractogram, and the constant intensity level at high azimuthal angles was taken as material background scattering and was substracted from the intensity profile.

The WAXD measurements were done by Mr. A. Bruggeman in the TNO Plastics and Rubber Research Institute in Delft, Netherlands.

9.2 Results and Discussion

9.2.1 Raman spectra

Spectra from the PES 3:3/C6 polyesters at various draw ratios λ (1.5, 2, 2.4, 2.6, 2.8, 3.1) and different polarization geometries (VV, VH, HV, HH) were obtained. Results for $\lambda = 2.4$ and for the three angles 90^o, $0^o$and 45^o are depicted in figures 2, 3 and 4, respectively. Looking at the spectra of figure 2, it becomes apparent that the peaks are much more pronounced in the VV mode rather than in the HV and HH modes; this means that vibrations along the direction of stretching are much stronger than in the other directions, and suggests a significant degree of molecular orientation along the stretching direction. Analogous observations hold for figure 3, where vibrations in the HH mode are more pronounced, while in and figure 4 the intensity of each band remains quite unaffected by changing polarization geometries.

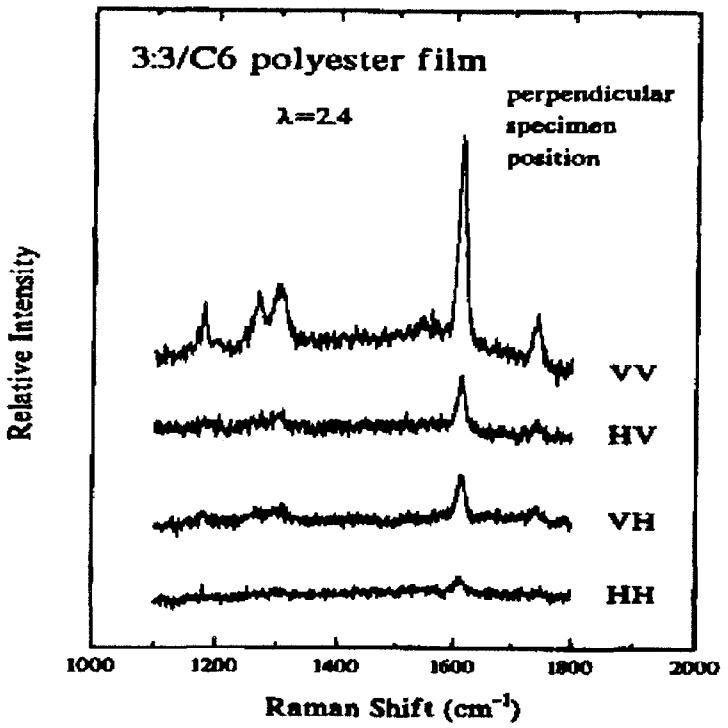

Figure 9.3: Raman spectra of the PES 3:3 / C6 polyester film with perpendicular specimen position and $\lambda = 2.4$.

In order to determine the degree of molecular orientation, it is important to focus our attention to a specific Raman band. This was chosen as the $1616cm^{-1}$

band, mainly for two reasons:

(i) this band is strong and well-resolved, and therefore its intensity can be determined accurately; and

(ii) it is a well-known Raman band, attributed to the $C = C$ stretching mode in the $C_1 - C_4$ direction of the benzene ring [31, 32].

This direction can vary as much as 6^o with respect to the main axis of the macromolecule, as it will be discussed later. This peak assignment is of crucial importance for the determination of P_2 and P_4, as it will become apparent below. Therefore, in the remaining of the paper the analysis of the Raman scattering intensities will refer to the $1616cm^{-1}$ line. It is now clear how one can estimate the direction of molecular orientation of the polyester films from figures 2-4 discussed above.

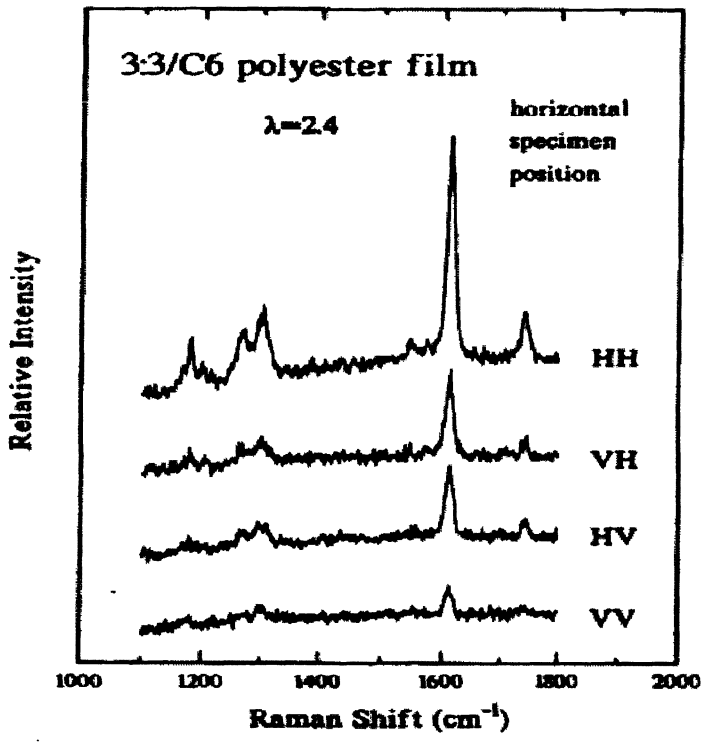

Figure 9.4: Raman spectra of the PES 3:3 / C6 polyester film with horizontal specimen position and $\lambda = 2.4$.

An important implication from these experiments is the determination of the effect of draw ratio on the orientability of the polyester films. This effect is manifested in figure 5, which represents VV and HV Raman spectra at various draw ratios, λ, for the vertical sample geometry (figure 1a). One can clearly observe a progressive change of the relative Raman intensities as the draw ratio

varies. Since the depolarization ratio ($\sigma = I_{HV}\,/I_{VV}$) is related to the orientation of the films, one can in principle use the linear-linear plot in figure 6, in order to determine the effect of λ in inducing orientation. This is truly apparent, since the slope of σ versus λ decreases substantially at the high values of draw ratio; for a perfectly oriented material we expect the slope to approach zero.

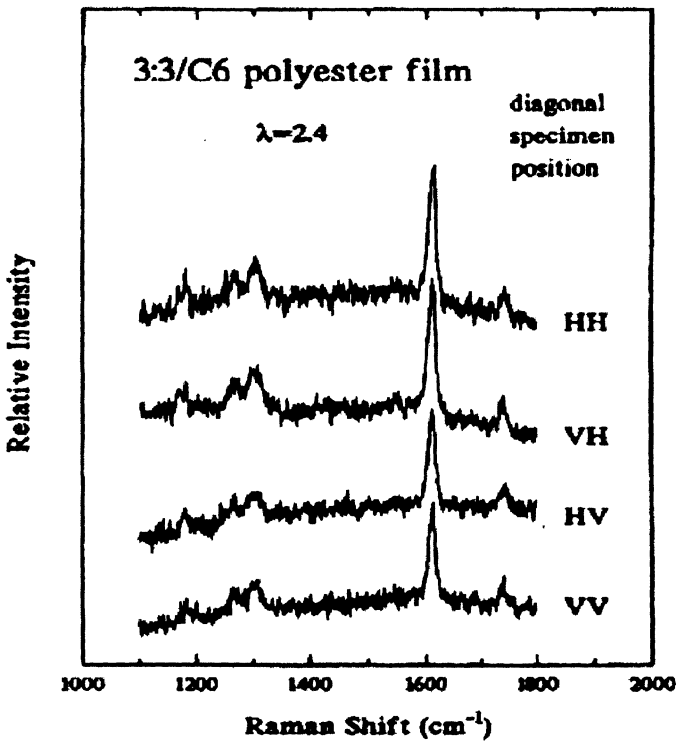

Figure 9.5: Raman spectra of the PES 3:3 / C6 polyester film with diagonal specimen position and $\lambda = 2.4$.

In order to quantify the molecular orientation, we adopt the analysis of Pigeon et al [29, 30], which is actually a special case of that of Kamitsos and Risen [33]; they are based on the theory of Bower [34], who has determined the molecular orientation in polyethylene films from their Raman spectra. Here we summarize the important points of the analysis. The total Raman scattering intensity I_s is given by

$$I_s = I_0 \sum_N (\sum_{i,j} I_i I'_j a_{ij})^2 \tag{9.1}$$

where I_0 is a constant depending on instrumental factors and the incident light intensity, a_{ij} are the components of the Raman tensor, i, j (each taking values from 1 to 3) refer to axes fixed in the sample, and I_i and I_j are the directions

cosines, which define, respectively, the polarization direction of the incident and scattered light with respect to the axes of the test sample. Summations inside the parenthesis are carried out over all i's and j's, whereas outside the parenthesis represent contribution of all scattering units, N, to the measured intensity. The experimental values are of the form $I_0 \sum a_{ij}\ a_{pq}$, where each a_{ij} can be expressed as a linear combination of the principal components α_1, α_2, and α_3 of the Raman tensor of the vibration investigated and the Euler angles defining the orientation of the principal axes of the tensor with respect to the axes of the sample. By assuming uniaxial symmetry with no preferred orientation around the main molecular axis, one can write:

$$\sum_{i,j,p,q} a_{ij}a_{pq} = 4\pi^2 N \sum_{l=0,2,4} M_{l00}A_{l00}^{ijpq} \tag{9.2}$$

where N is the number of structural units contributing to the Raman intensity and A_{l00}^{ijpq} is a sum of quadratic terms in α_1, α_2, and α_3, previously tabulated by Bower [34]. M_{l00} is expressed in terms of Legendre polynomials: $M_{l00} = 1/4\pi^2\{(2l+1)/2\}^{1/2} < P_l(cos\theta) >$. Under the above assumptions of uniaxial symmetry of the samples, the problem of determining the orientation moments P_l is reduced to a system of five nonlinear algebraic equations for the Raman scattering intensity

$$\begin{aligned} I_0\sum a_{22}^2 &= b[(3a_1^2+3a_2^2+3+2a_1a_2+2a_1+2a_2)/15 \\ &\quad +P_2(3a_1^2+3a_2^2-6+2a_1a_2-a_1-a_2)/21 \\ &\quad +3P_4(3a_1^2+3a_2^2+8+2a_1a_2-8a_1-8a_2)/280] \end{aligned} \tag{9.3}$$

$$\begin{aligned} I_0\sum a_{33}^2 &= b[(3a_1^2+3a_2^2+3+2a_1a_2+2a_1+2a_2)/15 \\ &\quad -2P_2(3a_1^2+3a_2^2-6+2a_1a_2-a_1-a_2)/21 \\ &\quad +P_4(3a_1^2+3a_2^2+8+2a_1a_2-8a_1-8a_2)/35] \end{aligned} \tag{9.4}$$

$$\begin{aligned} I_0\sum a_{21}^2 &= b[(a_1^2+a_2^2+1-a_1a_2-a_1-a_2)/15 \\ &\quad +P_2(a_1^2+a_2^2-2-4a_1a_2+2a_1+2a_2)/21 \\ &\quad +P_4(3a_1^2+3a_2^2+8+2a_1a_2-8a_1-8a_2)/280] \end{aligned} \tag{9.5}$$

$$\begin{aligned} I_0\sum a_{32}^2 &= b[(a_1^2+a_2^2+1-a_1a_2-a_1-a_2)/15 \\ &\quad -P_2(a_1^2+a_2^2-2-4a_1a_2+2a_1+2a_2)/42 \\ &\quad -P_4(3a_1^2+3a_2^2+8+2a_1a_2-8a_1-8a_2)/70] \end{aligned} \tag{9.6}$$

$$
\begin{aligned}
I_0 \sum a_{22}a_{33} &= b[(a_1^2 + a_2^2 + 1 + 4a_1a_2 + 4a_1 + 4a_2)/15 \\
&\quad -P_2(a_1^2 + a_2^2 - 2 + 10a_1a_2 - 5a_1 - 5a_2)/42 \\
&\quad -P_4(3a_1^2 + 3a_2^2 + 8 + 2a_1a_2 - 8a_1 - 8a_2)/70]
\end{aligned} \tag{9.7}
$$

where $b = I_0 N a_3^2$, $a_1 = \alpha_1/\alpha_3$, $a_2 = \alpha_2/\alpha_3$, and $P_2 =< P_2(cos\theta) >$ and $P_4 =< P_4(cos\theta) >$, as already mentioned. Tensor indices i, j refer to polarization of incident and scattered laser beam, respectively, which are also reflected in figure 1: Incident: H $\leftrightarrow$ 1; V $\leftrightarrow$ 2; scattered: H$\leftrightarrow$ 3; V$\leftrightarrow$ 2. The intensities at the left-hand-side of equations (2)-(6) can be obtained experimentally by measuring the Raman spectra at various combinations of polarization geometries and angles (γ') between molecular axes and laboratory-fixed reference frame (vertical, horizontal, diagonal). Spectra for the same $I_0 \sum a_{22}^2$, $I_0 \sum a_{33}^2$, $I_0 \sum a_{21}^2$, $I_0 \sum a_{32}^2$, respectively, were averaged in order to improve the accuracy of the measurements and minimize birefringence effects [29]; they were obtained by using $\gamma' = 0^o$ and 90^o. A special note shioild be made for the $I_0 \sum a_{22}a_{33}$ spectrum. This spectrum could not be measured directly, and it was calculated from other spectra ($I_0 \sum a_{22}^2$ and $I_0 \sum a_{33}^2$) and the HV spectra at $\gamma' = 45^o$. The latter involve some inaccuracy due to the potential birefringence problems which are likely to occur at 45^o. Nevertheless, in similar studies of PET orientation, it was shown [35] that the $1616cm^{-1}$ Raman band is only slightly affected by the birefringence, and thus the error involved in our measurements is considered small.

As already mentioned in the Introduction, attempts to solve the equations numerically revealed several problems, due to the fact that several acceptable solutions could be obtained, depending on the choice of initial conditions [29, 30]. This represents a nontrivial problem that cannot be resolved satisfactorily only by mathematical means; it is also imperative to impose the right physical restrictions on the system under investigation, i.e. to understand the structure of the molecular chain and the assignment of Raman lines. To this end a number of crucial boundary values and assumptions have been taken into consideration:

(a) Limiting values of the variables were chosen. In particular, $0 < P_2 < 1$, and $-0.39 < P_4 < 1$ [36] (actually one expects $P_4 > 0$, but a negative value of P_4 is physically meaningful, suggesting no preferred orientation around the draw direction). Further, the parameter b should be always positive, as implied by the analysis above.

(b) The $1616cm^{-1}$ line of the benzene ring vibration ($C_1 - C_4$) was used in our calculations,for the following reasons: (i) it is the strongest aline in the Raman spectrum, (ii) it occurs as an isolated and well localized line in the Raman spectrum of para-disubstituted benzene ring, with very small changes of frequency observed in a variety of related "model" compounds [37, 38], as also confirmed by vibrational calculations [37] and, (iii) is not directly affected by conformational changes and it is expected to give a reliable indication of the overall chain

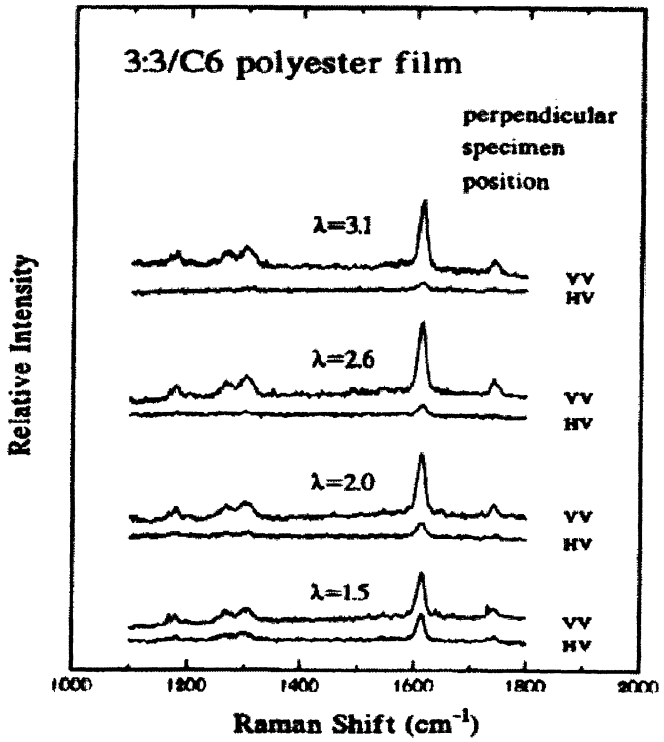

Figure 9.6: Raman spectra of the PES 3:3 / C6 polyester film with perpendicular specimen position, at several draw ratios (1.5 – 3.1)

orientation [?]. Thus it is very likely that one of the principal components of the Raman tensor coincides with the chain axis for this vibration (the deviation, estimated to be about 6^0 [28] is considered very small, since it does not change the resulting P_2 values significantly). Finally, and most importantly, symmetry considerations mentioned below are crucial to the choice of this specific Raman band.

(c) The Raman tensor of the $1616cm^{-1}$ line was assumed cylindrical, i.e. $a_1 = a_2$; this means that the two components of the polarizability tensor perpendicular to the plane of the ring, and perpendicular to the $C_1 - C_4$ direction are of the same sign and magnitude. Due to symmetry considerations, this assumption is viewed as legitimate; moreover, it was also justified in numerous studies of PET reported in the literature [31, 32, 35]; in particular in ref. 25 is important, since it clearly shows that a comparison of orientation moments calculated with and without the assumption of uniaxial Ramn tensor leads to the conclusion the assumption is reasonable.. Since the above is true, for an angle between the $C_1 - C_4$ direction in the benzene ring and the chain axis direction of about 19^o [31] it is safe to make the same assumptions for the 6^o case.

Draw Ratio	1.5	2.0	2.4	2.6	2.8	3.1
P_2	0.19	0.42	0.54	0.56	0.66	0.68
P_4	-0.30	0.06	0.20	0.21	0.21	0.37

Table1: P_2 and P_4 values determined from Raman scattering measurements (1616 cm^{-1}).

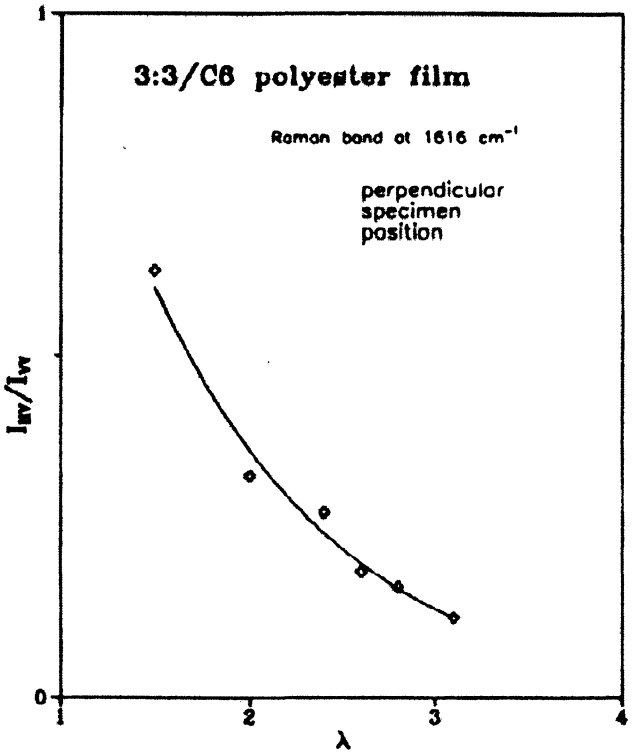

Figure 9.7: Experimental Raman depolarization ratio (I_{HV}/I_{VV}) of the PES 3:3 / C6 polyester film, as a function draw ratio. The line is drawn to guide the eye.

Using the above considerations, it is straightforward to simplify the original system of five equations and end-up with:

$$P_2 = \frac{(-x^2 - 2x)M - 1 + 4x}{(-x^2 + x)M - 4 + 4x} \tag{9.8}$$

$$P_4 = \frac{(8x^2 - 16x + 8)Q - 64x^2 - 32x - 24}{(8x^2 - 16x + 8)(2 + Q)} \tag{9.9}$$

$$b = \frac{f}{\frac{8x^2+4x+3}{15} + P_2\frac{8x^2-2x-6}{21} + P_4\frac{24x^2-48x+24}{280}} \tag{9.10}$$

where

$$M = \frac{8h - g}{k - w} \tag{9.11}$$

$$Q = \frac{2f + g}{2k + h} \tag{9.12}$$

and f, g, h, k, l are the experimental Raman scattering intensities (as functions of γ' and polarization), $I_0 \sum a_{22}^2$, $I_0 \sum a_{33}^2$, $I_0 \sum a_{21}^2$, $I_0 \sum a_{32}^2$ and $I_0 \sum a_{22} a_{33}$ respectively. Further, $x = a_1$ (under the assumption $a_1 = a_2$) and is determined from the depolarization ratio, σ, of the isotropic sample [10, 35]:

$$\sigma = (1 - x)^2 / [8x^2 + 4x + 3] \tag{9.13}$$

Results based on the above simplified approach are presented in table 1. A few remarks are in order: First of all, it is noted that the negative value P_4 at $\lambda = 1.5$ can be explained as in ref. 29, i.e., it corresponds to a distribution of particular draw ratio the distribution o $C_1 - C_4$ vibrations (also considered as main-chain orientation direction) in which all chain axes lie on a cone of angle a such that $P_2(cosa) = P_2$. As seen in table 1, the results follow the right qualitative trend, as suggested by figure 6, and are also in quantitative agreement with orientation results on similar systems [9, 25]. This represents a first qualitative test of the reliability of the above approach for analyzing the Raman data and determining the molecular orientation. It should be also noted that the values of P_4 fall within the acceptable range for a given P_2 value, according to the analysis of Bower [36] for uniaxially oriented polymers; this represents another confirmation of the consistency of the methodology employed here.

9.2.2 Infrared Spectra

The usefulness of the FTIR absorption measurements in determining molecular orientation originates from the fact that the infrared absorption of a characteristic group of the polymer is given by:

$$A \propto ((\partial \boldsymbol{\mu} / \partial r) \cdot \mathbf{E})^2 = ((\partial \mu / \partial r) E)^2 cos^2 \gamma \tag{9.14}$$

where $\partial \boldsymbol{\mu} / \partial r$ is the transition dipole moment, $\mathbf{E}$ is the electric field of the infrared radiation and γ is the angle between the dipole moment and the electric field. It is evident that maximum absorption is obtained when the radiation is polarized parallel to the dipole moment that develops during the vibration of a characteristic group, while no absorption will be measured for perpendicular polarization. For a random distribution of orientations of the absorbing group and, therefore, random orientation of the resulting dipole moments, the measured infrared absorption will be independent of polarization, whereas, when there is partial alignment, the absorption will depend on polarization of the infrared radiation. Therefore, by using linearly polarized infrared light the orientation of

the functional groups of a polymer can be studied. The absorption anisotropy is expressed by the dichroic ratio, D, defined as:

$$D = \frac{A_{\parallel}}{A_{\perp}} \tag{9.15}$$

where $A_{\parallel}$ and $A_{\perp}$ are the absorptions measured with the incident radiation being polarized parallel and perpendicular, respectively, to a reference direction. For the case of polymers the reference direction is usually the draw direction. The average of the second-order Legendre polynomial, known also as the Hermans-Stein orientation function of polymer chains, can be calculated from dichroic measurements by using the relationship [39, 40, 41, 42]

$$P_2 = \frac{(D-1)(D_o+2)}{(D+2)(D_o-1)} \tag{9.16}$$

where $D_o = 2cot^2\psi$ is the dichroic ratio for perfect orientation, with ψ the angle between the direction of the vibrational transition moment and the polymer chain axis. For vibrations for which $\psi = 90^o$ equation 9.16 reduces to

$$P_2 = 2(1-D)/(D+2) \tag{9.17}$$

while for $\psi = 0^o$ one obtains,

$$P_2 = (D-1)/(D+2) \tag{9.18}$$

Therefore, the second moment of the orientation function can be calculated from polarized infrared measurements.

Such measurements were performed on the same samples employed for the Raman study. Figures 7 and 8 depict the polarized absorption spectra obtained from the PES 3:3 / C6 samples with $\lambda = 1.5$ and 3.1, respectively. As shown in these figures, a number of infrared bands exhibit saturation effects when the radiation is polarized parallel to the stretching direction of the film. This is attributed to a combined effect resulting from the relatively large film thickness (about $30\mu m$), and from the strong absorption by the film under polarization of radiation.

Like in the Raman investigation, we employ sensitive probe-bands to quantify the molecular orientation induced by stretching. In the spectral region typical of CC stretching vibrations of the aromatic rings, four bands are observed at 1485, 1510, $1605cm^{-1}$ all of which exhibit parallel dichroism.. We focus on the band centered at $1605cm^{-1}$ because (i) this band is well resolved from the other CC components and (ii) it appears to be the infrared counterpart of $1616cm^{-1}$ Raman band. Indeed a, the para-disubstituted benzene ring of PES 3:3/C6 has no center of symmetry and thus the mode giving rise to the Raman band at $1616cm^{-1}$ becomes infrared active as well [43]. There are other examples of polymeric materials containing para-disubstituted benzene rings with no center of

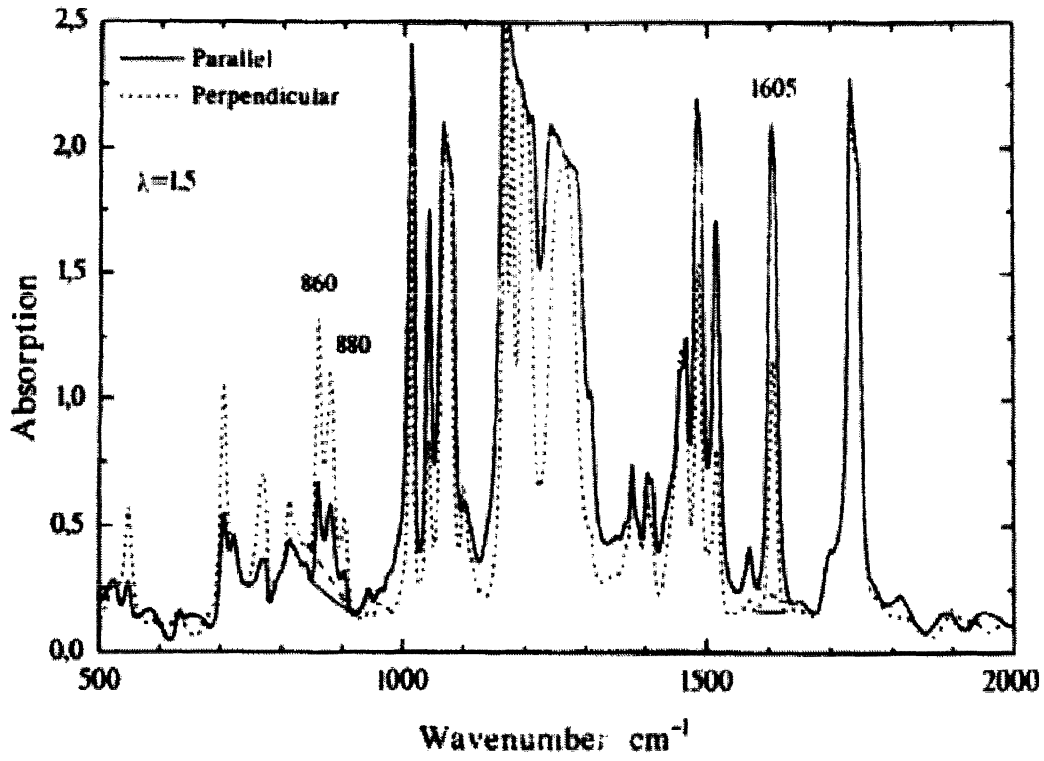

Figure 9.8: Polarized infrared absorption spectra for the PES 3:3 / C6 polyester film at draw ratio $\lambda = 1.5$. Solid lines represent polarization parallel to the stretching direction; dashed lines represent polarization perpendicular to the scattering direction. Base lines for the peaks at 860 cm^{-1} and 1605 cm^{-1} are drawn.

symmetry that exhibit strong infrared bands at $1605cm^{-1}$ with parallel dichroism [25, 44]. On these grounds we assign the infrared band at $1605cm^{-1}$ to the $C = C$ stretching vibration in the $C_1 - C_4$ direction in analogy with the Raman band at $1615cm^{-1}$[32].

The dichroic ratio D for the $1605cm^{-1}$ was determined by the baseline method [45], and is plotted in figure 9 versus draw ratio. Values of D were obtained for three samples only, $\lambda = 1.5$, 2.6 and 3.1, because all other samples showed saturation of the $1605cm^{-1}$ band in the parallel polarized spectra. A systematic increase of D with draw ratio is evident from figure 9 (in comparison to figure 8). Since the dipole moment for the $C = C$ stretching vibration is parallel to the $C_1 - C_4$ direction, and therefore parallel to the chain axis of the polymer, the trend of D suggests the development of chain axis orientation along the stretching direction. Assuming that $\psi = 0°$, eq. 9.18 can be used to calculate P_2 for the $1605cm^{-1}$ band. The results are given in Table 2. Comparisons with

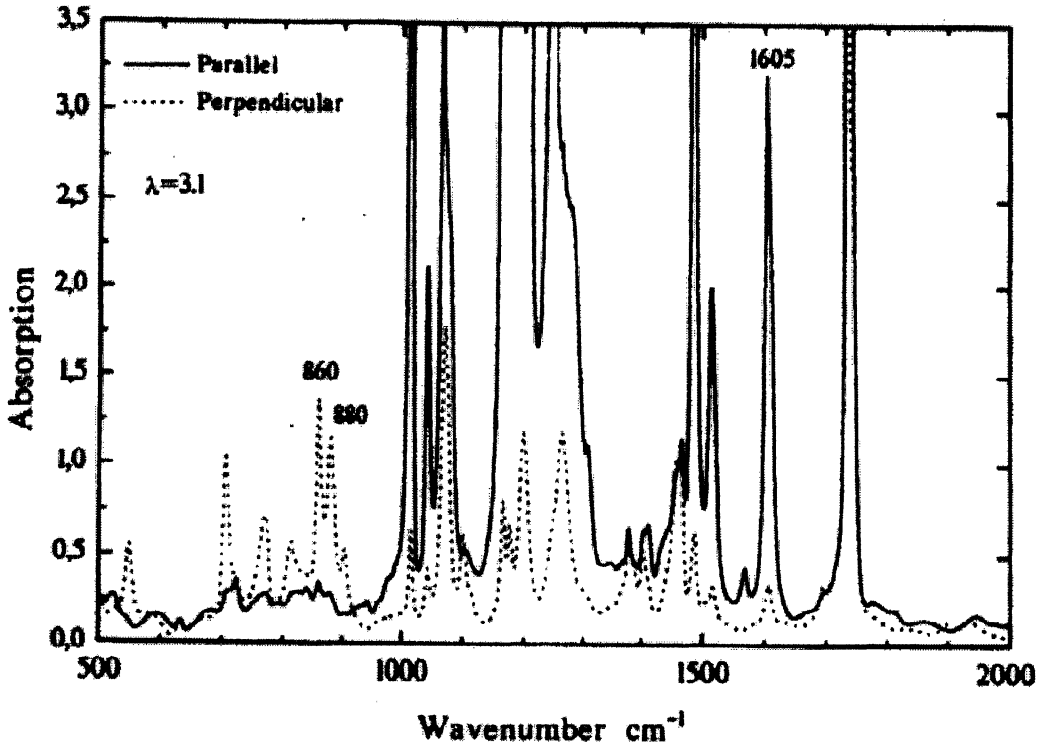

Figure 9.9: Polarized infrared absorption spectra for the PES 3:3 / C6 polyester film at draw ratio $\lambda = 3.1$. Solid lines represent polarization parallel to the stretching direction; dashed lines represent polarization perpendicular to the scattering direction.

the corresponding P_2 values obtained from the Raman analysis (Table 1) show similar results and the same trend with draw ratio. This observation confirms the fact that the two techniques are probing the same molecular mode, and therefore orientation, as it will be discussed below.

Draw Ratio	1.5	2.0	2.4	2.6	2.8	3.1
P_2 ($1605cm^{-1}$)	0.22	-	-	0.56	-	0.78
P_2 ($860cm^{-1}$)	0.47	0.68	0.73	0.78	0.78	0.83

Table2: P_2 values determined from FTIR measurements (1605 cm^{-1} and 860 cm^{-1})

Besides the 1605 cm^{-1} band, other infrared bands can be used also to investigate the tendency for molecular orientation in the polyester films. Of particular interest is the doublet at 860, 880 cm^{-1}, which exhibits polarization opposite to that of the $1605cm^{-1}$ band. This doublet can be assigned to the $C - H$

out-of-plane bending vibration of the benzene rings, with transition moment developing perpendicular to the plane of rings and therefore to the polymer axis [25, 44]. This fact explains the opposite polarization found to be exhibited by the 1605 cm^{-1} band and the 860, 880 cm^{-1} doublet. The dichroic ratio of the stronger component at 860 cm^{-1} was determined and is shown in Figure 9. The progressive decrease of D with λ is another manifestation of the induced molecular orientation upon stretching. Setting $\psi = 90^o$ for the vibrational mode giving rise to the 860^{-1} band, we calculate the corresponding P_2 for this mode by using equation 9.17. The results are included in Table 2. The increase of P_2 with draw ratio is well demonstrated, as in the case of the 1605 cm^{-1} band. The fact that the two bands give different values of P_2 at each λ is not unexpected, since they originate from vibrational modes of different segmental units of the polymer. Similar effects have been observed also in cases of other oriented polymers, including PVC [45] and polypropylene films [46].

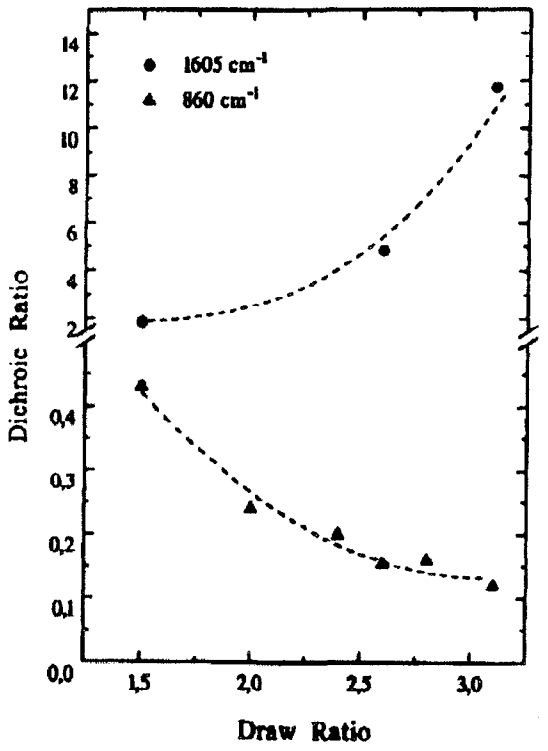

Figure 9.10: Dichroic ratios for the 860 cm^{-1} (bottom) and 1605 cm^{-1} (top) infrared bands as a function of draw ratio. Lines are drawn to guide the eye.

Another source for the difference between the P_2 values of the 860 and 880 cm^{-1} bands could be traced to the possibility that the corresponding transition moments are not exactly perpedicular and parallel, respectively, to the chain axes.

The direction of the dipole moment for the 860 cm^{-1} band is defined rather well, i.e., $\psi = 90^o$ [25, 43]; thus we may assume that $\psi \neq 0^o$ for the 1605 cm^{-1} band. Then the orientation function for the molecular chains, $P_{2,chain}$ can be obtained in terms of the dichroic ratio of the 1605 cm^{-1}, D, from the expression below, where ψ is the angle between the direction of the transition moment of the 1605cm^{-1} band and the chain axis:

$$P_{2,chain} = 2(\frac{D-1}{D+2})(\frac{1}{3\cos^2\psi - 1}) \tag{9.19}$$

Assuming that at the highest draw ratio, $\lambda = 3.1$, $P_{2,chain}$ can be approximated by the P_2 value of the 860 cm^{-1} band ($P_2 = 0.83$ from table 2), then from eq. 9.19 and the value of D at 1605 cm^{-1} (11.7), we get $\psi = 11.5^o$. This result suggests that the assumption made earlier that $\psi = 0^o$ is not unreasonable, at in any case, it does not affect the trend of P_2 at 1605 cm^{-1} with the draw ratio.

9.2.3 WAXD Results

The WAXD experimental intensity profiles of drawn tapes are convolutions of the orientation distribution and the scattering of a perfectly aligned system. Since the profile of a perfectly aligned system is not known, the narrowest peak obtained (width about 5°) represents an upper limit of this profile. The deconvolution has been performed according to a procedure of Alexander [47], and assuming a Lorentz-shape for all profiles. The degree of orientation was furthermore quantified by the full width at half maximum (FWHM) of the (100) reflection. Typical results are depicted in figures 10a and 10b, for draw ratios 2.0 and 3.1, respectively. From the azimuthal intensity distributions $I(\phi)$ the second moment of the orientation distribution was calculated by a numerical integration according to :

$$< \cos^2\theta >= \frac{\int_0^{\pi/2} I(\phi)\cos^2\phi d\phi}{\int_0^{\pi/2} I(\phi)\sin\phi d\phi} \tag{9.20}$$

The P_2 values thus determined are shown in Table 3 together with the FWHM values. The X-ray P_2 values shown here are calculated assuming a "perfect width" of 0°. Taking into account a "perfect" profile of a few degrees width, would lead to systematically higher values of P_2. The presented values exhibit a very small, but nevertheless clear increase of P_2 with draw ratio, and the significant differences with the Raman and FTIR P_2 values, especially at lower draw ratios. Here we use the WAXD data only for comparisons and for establishing trends of molecular orientation.

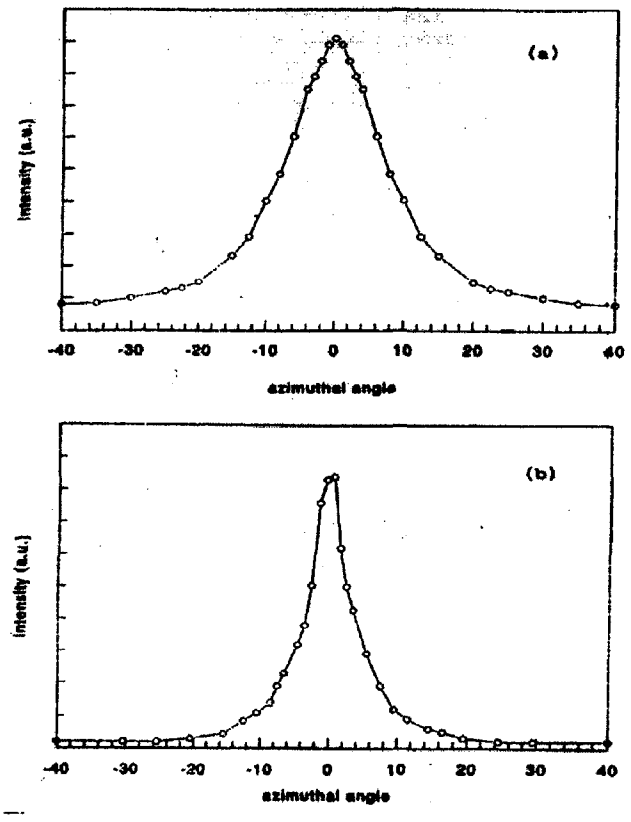

Figure 9.11: Azimuthal intensity distributions for the PES 3:3 / C6 polyester film, obtained by WAXD: (a) $\lambda = 2.0$; (b) $\lambda = 3.1$.

Draw Ratio	1.5	2.2	2.3	2.5	2.7	2.9	3.0	3.1
P_2	0.90	0.91	0.87	0.91	0.93	0.94	0.94	0.95
fwhm (deg)	15	14	12.6	14.3	13.1	11.8	8	6.7

Table3: P_2 and FWHM values determined from WAXD measurements.

9.2.4 Evaluation of Results

A compilation of the orientation data of the PES 3.3/C6 films obtained with the three techniques is presented in figure 11. Concerning P_4, the only conclusion that can be drawn is that is follows the right qualitative trend with draw ratio, and that its values fall within the range of the most probable ones, as already discussed; no further analysis can be made since there is no relevant information from FTIR or WAXD. Concerning P_2, it is very encouraging to note the excellent agreement between the Raman and FTIR data when the same vibrational mode is probed.

This is important since both spectroscopic techniques provide information on the molecular orientation by probing essentially the same band, namely the one originating from the $C = C$ vibration of the phenyl rings. Further, given the fact that the FTIR analysis is rather straightforward, the results suggest that the simplified analysis used for the Raman scattering data is indeed unambiguous and highly effective.

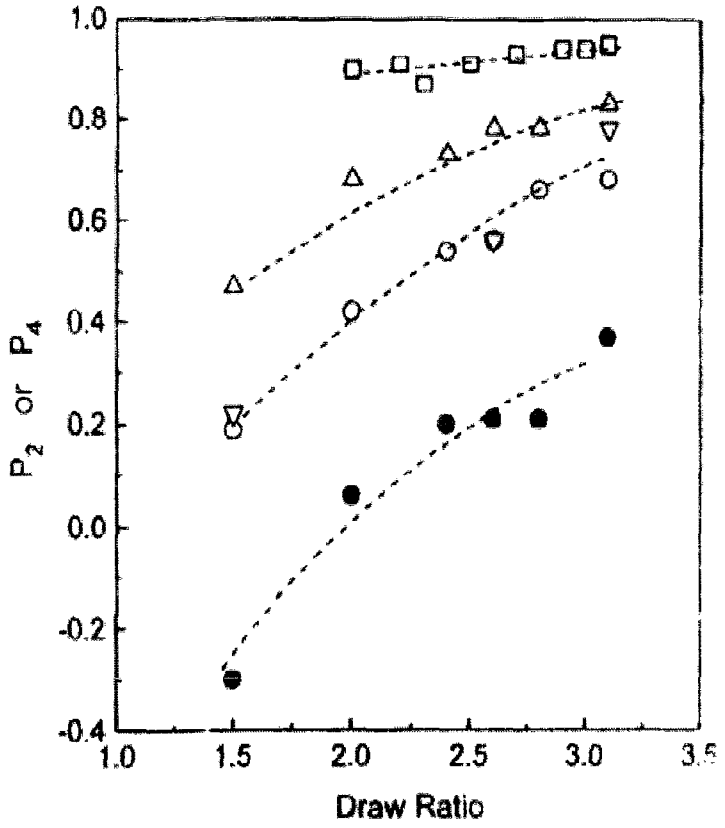

Figure 9.12: Second and fourth moments of the orientation distribution function, determined from Raman (P_2 and P_4), FTIR (P_2) and WAXD (P_2) measurements. Lines are drawn to guide the eye.

As far as the WAXD data are concerned, it is clear that a significant discrepancy exists. This observed discrepancy which amounts up to 30%, is too large to be accounted for by experimental uncertainties. We believe that it is justified by the fact that Raman and FTIR, which are sensitive to the vibration of a particular group, measure the average molecular orientation, while the WAXD orientation information originates from the liquid crystalline domains only. More than that, the polyester studied in this work is a material of rather small persistence length [27, 48, 49] and forms a far from perfect liquid crystalline domain, in lyotropic

phases. In our case this happens as the solvent is evaporated during film casting. Thus, Raman and FTIR determine the orientation in small areas frozen-in from liquid crystalline phase at some temperature, associated with observation on a molecular level (provided of course that the relative position between the vibrational groups probed and the main molecular axis is known). This is what we call "*molecular orientation*". On the other hand, WAXD looks at layer reflections, which are associated with much larger entities, and refer to the orientation of domains or crystallites, comprising of more than one molecules. This can be considered as a kind of *supramolecular domain orientation.* It is clear that the order within the layers can be low, whereas the layers relative to each other are highly oriented. In view of this qualitative model, the data of figure 11 can be understood, and the true effect of draw ratio on molecular orientation can be explained. More specifically, an 100% increase in the draw ratio leads to an over 250% increase in the value of P_2 of the 1616/1605 cm^{-1} band, and a corresponding one of 77% for the 860 cm^{-1} band. It is noted that, despite the difference in magnitudes of the 1605 cm^{-1} and 860 cm^{-1} bands, the trends are the same. Further, it is remarked that the significantly different dependence of WAXD and Raman/FTIR data on the draw ratio confirms that these two approaches look at different kind of orientation. It should be mentioned that somehow similar explanations, based on a two-domain amorphous-liquid crystalline model have been already presented in the literature [29, 30, 50] for other polyesteric materials, in order to explain similar discrepancies. This provides further justification for our interpretation, since these materials form apparently a far from prefect fully- liquid crystalline domain in lyotropic phases. Nevertheless, and despite the stability of the presented Raman-based methodology for extracting P_2 and P_4 (due to the assumptions made, the results do not depend on any choice of initial conditions as in previous works [29, 30]dealing with the solution of the system of five nonlinear equations) and the accuracy of the data presented, it is clear that more work is needed in the direction of the proposed model, mainly through theoretical support.

The existing models are mostly developed from continuum mechanical considerations. In particular, the affine deformation model of Kratky [?] can represent, to a good approximation, the orientation of rigid rods in a viscous matrix. The same essentially model was used by Kuhn and Grun [51] in order to describe the orientation of aggregates of anisotropic polymer segments. The model assumes that uniaxial deformation takes place by rotation of chains (or segments) under unconstrained conditions, while elongation may arise only from rotation, but not from shear. Under these conditions, the model predicts the second moment of the orientation distribution function as a function of draw ratio only. The agreement with the Raman and FTIR 1616/1605 cm^{-1} data is very good, but one should be careful in evaluating this, since the model does not contain any molecular parameter, and in that respect it is of little value for the present purposes. Another model of relevance is the rubber network model of Roe and Krigbaum [52]. It

describes the deformation of a crosslinked network, where the crosslinks can be considered as entanglements between chains. This model, however, has some inherent physical limitations when associated with the current rigid-rod polyesters; moreover, it considers the number of links per chain, n, as the adjustable parameter. In other words, it predicts P_2 as a function of n and λ. It can predict our Raman data with a decent accuracy when $n = 2$, which is considered as rather unrealistic. On these grounds, we believe that the rubber network model is not directly correlated to uniaxially oriented rigid-rod macromolecules. It is clear, however, that more work is needed in this direction.

9.3 Summary-Conclusions

Polarized Raman and FTIR spectroscopies have been successfully utilized in order to determine the molecular orientation of polyester films as a function of draw ratio. Results support the idea that while the liquid crystalline domains, probed by WAXD, are highly oriented even at low draw ratios, and dependence on them very weakly, the smaller-scale average molecular orientation inside these domains is smaller and depends on the draw ratio considerably. Raman scattering is a powerful tool for the determination of both the second and fourth moments of the segment orientation distribution function, when physical considerations regarding the structure of these materials are properly taken into account. A simplified approach for the analysis of the Raman spectra, based on the cylindrical symmetry of the Raman tensors at a specific vibrational normal mode, demonstrates the effectiveness of Raman spectroscopy for quantitative determination of the molecular orientation in rod-like polymers. Agreement between Raman and FTIR data is remarkable, manifesting the reliability of both techniques. Further, for these latter techniques, the effect of draw ratio on increasing molecular orientation is drastic. Finally, it is proposed that incorporation of polarization modulation techniques will make measurements faster and interpretation much easier, since the resulting equations are much simpler [12, 13], and require less restrictions than in the present case. This is the subject of future investigations in this direction.

References

[1] I.M. Ward. *Structure and Properties of Oriented Polymers.* Applied Science Publishers, London, 1975.

[2] I.M. Ward. *Developments in Oriented Polymers-I.* Applied Science Publishers, London, 1982.

[3] A.E. Zachariades and R.S. Porter. *The Strength and Stiffness of Polymers.* Marcel Dekker, New York, 1983.

[4] I.M. Ward. *Adv. Pol. Sci.*, 66:81, 1985.

[5] I.M. Ward. *Developments in Oriented Polymers-II.* Applied Science Publishers, London, 1982.

[6] C-P. Lafrance and R.E. Prud'homme. *Polymer*, 35:3927, 1994.

[7] G. Gustafsson, O. Inganas, H. Osterholm, and J. Laakso. *Polymer*, 32:1574, 1991.

[8] Jasse B., J. F. Tassin, L. Monnerie, and J. Laakso. *Prog. Colloid Polym. Sci.*, 92:8, 1993.

[9] Kaito A., M. Kyotani, and K. Nakayama. *Journal of Polymer Science:Polymer Physics Edition*, 31:1099, 1993.

[10] Purvis J. and D.I. Bower. *Polymer*, 15:645, 1974.

[11] Buffeteau T., B. Desbat, S. Besbes, M. Nafati, and L. Bokobza. *Polymer*, 35:2538, 1994.

[12] Archer L.A., G.G. Fuller, and L. Nunnelley. *Polymer*, 33:3574, 1992.

[13] Archer L.A. and G.G. Fuller. *Macromolecules*, 27:4359, 1994.

[14] Lafrance C-P., P. Chabot, M. Pigeon, R.E. Prud'homme, and M. Pezolet. *Polymer*, 34:5029, 1993.

[15] Satija S.K. and C.H. Wang. *J. Chem. Phys.*, 69:2739, 1978.

[16] Robinson M.E.R., D.I. Bower, and M.F. Maddams. *Journal of Polymer Science:Polymer Physics Edition*, 16:2115, 1978.

[17] L. Lauchlan and J.F. Rabolt. *Macromolecules*, 19:1049, 1986.

[18] G. Voyiatzis, G. Papatheodorou, E. Kamitsos, G. Chrysikos, S.H. Anastasisiadis, and G. Fytas. 1997.

[19] J. Purvis, D.I. Bower, and I.M. Ward. *Polymer*, 18:731, 1980.

[20] B. Jasse and J.L. Koenig. *Journal of Polymer Science:Polymer Physics Edition*, 16:2115, 1978.

[21] W. Li and R.E. Prud'homme. *Polymer*, 35:3260, 1994.

[22] E. Abtal and R.E. Prud'homme. *Polymer*, 34:4661, 1993.

[23] A. Kaito, K. Nakayama, and M. Kyotani. *Journal of Polymer Science:Polymer Physics Edition*, 29:1321, 1993.

[24] S.B. Damman, F.P.M. Mercx, and P.J. Lemstra. *Polymer*, 34:2726, 1993.

[25] A. Kaito, M. Kyotani, and K. Nakayama. *Macromolecules*, 24:3244, 1991.

[26] S. Jen, N.A. Clark, P.S. Pershan, and E.B. Priestley. *J. Chem. Phys.*, 66:4635, 1977.

[27] U. Tiesler, T. Pulina, M. Rehahn, and M. Ballauff. 243:299, 1994.

[28] A. Bruggeman, J.A.H.M. Buijs, and S.B. Damman. 1995.

[29] M. Pigeon, R.E. Prud'homme, and M. Pezolet. *Macromolecules*, 24:5687, 1991.

[30] M.J. Citra, D.B. Chase, R.M. Ikeda, and K.H. Gardner. *Macromolecules*, 28:4007, 1995.

[31] J. Purvis, D.I. Bower, and I.M. Ward. *Polymer*, 14:398, 1973.

[32] P. Lapersonne, D.I. Bower, and I.M. Ward. *Polymer*, 33:1266, 1992.

[33] E. Kamitsos and W.M. Risen Jr. *J. Chem. Phys.*, 79:477, 1983.

[34] D.I. Bower. *Journal of Polymer Science:Polymer Physics Edition*, 10:2135, 1972.

[35] J. Purvis and D.I. Bower. *Journal of Polymer Science:Polymer Physics Edition*, 14:1461, 1976.

[36] D.I. Bower. *Journal of Polymer Science:Polymer Physics Edition*, 19:93, 1981.

[37] F.J Boerio, S.K. BAhl, and G.E. McGraw. *Journal of Polymer Science:Polymer Physics Edition*, 14:1029, 1976.

[38] I.M. Ward and M.A. Wilding. *Polymer*, 18:327, 1977.

[39] R.D.B. Fraser. *J. Chem. Phys.*, 21:1511, 1953.

[40] R.D.B. Fraser. *J. Chem. Phys.*, 24:89, 1953.

[41] R.S. Stein. 31:335, 1958.

[42] S. Krimm. page 3, 1958.

[43] N.B. Colthup, L.H. Daly, and S.E. Wiberley. *Introduction to Infrared and Raman Spectroscopy.* Academic Press, New York, 1975.

[44] H Lei and Y. Zhao. *Polymer*, 35:104, 1994.

[45] S.A. Jabarin. *Polym. Eng. Sci.*, 31:638, 1991.

[46] I. Karacan, A.K. Taraiya, D.I. Bower, and I.M. Ward. *Polymer*, 34:2691, 1993.

[47] L.E. Alexander. *X-ray diffraction methods in polymer science.* Wiley Press, New York, 1969.

[48] G. Petekidis, D. Vlassopoulos, P. Galda, M. Rehahn, and M. Ballauff. *Macromolecules*, 29:8948, 1996.

[49] U. Tiesler, M. Rehahn, Ballauff M., G. Petekidis, D. Vlassopoulos, G. Maret, and H. Kramer. *Macromolecules*, 29:6832, 1996.

[50] A. Kaito, M. Kyotani, and K. Nakayama. *Journal of Polymer Science:Polymer Physics Edition*, 31:1099, 1993.

[51] W. Kuhn and F. Grun. *Kolloid-Z.*, 101:248, 1942.

[52] R.J. Roe and W.R. Krigbaum. *J. Appl. Phys.*, 35:2215, 1964.

Appendix A

Time-correlation functions

Correlation functions provide a concise method for expressing the degree to which two dynamical properties are correlated in time. Consider a property A that depends on the positions $q(t)$ and on the momenta $p(t)$of all particles in the system. The average value of $A(t)$ measured after t_0 is $\overline{A}(t) = \lim_{T\to\infty} \frac{1}{T} \int_{t_0}^{t_0+T} A(t)dt$; if it is independent of t_0 then A is a *stationary property.* The *time autocorrelation function* of $A(t)$is defined by:

$$< A(0)A(\tau) >= \lim_{T\to\infty} \frac{1}{T} \int_0^T A(t)A(t+\tau)dt \qquad \text{(A.1)}$$

In general $< A(0)^2 > \geq < A(0)A(\tau) >$, while for times τ large compared to the characteristic time of the fluctuations of $A(t)$ it is expected that $A(t)$ and $A(t+\tau)$ become totally uncorrelated and thus $\lim_{\tau\to\infty} < A(0)A(\tau) >=< A(0) >< A(\tau) >=< A >^2$. According to the above, the time-correlation function of A decays with time from $< A^2 >$ to $< A >^2$. The most usual decay of the correlation is a single exponential with a *relaxation time* τ_r. In light scattering as in several other applications it is more useful to use the fluctuation of a property: $\delta A(t) = A(t) - < A >$. Then the autocorrelation of the fluctuation decays according to $< \delta A(0)\delta A(\tau) >=< \delta A^2 > \exp(-\tau/\tau_r)$. The time-correlation functions that measured in experiments like light, neutron scattering or NMR spectroscopy are time-averages like eq. A.1, whereas in most theoretical investigations what is calculated is the ensemble-average time-correlation function defined by :

$$< A(0)A(\tau) >= \int d\mathbf{\Gamma}_0 \rho(\mathbf{\Gamma}_0) A(\mathbf{\Gamma}_0) A(\mathbf{\Gamma}_\tau) \qquad \text{(A.2)}$$

where $\mathbf{\Gamma}_0$ is the initial state of the system (with generalized coordinates $q_f(0)$ and generalized momenta $p_f(0)$) and $d\mathbf{\Gamma}_0\rho(\mathbf{\Gamma}_0)$ the probability of finding the system in the initial state $\mathbf{\Gamma}_0$. According to the *ergodic theorem* these two correlation functions are identical for ergodic systems.

Appendix B

Transport properties

B.1 Rodlike chains

For long, thin rigid rods the parallel diffusion is double the perpedicular one $D_{\|} = 2D_{\perp}$ and the isotropically averaged $D = \frac{D_{\|}+2D_{\perp}}{3}$ and the end-over-end rotational diffusion is $12D_{\perp}/L^2 = 9D/L^2$. The rotation of the rod around its own axis since it is not contribute in light scattering. We present here some models for the unrestricted transport properties of rigid and semistiff chains in the dilute region. Among many models the most important are:

a) The Kirkwood-Riesman model [1] for a linear array of beads where they computed the interactions between the beads for Θ solvent conditions. Their result is:

$$D = D' \ln(x) \tag{B.1}$$

$$D_R = D'_R \ln(x) \tag{B.2}$$

with $D' = (k_B T/3\pi\eta_s L)$ and $D'_R = (3k_B T/\pi\eta_s L^3)$; η_s being the solvent viscosity and $x = L/b$ the aspect ratio.

b) The improved Broesma model [2, 3, 4] for a smooth cylinder of aspect ratio $x > 4$ gives :

$$D = D'[\ln(2x) - 1/2(\gamma_{\|} - \gamma_{\perp})] \tag{B.3}$$

$$D_R = D'_R[\ln(2x) - \zeta] \tag{B.4}$$

The terms $\gamma_{||}$, $\gamma_{\perp}$and ζ are functions of the aspect ratio x:

$$\gamma_{||} = 1.27 - 7.4\{(\ln 2x)^{-1} - 0.34\}^2 \tag{B.5}$$

$$\gamma_{\perp} = 0.19 - 4.2\{(\ln 2x)^{-1} - 0.39\}^2 \tag{B.6}$$

$$\zeta = 1.45 - 7.5\{(\ln 2x)^{-1} - 0.27\}^2 \tag{B.7}$$

c) The relations of Tirado-Garcia de la Torre [5] have a subunit approach. In their approach they consider spheres made into rings and then rings stacked to form cylinders. Each sphere has a frictional interaction with the solvent and indirect hydrodynamic interactions with each other through the solvent. The results are derived numerically in the limit of numerous spheres of small diameters and hold also for relatively short rods $2 \leq x \leq 30$:

$$D = D'\{\ln(x) + \nu\}$$

$$D_R = D'_R\{\ln(x) + \delta\}$$

where ν and δ are functions of x:

$$v = 0.312 + 0.565/x - 0.1/x^2$$

$$\delta = -0.662 + 0.917/x - 0.05/x^2$$

The differences between the above models are essentially in the calculation of the end effect correction γ, ζ, ν and δ.

B.2 Semiflexible chains

The expressions for the diffusion coefficients of semiflexible rods involve the flexibility parameter of the chain, i.e. the persistence length l. Some of the models for semiflexible chains are:

a) The Hearst-Stockmayer model [6, 7, 8] for bending rods which provides expressions in the rodlike ($L < 2l$) and the flexible limit ($L > 2l$). In the stiff limit:

$$D = D'\{\ln(L/h) + 0.166(L/2l) - 1 + h/b\} \tag{B.8}$$

$$D_R = (D'_R/3)\{3\ln(L/h) - 7 + 4h/b + (L/2l)[2.25\ln(L/h) - 6.66 + 2h/b]\} \tag{B.9}$$

and in the flexible limit:

$$D = D'\{1.843\sqrt{L/2l} - \ln(h/2l) - 2.431 - h/b\} \tag{B.10}$$

$$D_R = (D'_R\pi L/6l)\{0.716\sqrt{L/2l} - 0.636\ln(h/2l) - 1.548 + 0.64h/b]\} \tag{B.11}$$

with h the length of the monomer repeat unit.

b) Yamakawa and Fujii [9] developed their diffusion coefficients based on the wormlike model. For $L > 4.556l$ they get:

$$D = D'(A_1\Lambda^{1/2} + A_2 + A_3\Lambda^{-1/2} + A_4\Lambda^{-1} + A_5\Lambda^{-3/2}) \tag{B.12}$$

where $\Lambda = L/2l$ and A_i involve $\Delta = b/2l$. For $L < 4.556l$ they get:

$$\begin{aligned} D &= D'(C_1 \ln(L/b) + C_2 + C_3\Lambda + C_4\Lambda^2 + C_5\Lambda^3 + C_6(b/L)\ln(L/b) \\ &\quad + C_7(b/L) + C_8(b/L)^2 + C_9(b/L)^3 + C_{10}(b/L)^4 + O[(b/L)^5]) \end{aligned} \tag{B.13}$$

where C_i are functions of Δ. For the explicit expressions of A_i and C_i see also references [9, 10].

c) Hagerman and Zimm [11] used Monte-Carlo simulations and a bead model to generate a representative ensemble of chain configurations. Then they calculate the rotational diffusion coefficients for each of these configurations and average over the ensemble to obtain the rotational diffusion of a semiflexible chain:

$$D_R = D_R(Broesma)/R \tag{B.14}$$

where

$$\begin{aligned} R &= [1.012 - 0.24813(L/l) + 0.033703(L/l)^2 - 0.0019177(L/l)^3] \\ &\quad \times [1 - 0.06469(L/l) + 0.01153(L/l)^2 - 0.0009893(L/l)^3] \end{aligned} \tag{B.15}$$

This rigid body approximation avoids the difficulties of the preaveraging models, but still ignores the fact that individual molecules can flex as they rotate.

Appendix C

Internal field

For the calculation of the scattered intensity from any dielectric medium it is necessary to calculate the local field, E_L in the position of the scatterer; a task which is not always easy. In the framework of Einstein-Smoluchowski scattering theory [12, 13] the main task for the solution of the scattering problem is to find a good equilibrium theory for $< \varepsilon >$, the mean dielectric constant of the scattering medium, and the knowledge of the important fluctuations. Then one has to calculate $\partial < \varepsilon > / \partial < \rho >$ for the case of polarized scattering (since the fluctuations of density ρ give rise to the polarized scattering) and $\partial < \varepsilon > / \partial < Q >$ in the case of depolarized scattering (since the fluctuating quantity for this kind of scattering is the orientational order parameter Q) [14]. The internal field, is tackled easier in the case of polarized scattering because the dielectric constant can be connected easily with any thermodynamic variable, and thus with $< \rho >$ and $\partial < \varepsilon > / \partial < \rho >$ can then be calculated. For a spherical cavity, the relation between the microscopic α_o and the macroscopic $< \varepsilon >$ is given by the Clausius-Mossotti relation $\frac{<\varepsilon>-1}{<\varepsilon>+2} = \frac{4\pi}{3}\alpha_o < \rho >$, and the local field in the cavity is $E_L = EL$ (with $L \equiv (\frac{n^2+2}{3})$the Lorentz local field). The internal field correction for the VV scattering is then found to be the fourth power of the Lorentz local field : $f_{VV}(n) = (\frac{n^2+2}{3})^4$ [14]. Although other local field factors have been suggested, on the base of different relations for $< \varepsilon >$, the fourth power correction given above has been generally accepted after exhaustive experimental testing [15].

On the other hand for depolarized light scattering the local field factor is still a matter of controversy; the main difficulty is that orientation is not a thermodynamic parameter and thus the calculation of $\partial < \varepsilon > / \partial < Q >$ is not straightforward [14]. Based on experimental support and some theoretical treatment the most widely used correction in DRS is $(\frac{n^2+2}{3})^2$. Nevertheless there are experiments [16, 17] which show that $f_{VH}(n)$is a decreasing function of n and thus no power law of L is correct. A generalization of the Einstein-Smoluchowski theory was presented by Keyes and Ladanyi [18, 19, 14] who used response and dielectric theories to connect ε with Q in an artificial ensemble with $\overline{Q} \neq 0$. Then

they calculate $\partial < \varepsilon > / \partial < Q >$ around $Q = 0$ (the equilibrium is isotropic) and using a dielectric theory in the dipole-induced dipole (DID) approximation. In this way they conclude that the internal field correction for the depolarized light scattering is of the form: $f_{VH}(n) = L^4 f'_{VH}(n)$ with $f'_{VH}(n)$ a decreasing function of n.The function $f'_{VH}(n)$ expresses the effect on the local field that a molecule feels, of the induced dipoles on its neighbors. This does not vanish only for non-spherical molecules due to the asymmetry in the interpair vectors and the correlation of the orientation of a neighbor molecule with its position. This extra local field induced by orientation will affect the depolarized light scattering. This effect is negligible in polarized scattering arising from density fluctuations which due not break the local symmetry; the later is the most important determinant of the local field. In view of the above no power law can give a good local field correction; nevertheless for most liquids $f_{VH}(n)$ is in the decreasing regime and this is why a L^2 factor seems to work better than a L^4.

For scattering from polymer solutions, a two component system, the density ρ is substituted by the concentration, c , of the polymer. Moreover in this case the intramolecular interactions contribute in the IFP although there is no experiment which can separate them from the intermolecular. There are two main model for the description of the total dipole moment of a polymer chain. The *Bond Additivity Approximation* (BAA) (or Valence optical scheme) [20, 21, 22] where the molecular polarizability is obtained by simply summing the bond polarizabilities: $\boldsymbol{\alpha}_M^{BAA} = \sum_{i=1}^{N} \boldsymbol{\alpha}_i$. In the BAA the optical anisotropy is a function of the relative orientations of the bonds:

$$\gamma^2 = \sum_{i=1}^{N} \Delta a_i [\Delta a_i + \sum_{i \neq j}^{N} \Delta a_j P_2(u_i \cdot u_j)] \tag{C.1}$$

while the isotropic polarizability is independent of the internal molecular coordinates $\alpha_0 = \sum_{i=1}^{N} \alpha_{0i}$. In this model the molecule is considered as a collection of independent scatterers and the scattering has rather a local nature. The optical anisotropy measures the intramolecular orientational pair correlations. In this model the optical anisotropy of an bonds can be used to calculate the optical anisotropy of the whole molecule by taking into account the conformation of the molecule. This was exactly the aim of several works by depolarize light scattering Fabry-Perot interferometry on small molecules [23, 24] and low-molecular weight nematogenic compounds [25, 26].

The other model is the *Interacting Atom Model* (IAM) [27, 14] where the molecular polarizability is defined as the tensor relating the total dipole moment, μ_M induced in the molecule, to the applied field E : $\mu_M = \boldsymbol{\alpha}_M \cdot E = \sum_{i=1}^{N} \mu_i$. The second equality suggests that in this model the additivity quantity is the dipole moments of each atom (μ_i) , the molecular polarizability is a property of

the whole molecule and the scattering is of collective rather than local nature. The main difference is in the optical anisotropy which is much more strongly dependent on the chain length than in BAA :

$$\gamma^2 = \frac{3}{2} trace(\hat{a}_M \cdot \hat{a}_M) \tag{C.2}$$

where $\hat{a}_M = a_M - a_0\hat{I}$ and $a_0 = \frac{1}{3}trace(\hat{a}_M)$. The experimental findings of the depolarization ration of short n-alkanes are in favor of the IAM model [14] which on the other hand gives inaccurate results for molecules with double and triple bonds.

The ambiguity in the calculation, or measurement of the $f'_{VH}(n)$ term in the local field correction shows that the true molecular anisotropy $< \gamma^2 >$ is difficult to be extracted by DRS ; what we can determine is an effective optical anisotropy $< \gamma^2_{eff} >= 15(\frac{\lambda}{2\pi})^4(\frac{3}{n^2+2})^4(\frac{R_{VH}}{\rho})$. This is expected to be smaller than the true molecular anisotropy and also solvent dependent. The BAA model is used because it can more easily predict values of $< \gamma^2_{eff} >$. From the theoretical point of view this is more justified when solvent molecules are more highly polarizable than polymer segments; the polymer-solvent DID interactions are then stronger leading to a screening of the intramolecular interactions. Moreover, the second power local field correction in DRS, although does not seem to be justified theoretically, can be used self consistently in the framework of BAA for the calculation of $< \gamma^2_{eff} >$ of molecules from the respective anisotropies of their constituents.

Appendix D

Effects of Laser Intensity and External Electric Field.

Solutions of the PPP/S series in TCE, obtain a yellow to brown color after some time at high concentrations. The origin of this effect is not yet clear (oxidation or degradation of the polymer has been ruled out); it may be due to some doping of the polymer or of some other specific interaction of the polymer with the solvent molecules which seem not to affect the molecular properties. These colored samples absorb in the wavelength of the incident laser which we normally use (532 nm).

In such cases it has been observed that changing the incident laser intensity (measurements with and without attenuator) we affect the dynamics of the slow mode, in the polarized geometry. The decrease of the incident intensity causes a decrease in the characteristic relaxation rate of the slow process, while the fast mode, attributed to the cooperative diffusion of the macromolecules, does not seem to be affected. Moreover the slow mode becomes sharper than single exponential as the incident intensity increases revealing some kind of ballistic motion (similar to our observations in chapter 7). This phenomenon is shown in fig. D.1 for three different concentrations. To check whether this is a result of the absorption of light by the solution or of the electric field of the Laser we perform the same experiment with a red Laser ($\lambda = 633$ nm) and also we imposed an external stationary electric field.

The measurements with the red laser do not exhibit any change in the dynamics at different scattering intensities, suggesting that the change of the dynamics is due to the absorption of the solutions in the wavelength of the green Laser (532 nm). In fig. D.3 the normalized field correlation functions measured in a solution of PPP/S-3 in TCE with both the green and the red laser and for two different incident intensities are shown. It is evident that for the 633 nm wavelength (red laser) there is no affect of the incident intensities on the dynamics whereas there is a strong effect for the 532 nm (green). Nevertheless, a similar change of the slow mode dynamics was observed when we impose an external electric field. In-

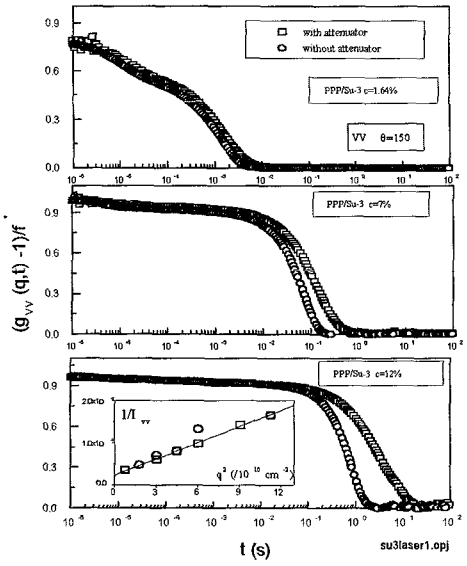

Figure D.1: Polarized correlation functions for two different incident intensities (with and without attenuation) at three different concentrations of PPP/Su-3 solutions in TCE. Inset: The q-dependence of the inverse of the scattered intensity for the two different incindent intensities.

creasing the applied electric field, a speed up of the dynamics of the slow mode is observed, as by increasing the incident intensity of the green Laser.

D.0.1 The Laser intensity

The incident intensity affects both the shape and the decay rate of the correlation function (fig. D.1). The smallest concentration where we observed such effects was $c = 1.64\%$ of S–3 in TCE. The change was more pronounced in 30^o angle where full intensity of the laser gave a sharper and faster slow mode compared to the results with a smaller incident intensity. Here it must be mentioned that changing the incident intensity there was also a change of the total contrast attributed to change of the instrumental factor f^* due to a change in the beam geometry as verified with standard solutions. At higher concentrations the effect of the laser intensity is larger (fig. D.1). At $c = 7.05\%$ of S–3 in TCE the slow mode becomes 17 times slower when we attenuate the incident intensity to 1.5% of the total, while the shape becomes significantly sharper than a single exponential ($\beta : 1.5 - 2.1$). On the other hand the fast, cooperative motion of the molecules does not seem to be affected, both in shape and time.

In order to quantify this finding, measurements at a constant angle ($\vartheta = 150^o$)

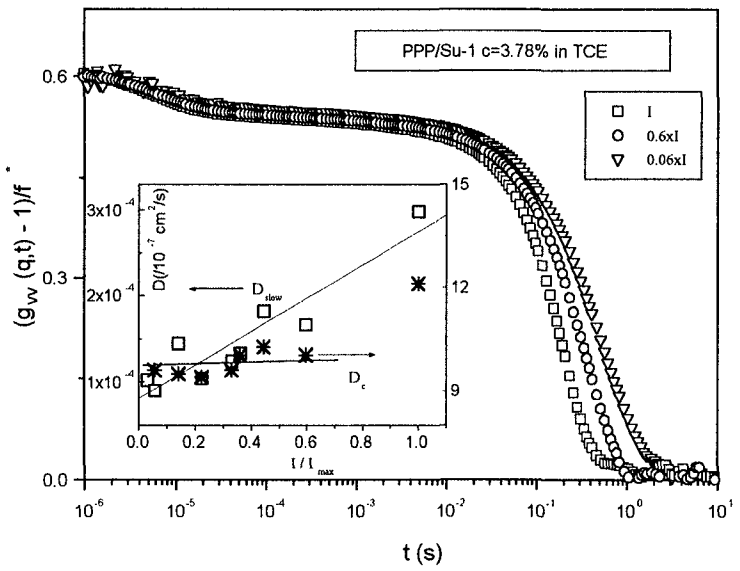

Figure D.2: Polarized correlation functions of a c=3.78% PPP/Su-1 solution in TCE, for different incindent Laser intensities. Inset: The slow and and the cooperative diffusion coefficient as measured at a scattering angle $\theta = 150^o$.

were done for several incident Laser intensities. These experiments were done in a solution of S-1 ($M_w = 189000$) in TCE at concentration $c = 3.78\%$ and temperature $T = 25^oC$ (Fig. D.2). Attenuating the incident beam to 2.8% of its maximum value we get an increase of the diffusion coefficient of the slow mode by a factor of 3; giving $\Delta D_{slow} = 2 \times 10^{-4}$ ($\times 10^{-7}$ cm^2/s).

Similar affect of the incident intensity was observed in all samples in TCE, whereas in the other solvents used (toluene and $CHCl_3$) only at high concentrations (above 20%) of S-10 in toluene did we observe some change in the slow mode dynamics.

D.0.2 The External Electric field

In the experiments with the external electric field, dynamic light scattering was done with a field from 200 up to 2000 Volts/cm. The measurements were done on the S-1 sample ($c = 3.78\%$ in TCE) at an angle of 150^o; q-dependence was checked only at 1200 and 2000 Volts/cm. There is a clear trend of the slow mode to become faster as we increase the electric field (fig. D.4). The change of the diffusion coefficient of the slow mode, calculated at $\theta = 150^o$, is $\Delta D_s = 1.7 \times 10^{-3}$ ($\times 10^{-7}$ cm^2/s) and corresponds to an electric field of 2000 Volts/cm (fig. D.2). If we compare the effects of the laser and the electric field we can

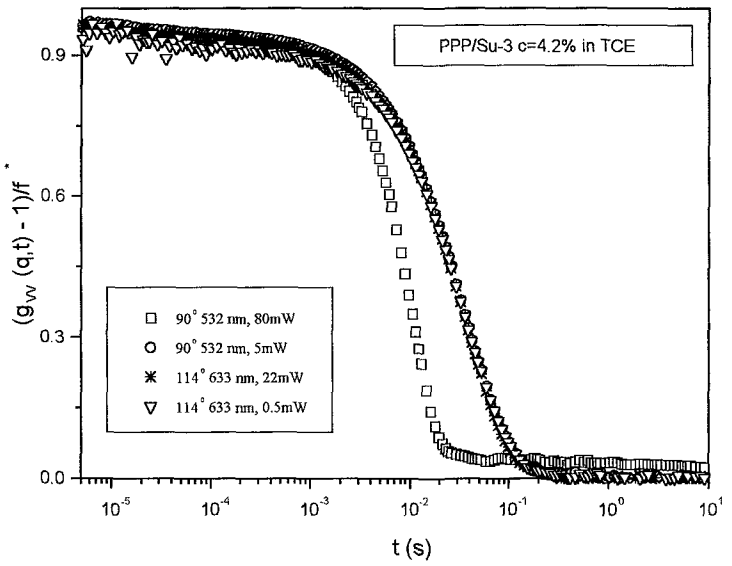

Figure D.3: Polarized correlation functions for a c=4.2% solution of PPP/Su-3 in TCE for two different wavelengths of the incindent intensity (red: 633 nm and green 532 nm) for two different intensities each.

estimate the electric field of the laser in the sample cell to be 238 Volts/cm. We can calculate the electric field of the laser from it power and the diameter at the focusing point. The full laser intensity was measured with a power meter before the focusing lens and found to be 58.6 mW and the focusing diameter is 0.1 mm. Thus the electric field of the laser in the scattering volume is calculated 255 V/cm, very similar to estimated external one producing for the same effect.

When we apply an electric field in the PPP/S solutions we measure a current ranging form $0.48\mu A$, to $1.21\mu A$ (for external field 200 to 600 V/cm) while in the pure TCE no electric current was found.

The above findings can be rationalized by a local heating of the solutions which creates a temperature gradient inside the sample. This will then create a convection towards the cooler areas with a convection velocity v. The result on the dynamics measured with PCS will be a larger apparent decay rate $\Gamma = q^2(D + v^2t)$ and a sharper than single exponential ($\exp(-\Gamma' t)^\beta$ with $\beta > 1$) correlation function (see also eq. 3.28 and discussion in chapter 7). For measurements with the green Laser the heating is caused by the absorption of the colored sample as has been verified by the measurements with the red Laser. The sample is the heated locally at the path of the beam in the cell resulting to a radial convection to the outer regions. These gives a convection velocity with a non vanishing component in the direction of the scattered beam; the later is needed so that a

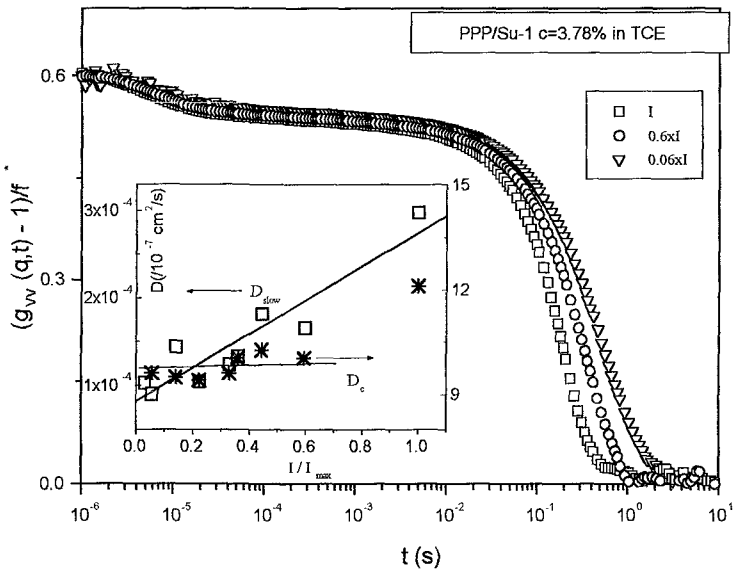

Figure D.4: Normalized field correlation function for three different values of the external elactric field. Inset: The change of the diffusion constent of the cooperative and the slow mode with respect ot the incident intensity.

ballistic motion is observable in a homodyne DLS experiment (see chapter 4 and 7). It is also worth mentioning that a separation of darker and lighter region which create rings around the path of the Laser beam, has been observed when the sample (S-1, $c = 3.78\%$ in TCE) was constantly illuminated by the full laser intensity for a long time (almost 30 hours). In the case of the external electric field the electric current which has been measured is responsible for the local heating of the sample resulting again to some convective motion in the sample cell.

References

[1] J. Riseman and J.G. Kirkwood. *J. Chem. Phys.*, 18:512, 1950.

[2] S. Broesma. *J. Chem. Phys.*, 32:1626, 1960.

[3] S. Broesma. *J. Chem. Phys.*, 74:6989, 1981.

[4] M.M. Tirado, C.L. Martinez, and J.G. de la Torre. *J. Chem. Phys.*, 81:2047, 1984.

[5] J.G. de la Torre, M.M. Tirado, and C.L. Martinez. *J. Chem. Phys.*, 23:611, 1984.

[6] J.E. Hearst and W.H. Stockmayer. *J. Chem. Phys.*, 7:1425, 1962.

[7] J.E. Hearst. *J. Chem. Phys.*, 38:1062, 1963.

[8] K. Zero and R. Pecora. *Dynamic Light Scattering, Applications of Photon Correlation Spectroscopy*, page 59. Plenum Press, New York and London, 1985.

[9] H. Yamakawa and M. Fujii. *Macromolecules*, 6:407, 1973.

[10] S.P Russo. *Dynamic Light Scattering: The Technique and Some Applications*, page 512. Oxford Science Publications, 1993.

[11] P. J. Hagerman and B. H. Zimm. *Biopolymers*, 20:1481, 1981.

[12] A. Einstein. *Ann.Phys*, 33:1275, 1910.

[13] M. Smoluchowski. *Ann. Phys*, 25:205, 1908.

[14] T. Keyes and B.M. Ladanyi. *Adv. Chem. Phys.*, 56:411, 1986.

[15] D. Beysens. *J. Chem. Phys.*, 64:2579, 1976.

[16] T.D. Gierke and W.H. Flygare. *J. Chem. Phys.*, 61:2231, 1974.

[17] A.K. Burnham, G.R. Alms, and W.H. Flygare. *J. Chem. Phys.*, 62:3289, 1975.

[18] T. Keyes. *J. Chem. Phys.*, 63:815, 1975.

[19] T. Keyes and B.M. Ladanyi. *Mol. Phys.*, 38:605, 1979.

[20] K.G. Denbigh. *Trans. Faraday Soc.*, 36:936, 1940.

[21] W. Kuhn and F. Grun. *Kolloid-Z.*, 101:248, 1942.

[22] P. Flory. *Statistical Mechanics of Chain Molecules, 2nd ed.* Hanser Publishers, Munchen, 1989.

[23] Y. Abe, A.E. Tonikelli, and Flory P.J. *Macromolecules*, 3:294, 1970.

[24] A.E. Tonikelli, Y. Abe, and Flory P.J. *Macromolecules*, 3:303, 1970.

[25] G. Fytas and A. Patkowski. *Dynamic Light Scattering: The Technique and Some Applications*, page 440. Oxford Press, 1993.

[26] G. Floudas, A. Patkowski, G. Fytas, and M. Ballauff. *J. Phys. Chem.*, 94:3215, 1990.

[27] J. Applequist, J.R. Carl, and K.K. Fung. *J. Am. Chem. Soc.*, 94:2952, 1972.

Chapter 10

Conclusions and Recommendations

In this work we investigated the dynamic behavior of a novel class of semistiff macromolecules, in solutions over a wide concentration regime. These polymers are well characterized poly-(p-phenylenes) (PPP) with large inherent optical anisotropy which uniquely enable the detailed study of their orientation fluctuations by depolarized dynamic light scattering as well as their concentration fluctuations by polarized light scattering. Their chain conformation and their aggregation behavior were also investigated providing full control of structure and dynamics of these systems. The main results of this dissertation can be summarized as follows:

I. Conformation The chain conformation of a series of polyesters (TPPE) and poly(p-phenylenes) (PPP-12) has been investigated in dilute solutions by means of depolarized Fabry-Perot interferometry [1]. By considering polydisperse wormlike chains, the persistence length, l, was determined from the depolarized Rayleigh intensity at infinite dilution and the weight average chain contour length, without involving optical anisotropies or the internal field problem. This general analysis showed that the effect of polymer non-uniformity is nearly negligible. A simple universal plot of the reciprocal of the specific depolarization ratio versus the reciprocal of the weight average chain length, was proposed for the determination of l and shown to work reasonably well, as proven by comparison with different techniques [2]. Results for the polyester series TPPE ($l = 19nm$) and the poly(p-phenylene) series PPP-12 ($l = 28nm$) confirm that poly(p-phenylenes) are stiffer molecules than polyesters. Moreover, by determining the effective anisotropy of oligomers, using the second power correction to the internal field, and comparing against the calculated values of the substituent units, it is shown that Flory's group additivity approximation works well for these semiflexible polymers.

II. Association Photon correlation spectroscopy in the polarized and depolarized geometries has been utilized in order to investigate the aggregation dynamics in toluene solutions of a hairy-rod polymer (PPP-12) [3]. Static and dynamic results from the dilute regime suggested that polymer molecules form small aggregates consisting of molecules in a nearly parallel arrangement, typically trimers, even at very low concentrations. In the semidilute regime, two new relaxation processes a slow and an ultra slow were detected, in addition to the faster cooperative diffusion and reorientation of the trimers. They were attributed to the formation of large anisotropic clusters, with inherent crystallization of side chains as revealed by X-ray scattering, which finally lead to phase separation. Assessment of the aggregation modes has been carried out using both single and multiple light scattering.

The concentration dependent dynamic study has also shown that these trimers are stable with concentration. In addition to these parallel arrangements of molecules, end-to-end association resulting in highly anisotropic, stable with concentration wormlike moieties, has been observed in P-12 and PPP/S-10 samples. The self-diffusion of clusters observed by VV dynamic light scattering slows down with concentration following the viscosity of the solution, and conforms with long time self diffusion measured by NMR (PPP-12) [4].

III. Dynamics The dynamics of concentration and orientation fluctuations of three series of PPP's was probed with polarized and depolarized PCS from dilute to highly concentrated regime ($c = 0.5 - 1400c^*$) in different solvents [5, 4, 6, 7]. The fact that in PPP/S, which was highly soluble, no nematic transition was observed allowed the investigation of the dynamics of these stiff molecules in unreachable, so far, highly concentrated isotropic solutions. The combined VV and VH experiments supplemented with some viscosity and self-diffusion data allowed a complete dynamic mapping of the system and revealed very interesting, novel features.

In these samples, the translational diffusion $D(c = 0)$ conforms with theoretical predictions and the known size of the polymer, while the rotational diffusion $D_R(c = 0)$ conforms with chains of smaller size, revealing the importance of internal bending motions in the depolarized light scattering. In addition in the PPP/S series with samples in a broad range of molecular weights, D_c is found to depend on M_w in both the dilute regime (revealing the stiff nature of the chain) and in the semidilute and concentrated regime in contrast to the observed behavior of flexible polymers. The cooperative diffusion coefficient is found to increase in all samples studied following an intermediate behavior between the flexible ($c^{0.75}$) and rodlike (c^1) predictions. Moreover in the concentrated regime ($c/c^{**} > 5$) D_c increases less strongly with c due to strong frictional effects. Its intensity exhibit a broad maximum with concentration, related to the osmotic modulus, $(\partial\pi/\partial c)_{T,p}$, scaling behavior with c which depending on M_w resembles

more or less the rodlike mean-field prediction. The cooperative friction coefficient deduced from light scattering I_c and D_c is found to be different from the self-diffusion friction deduced from NMR data.

For PPP/S samples where aggregation is minimum a second, weaker, diffusive, cooperative-like process is found in the polarized correlation function. We have excluded the possibility of a self-diffusion mode by measurements in a mixture of molecular weights. Moreover these two cooperative relaxation modes does not seem to conform with the mean field predictions for rigid rods near the nematic transition, although they might be of the same nature.

The VH correlation functions reflect rich orientational dynamics with some highly unusual characteristics. Two distinct VH processes were systematically found in PPP/S and PPP-12 samples. The fast process is related to the cooperative reorientational movements of parts of the stiff chain of the size of the Kuhn segments correlated over distance ξ. The slow mechanism is characterized by a decay rate which slows down unusually at high q and intensity which increases with q. We relate this mode with correlated reorientations of Kuhn-segment-pairs with preferred local orientational ordering (size $\sim q_{max}^{-1}$) which persists over the coherence length ξ ($> q_{max}^{-1}$). In this structural picture, the unexpected and unusual slowing down of Γ_s with q corroborates the notion that the most probable short wavelength fluctuations are long-lived. Another important finding is the very strong concentration dependence of the rotational diffusion coefficients of both the fast and the slow mode. The fast rotational diffusion, $D_{R,f}$ has a weaker concentration dependence than that of the slow mode, $D_{R,s}$. Both slow down much faster than the Doi-Edwards scaling prediction (c^{-2}) and prove how much the rotational diffusion can be slowed down in concentrated solutions of stiff polymers. Moreover, the larger M_w samples exhibit systematically weaker concentration dependence, implying that flexibility is more of dynamic rather than static nature. This behavior of the rotational diffusion is consistent with a strong increase of the zero-shear viscosity in aggreement with theories relating the two quantities. Both quantities can qualitatively be rationalized only with the prediction of "hole" theory for an exponentially decreasing with concentration parallel translational diffusion.

These findings for the diffusion coefficients (especially D_R) and the polarized and depolarized dynamic structure factors may provide important hints for the formulation of theories on the dynamics of such anisotropic systems.

IV. Molecular Orientation in Films Finally, polarized laser Raman and FTIR spectroscopies as well as wide angle X-ray diffraction have been employed in order to investigate the distribution of molecular orientation in uniaxially drawn films of polyesters [8]. Both the second ($< P_2(cos\theta) >$) and fourth ($< P_4(cos\theta) >$) moments of the segment orientation distribution function have been determined. Results reveal physically meaningful trends of both P_2 and P_4 with draw ratio.

A critical comparison among the three techniques confirms the sensitivity of Raman and FTIR to order at molecular level, when detecting the orientation of a particular segment, compared to similar WAXD results, that provide information on the larger scale liquid crystalline domain orientation only, and thus correspond to higher values of P_2.

Future work

In view of this work, there are some aspects of the dynamics of semistiff macromolecules that, to our opinion, are both interesting and important to be investigated experimentally and theoretically. We have already initiated further studies on the most promising, due to good solubility, PPP/S samples. At present both rheological (viscosity and dynamics) as well as self-diffusion (by NMR) experiments are conducted over a wide range of molecular weights of PPP/S. Another ongoing study is the investigation of the orientation fluctuations of PPP/S solutions near a wall, utilizing evanescent dynamic light scattering. It would also be interesting if the rotational diffusion of these series of wormlike polymers is measured in concentrations below the ones we were able to measure with PCS with the use of Fabry-Perot interferometry. The rotational dynamics can also be investigated by Electric Birefringence (Kerr effect) experiments. We have also started a study of the association of rodlike polymers in solution, by computer simulation in an effort to understand better the physical mechanisms involved. Finally, there is a need to study the phase behavior of these molecules and understand the absence of a nematic transition.

This work also bears into attention the need of theoretical understanding of the relaxation dynamics (concentration and orientation) and the concentration dependence of the transport properties of stiff polymers in the concentrated regime as well as of a theory for the polarized and depolarized dynamic structure factors in concentrated solutions of semirigid polymers.

Finally on the chemistry side, optically anisotropic rigid and semirigid fairly monodisperse rods with good solubility characteristics, which form anisotropic mesophases would be the model system for an investigation of pretransitional dynamics.

References

[1] G. Petekidis, D. Vlassopoulos, P. Galda, M. Rehahn, and M. Ballauff. *Macromolecules*, 29:8948, 1996.

[2] U. Tiesler, M. Rehahn, Ballauff M., G. Petekidis, D. Vlassopoulos, G. Maret, and H. Kramer. *Macromolecules*, 29:6832, 1996.

[3] G. Petekidis, D. Vlassopoulos, G. Fytas, N. Kountourakis, and S. Kumar. *Macromolecules*, 30:919, 1997.

[4] G. Petekidis, D. Vlassopoulos, G. Fytas, and G. Fleischer. *Macromolecules in press*, 1997.

[5] G. Petekidis, G. Fytas, and H. Witteler. *Colloid Polym. Sci.*, 272:1457, 1994.

[6] G. Petekidis, D. Vlassopoulos, G. Fytas, R. Rulkens, and G. Wegner. *in preparation*, 1997.

[7] G. Petekidis, D. Vlassopoulos, G. Fytas, R. Rulkens, G. Wegner, and G. Fleisher. *in preparation*, 1997.

[8] G. Voyiatzis, G. Petekidis, D. Vlassopoulos, E.I. Kamitsos, and A. Bruggeman. *Macromolecules*, 29:2244, 1996.